Copyright Warning & Restrictions

The copyright law of the United States (Title 17, United States Code) governs the making of photocopies or other reproductions of copyrighted material.

Under certain conditions specified in the law, libraries and archives are authorized to furnish a photocopy or other reproduction. One of these specified conditions is that the photocopy or reproduction is not to be "used for any purpose other than private study, scholarship, or research." If a, user makes a request for, or later uses, a photocopy or reproduction for purposes in excess of "fair use" that user may be liable for copyright infringement,

This institution reserves the right to refuse to accept a copying order if, in its judgment, fulfillment of the order would involve violation of copyright law.

Please Note: The author retains the copyright while the New Jersey Institute of Technology reserves the right to distribute this thesis or dissertation

Printing note: If you do not wish to print this page, then select "Pages from: first page # to: last page #" on the print dialog screen

DEPOSITION OF SUSPENSIONS IN LAMINAR FLOW IN THE ENTRANCE REGION OF A CHANNEL AND IN A DIFFUSER

BY

SHAWKI MAHMOUD ELDIGHIDY

A DISSERTATION

PRESENTED IN PARTIAL FULFILLMENT OF

THE REQUIREMENTS FOR THE DEGREE

OF

DOCTOR OF ENGINEERING SCIENCE IN MECHANICAL ENGINEERING

AT

NEW JERSEY INSTITUTE OF TECHNOLOGY

Newark, New Jersey
1975

ABSTRACT

In this investigation, the deposition of suspensions in laminar flow in the entrance region of a channel and a diffuser was considered.

The particulate phase was considered to be under the action of the electric field force due to electrostatic charges. In addition, a lift force acting on each particle at the wall arising from the fluid shear near the wall and an adhesive force between each particle and the wall due to the difference of the material properties for both particle and walls were considered as surface forces.

The suspension flow was assumed to be incompressible, laminar, dilute, and with negligible gravity effect.

The complete solution of the problem involved solving the Navier-Stokes equations for two-phase flow. Since the resulting governing equations are non-linear partial differential equations, finite difference and numerical techniques were used to obtain solutions. All the numerical work was carried out on an IBM 360 computer.

The complete flow characteristics of the particulate phase and the rate of deposition of the solid particles were studied under different flow conditions. Deposition due to surface adhesion only, electrostatic charge only and both surface adhesion and electrostatic charge including the lift-force action at the wall was considered.

Moreover, the case when the channel is connected to a diffuser which is considered as an approximate model for the splitter region of a fluidic device was discussed.

From this study, it was found that an appreciable amount of particle deposition can result because of the electrostatic charge on the solid particles. Also it was found that surface adhesion has a smaller effect on the rate of deposition than that due to electrostatic charge. The lift-force action at the wall has a negligible effect on the rate of deposition. In addition, it was concluded that the diffusive Peclet number has a considerable effect on the particle velocities, concentration and rate of deposition. The axial distribution of rate of deposition has a maximum only at low diffusive Peclet number.

Moreover, it was observed that the angle of divergence has a great effect on the rate of deposition in a diffuser flow. The pressure gradient and the rate of deposition increase with increasing diffuser angle. However, at larger diffuser angles, separation takes place and the rate of deposition increases rapidly in the presence of electric charge. In the absence of electric charge, the rate of deposition decreases rapidly with increasing diffuser angle.

APPROVAL OF DISSERTATION

DEPOSITION OF SUSPENSIONS IN LAMINAR FLOW IN THE ENTRANCE REGION OF A CHANNEL AND IN A DIFFUSER

BY

SHAWKI MAHMOUD ELDIGHIDY

FOR

DEPARTMENT OF MECHANICAL ENGINEERING

NEW JERSEY INSTITUTE OF TECHNOLOGY

BY

FACULTY COMMITTEE

APPROVED: _____ Chairman

_____

_____

_____

_____

NEWARK, NEW JERSEY

AUGUST, 1975

To my parents,

for their patience and encouragement

ACKNOWLEDGEMENTS

The author wishes to express his sincere gratitude to his advisor, Professor Rong-Yaw Chen, who provided many valuable suggestions, constant supervision, continuous guidance and encouragement throughout the course of investigation.

The author acknowledges with sincere appreciation the guidance and encouragement of Professor Robert A. Comparin, Chairman of the department, who initiated the study and provided technical advice and helpful suggestions during the research work.

The author wishes also to express his sincere gratitude to Professors J. V. Droughton, R. P. Kirchner, and R. I. Andrushkiw, who have kindly read through the original manuscript and provided valuable suggestions.

The author is grateful to the Mechanical Engineering Department of the New Jersey Institute of Technology for the teaching fellowship appointment during 1973-1974 academic year.

The research assistantship supported by the Harry Diamond Laboratories, in 1974-1975 is gratefully acknowledged.

Mrs. Alice Kulikowski typed the manuscript and her efforts are sincerely appreciated.

TABLE OF CONTENTS

LIST OF FIGURES

Figure

page

Figure page

LIST OF SYMBOLS

a	radius of a particle
a_d	radius of spherical sampler head
c_D	drag coefficient for a sphere
D_p	particle diffusivity
E	electric field intensity $E = E_y$
E_w	electric field intensity at the wall
E^*	dimensionless electric field intensity
f_w	adhesive force per unit mass of particles at the immediate vicinity of the wall
f_L	lift force per unit mass of particles acting on a particle by fluid shear
$\overline{F}$	inverse of relaxation time for momentum transfer given by equation (3-7)
F^*	a parameter that accounts for the deviation from Stokes' drag law, given by equation (3-8), $F^* = 1$ in the Stokes' law range
h	half the channel width
$\overline{K}$	an effectiveness parameter, accounts for a momentum transfer from the freely suspended particles to the fluid
K_{np}	Knudsen number of the particle phase
L_p	particle-fluid interaction length
m_p	mass of a particle
$\dot{m}$	rate of mass flow of the particles deposited on the wall

$\dot{m}^*$ dimensionless rate of deposition of particles

N_{DF} diffusion-response number which is the square root of the ratio of relaxation time to diffusion time

N_{ED} electro-diffusion number which is the ratio of displacement by electrostatic replusion to that by diffusion

N_m momentum-transfer number which is the ratio of relaxation time to transport time

N_R Reynolds number

N_{scp} particle Schmidt number

p static pressure of the fluid

p_o static pressure at inlet

P dimensionless static pressure of the fluid

q electric charge per particle

R^* dimensionless radius of a particle

u,v axial and vertical component of fluid velocity

u_p,v_p axial and vertical component of particle velocity

u_o inlet velocity (uniform)

u_1 fluid velocity at unit distance away from the stagnation point along the stagnation line in two-phase concave-type flow

U,V dimensionless axial and vertical component of fluid velocity

U_p,V_p dimensionless axial and vertical component of particle velocity

U_{pc},U_{pw} dimensionless axial component of particle velocity at the centerline and the wall respectively

V_{pw} dimensionless vertical component of particle velocity at the wall

$\vec{v}$	vectorial velocity of the fluid
$\vec{v}$	vectorial velocity of the particle cloud
w(x)	half the diffuser width at axial position x [w(x) ≡ h(x)]
W	dimensionless half diffuser width as defined in Appendix B
x,y	axial and vertical coordinates respectively
X,Y	dimensionless axial and vertical coordinates

Greek Letters

$\alpha,\beta,\gamma,\lambda$	dimensionless groups as defined in Appendix B
θ	half the diffuser angle
ε_o	permittivity of free space
$\bar{\bar{\mu}}$	viscosity of the material constituting the fluid phase
μ	viscosity of the fluid of suspension
μ_p	viscosity of the particulate phase in suspension, $\mu_p \simeq \rho_p D_p$
ν	kinematic viscosity of the fluid of suspension
ρ	density of the fluid phase
$\bar{\bar{\rho}}$	density of the material constituting the fluid phase
ρ_p	density of particle cloud (concentration)
$\bar{\bar{\rho}}_p$	density of the material constituting the particles
$\bar{\bar{\rho}}_d$	density of spherical sampler head
ρ_{pb}	packed bed density, i.e. particle cloud density deposited on the wall
ρ_{po}	inlet density of the particle cloud (uniform)
ρ_R	ratio of the density of the material constituting the fluid phase ($\bar{\bar{\rho}}$) to the density of the particle cloud at inlet (ρ_{po})

ρ^*_{pb} dimensionless packed bed density

ρ^*_p dimensionless density of the particle cloud (concentration)

ρ^*_{pc}, ρ^*_{pw} dimensionless density of the particle cloud at the centerline and the wall respectively

σ sticking probability accounts for electrical and viscous forces

σ_w sticking probability accounts for adhesive forces at the wall

σ'_w lifting probability which accounts for lift forces at the wall

Superscripts

* dimensionless quantities as defined

$\rightarrow$ vectorial quantity

Subscripts

b packed bed condition

c for centerline condition

o initial condition

p for particle phase

w for wall condition

1. INTRODUCTION

Two phase fluid-solid particle suspensions flow has been a subject of long term interest due to the frequent occurrence in many systems and the difficulty in obtaining satisfactory equations to explain the complex behavior exhibited by different systems.

There are many common examples of technologically important problems involving fluid-solid particle suspensions flows, such as problems connected with aerosol and paint sprays, air scrubbing systems, aircraft icing, blood flows, dust collectors, fluidized beds, heterogeneous reactors, metallized propellent rockets, pneumatic conveyers, rain erosion of guided missiles, rocket exhausts containing metal particles and many others.

One of the most important problems that has been investigated recently is the deposition of contaminants in fluidic devices, consequently serious changes in performance and plugging can be expected in such devices.

In a variety of cases of practical importance it is possible to treat the particle cloud as a continuum, then the flow of suspensions may be regarded, for the purpose of analysis, as a mixture of two interpenetrating continuous fluids.

The objective of this study of laminar flow of suspensions in the entrance region of channel and diffuser is to examine in detail the complete flow characteristics of the particulate phase under the

action of the electric field force due to electrostatic charges on the solid particles and channel or diffuser wall. In addition, a lift force acting on each particle at the wall arising from the fluid shear near the wall, and an adhesive force between each particle and the wall due to the difference of the material properties for both particle and walls will be considered as surface forces,hence they are included only in the problem as boundary conditions at the wall.

Also the characteristics of the rate of deposition curves for different flow parameters in both channel and diffuser flows will be discussed. In addition, and for the diffuser flow, the effect of the angle of divergence on the rate of deposition of the solid particles will be studied, consequently, the question concerning the effect of the pressure gradient on the rate of deposition can be answered.

Moreover, the case when the channel is connected to a diffuser which is considered as an approximate model for the splitter region of a fluidic device will be discussed.

Here it is meant by channel the constant area one i.e. the parallel-plate channel and it is meant by diffuser the straight wall diffuser.

The particulate concentration is assumed low enough (dilute suspension) such that the particles have no effect on the fluid phase. Incompressible, two-dimensional, steady and laminar flow for both channel and diffuser flows will be considered for the present investigation.

Since the resulting governing equations are non-linear partial differential equations, finite difference and numerical techniques were used to solve both problems of the channel and diffuser flows.

All the numerical work was carried out on an IBM 360 computer with accuracy of four significant figures for the channel flow problem and three significant figures for the diffuser flow problem.

In Chapter 2 a literature survey on the deposition of particles in two-phase flow is studied. The laminar flow of suspensions in the entrance region of both channel and diffuser is discussed in Chapters 3 and 4 respectively. Conclusions and recommendations for future study are given in Chapters 5 and 6 respectively.

2. LITERATURE SURVEY ON THE DEPOSITION OF PARTICLES IN TWO-PHASE FLOW

The problem of flow of suspensions and deposition of suspended particles from turbulent flows has been discussed and investigated recently by many investigators. For instance, the transport of suspended particles by turbulent streams of water has been studied by Kalinske and Van Driest [33].* The mixing and distribution of liquid droplets in high velocity gas streams were studied by Longwell and Weiss [41]. Only a few experiments have been reported on the important problem of deposition of droplets by Alexander and Coldren [2].

The problem of flow of suspensions and deposition of suspended particles with laminar flows has not been treated as widely as with turbulent flows.

The literature survey will be divided into two main sections:

1. External Flow, i.e. flow over a surface such as: flat plate, corner, sphere, an ellipsoid of revolution, cylinder and wedge, respectively.

2. Internal Flow, i.e. flow inside surfaces such as: channels and tubes, respectively.

*Numbers in brackets refer to items in the list of references.

2.1 External Flow

J. V. Healy [24] analyzed the flow of an ideal fluid, containing small spherical particles, past a cylinder and a flat plate of finite width standing normal to the stream, and the problem was treated by the method of small perturbations. The perturbed equations for arbitrary initial particle density are difficult to solve, even numercially. When the further assumption of small initial particle density is made, the problem is simplified considerably. Healy assumed: (1) incompresisble, potential, high-speed flow, (2) fluid-particle interaction is according to Stokes' drag law, (3) the particle-particle interaction is negligible, and (4) the density of the fluid is considerably less than that of the particle material, this assumption permits the absence of the pressure force terms in the particle momentum equation.

For this case the nonlinear equation governing the particle streamlines is given in differential form. The equation governing the particle density distribution is solved by the method of characteristics and the result given in integral form. The Runge-Kutta method is used to obtain numerical solutions and the results are presented graphically. Conformal mapping and analysis are used to find the particle streamlines and density distribution for the flow past a flat plate of finite width. For both bodies a particle-free zone exists, whose size depends only on the particle Stokes number, and in all cases the particle density increases monotonoically along the particle streamlines in the downstream direction. The critical particle Stokes number was found to be 1/8 for the cylinder and 1/4 for the plate.

D. H. Michael [44] considered the effect on the steady flow past a sphere of a uniform upstream distribution of dust particles having a small relaxation time. Using a potential solution as an upstream model of the gas flow at large Reynolds numbers N_R, an equation for the concentration of dust near the sphere was obtained and solved numerically.

It was shown that in the inviscid model, there existed a dust-free layer adjacent to the sphere. A drag force was computed, and it was also shown that particles did not collide with the sphere until the Stokes number, $2u\bar{\rho}_d a_d^2/9a\bar{\mu}$, was greater than 1/12 assuming that the gas flow did not change due to the presence of dust particles, and that was in agreement with the analysis done by Langmuir and Blodgett [36].

Michael's paper concludes with a discussion of the effect of a viscous boundary layer on the dust-free layer, depending upon the value of the Stokes number times the square root of Reynolds number. Michael's interest in this subject was aroused by a paper of Saffman [60] in which the Orr-Sommerfeld equation for small disturbances in plane parallel flow of a dusty gas was formulated.

Michael and Norey [45] calculated the trajectories for small particles introduced upstream into a fluid flowing past a fixed sphere. Unseparated potential flow is taken as the velocity profile for the fluid, and the effect of gravity is included in the formulation when it acts along the axis of symmetry.

Using a numerical procedure, particle trajectories which graze the sphere, and the corresponding collision efficiencies, were calculated for values of the Stokes number. When gravity was neglected, an analytic solution was obtained for large values of Stokes number which is in good agreement with the numerical results for Stokes number as low as 5. These results were compared with those of Langmuir and Blodgett [36]. When gravity was included, a critical value of the Stokes number was calculated for which no collisions occur until the Stokes number exceeds its critical value.

S. L. Soo [67] studied the relation between fraction impacted and collection efficiency of particles in a flowing suspension on a body.

The effects of inertia, diffusion and particle-surface interaction are expressed by parameters correlating relaxation time to diffusion time and deposition velocity by surface force to that by diffusion.

Morr and Soo [46] discussed the flow of a dust suspension over an ellipsoid of revolution. They performed an experimental work for measuring the particle deposition rate on the ellipsoid as well as the velocity and pressure distributions.

They classified the deposition of the solid particles on the ellipsoid as either inertial or diffusive. The particles deposited by inertia were very cohesive, tightly packed, and adhered to the surface of the ellipsoid close to the stagnation point, while the diffusive

deposition occurred in regions where the normal component of the particle cloud-mass mean motion was expected to be almost parallel to the surface; in such regions the deposits were slightly cohesive and adhered loosely to the surface of the ellipsoid. They calculated the fraction impacted efficiency for potential flow case by some simplifications in the momentum equations.

R. J. Forstrom et al [19] studied the fluid dynamics of particle (platelet) deposition for filtering walls that are related to Atherasclerosis. The analysis is applicable to the deposition of any rigid and spherical particle flowing near to a surface experiencing a fluid flux from fluid to wall. Particle deposition onto filtering surfaces is expected to occur when the drag force of filtration overcomes the fluid mechanic wall repulsive force. A nondimensional particle deposition parameter has been formulated and experimentally validated utilizing red blood cells.

The deposition parameter is applied to platelet deposition in the vasculature and shows that platelets are expected to contact arterial surfaces only in low shear, separated regions. This may be the link between the filtration and thrombosis theories of atherosclerosis. Platelet radius and plasma viscosity are predicted to be important parameters of atherosclerosis.

J. V. Healy [25] discussed the two-phase convex-type flows. The flow of an inviscid incompressible fluid, with imbedded identical spherical particles, around an arbitrary corner, was treated by the

method of small perturbations. Another application was made to concave-type flows in another paper. In both cases the approximate effects of separation were also considered.

The assumption of arbitrary initial particle density leads to a complex system of equations, which seems to have no simple solution. Assuming small initial particle density, the particle density distribution is given by a first-order partial differential equation and by solving it by the method of characteristics, yields ordinary differential equations, whose solutions are simple and analytic for unseparated flow and numerical only when separation is taken into account.

In the unseparated flow, spiral type curves will be obtained and the particle density increases monotonically in the downstream direction on all particle streamlines.

In the separated flow, Healy has found that the most effective result is the disappearance of the infinite velocity at the origin and the consequent considerable reduction in the magnitude of the perturbation.

J. V. Healy [26] discussed the two-phase concave-type flows, which is considered as an extension of his previous work in [25] concerning the two-phase convex-type flows.

He compared the particle streamlines found from the perturbation with those obtained by numerically integrating the unperturbed equations.

The agreement is found to be good for $u_1/\bar{F} \approx 0.2$ and excellent when $u_1/\bar{F} = 0.1$ or less, where u_1 is the fluid velocity at unit distance away from the stagnation point along the stagnation line and $\bar{F}$ is the inverse particle relaxation time.

The nature of concave corner flows abruptly changes when the angle θ through which the flow is deflected is $\pi/2$. For $\theta < \pi/2$, all particles collide directly except those approaching on streamlines close to the stagnation line. When $\theta = \pi/2$, the critical value of $(u_1/\bar{F})$ is $(u_1/\bar{F})_c = 0.25$, and for $\pi > \theta > \pi/2$, only particles approaching on streamlines near the stagnation line all collide.

It has been found that no particle-free zones exist in concave-type flows and the particle density increases monotonically in the downstream direction along all particle streamlines. The approximate effects of viscosity were also discussed at the end of the paper.

2.2 Internal Flow

Stukel and Soo [73] studied and investigated the turbulent flow of a suspension into a channel. An experimental investigation of the hydrodynamics of a suspension with 10 μ magnesia particles suspended in air over the inlet of a channel formed by two parallel plates was conducted for various flow velocities, plate gap widths, and mass flow ratios of solid particles to air. The study was undertaken to further the understanding of the aerodynamics of air pollution control equipment.

Experiments were carried out in a 12 in x 12 in section wind tunnel with flow velocities up to 120 ft/sec, plate gap widths of 1/4, 1 and 2 in., and mass flow ratios of particles to air varied from 0.01 to 0.1 lb. particles/lb air. They determined the particle and air velocities, the particulate mass flow and density distributions, and the particle size distribution as affected by the flow response. Measurement included a differential isokinetic sampling procedure for the measurement of the local mass flow of particles, $\rho_p u_p$, and a fiber optics probe for the measurement of the local particle concentration, ρ_p. Measurements of the velocities and static pressure of the gas phase were made with conventional Pitot static probes.

It was found that earlier methods of correlation based on the momentum integral method were valid, and that predictions of the boundary layer parameters of laminar motion could be extended to turbulent motion which exists in most of the air pollution control equipment.

The nature of the developing turbulent boundary layer for dilute suspensions is such that the density of particles is higher at the wall than at the core due to the presence of charge on the particles included by surface contacts. Further, a particle slip velocity brought about by the lack of particle-to-particle collisions in the suspension was observed at the wall, analogous to rarefied gas motions.

It was concluded that similarity laws for the scaling of equipment for air pollution control should include the momentum transfer number and the electroviscous number in addition to the Reynolds number N_R. The electroviscous number is especially important when particles possess large charge-to-mass ratios.

Yang and Peddieson [83] discussed the continuum theory of solid-fluid suspensions including solid-phase viscosity. They applied that theory to the solution of problems of one-dimensional, plane, parallel flow. The Stokes drag formula was assumed to govern the interphase force and both components were assumed to obey Newton's law of viscosity. They assumed no-slip condition for the dispersing phase and slip condition for the dispersed phase at a solid surface. The resulting equations were used to solve three steady-flow problems: (1) plane Poiseuille flow, (2) plane Couette flow, and (3) vertical film flow. They assumed incompressible Newtonian fluid with indeterminate pressure. It was also assumed that the solid phase obeys Newton's law of viscosity with (constant) viscosity coefficient μ_p. It was further assumed that the solid phase contributes nothing to the pressure of the mixture.

Closed-form solutions were obtained for these problems and used to evaluate the velocity profiles, skin friction coefficients, and

flow rates of both phases for a variety of numerical values of the parameters arising in the problem. These results were presented graphically.

They showed that the inclusion of solid-phase viscosity and the amount of particle slip allowed at the channel walls have important consequences in the problems solved. Some preliminary results were also given for an unsteady parallel-flow problem of the boundary layer type (Stokes' first problem).

Yang and Peddieson treated the particle cloud in their analysis as a continuum, then the suspension might be regarded, for the purpose of analysis, as a mixture of two interpenetrating continuous fluids.

Many authors have proposed sets of hydromechanical equations claimed by them to be appropriate for the analysis of two-phase solid-fluid flows.

Significant contributions have been made by Robinson [59], Van Deemter and Van Der Laan [79]. Hinze [28], Marble [42], Pigford and Baron [56], Murray [47], Anderson and Jackson [3], and Soo [65].

Soo's work appears to be the most general in that he began with the equations of the general theory of mixtures discussed by Truesdell and Toupin [76] and Truesdell and Noll [77].

The equations given by all of the above authors have similar forms but are not in complete agreement. It appears that more work

will be needed to resolve the discrepancies between the various theories. One of the best understood situations seems to be the case of negligible volume concentration of particles (i.e., a dilute suspension). Equations appropriate to this condition are discussed in the review article by Marble [43].

Yang and Peddieson discussed the problem of flows of solid-fluid suspensions without deposition.

Peddieson [53] studied the flow induced in a solid-fluid suspension by the impulsive motion of an infinite flat plate.

Many previous investigators have assumed that the solid phase behaves like an inviscid fluid. This assumption appears to be not universally valid. In fluidized beds, for instance, the viscosity of the solid phase is known to be large according to Jackson [31] and its neglect leads to qualitatively incorrect results in bed-stability calculations.

A continuum theory of solid-fluid suspensions including solid-phase viscous effects was formulated and used to solve the problem of finding the motion induced in a semi-infinite mass suspension by the impulsive motion of a bounding flat plate parallel to itself.

The appropriate partial differential equations were solved numerically using an implicit finite-difference method. Numerical results were obtained and examined for information concerning parametric trends.

An interesting result is that the fluid-phase skin-friction function is found to behave qualitatively differently when solid-phase viscous effects are important than when they are negligible.

Wang et al [80] has derived a complete series solution for the distribution and deposition of particles which are diffusing and settling in a stationary fluid between two horizontal plane surfaces after being uniformly distributed.

Separate expressions for the entire range of calculation are given as functions of two equations: (1) a dimensionless parameter which is the diffusion coefficient divided by the product of the settling velocity and plane separation, and (2) a dimensionless time variable which is the ratio of distance of fall to plane separation.

Numerical results show that it is better, as well as easier, to approximate deposition by the larger of the two separate effects for pure diffusion and for pure settling than by combining them as if they were independent probabilities.

Friedlander and Johnstone [20] found that when a stream of gas carrying suspended particles flows in turbulent motion past a surface, the particles are deposited due to the radial fluctuating component of velocity. They performed an experimental study of the rate of deposition of dust particles on the walls of tubes with an analysis of the mechanism of transport of particles in a turbulent stream.

Friedlander and Johnstone found that the net rate of deposition depends on both the rate of transport of the particles to the wall and

the rate of re-entrainment; the second effect was reduced to a minimum by allowing only a single layer of particles to accumulate on the surface and taking precautions to ensure adherence of all particles that struck the wall.

D. G. Thomas [78] has determined the minimum transport velocity (defined as the mean stream velocity required to prevent the accumulation of a layer of stationary or sliding particles on the bottom of a horizontal conduit) for flocculated thorium oxide and kaolin suspensions flowing in glass pipes. The pipes ranged from 1 to 4 in. in diameter, and the concentration was varied from 0.01 to 0.17 volume fraction solids. Two flow regimes were observed depending on the concentration of the suspension. In the first the suspension was sufficiently concentrated to be in the compaction zone and hence had an extremely low settling rate. The second regime was observed with more dilute suspensions which were in the hindered-settling zone and settled ten to one-hundred times faster than slurries which were in compaction.

The concentration for transition from one regime to the other was dependent on both the tube diameter and the degree of flocculation.

The suspension particles were smaller than the thickness of the laminar sublayer, and they settled according to Stokes' drag law.

Under these circumstances the relation obtained for dilute suspensions was found to be consistent with particle transfer in the radial direction owing to Bernoulli forces on the particle and the

action of turbulent fluctuations which penetrate the laminar sub-layer.

For concentrated suspension in compaction, the minimum transport velocity was given by a characteristic critical Reynolds number N_{R_c}.

Thomas [78] considered the case of small particle size to insure homogeneous flow of suspension.

Bourgeois and Grenier [7] studied the ratio of terminal velocity to minimum fluidizing velocity for spherical particles. The analogy between the states of a particle falling at its terminal velocity in a fluid and that of a particle in a bed, at incipient fluidization by the same fluid, suggests the possibility of a correlating minimum fluidizing and terminal velocities and of predicting the minimum fluidizing velocity.

A semi-theoretical curve has been obtained, relating (Re_t/Re_{mf}: terminal Reynolds number to minimum fluidizing Reynolds number) to the so-called fluidization number, $g\ \rho_{pb}\ (\bar{\rho}_p - \rho_{pb})\ (2a)^3/\bar{\mu}^2$, and it has been compared with new experimental data collected for this purpose in the range of fluidization number less than 10^8 and greater than 100.

Many authors have already proposed various empirical equations for predicting the minimum fluidizing velocity. Leva [37] in a graphical comparison of some of these correlations has shown that their agreement is rather erratic. In spite of their imperfections,

they have served a useful purpose in design work; further refinements are however desirable and should be based on a sound theoretical foundation. Among the proposed theoretical expressions, those of Narsimhan [48] and of Wen and Yu [81] are the most recent.

S. L. Soo [66] studied the pipe flow of suspensions. This study shows that fully developed pipe flow of a particulate suspension is defined by four dimensionless parameters of particle-fluid interactions in addition to the Reynolds number N_R.

Effects accounted for include the Magnus effect due to fluid shear, electrostatic repulsion due to electric charges on the particles and Brownian or turbulent diffusion. In the case of laminar liquid-solid suspension electrostatic effect is negligible, but shear effect is prominent. Solutions of the basic equations give the density distribution of particles with a peak at the center (Einstein, Jeffery) or at other radii between the center and the pipe wall (Segri et al) depending on the magnitudes of the various flow parameters.

In the case of a turbulent gas-solid suspension, the Magnus effect is significant only within the thickness of the laminar sublayer. However, charges induced on the particles by the impact of particles at the wall produce a higher density at the wall than at the pipe centerline. The velocity distribution of particles is characterized by a slip velocity at the wall and a lag in velocity in the core from the fluid phase.

In that study Soo neglected the effect of gravity on pipe flow of a suspension and he justified that assumption.

Soo and Tung [70] studied and analyzed the general case of a fully developed pipe flow of a suspension in a turbulent fluid with electrically charged particles or with significant gravity effect, or both, and for any inclination of the pipe with the direction of gravity.

Parameters defining the state of motion are: pipe flow Reynolds number, Froude number, electro-diffusion number, diffusion-response number, momentum-transfer number and particle Knudson number.

Comparison with experimental results is made for both gas-solid and liquid-solid suspensions.

It is shown that the gravity effect becomes significant in the case of large pipe diameters and large particle concentrations.

Soo and Tung [71] extended their previous studies of the fully developed flow of a suspension of particles in a turbulent fluid in gravitational and electric fields and a shear flow field, the effect of sedimentation was taken into account.

Additional considerations from previous studies are diffusion and settling under field forces, the sticking probability of a particle at the wall and that to a bed of similar particles.

The transient condition gives the rate of build-up of a bed of deposited particles. The method is applicable to pipes at any inclination to the direction of gravity.

Deposition by a field force may take place when the particle concentration at the pipe wall increases to its packed bed value or when particles start to adhere to the pipe wall. The former may result from a large concentration of particles, while the latter may occur even in a dilute suspension. In both cases, a layer of solid particles may build-up to a point such that a sliding bed will proceed downstream and may actually reach a condition of steady flow. However, an alternative situation is unsteady flow with formation and blow away of dunes or unsteady flow with particles moving from one dune to the next undergoing deceleration or acceleration as explained by Kennedy [34].

Soo and Rodgers [68] studied the occurrence of deposition due to field forces. They identified a sticking probability, σ, which depends on material properties. When all particles drifting to the wall stick to or settle at the wall $\sigma = 1$; $\sigma = 0$ for complete re-entrainment.

This sticking probability is related to the force of adhesion of particles to a surface.

Corn [14] showed that adhesive forces are either electrical or liquid (viscosity and surface tension) in origin.

The electrical forces include contact potential difference and dipole effect, space charge and electronic structure.

The gravity effect alone produces settling, but the fact that a particle may again become re-entrained gives $\sigma < 1$. Another sticking probability σ_w concerns adhesion of particles at the immediate vicinity of the wall. Opposite to settling is the lifting of a particle in the shear flow field of a fluid. This leads to a redistribution of density of particle clouds and erosion of a bed of deposited particles.

Soo and Tung [70,71] investigated the general case of a fully developed pipe flow of a suspension in a turbulent fluid in gravitational and electric fields and a shear flow field. Although they claimed that the method of solution could be extended to a laminar flow field, they did not carry out any study on laminar flow.

Chua and Wang [11] conducted an experimental investigation of the deposition of submicron particles from steady flows in a branched tube. Local rates of deposition of submicron particles from steady flows were measured along the inner and outer walls of the daughter branches of a symmetrical Y-shaped glass model of a junction with dimension based on the data of the secondary and tertiary branchi of an average human respiratory tract.

Monodisperse polystyrene latex microspheres were used to generate the aerosol by a collision-type atomizer. The particles were 0.109μ in diameter and were electrically neutralized by bipoleions. The aerosol passed through the daughter tubes at three constant

inspiratory flow rates, 31.25, 62.5 and 125 ml/sec, which correspond to low, normal and stressed breathing rates of average men.

At all flow rates, the deposition rates along the inner walls were observed to have a maximum at the branch point and a second maximum at approximately two diameters distance from the branch point, while the deposition rates along the outer walls appeared to have a maximum at one diameter distance from the entrance to the daughter branch.

Futhermore, the deposition rates were higher by one order of magnitude than the values calculated from the equation of convective diffusion with the assumption of a parabolic velocity profile. The data suggest that asymmetric flow profiles and secondary flows in daughter tubes have significant and considerable effects on the rates of particle deposition.

Chua and Wang plotted some curves of deposition rate per unit concentration, i.e. the so-called velocity of deposition versus the distance from junction for all flow rates mentioned before, and they compared their results with those of Levich [38].

Hughmark [30] studied the solid particle deposition from a turbulent gas stream. He did an experiment to estimate the particle velocity as a function of the stopping distance (the distance that a particle with a given initial velocity will move through a stagnant fluid). And he claimed that data for 0.8 μ particles in the 0.54 cm diameter pipe are not shown because these data are not in

agreement with the other particle data, also he added that the assumptions of equal particle and gas diffusion, stopping distance, and particle velocity equal to fluctuating velocity appear to be consistent with the experimental data.

Singh and Byers [63] did an experimental study of particle deposition due to thermal force from hot dust-laden gas in turbulent flow downward in an externally cooled vertical tube. Thermal force is the term used to describe the force experienced by a suspended particle due to a temperature gradient in the gas. This temperature gradient causes small particles to travel in the direction of decreasing temperature. They showed that small particles deposited closer to the inlet and the larger ones travelled farther downstream before depositing, also they found that no deposition took place for particles larger than 0.75μm.

The resulting data for particle size and average temperature in the laminar sublayer along the tube length indicated that the thermal accommodation coefficients decreased rapidly with increasing temperature. Collection efficiency was determined experimentally as a function of particle size for a turbulent stream flowing through a concentric tube annulus with the inner tube heated and the outer cooled. Overall efficiency was found to increase from 19.5% for the pipe flow to about 29% for the annulus. The range of the particle size distribution for the annulus flow was from 0.35 to 1.2μm

Peddieson [55] studied the motion of a two-phase (dust-carrier gas) suspension in the vicinity of a sphere or a circular cylinder.

The problem of analyzing the flow of a fluid containing solid particles or droplets past such bodies has been of interest for a long time because of the existence of such flows in several situations of engineering interest. These include the formation of ice on airplane wings, the erosion of missile surfaces due to high-speed raindrop impacts, and the collection and sampling of dust for the purposes of monitoring and controlling air pollution.

A knowledge of the rate of dust collection by a single isolated element can be used to estimate the rate of collection of the bed as a whole. Also the heads of various sampling devices often take the form of spheres or cylinders.

Some early papers in this field are those by Taylor [75], Langmuir and Blodgett [36], and Robinson [59]. The work of these authors and many others is reviewed in the book by Fuchs [22] and the conference proceedings edited by Richardson [58].

Most of this earlier work was directed toward finding the so-called collection efficiencies for bodies of various shapes.

(The collection efficiency is a measure of the rate at which particulate material is collected on the surface of the body).

Various extensions of that work are contained in the papers of Paretsky, Theodore, Pfeffer, and Squires [51], Spielman and Goren [72], Flint and Howarth [18], Dawson [17], Michael and Norey [45], and O'Neill [49].

All of the preceding papers have contained the assumption that the void fraction of the two-phase suspension was large, (the void fraction is the ratio of fluid volume to total suspension volume).

Peddieson [54] discussed the theoretical prediction of the performance of dust collectors.

A state of multiphase flow exists in such devices. In a dry collector there are two phases, dust and the carrier gas. In a wet collector an additional phase, consisting of water droplets, is present.

R. H. Boll [6] developed a mathematical model of venturi scrubber performance and compared with experimental data on pressure drop and particle collection.

It comprises simultaneous differential equations of drop motion, momentum exchange, and particle impaction on drops. They are readily integrated by computer for the whole venturi, given its configuration and operating conditions. Provided liquor distribution is reasonably uniform, pressure drop prediction is quite good for a wide variety of venturi sizes and shapes.

Accuracy of prediction of particle collection is only fair, discrepancies are thought to be due to either maldistribution of spray liquor or condensation of water vapor. Thus, provided these conditions are voided, the model can be used to optimize design and operating conditions for specific applications.

Pai and Hsieh [50] studied the interaction terms in gas-solid two-phase flows. From both experimental data and theoretical results of the two-phase flow, they obtained the complete expression of the interaction force between a gas and solid particle at low Reynolds number flow. The interaction force contains two terms: one is proportional to the difference between the velocities of the gas and the solid particle with a coefficient as a function of volume fraction Z and the other is proportional to the product of the total pressure of the mixture and the gradient of solid volume fraction. The second term is new. When $Z \to 0$ the completion expression of interaction force reduces to the well-known expression of Stokes formula.

Crooke and Walsh [15] studied the flow of a dusty gas through an infinitely long pipe. They discussed several boundary value problems arising from Saffman's formulation of the equations of two-dimensional flow for dusty gases.

They derived a set of linear partial differential equations representing two-dimensional flow and obtained solutions to these equations for rectangular and circular geometries. They examined both steady-state and transient cases.

The general solution for two-dimensional flow through arbitrary cross-sections in terms of eigenfunction expansions for the geometry of these cross-sections was obtained.

They developed a method for the construction of solutions for the flow of a viscous, incompressible gas with suspended dust particles

when the flow domain possesses special geometry. They did not consider any change in the number density (N) of the particles, i.e. the case of no particle deposition.

Comparin et al [13] studied experimentally the deposition of contaminants in fluidic devices. They found that serious changes in performance and plugging can be expected in such devices.

It is an interesting point to further the study analytically for the deposition of contaminants in fluidic devices particularly in the splitter region (output region) which can be approximated to a parallel-plate channel connected to a straight wall diffuser.

3. LAMINAR FLOW OF SUSPENSIONS IN THE ENTRANCE REGION OF A CHANNEL

Internal flows of suspensions have been extensively studied as mentioned in Chapter 2. However, laminar flows of suspensions in channels, especially in the entrance regions, have not been investigated due to the fact that a complete solution of the problem will involve solving the Navier-Stokes equations, which is a formidable task. The availability of large, high speed digital computers and the greater understanding of the use of numerical methods for solving non-linear partial differential equations have made the numerical solution of the equations of motion feasible, thus eliminating much of the need for approximation in solving fluid mechanics problems.

An experimental study by Stukel and Soo [73] of turbulent flow of a suspension into a channel has found that considerable amount of particle deposition occurred due to the electrostatic charge on the particles. Soo further introduced the concept of a sticking factor, σ which depends on both the solid particle and channel wall material. When $\sigma = 1.0$, all particles reaching the channel wall are assumed to stick to the wall, whereas at $\sigma = 0$, every particle is reentrained by the fluid flow stream after reaching the wall.

In this chapter, a numerical scheme is presented to study the laminar flow of suspensions in the entrance region of a channel, including the rate of deposition of the solid particles on the channel wall.

The suspension channel flow is considered at conditions under which a finite layer of particles is deposited at the channel wall, due to the electrostatic charge and wall adhesion. The electrostatic charge is generated by the collision among the solid particles themselves and also by the collision between the solid particles and the channel wall. Experiments by Kunkel [35] showed that all dust particles become electrostatically charged upon being dispersed into a cloud.

The suspension flow is laminar and is considered to be incompressible which is also true as a good approximation for compressible flow at very low Mach numbers.

Also the case of low particulate concentration (dilute suspension) will be considered such that the particles have no effect on the fluid phase. Due to dilute suspension assumption and since the solid particles are very small (size of order 2μ diameter), the effect of gravity can be neglected. Further it will be assumed that the thickness of the layer of deposit is much smaller than the channel width, so that the effective reduction in channel width is not enough to change appreciably the fluid velocity distribution.

To get the governing equations, one writes the assumptions as follows:

Assumptions

(1) Incompressible, steady flow

(2) Two-dimensional, laminar flow

(3) Negligible gravity effect

(4) Negligible axial component of the electric field intensity ($E_x = 0$)

(5) Dilute suspension ($\rho > \rho_p$, $\bar{K} = 0$)

(6) Fluid-particle interaction is according to Stokes' drag law

(7) Particle-particle interaction is negligible

(8) Thickness of the layer of deposit is much smaller than the channel width

In accordance with the boundary layer simplification by Schlichting [62], the equation for the normal component of fluid momentum reduces to $(\partial p/\partial y) = 0$, therefore p is a function of x only and one can replace the partial derivative term $(\partial p/\partial x)$ in the equation for the axial component of fluid momentum, by the total derivative term (dp/dx).

Subject to these assumptions, the governing equations will be:

3.1 Governing Equations

(a) Fluid Phase

$$\frac{\partial u}{\partial x} + \frac{\partial v}{\partial y} = 0 \tag{3-1}$$

$$u \frac{\partial u}{\partial x} + v \frac{\partial u}{\partial y} = - \frac{1}{\rho} \frac{dp}{dx} + \frac{\mu}{\rho} \frac{\partial^2 u}{\partial y^2} \tag{3-2}$$

(b) Particle Phase

$$\frac{\partial (\rho_p u_p)}{\partial x} + \frac{\partial (\rho_p v_p)}{\partial y} = 0 \tag{3-3}$$

$$u_p \frac{\partial u_p}{\partial x} + v_p \frac{\partial u_p}{\partial y} = \bar{F} (u - u_p) + \frac{D_p}{\rho_p} \frac{\partial}{\partial y} \left(\rho_p \frac{\partial u_p}{\partial y}\right) \tag{3-4}$$

$$u_p \frac{\partial v_p}{\partial x} + v_p \frac{\partial v_p}{\partial y} = \bar{F} (v - v_p) + \left(\frac{q}{m_p}\right) E_y \tag{3-5}$$

$$\frac{\partial E_y}{\partial y} = \frac{\rho_p q}{\varepsilon_o m_p} \tag{3-6}$$

where $$\bar{F} = F^* \left[9(\bar{\mu}/2a^2)\rho_p\right]\left[1 + (\rho/2\bar{\rho}_p)\right]^{-1} \tag{3-7}$$

and $$F^* = (c_D/24)\left[2a(\bar{\rho}\left|\vec{v} - \vec{v}_p\right|)/\bar{\mu}\right]. \tag{3-8}$$

The continuity equation of the particle phase (3-3) can be expanded in the form

$$\rho_p \frac{\partial u_p}{\partial x} + u_p \frac{\partial \rho_p}{\partial x} + \rho_p \frac{\partial v_p}{\partial y} + v_p \frac{\partial \rho_p}{\partial y} = 0$$

which contains partial derivatives of the same order for u_p, v_p and ρ_p.

Looking at equations (3-4), (3-5) and (3-6) one can see that the variables of highest order derivatives are u_p, v_p and E_y, respectively. This means that equation (3-4) is a fundamental equation for u_p, also equation (3-5) is a fundamental equation for v_p and equation (3-6) is a fundamental equation for E_y. One still needs a fundamental equation for ρ_p, i.e. an equation where ρ_p has the highest order derivative and this is done by replacing the continuity equation of the particle phase with the diffusion equation as follows:

Equations (3-1) and (3-3) can be combined to give:

$$u \frac{\partial \rho_p}{\partial x} + v \frac{\partial \rho_p}{\partial y} = - \frac{\partial}{\partial x}\left[\rho_p(u_p - u)\right] - \frac{\partial}{\partial y}\left[\rho_p(v_p - v)\right] \tag{3-9}$$

Let $j_{px} = \rho_p (u_p - u)$

$j_{py} = \rho_p (v_p - v)$

j_{px} and j_{py} are the mass fluxes in the x - and y - direction respectively under the effect of both external field force and self-diffusion of the particles. Equation (3-9) can be written as follows:

$$u \frac{\partial \rho_p}{\partial x} + v \frac{\partial \rho_p}{\partial y} = - \frac{\partial j_{px}}{\partial x} - \frac{\partial j_{py}}{\partial y} \qquad (3\text{-}10a)$$

For the present investigation, it is assumed $\frac{\partial j_{px}}{\partial x} << \frac{\partial j_{py}}{\partial y}$, therefore equation (3-10a) becomes

$$u \frac{\partial \rho_p}{\partial x} + v \frac{\partial \rho_p}{\partial y} = - \frac{\partial j_{py}}{\partial y} \qquad (3\text{-}10b)$$

From Fick's law one has

$$j_{py} = \left(\frac{q}{m_p}\right) \frac{\rho_p E_y}{\bar{F}} - D_p \frac{\partial \rho_p}{\partial y} \qquad (3\text{-}11)$$

which means that the mass flux of the solid particles in the y-direction is due to both external field force and self-diffusion of the particles.

Substituting Eq. (3-11) into Eq. (3-10b), one gets the diffusion equation:

$$u \frac{\partial \rho_p}{\partial x} + v \frac{\partial \rho_p}{\partial y} = - \frac{\partial}{\partial y} \left[\left(\frac{q}{m_p}\right) \frac{\rho_p E_y}{\bar{F}}\right] + D_p \frac{\partial^2 \rho_p}{\partial y^2} \qquad (3\text{-}12)$$

Therefore the system of equations that has to be solved is as follows:

$$\frac{\partial u}{\partial x} + \frac{\partial v}{\partial y} = 0 \qquad (3\text{-}1)$$

$$u \frac{\partial u}{\partial x} + v \frac{\partial u}{\partial y} = - \frac{1}{\rho} \frac{dp}{dx} + \frac{\mu}{\rho} \frac{\partial^2 u}{\partial y^2} \qquad (3\text{-}2)$$

$$u_p \frac{\partial u_p}{\partial x} + v_p \frac{\partial u_p}{\partial y} = \bar{F} (u - u_p) + \frac{D_p}{\rho_p} \frac{\partial}{\partial y} \left(\rho_p \frac{\partial u_p}{\partial y}\right) \qquad (3\text{-}4)$$

$$u_p \frac{\partial v_p}{\partial x} + v_p \frac{\partial v_p}{\partial y} = \bar{F}\,(v - v_p) + \left(\frac{q}{m_p}\right) E_y \qquad (3\text{-}5)$$

$$u \frac{\partial \rho_p}{\partial x} + v \frac{\partial \rho_p}{\partial y} = -\frac{\partial}{\partial y}\left[\left(\frac{q}{m_p}\right)\frac{\rho_p E_y}{\bar{F}}\right] + D_p \frac{\partial^2 \rho_p}{\partial y^2} \qquad (3\text{-}12)$$

$$\frac{\partial E_y}{\partial y} = \left(\frac{\rho_p q}{\varepsilon_o m_p}\right) \cdot \qquad (3\text{-}6)$$

The purpose of solving these equations is to determine the rate of deposition of the particles on the channel wall which can be obtained from the equation of conservation of mass of the particle phase as follows:

$$-\frac{\partial}{\partial x}\int_o^h \rho_p u_p dy = \sigma \rho_{pw} v_{pw} + \sigma_w \rho_{pw} f_w/\bar{F} - \sigma_w' \rho_{pb} f_L/\bar{F} \qquad (3\text{-}13)$$

where σ is the sticking probability accounts for electrical and viscous forces,

σ_w is the sticking probability accounts for adhesive forces at the wall,

σ_w' is the lifting probability which accounts for lift forces at the wall,

f_w is the adhesive force per unit mass of particles at the immediate vicinity of the wall,

f_L is the lift force per unit mass of particles acting on a particle by fluid shear near the wall, and it is given by Soo and Tung [71] as follows:

$$f_L = 1.54 \frac{\rho}{\bar{\rho}_p} \frac{\sqrt{\nu}}{a} \left|\frac{\partial u}{\partial y}\right|^{\frac{1}{2}} \left(u_p - u + a\left|\frac{\partial u}{\partial y}\right|\right). \qquad (3.14)$$

The right-hand side of equation (3-13) consists of three terms. The first term ($\sigma\rho_{pw}v_{pw}$) is the rate of deposition of particles per unit area due to electric charge. The relation of v_{pw} and E_w (electric field intensity at the wall) is derived in Appendix A and it is given by Eq. (A-7).

The second term ($\sigma_w\rho_{pw}f_w/\bar{F}$) is the rate of deposition of particles per unit area due to surface adhesion. This term depends upon material and surface properties. The quantity $\sigma_w f_w/4\bar{F}$ is the deposition velocity defined by Friedlander and Johnstone[20].

The third term ($-\sigma_w'\rho_{pb}f_L/\bar{F}$) is the rate of lifting of particles per unit area due to lift forces at the channel wall. The minus sign indicates lifting of particles, i.e. decrease in rate of deposition. For given fluid and particle phases with fixed particle size, the lift force per unit mass f_L will be a function of the axial velocities difference $(u_p - u)$ and the axial velocity gradient of the fluid phase $(\partial u/\partial y)$. This means that the lift force f_L at the wall is a function of the axial position x. It is worth noticing that the lift force in the governing equations was neglected because of neglecting the gravity effect since the suspension is dilute and the solid particles are very small. However, the lift force f_L was considered as a surface force arising from the fluid shear near the wall.

Combining Eq. (3-14) with Eq. (3-13) then the resulting equation for the rate of deposition of the particles will include the variables:

$$\left(u,\ u_p,\ \frac{\partial u}{\partial y}\right)_{@\text{ the wall}},\ v_{pw} \text{ and } \rho_{pw}.$$

The factors σ, σ_w, σ_w' and the quantities f_w and ρ_{pb} can be assigned reasonable values according to experiments and previous work by others such as Soo and Tung [71] and $\bar{F}$ can be calculated from Eq. (3-7) after some simplifications as indicated in Appendix B.

Equations (3-1), (3-2), (3-4), (3-5), (3-6) and (3-12) to (3-14) can be non-dimensionalized as given in Appendix B, as follows:

$$\frac{\partial U}{\partial X} + \frac{\partial V}{\partial Y} = 0 \tag{3-15}$$

$$U \frac{\partial U}{\partial X} + V \frac{\partial U}{\partial Y} = - \frac{dP}{dX} + \frac{1}{N_R} \frac{\partial^2 U}{\partial Y^2} \tag{3-16}$$

$$U_p \frac{\partial U_p}{\partial X} + V_p \frac{\partial U_p}{\partial Y} = \frac{1}{N_m} (U - U_p) + \frac{1}{\beta \rho_p^*} \frac{\partial}{\partial Y} (\rho_p^* \frac{\partial U_p}{\partial Y}) \tag{3-17}$$

$$U_p \frac{\partial V_p}{\partial X} + V_p \frac{\partial V_p}{\partial Y} = \frac{1}{N_m} (V - V_p) + \frac{1}{\beta N_m} E^* \tag{3-18}$$

$$\beta (U \frac{\partial \rho_p^*}{\partial X} + V \frac{\partial \rho_p^*}{\partial Y}) = \frac{\partial^2 \rho_p^*}{\partial Y^2} - E^* \frac{\partial \rho_p^*}{\partial Y} - 4\alpha \rho_p^{*2} \tag{3-19}$$

$$\frac{\partial E^*}{\partial Y} = 4\alpha \rho_p^* \tag{3-20}$$

$$\dot{m}^* = \rho_{pw}^* (\sigma V_{pw} + \sigma_w \lambda/\beta) - \sigma_w' \rho_{pb}^* \gamma/\beta \tag{3-21}$$

where $$\gamma = (1.54\beta N_m \rho_R / R^* N_R^{1/2}) (U_p - U + R^* \left| \frac{\partial U}{\partial Y} \right|) \left| \frac{\partial U}{\partial Y} \right|^{-1/2} \tag{3-21a}$$

calculated at the wall.

The physical meaning and order of magnitude of the dimensionless quantities and parameters are explained in Appendix B.

Equation (3-19) is the Diffusion equation, while Eq. (3-20)[given

by the Gauss law] is the Poisson equation. The unknowns in the above equations [Eq. (3-15) through Eq. (3-21)] are:

$$U,\ V,\ P,\ U_p,\ V_p,\ \rho_p^*,\ E^*\ \text{and}\ \dot{m}^*$$

Note that the solution depends on Reynolds number N_R as well as the momentum-transfer number N_m, the diffusive Peclet number β, the electrostatic charge parameter α and the boundary conditions.

3.2 Boundary Conditions

Referring to Fig. (3.1) and considering symmetrical flow through the channel with uniform inlet conditions, the boundary conditions will be:

@ x = 0 (at the channel inlet)

$(0 \le y \le h)$

$$\left.\begin{aligned} u = u_p = u_o &\quad \text{uniform} \\ v = v_p = 0 & \\ \rho_p = \rho_{po} &\quad \text{uniform} \\ p = p_o &\quad \text{uniform} \\ E_y = 0 & \end{aligned}\right\} \quad (3\text{-}22)$$

@ y = 0 (at the centerline of the channel)

$(x > 0)$

$$\left.\begin{aligned} \frac{\partial u}{\partial y} = \frac{\partial u_p}{\partial y} = 0 &\quad \text{symmetry} \\ v = v_p = 0 & \\ \frac{\partial \rho_p}{\partial y} = 0 &\quad \text{symmetry} \\ E_y = 0 & \end{aligned}\right\} \quad (3\text{-}23)$$

$$
\begin{aligned}
&\underline{@\ y = h} \qquad\qquad \text{(at the channel wall)} \\
&(x > 0) \\
&u = v = 0 \qquad\qquad \text{no slip condition} \\
&u_p = -L_p \left.\frac{\partial u_p}{\partial y}\right|_{y=h} \qquad \text{particle slip condition} \qquad \text{Case I} \\
\text{or}\ &\left[\begin{array}{ll} u_p = u_o(1 - x\bar{F}/u_o) - L_p \left.\dfrac{\partial u_p}{\partial y}\right|_{y=h} & (x < u_o/\bar{F}) \\ u_p = -L_p \left.\dfrac{\partial u_p}{\partial y}\right|_{y=h} & (x \geq u_o/\bar{F}) \end{array}\right] \text{Case II} \\
&D_p \left.\frac{\partial \rho_p}{\partial y}\right|_{y=h} = (1-\sigma)\rho_{pw} \frac{qE_w}{m_p \bar{F}} - \sigma_w \rho_{pw} \frac{f_w}{\bar{F}} + \sigma'_w \rho_{pb} \frac{f_L}{\bar{F}}
\end{aligned}
\qquad (3\text{-}24)
$$

where $f_L = 1.54 \dfrac{\rho}{\rho_p} \dfrac{\sqrt{\nu}}{a} \left|\dfrac{\partial u}{\partial y}\right|^{\frac{1}{2}} (u_p - u + a \left|\dfrac{\partial u}{\partial y}\right|)$,

and L_p is the particle-fluid interaction length. When the fluid is in laminar motion, L_p is the free path over which a particle changes its direction because of diffusion D_p. The existence of L_p explains the experimental result that the particles are in a slip motion with velocity u_{pw} at the wall as in the case of a rarefied gas, the expression for L_p as a free path is given by John [32] as follows:

$$L_p = \bar{l} = \frac{3\mu}{\rho a \sqrt{\frac{8}{\pi\gamma}}}$$

where $a = \sqrt{\gamma g_c RT}$ (Velocity of sound)

therefore
$$L_p = \frac{3\nu}{\sqrt{\frac{8}{\pi} g_c RT}} \qquad (3\text{-}24a)$$

where ν = Kinematic viscosity of the fluid (air)

R = Gas constant

T = Temperature of the gas

g_c = Gravitational constant

So for a given pressure and temperature (say 1 atm and 20 deg C) the interaction length, L_p, can be calculated as shown in Appendix B.

The last boundary condition in (3-24) of the particle cloud density gradient at the wall is derived in Appendix A. It is based on the equation of conservation of mass of the particle phase, from which one can find the rate of deposition of the particles on the channel wall as given in Eq. (3-13).

It is worth noticing that two cases for the slip condition of the particles at the wall were considered. Case I is the regular slip condition and Case II is the modified slip condition where the excess term $u_o(1 - x\bar{F}/u_o)$ @ $x < u_o/\bar{F}$ was introduced to account for the distance that the solid particles will travel before they start to deposit on the wall when $L_p = 0$ (i.e. Knudsen number $K_{np} = 0$). The value of the distance x depends on the relaxation time of the particles $(1/\bar{F})$, the higher the relaxation time of particles the greater the distance x will be and vice versa.

The above equations of the boundary conditions can be non-dimensionalized as follows:

$$\begin{array}{lll} \underline{@\ X = 0} & \text{(at the channel inlet)} & \\ (0 \leq Y \leq 1) & & \\ U = U_p = 1 & \text{uniform} & (1,2) \\ V = V_p = 0 & & (3,4) \end{array} \Bigg] \quad (3\text{-}25)$$

$$\left.\begin{array}{lll} \rho_p^* = 1 & \text{uniform} & (5) \\ P = 0 & & (6) \\ E^* = 0 & & (7) \end{array}\right] \quad (3\text{-}25)$$

@ Y = 0 (at the centerline of the channel)

(X > 0)

$$\left.\begin{array}{lll} \dfrac{\partial U}{\partial Y} = \dfrac{\partial U_p}{\partial Y} = 0 & \text{symmetry} & (8,9) \\ V = V_p = 0 & & (10,11) \\ \dfrac{\partial \rho_p^*}{\partial Y} = 0 & \text{symmetry} & (12) \\ E^* = 0 & & (13) \end{array}\right] \quad (3\text{-}26)$$

@ Y = 1 (at the channel wall)

(X > 0)

$$\left.\begin{array}{lll} U = V = 0 & \text{no slip condition} & (14,15) \\ U_p = -K_{np} \left.\dfrac{\partial U_p}{\partial Y}\right|_{Y=1} & \text{particle slip condition} \quad \text{Case I} & (16) \\ \text{or} \quad \left[\begin{array}{ll} U_p = (1 - X/N_m) - K_{np} \left.\dfrac{\partial U_p}{\partial Y}\right|_{Y=1} & X < N_m \\ U_p = -K_{np} \left.\dfrac{\partial U_p}{\partial Y}\right|_{Y=1} & X \geq N_m \end{array}\right] & \text{Case II} \quad (16) \\ \left.\dfrac{\partial \rho_p^*}{\partial Y}\right|_{Y=1} = (1-\sigma) E_w^* \rho_{pw}^* - \sigma_w \lambda \rho_{pw}^* + \sigma_w' \gamma \rho_{pb}^* & & (17) \end{array}\right] \quad (3\text{-}27)$$

where $\gamma = (1.54\ \beta N_m \rho_R / R^* N_R^{1/2})(U_p - U + R^* \left|\frac{\partial U}{\partial Y}\right|) \left|\frac{\partial U}{\partial Y}\right|^{1/2}$.

The above equations (3-25) to (3-27) represent 17 boundary conditions and these conditions are necessary and sufficient to solve the system of equations given in Section 3.1 [Eq. (3-15) to Eq. (3-21)].

3.3 Method of Solution

Equations (3-15) to (3-21) in Section 3.1 with the boundary conditions (3-25), (3-26) and (3-27) in Section 3.2 can be solved together for the unknowns U, V, P, U_p, V_p, ρ_p^*, E^*, and $\dot{m}^*$ by the finite difference technique [12, 64]. These equations are written in a finite difference form as shown in Appendix C.

A square mesh is superimposed on the flow field internal to the channel. The finite difference coordinates are chosen to correspond to the spatial coordinates shown in Fig. (3.1) so that i = 1 corresponds to X = 0, and j = 2 corresponds to Y = 0, a positive change in the X-coordinate of ΔX, which is taken as 0.1, increases i by 1, similarly a positive change in the Y-coordinate of ΔY, which is taken as 0.1 (corresponding to 10 equal intervals in the Y-direction, i.e. n = 10) increases j by 1. When Y = 1, at the channel wall, j = n+2. Eleven mesh points in the Y-direction and up to 141 mesh points in the X-direction were used, i.e. X = 14 which is equivalent to 7 times the channel width. The finite difference grid is illustrated in Fig. (3.2).

The quantities U, V, P, U_p, V_p, ρ_p^* and E^* at each point in the column i = 1 are known as boundary conditions (3-25). By substituting the values of U , U_{p_1}, V_{p_1} and $\rho_{p_1}^*$ (uniform conditions) into equation (C-25) after replacing the subscript (i + 1) with i, then one can calculate the deposition rate (DPR $\equiv \dot{m}^*$) at i = 1. From the quantities U_1, V_1, P_1, U_{p_1}, V_{p_1}, $\rho_{p_1}^*$ and E_1^*, by use of the finite difference equations which take the form of the matrix equation:

$$A_i \; X_{i+1} = B_i$$

where A_i is the matrix of coefficients at axial position i,

B_i is the column vector at the same axial position i,

and X_{i+1} is the variable column vector at axial position (i+1).

A_i and B_i are in terms of U_i, V_i, P_i, U_{p_i}, V_{p_i}, $\rho^*_{p_i}$, and E^*_i. But X_{i+1} is in terms of U_{i+1}, V_{i+1}, P_{i+1}, $U_{p_{i+1}}$, $V_{p_{i+1}}$, $\rho^*_{p_{i+1}}$ and E^*_{i+1}. So for i = 1, A_1 and B_1 are known, hence one can determine X_2, i.e. U_2, V_2, P_2, U_{p_2}, V_{p_2}, $\rho^*_{p_2}$ and E^*_2. Substituting the values of U_2, U_{p_2}, V_{p_2}, and $\rho^*_{p_2}$ taken at the wall (i.e. @ j = 12) into equation (C-25) then the deposition rate DPR_2 can be determined.

In the same manner the solution is carried on downstream, finding U, V, P, U_p, V_p, ρ^*_p and E^* for the (i+1)th column when these quantities are known in the ith column. Substituting the values of U_{i+1}, $U_{p_{i+1}}$, $V_{p_{i+1}}$ and $\rho^*_{p_{i+1}}$ taken at the wall, into equation (C-25) then one can find the deposition rate DPR_{i+1}, i.e. $\dot{m}^*$ at the axial position i+1.

The numerical procedures are shown in Appendix C. For the solution of the matrix equation AX = B, a computer program has been written using a subroutine called (LEQT2F) which in turn uses other subroutines (LUDATF & LUELMF) to solve the given matrix equation numerically and by the Crout reduction technique [21] which is the modified Gauss elimination technique. A matrix size of A was considered to be (60 x 60) and an accuracy of four significant figures

in the computations was assumed.

As far as the stability requirement is concerned, Berezin [4] and Quarmby [57] indicated that the general condition for stability is

$$(\Delta X/N_R)/(\Delta Y)^2 < 0.5$$

with $\Delta X = \Delta Y = 0.1$,

for $N_R = 1000$ $\quad (\Delta X/N_R)/(\Delta Y)^2 = 0.01 \quad < 0.5$

and for $N_R = 100$ $\quad (\Delta X/N_R)/(\Delta Y)^2 = 0.1 \quad < 0.5$

Therefore the stability requirement is satisfied.

Moreover, different mesh sizes ($\Delta X = 0.05$, 0.2, and 0.3) were used during the course of analysis. The solutions for these mesh sizes were found to be in agreement with the solution for the chosen mesh size ($\Delta X = 0.1$).

3.4 Results and Discussion

In this section, the complete flow characteristics of laminar flow of suspensions in the entrance region of channel will be examined in detail. The fluid phase will be discussed briefly, since it has been done by Quarmby [57] and others. However, the particulate phase will be studied extensively due to the fact that the solution of the problem is a parametric type, and the interest is to find out which flow parameters affect considerably the rate of deposition of the solid particles. Some of these parameters as well as dimensionless quantities needed to solve the problem, can be calculated as indicated Appendix B, while the others can be estimated and taken from previous results and experiments that have been done by others [10,71].

3.4.1 Fluid Phase

Fig. (3.4) shows the axial velocity distribution of the fluid phase U. The centerline velocity, U_c, increases downstream until it approaches a value of 1.5 when the flow becomes fully developed. As a check with Quarmby's solution [57], at X = 14, U_c = 1.16 while the corresponding value obtained by Quarmby (with K_n = 0) is U = 1.20 which means that the solution is different by 3.3% at that specific point. Such a difference is mainly due to the fact that a horizontal mesh size of $\Delta X = 0.1$ was assumed, while Quarmby has considered $\Delta X = 0.0001$ and of course the smaller the mesh size, the better the results one obtains. But since the problem involves solving for the fluid and particulate phases at the same time and the interest is to examine the flow characteristics of the particulate phase, then an approximate solution for the fluid phase (by selecting $\Delta X = 0.1$) is reasonable for reducing computing time.

Fig. (3.5) shows the vertical velocity distribution of the fluid phase V. Here, the values of V are negative, which means that the direction of motion of the fluid elements in the vertical direction is away from the wall, and this result is analogous to the result obtained by Hornbeck [29] for pipe flow. Also it can be observed that the absolute value of V decreases downstream until it becomes zero when the flow becomes fully developed.

Fig. (3.6) shows the axial distribution of the fluid static pressure P. It is clear that the pressure decreases along the X-axis and this is true since the fluid is accelerated.

3.4.2.1 Flow of Suspensions without Deposition

This case is studied for the purpose of finding the flow parameters that affect the velocity field and concentration of particles.

Fig. (3.7) shows a comparison of axial velocities of fluid and particle phases U and U_p respectively with no deposition. It is obvious that $U > U_p$ except at the wall. Such a difference $(U - U_p)$ is caused by the difference in the momentum of both fluid and particles. Also it can be seen that U_{pc}, the axial velocity of the particle at the centerline of the channel, increases downstream until it matches the fluid stream velocity in the fully developed region.

It is worth noticing that the profile of U_p at $X = 1$ and near the wall is curved due to the slip condition at the wall in Case II where $(1 - X/N_m) > - K_{np} \left.\frac{\partial U_p}{\partial Y}\right|_{Y=1}$ for $X < N_m$.

Fig.(3.8) shows a comparison of vertical velocities of fluid and particle phases, V and V_p, with no deposition. It is clear that both V and V_p are negative, therefore both the fluid elements and the particles are moving towards the centerline of the channel. Also the absolute value of $(V - V_p)$ increases with X at the beginning, then starts to decrease until it reaches zero at very large X, i.e. when the flow becomes fully developed.

Fig. (3.9) indicates that the particle velocity, U_p, increases with increasing the diffusive Peclet number β. It is clear that the particle velocity profile becomes close to that of the fluid phase at higher β due to the fact that increasing the diffusive Peclet

3.4.2 Particle Phase

In this section, the discussion of the particulate phase will be divided into four main parts as follows:

(1) Flow of suspensions without deposition

(2) Flow of suspensions with deposition due to surface adhesion only

(3) Flow of suspensions with deposition dut to electric charge only

(4) Flow of suspensions with deposition due to both electric charge and surface adhesion including lift-force action at the wall (general case).

It should be noted that the discussion and related figures in the particulate phase are focussed on Case II for the particle slip condition at the wall (boundary condition 3-27), unless otherwise stated. However, the only difference between the effect of Case I and Case II is some changes in the velocity profiles and rate of deposition of particles within a distance $X = N_m$, where N_m is the momentum-transfer number.

In each case the velocity profiles of the particles U_p and V_p will be discussed. Particle cloud density distribution, i.e. the particle concentration ρ_p^* and also the electric field intensity E^* will be considered. In addition, the characteristic curves of the rate of deposition of particles will be discussed in a way that shows the most important parameters.

number increases the momentum transfer from the fluid elements to the solid particles.

Fig. (3.10) illustrates the effect of the diffusive Peclet number, β, on the vertical velocity of the particles with no deposition. It is shown that the absolute value of V_p decreases with increasing diffusive Peclet number, i.e. when the particles become more accelerated.

The computer results indicate that the diffusive Peclet number has no effect on the distribution of the particle concentration ρ_p^* which is uniform in a flow of suspension without deposition.

3.4.2.2 Flow of Suspensions with Deposition Due to Surface Adhesion Only

In this section, the effects of the surface adhesion on the particulate phase characteristics will be discussed. The surface adhesion is caused by the adhesive force between the particles and the wall due to the difference of the material properties of the particles and the channel wall.

The computer results show that the surface adhesion has a very little effect on the particles velocity profiles U_p and V_p. And the most effective parameter that changes these velocity profiles is the diffusive Peclet number β. However, the surface adhesion has a great influence on the distribution of the particle concentration, ρ_p^*, and the rate of deposition, $\dot{m}^*$, as shown in next figures.

Fig. (3.11) shows the particle cloud density distribution, i.e. the particle concentration, ρ_p^*, for a surface adhesion parameter ($\sigma_w\lambda = 0.1$) and at low diffusive Peclet number ($\beta = 4$). It is worth noticing that the concentration, ρ_p^*, decreases downstream, moreover the decrease of the concentration at the wall is greater than that at the centerline.

Fig. (3.12) illustrates the influence of the surface adhesion parameter ($\sigma_w\lambda = 0.1, 1.0, 100$) on the distribution of the particle concentration ρ_p^*, for $\beta = 40$. It is clear that at higher surface adhesion, the particle concentration drops faster especially at the wall as shown in Fig. (3.13), moreover at a value of $\sigma_w\lambda = 100$, the particle concentration at the wall ρ_{pw}^* becomes practically zero further downstream, and this is the case of complete absorption. In addition and by comparing Fig. (3.12) for $\sigma_w\lambda = 0.1$ where $\beta = 40$ with Fig. (3.11) where $\beta = 4$, it can be seen that when one increases the diffusive Peclet number β, the particle concentration becomes more uniform particularly at the centerline of the channel as also indicated in Fig. (3.14).

Fig. (3.14) indicates the effect of surface adhesion on particle concentration for $\beta = 10^7$. It is obvious that $\rho_p^* = 1.0$ at $Y = 0$ up to 0.6 and the only change in concentration occurs near the wall. Form Fig. (3.15) one can observe that the particle concentration at the wall decreases rapidly with increasing surface adhesion. From the computer results at $X = 14$, $\sigma_w\lambda = 1000$ the particle concentration at the wall $\rho_{pw}^* = 0.0055$, i.e. the case of complete

absorption where $\rho^*_{pw} = 0$, occurs approximately when $\sigma_w\lambda = 1000$ for $\beta = 10^7$ while the complete absorption case happens when $\sigma_w\lambda \simeq 100$ for $\beta = 40$ as shown in Fig. (3.13). From this result it can be seen that the diffusive Peclet number, β, has a considerable effect on the particle concentration. Moreover, the surface adhesion parameter, $\sigma_w\lambda$, has a serious effect on particle concentration especially at low β. It is worth noticing that the absolute value of the particle cloud density gradient at the wall i.e. $(\partial\rho^*_p/\partial Y)_{Y=1}$ increases with increasing the surface adhesion parameter, $\sigma_w\lambda$, as shown in Fig. (3.12) and Fig. (3.14). And by looking at equations (A-10) and (3-21) one can notice that the rate of deposition, $\dot{m}^*$, increases as $(\partial\rho^*_p/\partial Y)_{Y=1}$ increases in case of adhesion only, consequently, $\dot{m}^*$ increases with increasing $\sigma_w\lambda$ as indicated in Fig. (3.17) and Fig. (3.18).

Fig. (3.16) shows the axial distribution of the rate of deposition of solid particles, $\dot{m}^*$, due to surface adhesion only where $\sigma_w\lambda = 0.1$ and $\beta = 4$. It is evident that the rate of deposition decreases downstream, which is to be expected since the particle concentration at the wall, ρ^*_{pw}, decreases because of surface adhesion and particle absorption at the wall.

Fig. (3.17) and Fig. (3.18) show the effect of surface adhesion on the rate of deposition due to adhesion only for $\beta = 40$ and $\beta = 10^7$ respectively. It is clear that $\dot{m}^*$ increases with increasing $\sigma_w\lambda$. Also the rate of deposition increases rapidly at inlet and slowly further downstream with increasing surface adhesion until the case

of complete absorption is reached where all particles are deposited at the inlet.

Fig. (3.19) illustrates the effect of the lift forces on the rate of deposition of particles in case of no electric charge, i.e. deposition is due to surface adhesion only.

It is clear that without lift forces ($\sigma_w' = 0$) the rate of deposition, $\dot{m}^*$, decreases along the X-axis, while with lift forces ($\sigma_w' = 10^{-6}$) the rate of deposition increases up to X = 5 then decreases slightly. The main result from such a figure is that lifting reduces the rate of deposition slightly as it will be seen later in Fig. (3.47) and Fig. (3.48) when electric charge is considered. Here, it should be emphasized that the lift forces acting on the particles at the wall arising from the fluid shear near the wall are not considered as field forces but rather surface forces because of the small particle size and negligible gravity effect. For that reason the lift forces have a very little effect on the solution for the rate of deposition.

3.4.2.3 Flow of Suspensions with Deposition Due to Electric Charge Only

Stukel and Soo [73] conducted an experiment for a turbulent flow of a suspension into a channel. They found that an appreciable amount of particle deposition occurred due to the electrostatic charge on the particles. That electrostatic charge is generated by the collisions between the solid particles themselves and also by

the collisions between the solid particles and the channel wall. For that reason, the case of deposition due to electric charge only will be considered in this section.

The computer results indicate that the electrostatic charge has a very little effect on the particles velocity profiles, U_p and V_p, at large diffusive Peclet number ($\beta = 10^7$). However, as β decreases (say $\beta = 40$) then the electrostatic charge affects the particle velocity profiles particularly V_p as shown in Fig. (3.23) where V_p becomes positive. In other words the particle velocity profiles, U_p and V_p, are mainly sensitive to the diffusive Peclet number, β, as mentioned in the previous article.

Fig.(3.20) shows the particle cloud density distribution, i.e. the particle concentration, ρ_p^*, due to electric charge only. It is clear that the electrostatic charge tends to increase the particle concentration at the wall, ρ_{pw}^*. Note that this is opposite to the effect of surface adhesion that causes a decrease in ρ_{pw}^* as discussed in the previous section. However, the particle concentration at the channel centerline remains constant and uniform because of the high diffusive Peclet number ($\beta = 10^7$).

Fig. (3.21) illustrates the influence of the electrostatic charge and surface adhesion, on the rate of deposition. It is clear that the rate of deposition, $\dot{m}^*$, due to electric charge only is greater than that due to surface adhesion only as one moves further downstream. From the upper curve (electric charge only) it can be observed that $\dot{m}^*$ increases rapidly up to X = 2, then increases again

but slightly and linearly, i.e. $\dot{m}^*$ has no maximum. Such a maximum exists only if β is small as shown in Fig. (3.45), which means that the Peclet number of diffusion has a serious effect on the shape of the rate of deposition curve as it will be seen in the next article. Also from the lower curve (adhesion only) it can be noticed that $\dot{m}^*$ decreases slightly and almost linearly along the X-axis.

3.4.2.4 Flow of Suspensions with Deposition Due to Both Electric Charge and Surface Adhesion Including Lift-Force Action at the Wall (General Case)

The general case where deposition is due to both electrostatic charge on the particles and adhesion at the channel wall including the lift-force action will be discussed in this section. A comparative type of study will be presented to investigate the effects of all different flow parameters and dimensionless numbers, on the rate of deposition.

Fig. (3.22) and Fig. (3.23) show the effect of Case I and Case II, i.e. the particle slip condition at the wall given by (3-27), on the distribution of axial and vertical velocities of particles U_p and V_p. Case I is the regular slip condition of the particles at the wall and Case II is the modified slip condition where the excess term $u_o(1 - x\bar{F}/u_o)$ @ $x < u_o/\bar{F}$ is introduced to account for the distance that the solid particles will travel before they start to deposit on the wall when $K_{np} = 0$. From these two figures, i.e. Fig. (3.22) and Fig. (3.23), it is clear that there is no difference between Case I and Case II except at the beginning where $X < N_m$. It

is worth noticing that V_p is positive as shown in Fig. (3.23), i.e. the particles are moving in the positive Y-direction (toward the wall) and this is due to the electrostatic charge on particles when the diffusive Peclet number, β, is small, however for large β, V_p remains negative as discussed in Section 3.4.2.3.

Fig. (3.24) shows the distribution of the particle concentration, ρ_p^*, in Cases I and II. It is clear that the distribution is identical in both cases and the concentration at the wall is greater than that at the centerline, i.e. $\rho_{pw}^* > \rho_{pc}^*$. Also it can be seen that both ρ_{pw}^* and ρ_{pc}^* decrease downstream as shown in Fig. (3.25) and Fig. (3.26). This result is analogous to the result obtained by Soo and Tung [71] for suspension flow in a pipe.

Fig. (3.27) indicates the effect of the sticking factor, σ (for electroviscous forces) on the particle concentration, ρ_p^*. It is shown that ρ_p^* decreases with increasing σ and that the decrease is greater at the wall than at the centerline. However, the maximum value for σ is 1.0, i.e. it is limited and from that one can observe that more decrease in ρ_{pw}^* can be achieved by increasing the surface adhesion parameter, $\sigma_w\lambda$, as mentioned before.

Fig. (3.28) shows the distribution of the particle concentration, ρ_p^*, at large diffusive Peclet number ($\beta = 10^7$). It can be noticed that the concentration is uniform at the centerline while it increases at the wall due to electric charge as also shown in Fig. (3.20) for the case of deposition due to electric charge only. However, surface adhesion tends to decrease the concentration at the wall as shown in

Fig. (3.13).

Fig. (3.29) and Fig. (3.30) indicate that the electric field intensity distribution, E^*, in Cases I and II is almost linear. Moreover, all curves of different axial positions coincide on one curve by increasing the diffusive Peclet number, β.

Now for the rate of deposition curves, two main sets of parameters and dimensionless quantities will be considered. For the first set: ($K_{np} = 0.0001$, $N_m = 2$, $N_R = 1000$, $R^* = 0.002$, $\alpha = 1.0$, $\beta = 40$, $\sigma = 0.5$, $\sigma_w^{\lambda} = 0.1$, $\sigma_w' = 10^{-6}$, $\rho_R = 300$, $\rho_{pb}^* = 0.3$), and for the second set: ($K_{np} = 0.0001$, $N_m = 2$, $N_R = 1000$, $R^* = 0.002$, $\alpha = 1.0$, $\beta = 10^7$, $\sigma = 0.5$, $\sigma_w^{\lambda} = 1.0$, $\sigma_w' = 10^{-10}$, $\rho_R = 300$, $\rho_{pb}^* = 0.3$). The difference between the two sets is the values underlined, particularly the Peclet number of diffusion, β. To investigate the effect of each of these parameters and numbers on the deposition rate, $\dot{m}^*$, one must vary the value of each one at a time keeping all others constant. The physical meaning and order of magnitude of these parameters and numbers are discussed in Appendix B.

Fig. (3.31) and Fig. (3.32) indicate the effect of the slip condition of the particles at the channel wall (Cases I and II) on the rate of deposition, $\dot{m}^*$, for the two sets of parameters and numbers mentioned above. It is clear from both figures that in Case II one has lesser rate of deposition than that in Case I near the channel inlet, i.e. the more the slip of particles at the wall, the lesser the rate of deposition. But further downstream ($X \geq N_m$) the two cases I and II have equal rate of deposition.

From Fig. (3.31) it is evident that a maximum rate of deposition occurs at approximately one channel width for Case II. This result is analogous to the result obtained by Chau and Wang [11] who conducted an experimental work for a flow of suspensions in a branched tube and observed that a maximum rate of deposition occurs at the branch point and a second maximum at approximately two diameters distance from the branch point along the inner walls, while a maximum rate of deposition occurs at one diameter distance along the outer walls.

However, for large diffusive Peclet number, the rate of deposition increases along the X-axis without showing a maximum as seen in Fig. (3.32).

Fig. (3.33) and Fig. (3.34) illustrate the effect of the particle size, R^*, on the rate of deposition, $\dot{m}^*$. It is obvious that by increasing the particle size from 2 to 20 μ diameters, the rate of deposition increases very little near the channel inlet.

Fig. (3.35) shows the effect of particle Knudsen number, K_{np}, on the rate of deposition, $\dot{m}^*$. It is shown that by decreasing the Knudsen number from 0.01 to 0.0001, the rate of deposition increases but very little and only near the channel inlet.

Fig. (3.36) and Fig. (3.37) indicate the effect of the momentum-transfer number, N_m, on the rate of deposition. The rate of deposition decreases with increasing momentum-transfer number, and the maximum rate of deposition occurs approximately at $X = N_m$ for low

diffusive Peclet number (β = 40) as shown in Fig. (3.36). But for high diffusive Peclet number ($\beta = 10^7$) the rate of deposition has no maximum as depicted in Fig. (3.37).

From Fig. (3.38) and Fig. (3.39) one can observe that Reynolds number, N_R, has a very little effect on the rate of deposition $\dot{m}^*$ and in general the larger the Reynolds number, the lesser the rate of deposition.

Fig. (3.40) shows the effect of the electrostatic charge on the rate of deposition at small diffusive Peclet number (β = 40). It is clear that whenever one increases the electrostatic charge parameter, α, the rate of deposition increases downstream. Now as the diffusive Peclet number increases ($\beta = 10^7$) then by increasing the electrostatic charge parameter, the rate of deposition increases also and continuously as indicated in Fig. (3.41). From both Fig. (3.40) and Fig. (3.41) one can see the serious effect of the electrostatic charge on the rate of deposition.

The effect of the diffusive Peclet number, β, on the rate of deposition of particles, $\dot{m}^*$, is shown in Fig. (3.42). It is clear that the larger the value of β, the smaller the rate of deposition, $\dot{m}^*$, near the channel inlet. However, the larger the value of β, the larger the modified rate of deposition, $\beta\dot{m}^*$, (defined in Appendix B) as shown in Fig. (3.43).

Fig.(3.44) illustrates the influence of the surface adhesion on the rate of deposition. It is shown that increasing the surface

adhesion parameter, $\sigma_w\lambda$, increases the rate of deposition and shifts the maximum rate of deposition to the inlet of the channel, and if we keep increasing $\sigma_w\lambda$ until the case for complete absorption ($\rho^*_{pw} = 0$) is reached, then all the particles will deposit at the inlet of the channel.

Fig. (3.45) indicates the effect of each of the electrostatic charge and surface adhesion on the rate of deposition. It is evident that with electric charge, the rate of deposition gets larger than that with surface adhesion only. In other words the effect of the electrostatic charge is predominant.

The effect of the electroviscous-sticking factor, σ, on the rate of deposition is depicted in Fig. (3.46). Now by increasing the value of σ, the rate of deposition, $\dot{m}^*$, increases. One must keep in mind that $0 \leq \sigma \leq 1.0$, and that it is a probability factor of sticking.

Fig. (3.47) and Fig. (3.48) indicate the effect of the lift forces at the wall on the rate of deposition. It is clear that the lift forces tend to reduce the rate of deposition but very little as also indicated in Fig. (3.19).

The influence of the electrostatic charge on the modified rate of deposition, $\beta\dot{m}^*$, is shown in Fig. (3.49) and Fig. (3.50). And as it was mentioned before that increasing α, increases the rate of deposition, $\dot{m}^*$, it also increases the modified rate of deposition, $\beta\dot{m}^*$.

Fig. (3.51) shows the effect of the diffusive Peclet number, β, on the modified rate of deposition, $\beta\dot{m}^*$. It is clear that increasing β increases $\beta\dot{m}^*$ considerably until β reaches a value of approximately 1000 then any further increase in β will not cause an appreciable change in $\beta\dot{m}^*$, i.e. the modified rate of deposition is limited regardless to the value of the diffusive Peclet number.

Fig. (3.52) indicates the influence of the electrostatic charge on the rate of deposition of particles at high surface adhesion ($\sigma_w\lambda = 1000$).

It is clear that the greater the value of α, the greater the rate of deposition, $\dot{m}^*$. Comparing Fig. (3.50) with Fig. (3.52) one can see that surface adhesion tends to decrease the rate of deposition downstream.

From this study, it was found that a considerable amount of particle deposition can result due to the electrostatic charge on the solid particles, i.e. the electrostatic charge parameter, α, is one of the most important parameters in particle deposition. Also, it was found that the diffusive Peclet number, β, has an appreciable effect on the particle velocities, U_p & V_p, and concentration, ρ_p^*, and rate of deposition, $\dot{m}^*$. The rate of deposition curve shows a maximum only at low β and in the presence of electric charge ($\alpha > 0$).

Moreover, surface adhesion has a smaller effect on the rate of deposition than that due to electric charge and the rate of deposition curve for adhesion only is a decreasing type curve.

In addition lift-force action at the channel wall has a negligible effect on the rate of deposition.

In other words, the important parameters for the rate of deposition in a channel flow are as follows:

α the electrostatic charge parameter

β the diffusive Peclet number

4. LAMINAR FLOW OF SUSPENSIONS IN THE ENTRANCE REGION OF A DIFFUSER

The single-phase diffuser flow problem with turbulent flow has been studied experimentally by Carlson et al [8], Wolf and Johnston [82] and others. Two-dimensional diffuser performance with subsonic, two-phase, air-water flow has been discussed by Hench and Johnston [27]. They concluded that diffusers with air-water mixtures have the same general performance and characteristics as single-phase diffusers. Also they found that the pressure recovery of diffusers with two-phase flow deteriorates with increasing air flow, especially after the two-phase flow regime changes form bubbly to turbulent.

In addition the radial diffuser and converging channel and tube flows with laminar flow have been investigated analytically by Parmet and Saibel [52], Limberg [39, 40], Sutterby [74] and many others.

Schlichting [62] discussed the flow in convergent and divergent channels for some special cases. He stated that in a divergent channel the shape of the velocity profiles is markedly affected by the Reynolds number and by the angle of divergence.

Hamel [23] studied the two and three-dimensional flows whose streamlines are identical with those of a potential flow. He found that for larger angles of divergence back flow occurs earlier.

Blasius [5] investigated the two-dimensional and axi-symmetrical flow through channels with small angles of divergence. He showed that laminar flow can support only a very small pressure increase

without the incidence of separation. The condition for the avoidance of back flow at the wall in a divergent tube of radius R(x) was found to be $(dR/dx) < 12/N_R$ (condition for separation), where $N_R = \bar{u}d/\nu$ denotes the Reynolds number referred to the mean velocity of the flow through the tube and to its diameter.

In more modern times Abramowitz [1] extended these calculations (of divergent tubes) for divergent channels, and found that the point of separation moves downstream from the channel entrance as the Reynolds number is increased and as the angle of divergence is decreased.

However, the laminar diffuser flow of suspensions as a two-phase flow problem has not been investigated.

In this chapter, a numerical scheme is presented to study the laminar flow of suspensions in the entrance region of a diffuser, with emphasis on the rate of deposition of the solid particles on the diffuser wall.

The suspension diffuser flow is considered at conditions under which a finite layer of particles is deposited at the diffuser wall, due to the electrostatic charge and wall adhesion. The suspension flow is assumed to be incompressible, laminar, dilute with negligible gravity effect.

4.1 Governing Equations

Having the same assumptions as in Chapter 3, the governing equations will be exactly the same as for the channel flow described

in section 3.1, except that the equation for the rate of deposition, i.e. Eq. (3-13) will include h(x) instead of h and the equation is still valid for the diffuser flow as mentioned in Appendix A. Here the unknowns that one is looking for in this case for the diffuser flow are the same as for the channel flow.

4.2 Boundary Conditions

Two different cases for the boundary conditions of the diffuser flow will be considered. The first case is for a single diffuser assuming uniform boundary conditions at the inlet. The second case is for a diffuser connected to a constant area channel of length $x = 2h$ (one channel width). In that case, the results of the channel flow at exit ($x = 2h$) will be taken as the boundary conditions at the diffuser inlet.

The purpose of considering the second case is due to the fact that in an actual fluidic device, the splitter region can be considered as a diffuser connected to a constant area channel. This is done to simplify the problem, however in the actual fluidic device, the diffuser section is not symmetric and moreover, all boundary conditions are nonuniform.

In both cases for the boundary conditions, symmetrical flow through the diffuser will be assumed.

Referring to Fig. (4.1), the boundary conditions for a single diffuser with uniform inlet conditions will be:

@ x = 0 (at the diffuser inlet)

$(0 \leq y \leq h)$

$$\left.\begin{array}{ll} u = u_p = u_o & \text{uniform} \\ v = v_p = 0 & \\ \rho_p = \rho_{po} & \text{uniform} \\ p = p_o & \text{uniform} \\ E_y = 0 & \end{array}\right] \quad (3\text{-}22)$$

@ y = 0 (at the diffuser centerline)

$(x > 0)$

$$\left.\begin{array}{ll} \dfrac{\partial u}{\partial y} = \dfrac{\partial u_p}{\partial y} = 0 & \text{symmetry} \\ v = v_p = 0 & \\ \dfrac{\partial \rho_p}{\partial y} = 0 & \text{symmetry} \\ E_y = 0 & \end{array}\right] \quad (3\text{-}23)$$

@ y = h(x) (at the diffuser wall) $h(x) \equiv w(x)$

$(x > 0)$

$$\left.\begin{array}{ll} u = v = 0 & \text{no slip condition} \\ u_p = -L_p \left.\dfrac{\partial u_p}{\partial y}\right|_{y=h(x)} & \text{particle slip condition Case I} \\ \text{or} \quad \left[\begin{array}{ll} u_p = u_o(1-x\bar{F}/u_o) - L_p \left.\dfrac{\partial u_p}{\partial y}\right|_{y=h(x)} & x < (u_o/\bar{F}) \\ u_p = -L_p \left.\dfrac{\partial u_p}{\partial y}\right|_{y=h(x)} & x \geq (u_o/\bar{F}) \end{array}\right] & \text{Case II} \\ D_p \left.\dfrac{\partial \rho_p}{\partial y}\right|_{y=h(x)} = (1-\sigma)\rho_{pw} \dfrac{qE_w}{m_p \bar{F}} - \sigma_w \rho_{pw} \dfrac{f_w}{\bar{F}} + \sigma'_w \rho_{pb} \dfrac{f_L}{\bar{F}} . & \end{array}\right] \quad (3\text{-}24)$$

Similar to Chapter 3, section 3.2, the dimensionless form of the boundary conditions is as follows:

$\underline{@\ X = 0}$ (at the diffuser inlet)

$(0 \leq Y \leq 1)$

$$\left.\begin{aligned} U = U_p &= 1 \qquad \text{uniform} \\ V = V_p &= 0 \\ \rho^*_p &= 1 \qquad \text{uniform} \\ P &= 0 \\ E^* &= 0 \end{aligned}\right] \quad (3\text{-}25)$$

$\underline{@\ Y = 0}$ (at the diffuser centerline)

$(X > 0)$

$$\left.\begin{aligned} \frac{\partial U}{\partial Y} = \frac{\partial U_p}{\partial Y} &= 0 \qquad \text{symmetry} \\ V = V_p &= 0 \\ \frac{\partial \rho^*_p}{\partial Y} &= 0 \qquad \text{symmetry} \\ E^* &= 0 \end{aligned}\right] \quad (3\text{-}26)$$

$\underline{@\ Y = W}$ (at the diffuser wall) $\quad W = w(x)/h$ $\quad (W \geq 1)$

$(X > 0)$

$$\left.\begin{aligned} &U = V = 0 \qquad \text{no slip condition} \\ &U_p = -K_{np} \left.\frac{\partial U_p}{\partial Y}\right|_{Y=W} \qquad \text{particle slip condition} \qquad \text{Case I} \\ \text{or} \quad &\left[\begin{aligned} U_p &= (1-X/N_m) - K_{np} \left.\frac{\partial U_p}{\partial Y}\right|_{Y=W} \qquad (X < N_m) \\ U_p &= -K_{np} \left.\frac{\partial U_p}{\partial Y}\right|_{Y=W} \qquad (X \geq N_m) \end{aligned}\right] \qquad \text{Case II} \\ &\left.\frac{\partial \rho^*_p}{\partial Y}\right|_{Y=W} = (1-\sigma) E^*_w \rho^*_{pw} - \sigma_w \lambda \rho^*_{pw} + \sigma'_w \gamma \rho^*_{pb} \ . \end{aligned}\right] \quad (3\text{-}27)$$

The boundary conditions for a diffuser connected to a constant area channel of length x = 2h, will be the same as for diffuser alone except the inlet conditions i.e. @ X = 0 where the results of the channel flow at x = 2h are taken to be the inlet boundary conditions of the diffuser flow, and this is the case of nonumiform inlet conditions.

4.3 Method of Solution

Equations (3-15) through (3-21) in section 4.1, with the boundary conditions in section 4.2, can be solved together for the unknowns U, V, P, U_p, V_p, ρ_p^*, E^* and $\dot{m}^*$ by the finite difference technique as in the case of the channel flow.

Trying to keep the matrix size constant at all axial positions to avoid singularity problems, and since the width of the diffuser is a function of axial position, a trapezoid mesh is superimposed on the flow field internal to the diffuser, recognizing that the diffuser angle is small (4^o to 15^o).

The finite difference coordinates are chosen to correspond to the spatial coordinates shown in Fig. (4.1) so that i = 1 corresponds to X = 0, and j = 2 corresponds to Y = 0, a positive change in the X-coordinate of ΔX, which is taken as 0.1, increases i by 1. But the positive change in the Y-coordinate of ΔY varies from one axial position to another by a value equal to $(\tan\theta)/n^2$ where θ is half the diffuser angle and n is the number of equal intervals in the Y-coordinate (it was considered n = 10). For example, if $\theta = 2^o$, then $(\Delta Y_{i+1} - \Delta Y_i) = 0.00034921$. Each change of ΔY in the Y-coordinate

increases j by 1, when Y = 1, at the diffuser wall, j = n + 2. Eleven mesh points in the Y-direction and up to 141 mesh points in the X-direction were used.

The finite difference grid is illustrated in Fig. (4.2).

The quantities U, V, P, U_p, V_p, ρ_p^* and E^* at each point in the column i = 1 are known as boundary conditions (3-25) or results of channel flow at X = 2 for the case when the diffuser is connected to a constant area channel.

By substituting the values of U_1, U_{p_1}, V_{p_1} and $\rho_{p_1}^*$ taken at the wall into equation (C-25) after replacing (i + 1) with i, then the rate of deposition (DPR $\equiv \dot{m}^*$) at i = 1 can be calculated.

From the quantities U_1, V_1, P_1, U_{p_1}, V_{p_1}, $\rho_{p_1}^*$, and E_1^*, by use of the finite difference equations which take the form of the matrix equation:

$$A_i \, X_{i+1} = B_i$$

Where A_i is the matrix of coefficients at axial position i, B_i is the column vector at the same axial position, and X_{i+1} is the variable column vector at axial position (i+1). A_i and B_i are in terms of U_i, V_i, P_i, U_{p_i}, V_{p_i}, $\rho_{p_i}^*$, E_i^* and S_i where $S_i = \Delta Y_i = W_i/n$ and $W_{i+1} = w_i + \tan\theta/n$, ($w_1 = 1$, $n = 10$). But X_{i+1} is in terms of U_{i+1}, V_{i+1}, P_{i+1}, $U_{p_{i+1}}$, $V_{p_{i+1}}$, $\rho_{p_{i+1}}^*$ and E_{i+1}^*. Therefore, at i = 1, A_1 and B_1 are known, hence one can determine X_2, i.e. U_2, V_2, P_2, U_{p_2}, V_{p_2}, $\rho_{p_2}^*$ and E_2^*. Substituting the values of U_2, U_{p_2}, V_{p_2} and $\rho_{p_2}^*$ taken at the wall (j = 12) into equation (C-25) then the deposition

rate DPR_2 can be evaluated.

In the same manner the solution is carried on downstream, finding U, V, P, U_p, V_p, ρ_p^* and E^* for the (i+1)th column when these quantities are known in the i th column, and upon substituting the values of $U_{i+1}, U_{p_{i+1}}, V_{p_{i+1}}$ and $\rho^*_{p_{i+1}}$ taken at the wall, into equation (C-25) then one can determine the deposition rate $DPR_{(i+1)}$. The numerical procedures are shown in Appendix C.

The computer program used for solving the channel flow problem is also used for solving the diffuser flow problem after making the necessary changes concerning the diffuser angle and its related variables.

4.4 Results and Discussion

In this section, the complete flow characteristics of the laminar flow of suspensions in the entrance region of a diffuser will be discussed. The fluid phase will be examined briefly, however the particulate phase will be studied extensively due to the fact that the solution of the problem is a parametric type and the goal is to find the most important parameters for the rate of deposition. Moreover, the effect of the diffuser angle as one of the most important parameters on the rate of deposition will be examined, consequently the question concerning the effect of the pressure gradient on the rate of deposition in a diffuser flow can be answered.

4.4.1 Fluid Phase

Fig. (4.4) shows the axial velocity distribution of the fluid

phase, U. It is clear that the centerline velocity, U_c, decreases downstream, and the numerical value of the velocity gradient at the wall $(\partial U/\partial Y)_w$ decreases along the X-axis. Moreover, there is no back flow, i.e. no separation within 14h distance, since the chosen angle of the diffuser is small ($2\theta = 4^o$).

Fig. (4.5) shows the vertical velocity distribution of the fluid phase, V. Here, the values of V are negative, which means that the direction of motion of the fluid elements in the normal direction is away from the wall. Also it can be seen that the absolute value of V increases then decreases along the X-axis.

Fig. (4.6) illustrates the effect of the diffuser angle (2θ) on the fluid static pressure distribution, P. It is evident that the pressure increases as the diffuser angle is increased until separation occurs. Also at larger angles separation takes place as investigated by Abramowitz [1].

4.4.2 Particle Phase

In this section, three cases will be considered:

(1) Deposition due to surface adhesion only

(2) Flow of suspensions with deposition due to both electric charge and surface adhesion including lift-force action at the wall with uniform inlet conditions

(3) Deposition due to both electric charge and surface adhesion including lift-force action at the wall with nonumiform inlet conditions (diffuser connected to a channel).

Similar to section 3.4, the discussion and related figures in the particulate phase are concentrated on Case II for the particle slip condition at the wall (boundary condition 3-27), unless otherwise stated.

In Cases (1) and (3) only the rate of deposition curves will be discussed. However, in Case (2), the velocity profiles U_p and V_p, particle concentration ρ_p^*, electric field intensity E^* and the rate of deposition, $\dot{m}^*$, will be examined. A comparative type of study for $\dot{m}^*$ with different flow parameters and numbers as well as the diffuser angle is made.

4.4.2.1 Deposition Due to Surface Adhesion Only

Fig. (4.7) indicates the effect of the diffuser angle on the rate of deposition due to surface adhesion only. It is clear that the rate of deposition decreases downstream. Also it can be seen that the diffuser angle (20) has a great effect on the deposition rate, $\dot{m}^*$. As one increases the diffuser angle, the rate of deposition decreases until the point of separation is reached where the rate of deposition decreases rapidly.

The results at $\theta = 0$, are the same as for the constant area channel flow with $\sigma_w \lambda = 1.0$ shown in Fig. (3.18).

4.4.2.2 Flow of Suspensions with Deposition Due to Both Electric Charge and Surface Adhesion Including Lift-Force Action at the Wall (with Uniform Inlet Conditions)

A comparison of axial velocities of fluid and particle phases

U and U_p respectively is shown in Fig. (4.8). It is evident that the centerline velocities U_c and U_{pc} are close to each other, however at the wall and near the inlet there is a significant difference in the velocities U_w and U_{pw} due to the slip condition of the particles (Case II in boundary condition 3-27).

Fig. (4.9) shows the vertical velocity distribution of the particles, V_p. Here, the values of V_p are positive, which means that the particles are moving toward the wall, while the fluid elements are moving away from the wall.

This difference is due to the electrostatic charge on the particles when the diffusive Peclet number, β, is small. However, for large β, the sign of V_p remains negative as shown in Fig. (4.20).

Fig. (4.10) shows the distribution of the particle concentration, ρ_p^*. It is shown that the concentration at the wall is greater than that at the centerline, i.e. $\rho_{pw}^* > \rho_{pc}^*$ at any axial position. Also the centerline concentration decreases downstream, similar to the case of channel flow.

From Fig. (4.11) it can be observed that the distribution of the electric field intensity, E^*, is almost linear.

Fig. (4.12) indicates the effect of the particle slip condition at the wall, i.e. Case I and Case II, on the rate of deposition, $\dot{m}^*$. It is clear that in Case II one has a lesser rate of deposition than that in Case I near the diffuser inlet, i.e. the greater the slip of particles at the wall, the lesser the rate of deposition, but further

downstream the two cases are identical.

The computer results indicate that the particle size, R^*, has a negligible effect on the rate of deposition, especially for particles of 2 to 20μ diameters. Also the particle Knudsen number, K_{np}, has a negligible influence on the rate of deposition, particularly for a range of K_{np} = 0.0001 to 0.01.

From Fig. (4.13) it can be observed that by increasing the momentum-transfer number, N_m, the rate of deposition, $\dot{m}^*$, decreases near the diffuser inlet and N_m has no effect at all downstream.

The effect of Reynolds number, N_R, on the rate of deposition is shown in Fig. (4.14). It can be noticed that N_R has a very little effect on $\dot{m}^*$.

Fig. (4.15) shows the effect of the electrostatic charge parameter, α, on the rate of deposition. It is clear that whenever α is increased, the rate of deposition $\dot{m}^*$ increases rapidly at the diffuser inlet and then decreases downstream.

The effect of the diffusive Peclet number, β, on the rate of deposition, $\dot{m}^*$, is depicted in Fig. (4.16). It can be noticed that $\dot{m}^*$ decreases with increasing β.

Fig. (4.17) shows the effect of the surface adhesion parameter, $\sigma_w\lambda$, on the rate of deposition. It is clear that when $\sigma_w\lambda$ is increased, the rate of deposition, $\dot{m}^*$, increases but to a certain limit, where further increase in $\sigma_w\lambda$ will cause a rapid decrease in the particle concentration at the wall until the case of complete absorp-

tion of particles at the wall is reached, then all particles will deposit at diffuser inlet.

The effect of the diffuser angle on the rate of deposition at low diffusive Peclet number is shown in Fig. (4.18). It is evident that the larger the diffuser angle, the greater the rate of deposition. However, at larger angles, separation takes place within 14h distance.

Fig. (4.19) shows a comparison of the axial velocities of fluid and particle phases U and U_p at large Peclet number of diffusion ($\beta = 10^7$). It is clear that the two velocities are close to each other except at the beginning (X = 1) due to the particle slip condition at the wall.

From Fig. (4.20) it can be noticed that the difference between the vertical velocities V and V_p increases at the beginning then decreases further downstream until it reaches zero when the flow becomes fully developed.

Fig. (4.21) indicates the distribution of the particle concentration, ρ_p^*, at high diffusive Peclet number. It is shown that ρ_p^* is uniform and constant at the centerline while it increases at the wall due to electric charge.

From Fig. (4.22) it can be seen that the distribution of the electric field intensity, E^*, is linear at all axial positions when ($\beta = 10^7$).

Fig. (4.23) illustrates the effect of the diffuser angle (2θ) on the rate of deposition, $\dot{m}^*$, with $\beta = 10^7$. It is shown that the rate of deposition always increases with increasing diffuser angle. Moreover, at larger diffuser angle, separation takes place and the rate of deposition increases rapidly. By comparing Fig. (4.23) with Fig. (4.18) one can see the serious effect of the diffusive Peclet number, β, on the shape of the deposition curve. But from both figures it can be concluded that the larger the diffuser angle, the greater the rate of deposition, and since the pressure gradient (dP/dX) increases by increasing the diffuser angle (2θ) as shown in Fig. (4.6), consequently the higher the pressure gradient, the greater the rate of deposition, $\dot{m}^*$.

It is worth noticing that the shape of the deposition curves shown in Fig. (4.23) is agreeable with the actual results of contamination buildup with time shown in Figures 27, 32 and 38 given by Comparin et al [13]. From these figures (27, 32 and 38) one can observe that greater deposition occurs at the top plates (more divergence) while lesser deposition occurs at the bottom plates (less divergence).

4.4.2.3 Deposition Due to Both Electric Charge and Surface Adhesion Including Lift-Force Action at the Wall with Nonuniform Inlet Conditions

This is the case when the diffuser is connected to a constant area channel. A channel of length equivalent to its width, i.e. $x = 2h$, is connected to a diffuser of angle (2θ), where the selected values for 2θ are 4^o and 15^o.

This is done as an approximate model for the splitter region in an actual fluidic device. Hence, the results of the channel flow at X = 2 will be considered as the inlet conditions for the diffuser flow.

Fig. (4.24) shows the effect of the diffuser angle and inlet conditions on the rate of deposition. Here, it can be noticed that the rate of deposition increases gradually at smaller angles of divergence, however at larger angles the rate of deposition increases rapidly and separation takes place earlier. Also one notices that nonuniform inlet conditions affect the rate of deposition within a distance of X = 2, and the effect is negligible downstream.

Fig. (4.25) and Fig. (4.26) show the axial distribution of the rate of deposition, $\dot{m}^*$, in case of a channel connected to a diffuser when the angle of divergence $2\theta = 4^o$ and 15^o, respectively. From these figures one can see that at $2\theta = 15^o$ separation occurs at X = 1.7 from the diffuser inlet, while at $2\theta = 4^o$ no separation at all.

From this analysis it was found that the conclusions obtained in section 3.4 for the channel flow are the same for the diffuser flow. In addition to that, it was found that the angle of divergence has a serious effect on the rate of deposition in a diffuser flow. By increasing the angle of divergence, the pressure gradient increases and also the rate of deposition increases. But at larger diffuser angles, separation takes place and the rate of deposition increases rapidly in the presence of electric charge. However, in

the absence of electric charge, the rate of deposition decreases rapidly with increasing angle of divergence.

In other words, the most important parameters for the rate of deposition in a diffuser flow are as follows:

α the electrostatic charge parameter

β the diffusive Peclet number

2θ the diffuser angle

5. CONCLUSIONS

From this investigation, the conclusions reached for both channel and diffuser flows can be given as follows:

(1) An appreciable amount of particle deposition can result because of the electrostatic charge on the solid particles, i.e. the electrostatic charge parameter, α, is one of the most important parameters.

(2) The diffusive Peclet number, β, has a considerable effect of the particle velocity profiles U_p and V_p, concentration ρ_p^* and rate of deposition of particles $\dot{m}^*$. The rate of deposition curve shows a maximum only at low β.

(3) Surface adhesion has a smaller effect on the rate of deposition than that due to electric charge.

(4) Lift-force action at the wall has a negligible effect on the rate of deposition.

In addition to that, it was found that the angle of divergence has a great effect on the rate of deposition in a diffuser flow. By increasing the diffuser angle, the pressure gradient increases and also the rate of deposition increases. However, at larger diffuser angles, separation takes place earlier and the rate of deposition increases rapidly in the presence of electric charge. However, in the absence of electric charge the rate of deposition decreases rapidly with increasing diffuser angle.

In other words, the most effective parameters and numbers on

the rate of deposition are:

Channel and diffuser flows

(i) α the electrostatic charge parameter

(ii) β the diffusive Peclet number

Diffuser flow only

(iii) 2θ the diffuser angle

6. RECOMMENDATIONS FOR FUTURE STUDY

The information regarding some of the flow parameters such as electrostatic charge parameter, α, and surface adhesion parameter, $\sigma_w\lambda$, is insufficient for a flow in a fluidic device.

Experiments may be conducted to measure the electrostatic charges on the particles in order to calculate the electrostatic charge parameter, α.

An experimental study might also be undertaken using different materials for both particles and channel or diffuser wall to measure the surface adhesive force, hence the surface adhesion parameter, $\sigma_w\lambda$, can be obtained.

Also the effect of both electrostatic charge and surface adhesion on rate of deposition of particles can be shown experimentally.

In this investigation, the case of solid particles suspended in air, i.e. two-phase flow was considered. Attempts should be made to extend this study in the presence of oil particles and solid particles in the air, i.e. three-phase flow, which is the actual case expecially when one deals with air from a compressor. Such a study will show the influence of the oil particles on the rate of deposition of the solid particles.

Moreover, it would be of interest to further the study of deposition of suspensions in laminar flow in both channel and diffuser under the action of gravitational and electric fields and a shear

flow field. This is the case when one deals with particles of large size and dense suspension.

REFERENCES

1. Abramowitz, M.,"On Backflow of a Viscous Fluid in a Diverging Channel", Journal of Math. Phys., Vol. 28, 1949, pp. 1-21.

2. Alexander, L. G. and Coldren, C. L., "Droplet Transfer from Suspending Air to Duct Walls", Ind. Eng. Chem., Vol. 43, 1951, p. 1325.

3. Anderson, T. B. and Jackson, R., "A Fluid Mechanical Description of Fluidized Beds", Ind. Eng. Chem. Fundam., Vol. 6, 1967, p. 527.

4. Berezin, J. S. and Zhidkov, N. P., Computing Mehtods, Pergamon Press, London, Vol. II, 1965, pp. 534-544.

5. Blasius, H., "Laminare Strömung in Kanälen wechselnder Breite", Z. Math. und Physik, Vol. 58, 1910, p. 225.

6. Boll, R. H., "Particle Collection and Pressure Drop in Venturi Scrubbers", Ind. Eng. Chem. Fundam., Vol. 12, No. 1, 1973, pp. 40-49.

7. Bourgeois, P. and Grenier, P., "The Ratio of Terminal Velocity to Minimum Fluidizing Velocity for Spherical Particles", Can. J. Chem. Eng., Vol. 46, 1968, pp. 325-328.

8. Carlson, J. J., Johnston, J. P. and Sagi, C. J., "Effects of Wall Shape on Flow Regimes and Performance in Straight, Two-Dimensional Diffusers", Journal of Basic Engineering, Transactions of the ASME, 1967, pp. 151-160.

9. Cheng, L. and Soo, S. L., "Charging of Dust Particles by Impact", J. Appl. Phys., Vol. 41, No. 2, 1970, pp. 585-591.

10. Cheng, L., Soo, S. L. and Tung, S. K., "Electrical Measurement of Flow Rate of Pulverized Coal Suspension", Journal of Engineering for Power, Transactions of the ASME, 1970, pp. 135-149.

11. Chua, J. H. and Wang, C. S., "Deposition of Submicron Particles from Steady Flows in a Branched Tube", J. Res. Assoc. Powder Tech., Vol. 9, 1972, pp. 37-45.

12. Cohen, A. M., Numerical Analysis, Halsted Press, 1972, Chapter 12.

13. Comparin, R. A., Moses, H. L. and Rowell, E. E.,III, "Contamination Effects in a Laminar Proportional Amplifier", Fluidic, State-of-the-Art Symposium, Sept. 30 - Oct. 3, Vol. 1, 1974, pp. 247-259, U.S. Army (H.D.L.) Material Command.

14. Corn, M., "The Adhesion of Solid Particles to Solid Surfaces", J. Air Pollution Control Assoc., Vol. 11(1), 1961, pp. 523-528 and Vol. 11(12), 1961, pp. 566-575, 584.

15. Crooke, P. S. and Walsh, R. A., "The Flow of a Dusty Gas through an Infinitely Long Pipe", Powder Technology, Vol. 9, 1974, pp. 111-119.

16. Davies, C. N., Aerosol Science, Academic Press, London and New York, 1966, Chapter XII.

17. Dawson, S. V., "Theory of Collection of Airborn Particles by Fibrous Filters", Ph.D. Dissertation, Howard School of Public Health, 1969.

18. Flint, L. R. and Howarth, W. J., "The Collision Efficiency of Small Particles with Spherical Air Bubbles", Chem. Eng. Sci., Vol. 26, 1971, p. 1155.

19. Forstrom, R. J., Voss, G. O. and Blackshear, P. L., Jr., "Fluid Dynamics of Particle (Platelet) Deposition for Filtering Walls; Relationship to Atherosclerosis", Journal of Fluids Engineering, Transactions of the ASME, 1973.

20. Friedlander, S. K. and Johnstone, H. F., "Deposition of Suspended Particles from Turbulent Gas Streams", Ind. and Eng. Chem., Vol. 49, No. 7, 1957, pp. 1151-1156.

21. Fröberg, C-E., Introduction to Numerical Analysis, Addison-Wesley Publishing Company, second edition, 1968, Chapters 4 and 15.

22. Fuchs, N., Mechanics of Aerosols, Pergamon Press, 1964.

23. Hamel, G., "Spiralförmige Bewegung Zäher Flüssigkeiten", Jahresber. d. Dt. Mathematicker-Vereinigung, Vol. 25, 1916, pp. 34-60.

24. Healy, J. V., "Perturbed Two-Phase Cylindrical Type Flows", The Physics of Fluids, Vol. 13, No. 3, 1969, pp. 551-557.

25. Healy, J. V., "Two-Phase Convex-Type Corner Flows", J. Fluid Mech., Vol. 41, Part 4, 1970, pp. 759-768.

26. Healy, J. V., "Two-Phase Concave-Type Corner Flows", J. Fluid Mech., Vol. 46, Part 1, 1971, pp. 33-42.

27. Hench, J. E. and Johnston, J. P., "Two-Dimensional Diffuser Performance with Subsonic, Two-Phase Air-Water Flow", Journal of Basic Engineering, Transactions of the ASME, 1972, pp. 105-121.

28. Hinze, J. O.,"Momentum and Mechanical-Energy Balance Equations for a Flowing Homogeneous Suspension with Slip between the Two Phases", Appl. Sci. Res., A11, 1962, p. 33.

29. Hornbeck, R. W., "The Entry Problem in Pipes with Porous Walls", Master Thesis - Carnegie Institute of Technology, Pittsburgh 13, Pennsylvania, 1961.

30. Hughmark, G. A., "Solid Particle Deposition from a Turbulent Gas Stream", A.I.Ch.E. Journal, Vol. 18, No. 2, 1972, p. 451.

31. Jackson, R., "The Present Status of Fluid Mechanical Theories of Fluidization", Chemical Eng. Progress Symposium Series, Vol. 66, No. 105, 1970, pp. 3-13.

32. John, J. E., Gas Dynamics, Allyn and Bacon, Inc., Fourth printing, 1973, Chapter 16.

33. Kalinske, A. A. and Van Driest, E. R., Proceedings of Fifth International Congress on Applied Mechanics, Cambridge, Mass., 1938, p. 416.

34. Kennedy, J. F., "The Formation of Sediment Ripples, Dunes and Antidunes", Ann. Rev. Fluid Mech., Vol. 1, 1969, pp. 147-168.

35. Kunkel, W. B., "The Static Electrification of Dust Particles on Dispersion into a Cloud", J. Appl. Phys., Vol. 21, 1950, pp. 820-832.

36. Langmuir, I. and Blodgett, K., "A Mathematical Investigation of Water Droplet Trajectories", Army Air Forces Technical Report No. 5418, 1946.

37. Leva, M., Fluidization, McGraw-Hill Book Co., New York, 1959, p. 47.

38. Levich, V. G., Physicochemical Hydrodynamics, Prentice-Hall, Englewood Cliffs, N. J., 1962, p. 115.

39. Limberg, H., "Computation of Laminar Inlet Flow in Convergent Channels for Some Models", (in German) Rev. Mechan. Appl., Vol. 8, 1963, pp. 59-75.

40. Limberg, H., "Lmainar Inlet Flow in a Convergent Axial Symmetrical Nozzle", (in German) Rev. Mechan. Appl., Vol. 8, 1963, pp. 997-1015.

41. Longwell, J. P. and Weiss, M. A., "Mixing and Distribution of Liquids in High Velocity Air Streams", Ind. Eng. Chem., Vol. 45, 1953, p. 667.

42. Marble, F. E., "Dynamics of a Gas Containing Small Solid Particles", Proc. 5th AGARD Colloq., Combust. Propul., Pergamon Press, 1963, p. 175.

43. Marble, F. E., "Dynamics of Dusty Gases", Annual Review of Fluid Mechanics, Vol. 3 (M. Van Dyke, W. Vincenti and J. Wehausen, eds), 1970, p. 397.

44. Michael, D. H., "The Steady Motion of a Sphere in a Dusty Gas", J. Fluid Mech., Vol. 31, Part 1, 1968, pp. 175-192.

45. Michael, D. H. and Norey, P. W., "Particle Collision Efficiencies for a Sphere", J. Fluid Mech., Vol. 37, Part 3, 1969, pp. 565-575.

46. Morr, G. F. and Soo, S. L., "Flow of a Dust Suspension over an Ellipsoid of Revolution", (Water and Air Pollution Symposium on Flow Status in Air & Water Pollution), presented at the joint meeting of the Fluids Eng. Division and the Appl. Mech. Division, Georgia Institute of Technology, June 1973.

47. Murray, J. D., "On the Mathematics of Fluidization", J. Fluid Mech., Vol. 21, 1965, p. 465, Vol. 22, 1965, p. 57.

48. Narsimhan, G., "On a generalized Expression for Prediction of Minimum Fluidization Velocity", A.I.Ch.E. Journal, Vol. 11, 1965, p. 550.

49. O'Neill, M. E., "On the Collection Efficiency of a Spherical Sampler with Suction", Chem. Eng. Sci., Vol. 27, 1972, pp. 519-528.

50. Pai, S. I. and Hsieh, T., "Interaction Terms in Gas-Solid Two-Phase Flows", Z. Flugwiss. 21, 1973, Heft 12, pp. 442-445.

51. Paretsky, L., Theodore, L., Pfeffer, R. and Squires, A. M., "Panel Bed Filters for Simultaneous Removal of Fly Ash and Sulfur Dioxide", J. Air Pol. Cont. Assoc., Vol. 21, 1971, p. 204.

52. Parmet, I. L. and Saibel, E., "Flow and Boundary Layer Development in a Radial Diffuser", Revue Roumaine des Sciences Technique - Ser. D Mecanique Appl., Vol. 11, 1966, pp. 275-284.

53. Peddieson, J., Jr., "Flow Induced in a Solid-Fluid Suspension by Impulsive Motion of an Infinite Flat Plate", - presented at Ninth Annual Meeting of Society of Engineering Science, 1971.

54. Peddieson, J., Jr., "The Hydrodynamics of Dust Collection", - Proceedings of the 18th Annual Technical Meeting of the INstitute of Environmental Sciences, 1972.

55. Peddieson, J., Jr., "Dust Collection at Moderate Void Fractions",- Proceedings of the Annual Technical Meeting of the Institute of Environmental Sciences, 1973.

56. Pigford, R. L. and Baron, T., "Hydrodynamic Stability of a Fluidized Bed", Ind. Eng. Chem. Fundam., Vol. 4, 1965, p. 81.

57. Quarmby, A., "A Finite Difference Analysis of Developing Slip Flow", Appl. Sci. Res., Vol. 19, 1968, pp. 18-33.

58. Richardson, E. G., Aerodynamic Capture of Particles, Pergamon Press, 1960.

59. Robinson, A., "On the Motion of Small Particles in a Potential Field of Flow", Comm. Pure Appl. Math., Vol. 9, 1956, p. 69.

60. Saffman, P. G., "On the Stability of Laminar Flow of a Dusty Gas", J. Fluid Mech., Vol. 13, 1962, pp. 120-128.

61. Saffman, P. G., "The Lift on a Small Sphere in a Slow Shear Flow", J. Fluid Mech., Vol. 22, 1965, pp. 385-400.

62. Schlichting, H., Boundary Layer Theory, McGraw-Hill Book Co., 6th Edition, 1968, Chapters 4 and 7.

63. Singh, B. and Byers, R., "Particle Deposition Due to Thermal Force in the Transition and Near-Continuum Regimes", Ind. Eng. Chem. Fundam., Vol. 11, No. 1, 1972, pp. 127-133.

64. Smith, G. D., Numerical Solution of Partial Differential Equations, Oxford University Press, New York and London, 1965.

65. Soo, S. L., Fluid Dynamics of Multiphase Systems, Blaisdell Publishing Co., 1967, Chapters 6 and 8.

66. Soo, S. L., "Pipe Flow of Suspensions", Appl. Sci. Res., Vol. 21, 1969, pp. 68-84.

67. Soo, S. L., "Effect of Diffusion on Collection and Impaction of a Sphere", Powder Technology, Vol. 7, 1973, pp. 267-269.

68. Soo, S. L. and Rodgers, L. W., "Further Studies on the Electro-Aerodynamic Precipitator", Powder Technology, Vol. 5, 1971, pp. 43-50.

69. Soo, S. L., Stukel, J. J. and Hughes, J. M., "Measurement of Mass Flow Density of Aerosols in Transfer", Environmental Science and Technology Industrial and Engineering Chemistry, Vol. 3, No. 4, 1969, pp. 386-393.

70. Soo, S. L. and Tung, S. K., "Pipe Flow of Suspensions in Turbulent Fluid, Electrostatic and Gravity Effects", Appl. Sci. Res., Vol. 24, 1971, pp. 83-97.

71. Soo, S. L. and Tung, S. K., "Deposition and Entrainment in Pipe Flow of a Suspension", Powder Technology, Vol. 6, 1972, pp. 283-294.

72. Spielman, L. A. and Goren, S. L., "Capture of Small Particles by London Forces from Low Speed Liquid Flows", Environ. Sci. and Technol., Vol. 4, No. 2, 1970, p. 135.

73. Stukel, J. J. and Soo, S. L., "Turbulent Flow of a Suspension into a Channel", Powder Technology, Vol. 2, 1968/1969, pp. 278-289.

74. Sutterby, J. L., "Finite Difference Analysis of Viscous Laminar Converging Flow in Conical Tubes", Appl. Sci. Res., Section A, Vol. 15, 1965, pp. 241-252.

75. Taylor, G. I., "Notes on Possible Equipment and Technique for Experiments on Icing of Aircrafts", A.R.C. Technical Report R & M No. 2024, 1940.

76. Truesdell, C. and Toupin, R., "The Classical Field Theories", Handbuch der Physic III/1 (S. Flugge, ed.), 1960, p. 469.

77. Truesdell, C. and Noll, W., "The Nonlinear Field Theories of Mechanics", Handbuch der Physic III/3 (S. Flugge, ed.), 1965, p. 537.

78. Thomas, D. G., "Transport Characteristics of Suspensions:II, Minimum Transport Velocity for Flocculated Suspensions in Horizontal Pipes", A.I.Ch.E. Journal, Vol. 7, No. 3, 1961, pp. 423-430.

79. Van Deemter, J. J. and Van Der Laan, E. T., "Momentum and Energy Balances for Dispersed Two-Phase Flow", Appl. Sci. Res., A10, 1961, p. 102.

80. Wang, C. S., Altshuler, B. and Palmes, E. D., "The Distribution and Deposition of Particles Suspended between Parallel Plane Surfaces", J. Colloid and Interface Science, Vol. 26, 1968, pp. 41-44.

81. Wen, C. Y. and Yu, Y. H., "Mechanics of Fluidizations", Chem. Eng. Progr. Symposium Series, Vol. 62, No. 62, 1966, p. 100.

82. Wolf, S. and Johnston, J. P., "Effects of Nonuniform Inlet Velocity Profiles on Flow Regimes and Performance in Two-Dimensional Diffusers", Journal of Basic Engineering, Transactions of the ASME, 1969, pp. 462-474.

83. Yang, Y. C. and Peddieson, J., Jr., "Some Parallel Flows of Solid-Fluid Suspension", - presented at Ninth Annual Meeting of Society of Engineering Science, 1971.

Appendix A

DERIVATION OF THE BOUNDARY CONDITION OF THE PARTICLE CLOUD DENSITY GRADIENT AT THE WALL

From the continuity equations of the fluid and particulate phases discussed in section 3.1 one has:

$$\frac{\partial u}{\partial x} + \frac{\partial v}{\partial y} = 0 \qquad (3\text{-}1)$$

and

$$\frac{\partial (\rho_p u_p)}{\partial x} + \frac{\partial (\rho_p v_p)}{\partial y} = 0 \qquad (3\text{-}3)$$

Combining these two equations, one can get the following:

$$u \frac{\partial \rho_p}{\partial x} + v \frac{\partial \rho_p}{\partial y} = - \frac{\partial}{\partial x} [\rho_p (u_p - u)] - \frac{\partial}{\partial y} [\rho_p (v_p - v)] \qquad (3\text{-}9)$$

Let $J_{px} = \rho_p (u_p - u)$

$$J_{py} = \rho_p (v_p - v)$$

J_{px} and J_{py} are the mass fluxes in the x- and y-direction respectively under the effect of both external field force and self-diffusion of the particles.

Therefore equation (3-9) can be written in the form:

$$u \frac{\partial \rho_p}{\partial x} + v \frac{\partial \rho_p}{\partial y} = - \frac{\partial J_{px}}{\partial x} - \frac{\partial J_{py}}{\partial y} \qquad (A\text{-}1)$$

From the momentum equation of the particulate phase in the x-direction one has:

$$u_p \frac{\partial u_p}{\partial x} + v_p \frac{\partial u_p}{\partial y} = \bar{F} (u - u_p) + \frac{D_p}{\rho_p} \frac{\partial}{\partial y} (\rho_p \frac{\partial u_p}{\partial y}) \qquad (3\text{-}4)$$

Multiplying both sides of this equation by $(\rho_p/\bar{F})$ it follows

$$\frac{1}{\bar{F}}\left(\rho_p u_p \frac{\partial u_p}{\partial x} + \rho_p v_p \frac{\partial u_p}{\partial y}\right) = -\rho_p (u_p - u) + \frac{D_p}{\bar{F}} \frac{\partial}{\partial y}\left(\rho_p \frac{\partial u_p}{\partial y}\right)$$

By differentiating partially with respect to x, then one obtains

$$\frac{1}{\bar{F}} \frac{\partial}{\partial x}\left(\rho_p u_p \frac{\partial u_p}{\partial x} + \rho_p v_p \frac{\partial u_p}{\partial y}\right) = -\frac{\partial}{\partial x}[\rho_p (u_p - u)] + \frac{D_p}{\bar{F}} \frac{\partial^2}{\partial x \partial y}\left(\rho_p \frac{\partial u_p}{\partial y}\right)$$

$$\therefore \quad \frac{1}{\bar{F}}\left[\frac{\partial(\rho_p u_p)}{\partial x}\left(\frac{\partial u_p}{\partial x}\right) + \rho_p u_p \frac{\partial^2 u_p}{\partial x^2} + \frac{\partial(\rho_p v_p)}{\partial x}\left(\frac{\partial u_p}{\partial y}\right) + \rho_p v_p \frac{\partial^2 u_p}{\partial x \partial y}\right]$$

$$= -\frac{\partial}{\partial x}[\rho_p (u_p - u)] + \frac{D_p}{\bar{F}}\left[\frac{\partial^2 \rho_p}{\partial x \partial y}\left(\frac{\partial u_p}{\partial y}\right) + \rho_p \frac{\partial^3 u_p}{\partial x \partial y^2}\right]$$

Neglecting all higher order terms and assuming that the quantities $\partial(\rho_p u_p)/\partial x$ and $\partial(\rho_p v_p)/\partial x$ are negligible at the channel or diffuser wall, then one gets

$$\frac{\partial}{\partial x}[\rho_p (u_p - u)] \simeq 0 \tag{A-2}$$

i.e. $$\frac{\partial J_{px}}{\partial x} \simeq 0$$

Substituting from equation (A-2) into equation (A-1), then one can write

$$u \frac{\partial \rho_p}{\partial x} + v \frac{\partial \rho_p}{\partial y} = -\frac{\partial J_{py}}{\partial y} \tag{A-3}$$

which is the same as equation (3-11) in section 3.1. Now using Fick's law one has

$$J_{py} = \left(\frac{q}{m_p}\right) \frac{\rho_p E_y}{\bar{F}} - D_p \frac{\partial \rho_p}{\partial y} \tag{F}$$

which indicates that the particle mass flux is due to the effect of

both external field force (electric field force) and self-diffusion of the particles. Substituting equation (F) into equation (A-3), it follows

$$u \frac{\partial \rho_p}{\partial x} + v \frac{\partial \rho_p}{\partial y} = - \frac{\partial}{\partial y} \left[\left(\frac{q}{m_p}\right) \frac{\rho_p E_y}{\bar{F}} \right] + \frac{\partial}{\partial y} \left(D_p \frac{\partial \rho_p}{\partial y}\right) \qquad \text{(A-4)}$$

Integrating equation (A-4) w.r.t. y and taking the limits of integration from y = 0 to y = h, one obtains

$$\int_o^h u \frac{\partial \rho_p}{\partial x} dy + \int_o^h v \frac{\partial \rho_p}{\partial y} dy = \int_o^h - \frac{\partial}{\partial y} \left[\left(\frac{q}{m_p}\right) \frac{\rho_p E_y}{\bar{F}} \right] dy + \int_o^h \frac{\partial}{\partial y} \left(D_p \frac{\partial \rho_p}{\partial y}\right) dy$$

$$= - \left[\left(\frac{q}{m_p}\right) \frac{\rho_p E_y}{\bar{F}} \right]_o^h + \left[D_p \frac{\partial \rho_p}{\partial y} \right]_o^h$$

$$= - \left(\frac{q}{m_p}\right) \frac{\rho_{pw} E_w}{\bar{F}} + \left(\frac{q}{m_p}\right) \frac{\rho_{po} E_o}{\bar{F}} + D_p \frac{\partial \rho_p}{\partial y}\bigg|_{y=h} - D_p \frac{\partial \rho_p}{\partial y}\bigg|_{y=0}$$

Applying the boundary condition (3-23) in section 3.2, one gets:

$$\int_o^h u \frac{\partial \rho_p}{\partial x} dy + \int_o^h v \frac{\partial \rho_p}{\partial y} dy = D_p \frac{\partial \rho_p}{\partial y}\bigg|_{y=h} - \left(\frac{q}{m_p}\right) \frac{\rho_{pw} E_w}{\bar{F}}$$

$$\therefore \quad D_p \frac{\partial \rho_p}{\partial y}\bigg|_{y=h} = \rho_{pw} \left(\frac{qE_w}{m_p \bar{F}}\right) + \int_o^h u \frac{\partial \rho_p}{\partial x} dy + \int_o^h v \frac{\partial \rho_p}{\partial y} dy$$

Carrying out integration by parts for the second integral term on the right-hand side of this equation, one can write

$$D_p \frac{\partial \rho_p}{\partial y}\bigg|_{y=h} = \rho_{pw} \left(\frac{qE_w}{m_p \bar{F}}\right) + \int_o^h u \frac{\partial \rho_p}{\partial x} dy + \left[\rho_p v\right]_o^h - \int_o^h \rho_p \frac{\partial v}{\partial y} dy$$

Once again, applying the boundary conditions (3-23) and (3-24) in section 3.2, it follows

$$D_p \frac{\partial \rho_p}{\partial y}\bigg|_{y=h} = \rho_{pw} \left(\frac{qE_w}{m_p \bar{F}}\right) + \int_o^h u \frac{\partial \rho_p}{\partial x} dy - \int_o^h \rho_p \frac{\partial v}{\partial y} dy \qquad (A-5)$$

But from the continuity equation of the fluid phase, equation (3-1), one has

$$\frac{\partial u}{\partial x} = - \frac{\partial v}{\partial y}$$

Substituting into equation (A-5) gives

$$D_p \frac{\partial \rho_p}{\partial y}\bigg|_{y=h} = \rho_{pw} \left(\frac{qE_w}{m_p \bar{F}}\right) + \int_o^h u \frac{\partial \rho_p}{\partial x} dy + \int_o^h \rho_p \frac{\partial u}{\partial x} dy$$

$$= \rho_{pw} \left(\frac{qE_w}{m_p \bar{F}}\right) + \int_o^h \frac{\partial (\rho_p u)}{\partial x} dy$$

Applying Leibnitz's rule for differentiating an integral, one obtains

$$D_p \frac{\partial \rho_p}{\partial y}\bigg|_{y=h} = \rho_{pw} \left(\frac{qE_w}{m_p \bar{F}}\right) + \frac{\partial}{\partial x} \int_o^h (\rho_p u) dy - (\rho_p u)_h \frac{dh}{dx}$$

for channel flow $\frac{dh}{dx} = 0$, but for diffuser flow $\frac{dh}{dx} \neq 0$, however for both cases $(\rho_p u)_h = 0$ due to the no slip condition at the wall for the fluid phase, hence one gets:

$$D_p \frac{\partial \rho_p}{\partial y}\bigg|_{y=h} = \rho_{pw} \left(\frac{qE_w}{m_p \bar{F}}\right) + \frac{\partial}{\partial x} \int_o^h (\rho_p u) dy$$

$$= \rho_{pw} \left(\frac{qE_w}{m_p \bar{F}}\right) + \frac{\partial}{\partial x} \int_o^h \rho_p u_p dy - \int_o^h \frac{\partial}{\partial x} [\rho_p (u_p - u)] dy$$

But from equation (A-2) one has $\frac{\partial}{\partial x}[\rho_p(u_p - u)] \simeq 0$

$$\therefore \quad D_p \left.\frac{\partial \rho_p}{\partial y}\right|_{y=h} = \rho_{pw}\left(\frac{qE_w}{m_p \bar{F}}\right) + \frac{\partial}{\partial x}\int_o^h \rho_p u_p \, dy \qquad \text{(A-6)}$$

And from the momentum equation of the particulate phase in the y-direction, one has

$$u_p \frac{\partial v_p}{\partial x} + v_p \frac{\partial v_p}{\partial y} = \bar{F}(v - v_p) + \left(\frac{q}{m_p}\right)E_y \qquad \text{(3-5)}$$

Neglecting all the inertia terms relative to the other terms, and since at the wall v = 0 (no slip condition of the fluid phase), then equation (3-5) becomes

$$v_{pw} \simeq \left(\frac{qE_w}{m_p \bar{F}}\right) \qquad \text{(A-7)}$$

For the rate of deposition of the solid particles, the equation of conservation of mass has been used as follows:

$$-\frac{\partial}{\partial x}\int_o^h \rho_p u_p dy = \sigma \rho_{pw} v_{pw} + \sigma_w \rho_{pw} f_w/\bar{F} - \sigma_w' \rho_{pb} f_L/\bar{F} \qquad \text{(3-13)}$$

Substituting from equation (A-7) into equation (3-13) gives

$$-\frac{\partial}{\partial x}\int_o^h \rho_p u_p dy = \sigma \rho_{pw}\left(\frac{qE_w}{m_p \bar{F}}\right) + \sigma_w \rho_{pw} f_w/\bar{F} - \sigma_w' \rho_{pb} f_L/\bar{F}$$

$$\text{i.e.} \quad \frac{\partial}{\partial x}\int_o^h \rho_p u_p dy = -\sigma \rho_{pw}\left(\frac{qE_w}{m_p \bar{F}}\right) - \sigma_w \rho_{pw} f_w/\bar{F} + \sigma_w' \rho_{pb} f_L/\bar{F} \qquad \text{(A-8)}$$

Substituting from equation (A-8) into equation (A-6) follows

$$D_p \left.\frac{\partial \rho_p}{\partial y}\right|_{y=h} = \rho_{pw}\left(\frac{qE_w}{m_p \bar{F}}\right) - \sigma \rho_{pw}\left(\frac{qE_w}{m_p \bar{F}}\right) - \sigma_w \rho_{pw} f_w/\bar{F} + \sigma_w' \rho_{pb} f_L/\bar{F}$$

$$\therefore \quad D_p \left.\frac{\partial \rho_p}{\partial y}\right|_{y=h} = (1 - \sigma)\rho_{pw}\frac{qE_w}{m_p \bar{F}} - \sigma_w \rho_{pw} f_w/\bar{F} + \sigma_w' \rho_{pb} f_L/\bar{F} \qquad \text{(A-9)}$$

This is the boundary condition of the particle cloud density gradient at the wall, which is used in (3-24), sections (3.2) and (4.2) for the boundary conditions.

And by non-dimensionalizing of equation (A-9), one gets the following:

(1) channel flow

$$\left.\frac{\partial \rho_p^*}{\partial Y}\right|_{Y=1} = (1 - \sigma)\, E_w^* \rho_{pw}^* - \sigma_w \lambda \rho_{pw}^* + \sigma_w' \gamma \rho_{pb}^* \qquad \text{(A-10)}$$

(2) diffuser flow

$$\left.\frac{\partial \rho_p^*}{\partial Y}\right|_{Y=W} = (1 - \sigma) E_w^* \rho_{pw}^* - \sigma_w \lambda \rho_{pw}^* + \sigma_w' \gamma \rho_{pb}^* \qquad \text{(A-11)}$$

Appendix B

DIMENSIONLESS QUANTITIES AND PARAMETERS PHYSICAL MEANING AND ORDER OF MAGNITUDE

(1) Dimensionless Quantities and Parameters

$$X = x/h$$

$$Y = y/h$$

$$R^* = a/h$$

$$W = w(x)/h$$

$$U = u/u_o$$

$$V = v/u_o$$

$$U_p = u_p/u_o$$

$$V_p = v_p/u_o$$

$$P = (p - p_o)/(\rho u_o^2)$$

$$N_{DF} = \left(\frac{D_p}{\bar{F}h^2}\right)^{1/3}$$

$$N_{ED} = \left(\frac{\rho_{po}}{4\varepsilon_o}\right)^{1/2} \left(\frac{q}{m_p}\right)\left(\frac{h^2}{D_p}\right)$$

$$N_m = u_o/h\bar{F}$$

$$N_R = u_o h/\nu$$

$$K_{np} = L_p/h$$

$$\dot{m}^* = \dot{m}/(\rho_{po} u_o)$$

$$\beta\dot{m}^* = \dot{m}/[\rho_{po}(D_p/h)]$$

$$E^* = \left(\frac{q}{m_p}\right)\left(\frac{h}{\bar{F}D_p}\right)E$$

$$\rho_p^* = \rho_p/\rho_{po}$$

$$\rho^{*}_{pb} = \rho_{pb}/\bar{\rho}_{p}$$

$$\rho_{R} = \bar{\rho}/\rho_{po}$$

$$\alpha = (N_{ED}\ N_{DF})^{2} = \left(\frac{\rho_{po}}{4\epsilon_{o}}\right)\left(\frac{q}{m_{p}}\right)^{2}\left(\frac{h^{2}}{\bar{F}D_{p}}\right)$$

$$\beta = (N_{m}/N_{DF}^{2}) = u_{o}h/D_{p}$$

$$\gamma = (hf_{L})/(\bar{F}D_{p})$$

$$\lambda = (hf_{w})/(\bar{F}D_{p})$$

(2) Physical Meaning

$$N_{DF} = \left(\frac{D_{p}}{\bar{F}h^{2}}\right)^{\frac{1}{2}}$$ Diffusion response number

which is the square root of the ratio of relaxation time $(1/\bar{F})$ to diffusion time (h^{2}/D_{p}).

$$N_{ED} = \left(\frac{\rho_{po}}{4\epsilon_{o}}\right)^{\frac{1}{2}}\left(\frac{q}{m_{p}}\right)\left(\frac{h^{2}}{D_{p}}\right)$$ Electro-diffusion number

which is the ratio of displacement by electrostatic repulsion to that by diffusion.

$$N_{m} = u_{o}/h\bar{F}$$ Momentum-transfer number

which is the ratio of relaxation time $(1/\bar{F})$ to transport time (h/u_{o}).

$$N_{R} = u_{o}h/\nu$$ Reynolds number (based on half channel width)

which is the ratio of inertia forces to viscous forces.

$N_{scp} = \nu/D_p$ Schmidt number of particle

which is the ratio of viscous forces to particle diffusive forces, it is analogous to Prandtl number in heat transfer.

$K_{np} = L_p/h$ Knudsen number of particle

which is the ratio of particle-fluid interaction length (L_p) to half channel width (h). This number governs the particle slip condition at the wall.

$\alpha = (N_{ED}N_{DF})^2 = (\frac{po}{4\varepsilon_o})(\frac{q}{m_p})^2(\frac{h^2}{\bar{F}D_p})$ Electrostatic-charge parameter

which characterizes the electrostatic charge of solid particles.

$\beta = (N_m/N_{DF}^2) = N_{scp}\ N_R = U_o h/D_p$ Diffusive Peclet number

which is the ratio of inertia forces to diffusive forces. This number is a momentum-diffusion parameter.

$\gamma = (hf_L)/(\bar{F}D_p)$ Lift-force parameter

which is the ratio of lift forces at the wall to diffusive forces of particles.

$\lambda = (hf_w)/(\bar{F}D_p)$ Adhesive-force parameter

which is the ratio of wall adhesive forces to diffusive forces of particles. Note that ($\sigma_w\lambda$) was used as a surface adhesion parameter.

$\dot{m}^* = \dot{m}/(\rho_{po}u_o)$ Dimensionless rate of deposition of particles

which is the ratio of the rate of deposition of the particles to the mass flow rate of the particles at inlet.

$\beta\dot{m}^* = \dot{m}/[\rho_{po}(D_p/h)]$ Dimensionless-modified rate of deposition of particles

which is the ratio of the rate of deposition of the particles to the modified mass flow rate of the particles at inlet $[\rho_{po}(D_p/h)]$ which is the product of the inlet particle concentration ρ_{po} times the diffusion velocity (D_p/h).

(3) Order of Magnitude

Some of the parameters and dimensionless quantities can be calculated, while the others can be estimated and taken from previous experiments (Cheng et al [10]).

From the actual size of a fluidic device one has h = 0.05 cm.

Considering solid particles of diameters

$2a = 2\mu$ and

$2a = 20\mu$

the particle size parameter $R^* = a/h$ can be calculated and the result is as follows:

$R^* = 0.002$ for particles of 2μ diameter

$R^* = 0.02$ for particles of 20μ diameter

For air as a fluid phase with a pressure p = 1 atm and temperature T = 20 deg C, then by using equation (3-24a) the particle-fluid interaction length, L_p, can be calculated and the result is as follows:

$L_p = 6.5 \times 10^{-6}$ cm.

Hence the particle Knudsen number, $K_{np} = L_p/h$, can be evaluated and the result is:

$K_{np} = 0.00013$.

A range for K_{np} as (0.0001 - 0.01) will be considered.

Assuming a uniform inlet velocity u_o = 3000 cm/S the Reynolds number can be determined, $N_R = u_o h/\nu$ based on half the channel width, and the result is

N_R= 1000.

A range for N_R as (100-1000) will be taken. For the momentum-transfer number, one has

$$N_m = u_o/h\bar{F}$$

where $$\bar{F} = F^*[9(\bar{\mu}/2a^2)\bar{\rho}_p][1 + (\bar{\rho}/2\bar{\rho}_p)]^{-1} \qquad (3\text{-}7)$$

and $$F^* = (c_D/24)[2a(\bar{\rho}\,|\vec{v} - \vec{v}_p|)/\bar{\mu}]. \qquad (3\text{-}8)$$

In the Stokes' law range F^*= 1 as given by Soo and Tung [71], and assuming that $\bar{\rho} << \bar{\rho}_p$, then the second bracket in equation (3-7) can be dropped, i.e.

$$\bar{F} = 9\bar{\mu}\bar{\rho}_p/2a^2.$$

Then for a particle density $\bar{\rho}_p$ = 3.7 g/cm^3, the inverse of the relaxation time $\bar{F}$ can be obtained, and the result is

$\bar{F} \simeq 22000$ S^{-1} for particles of 2μ diameter

and $\bar{F} \simeq 220$ S^{-1} for particles of 20μ diameter.

Hence the momentum-transfer number N_m can be calculated, and the result is as follows:

N_m = 2.7 for particles of 2μ diameter

and N_m = 270 for particles of 20μ diameter.

For the electrostatic charge parameter α,

$$\alpha = \left(\frac{\rho_{po}}{4\varepsilon_o}\right)\left(\frac{q}{m_p}\right)^2\left(\frac{h^2}{\bar{F}D_p}\right)$$

where

$\varepsilon_o = 8.85434 \times 10^{-12}$ $C^2/N.m^2$ (free space permittivity).

From the experimental work by Cheng et al [10] for an air velocity of 35 m/s (close to $u_o = 30$ m/s):

$(q/m_p) = 1.633 \times 10^{-3}$ C/Kg

and this is the electrostatic charge to mass ratio, required to evaluate α.

Assuming an inlet particle concentration, ρ_{po} of

$\rho_{po} = 4.6 \times 10^{-6}$ g/cm^3

according to Davies [16] the coefficient of diffusion D_p is as follows:

$D_p = 1.3 \times 10^{-7}$ cm^2/s for particles of 2μ diameter

and $D_p = 1.2 \times 10^{-8}$ cm^2/s for particles of 20μ diameter.

Hence one can determine the electrostatic charge parameter, α, and the result is:

$\alpha \simeq 467$ for particles of 2μ diameter

A range for α of zero to 400 will be considered.

For the diffusive Peclet number $\beta = u_o h/D_p$.

Subtituting numerical values,

$\beta \simeq 1.2 \times 10^9$ for particles of 2μ diameter

A range for β of 4 to 10^7 will be assigned.

The surface adhesion parameter $\sigma_w \lambda$ is assigned the values 0, 0.1, 1.0, 10 and 100 in accordance with the studies by Soo and Tung [71].

Since the electroviscous-sticking factor σ and the lifting factor σ_w' can only have values between 0 and 1.0, values of 0.5 and 1.0

for σ and 0, 10^{-10} and 10^{-6} for σ_w' were assigned. It should be noted that for higher values of σ_w', the results are unrealistic.

For the density ratio

$$\rho_R = \bar{\rho}/\rho_{po},$$

$$\bar{\rho} = \rho_{air} = 0.00138 \quad g/cm^3$$

and $\rho_{po} = 4.6 \times 10^{-6}$ g/cm^3 (assumed)

hence

$$\rho_R = 300.$$

The dimensionless packed bed density, $\rho^*_{pb} = \rho_{pb}/\bar{\rho}_p$, will be assumed to be 0.3 as a reasonable value.

Appendix C

NUMERICAL PROCEDURES FOR SOLVING THE EQUATIONS DERIVED IN CHAPTERS 3 and 4

The governing equations (3-15) to (3-20) can be written in finite difference form as follows:

$$\frac{(U_{i+1,j} - U_{i,j})}{H} + \frac{(V_{i+1,j+1} - V_{i+1,j})}{S} = 0 \qquad \text{(C-1)}$$

$$U_{i+1,j}\left(\frac{U_{i+1,j} - U_{i,j}}{H}\right) + V_{i+1,j}\left(\frac{U_{i+1,j+1} - U_{i+1,j-1}}{2S}\right) = -\frac{(P_{i+1} - P_i)}{H} + \frac{(U_{i+1,j+1} - 2u_{i+1,j} + U_{i+1,j-1})}{N_R S^2} \qquad \text{(C-2)}$$

$$U_{p_{i+1,j}}\left(\frac{U_{p_{i+1,j}} - U_{p_{i,j}}}{H}\right) + V_{p_{i+1,j}}\left(\frac{U_{p_{i+1,j+1}} - U_{p_{i+1,j-1}}}{2S}\right) = \frac{(U_{i+1,j} - U_{p_{i+1,j}})}{N_m} + \frac{(U_{p_{i+1,j+1}} - 2U_{p_{i+1,j}} + U_{p_{i+1,j-1}})}{\beta S^2} + \frac{(\rho^*_{p_{i+1,j+1}} - \rho^*_{p_{i+1,j-1}})(U_{p_{i+1,j+1}} - U_{p_{i+1,j-1}})}{4\beta S^2 \rho^*_{p_{i+1,j}}} \qquad \text{(C-3)}$$

$$U_{p_{i+1,j}}\left(\frac{V_{p_{i+1,j}} - V_{p_{i,j}}}{H}\right) + V_{p_{i+1,j}}\left(\frac{V_{p_{i+1,j+1}} - V_{p_{i+1,j}}}{S}\right) = \frac{(V_{i+1,j} - V_{p_{i+1,j}})}{N_m} + \frac{E^*_{i+1,j}}{\beta N_m} \qquad \text{(C-4)}$$

$$U_{i+1,j}\left(\frac{{}^{*}\rho p_{i+1,j}-{}^{*}\rho p_{i,j}}{H}\right)+V_{i+1,j}\left(\frac{{}^{*}\rho p_{i+1,j+1}-{}^{*}\rho p_{i+1,j-1}}{2S}\right)$$

$$=\frac{({}^{*}\rho p_{i+1,j+1}-2{}^{*}\rho p_{i+1,j}+{}^{*}\rho p_{i+1,j-1})}{\beta S^2}$$

$$-E^{*}_{i+1,j}\left(\frac{{}^{*}\rho p_{i+1,j+1}-{}^{*}\rho p_{i+1,j-1}}{2\beta S}\right)-\frac{4\alpha}{\beta}\,{}^{*}\rho p_{i+1,j} \qquad \text{(C-5)}$$

$$\left(\frac{E^{*}_{i+1,j+1}-E^{*}_{i+1,j}}{S}\right)=4\alpha\rho^{*}_{i+1,j} \qquad \text{(C-6)}$$

Neglecting the second term on the left-hand side of equation (C-4) since it is small compared with the other terms, and by linearizing these equations, one will get the following:

$$\left(\frac{U_{i+1,j}-U_{i,j}}{H}\right)+\left(\frac{V_{i+1,j+1}-V_{i+1,j}}{S}\right)=0 \qquad \text{(C-1)}$$

$$U_{i,j}\left(\frac{U_{i+1,j}-U_{i,j}}{H}\right)+V_{i,j}\left(\frac{U_{i+1,j+1}-U_{i+1,j-1}}{2S}\right)=-\left(\frac{P_{i+1}-P_{i}}{H}\right)$$

$$+\frac{(U_{i+1,j+1}-2U_{i+1,j}+U_{i+1,j-1})}{N_R S^2} \qquad \text{(C-7)}$$

$$U_{p_{i,j}}\left(\frac{{}^{U}p_{i+1,j}-{}^{U}p_{i,j}}{H}\right)+V_{p_{i,j}}\left(\frac{{}^{U}p_{i+1,j+1}-{}^{U}p_{i+1,j-1}}{2S}\right)$$

$$=\frac{(U_{i+1,j}-{}^{U}p_{i+1,j})}{N_m}+\frac{({}^{U}p_{i+1,j+1}-2{}^{U}p_{i+1,j}+{}^{U}p_{i+1,j-1})}{\beta S^2}$$

$$+\frac{({}^{*}\rho p_{i,j+1}-{}^{*}\rho p_{i,j-1})({}^{U}p_{i+1,j+1}-{}^{U}p_{i+1,j-1})}{4\beta S^2\rho^{*}_{p_{i,j}}} \qquad \text{(C-8)}$$

$$U_{P_{i,j}}\left(\frac{V_{P_{i+1,j}} - V_{P_{i,j}}}{H}\right) = \left(\frac{V_{i+1,j} - V_{P_{i+1,j}}}{N_m}\right) + \frac{E^*_{i+1,j}}{\beta N_m} \qquad \text{(C-9)}$$

$$U_{i,j}\left(\frac{\rho^*_{P_{i,1,j}} - \rho^*_{P_{i,j}}}{H}\right) + V_{i,j}\left(\frac{\rho^*_{P_{i+1,j+1}} - \rho^*_{P_{i+1,j-1}}}{2S}\right)$$

$$= \left(\frac{\rho^*_{P_{i+1,j+1}} - 2\rho^*_{P_{i+1,j}} + \rho^*_{P_{i+1,j-1}}}{\beta S^2}\right)$$

$$- E^*_{i,j}\left(\frac{\rho^*_{P_{i+1,j+1}} - \rho^*_{P_{i+1,j-1}}}{2\beta S}\right) - \frac{4\alpha}{\beta}\rho^*_{P_{i,j}}\rho^*_{P_{i+1,j}} \qquad \text{(C-10)}$$

$$\left(\frac{E^*_{i+1,j+1} - E^*_{i+1,j}}{S}\right) = 4\alpha\rho^*_{P_{i+1,j}} \qquad \text{(C-6)}$$

where H and S are the step sizes in the axial and normal directions respectively.

For the channel flow $H = S = 0.1$ (constant) .

But for the diffuser flow $H = 0.1$ (constant) while S varies according to the diffuser angle (2θ). Different values for angle θ will be considered, particularly $\theta = 2^o$, 2.5^o, 4^o, 5^o and 7.5^o. For an actual fluidic amplifier, the diffuser angle in the splitter region is about 15^o, i.e. $\theta = 7.5^o$.

In each case the width of the diffuser will be a function of axial position and one can write:

$$W_{i+1} = W_i + \tan\theta/N \qquad [W = w(x)/h]$$

and $S_{i+1} = W_{i+1}/N$

where $N = 10$, $W_1 = 1$ and $S_1 = 0.1$.

For example when $\theta = 2^{o}$ ($\tan \theta = 0.034921$)

then $W_2 = 1.0034921$ $S_2 = 0.10034921$

$W_3 = 1.0069842$ $S_3 = 0.10069842$

$W_4 = 1.0104763$ $S_4 = 0.10104763$

$W_5 = 1.0139684$ $S_5 = 0.10139684$

....

and so on.

For both the channel and diffuser flows

$i = 1(1)m$ (m is taken up to 140)

$j = 2(1)n+1$ (n is taken 10)

where m and n are the numbers of equal intervals in the x- and y-direction respectively. The finite difference grids of both the channel and diffuser flows are shown in Fig. (3.2) and (4.2) respectively.

The equations of the boundary conditions (3-25), (3-26) and (3-27) can be written in finite difference form as follows:

@ i = 1 [at inlet, corresponds to X = 0, since
$(2 \leq j \leq n+2)$ X = H (i-1)]

$U_{1,j} = U_{p_{1,j}} = 1$ uniform

$V_{1,j} = V_{p_{1,j}} = 0$

$\rho^{*}_{p_{1,j}} = 1$ uniform

$P_{1,j} = P_1 = 0$

$E_{1,j} = 0$

These uniform inlet boundary conditions are applied for both channel and diffuser flows when there is no connection between the two.

But when one deals with a diffuser connected to a channel, then the inlet conditions of the diffuser flow are the exit conditions of the channel flow.

$\underline{@\ j = 2}$ $\quad (i > 1)$ [at the channel or diffuser centerline, corresponds to Y = 0, since Y = S(j-2)]

$$\frac{U_{i+1,3} - U_{i+1,1}}{2S} = \frac{U_{p_{i+1,3}} - U_{p_{i+1,1}}}{2S} = 0 \rightarrow \begin{cases} U_{i+1,3} = U_{i+1,1} \\ U_{p_{i+1,3}} = U_{p_{i+1,1}} \end{cases} \quad \text{symmetry}$$

$$V_{i+1,2} = V_{p_{i+1,2}} = 0$$

$$\frac{\rho^*_{p_{i+1,3}} - \rho^*_{p_{i+1,1}}}{2S} = 0 \rightarrow \rho^*_{p_{i+1,3}} = \rho^*_{p_{i+1,1}} \quad \text{symmetry}$$

$$E^*_{i+1,2} = 0$$

$\underline{@\ j = n+2}$ $\quad (i > 1)$ [at the wall, corresponds to Y = 1 for channel flow and Y = W for diffuser flow]

$$U_{i+1,n+2} = V_{i+1,n+2} = 0 \qquad \text{(no slip-fluid phase)}$$

$$U_{p_{i+1,n+2}} = \left(\frac{K_{np}/S}{1 + K_{np}/S}\right) U_{p_{i+1,n+1}} \qquad \text{(slip-particle phase) Case 1}$$

$$\text{or} \quad \left[\begin{array}{ll} U_{p_{i+1,n+2}} = \dfrac{(1 - \frac{H(i-1)}{N_m})}{(1 + K_{np}/S)} + (\dfrac{K_{np}/S}{1 + K_{np}/S}) U_{p_{i+1,n+1}} & i < (N_m/H)+1 \\ U_{p_{i+1,n+2}} = (\dfrac{K_{np}/S}{1 + K_{np}/S}) U_{p_{i+1,n+1}} & i \geq (N_m/H)+1 \end{array} \right] \text{Case II}$$

$$(\frac{\rho^*_{p_{i+1,n+2}} - \rho^*_{p_{i+1,n+1}}}{S}) = (1 - \sigma) E^*_{i+1,n+2} \rho^*_{p_{i+1,n+2}} - \sigma_w \lambda \rho^*_{p_{i+1,n+2}} + \sigma'_w \gamma_{i+1,n+2} \rho^*_{pb}$$

which can be written in the following approximate form:

$$\rho^*_{p_{i+1,n+2}} = \rho^*_{p_{i+1,n+2}} \{ (1 + S\sigma'_w \gamma_{i,n+2} \rho^*_{pb} / \rho^*_{p_{i,n+1}}) / [1 - S(1-\sigma) E^*_{i,n+2} + S\sigma_w \lambda] \}$$

Let ($\xi = S/H$), then equations (C-1), (C-7) to (C-10) and (C-6) can be written in the form:

$$V_{i+1,j+1} - V_{i+1,j} + \xi U_{i+1,j} = (\xi U_{i,j}) \tag{C-11}$$

$$-(\frac{V_{i,j}}{2S} + \frac{1}{S^2 N_R}) U_{i+1,j-1} + (\frac{U_{i,j}}{H} + \frac{2}{S^2 N_R}) U_{i+1,j} + (\frac{V_{i,j}}{2S} - \frac{1}{S^2 N_R}) U_{i+1,j+1} + \frac{P_{i+1}}{H} = (\frac{U^2_{i,j} + P_i}{H}) \tag{C-12}$$

$$(-\frac{V_{p_{i,j}}}{2S} - \frac{1}{S^2 \beta} + \frac{\rho^*_{p_{i,j+1}} - \rho^*_{p_{i,j-1}}}{4S^2 \beta \rho^*_{p_{i,j}}}) U_{p_{i+1,j-1}} + (\frac{1}{N_m} + \frac{2}{S^2 \beta} + \frac{U_{p_{i,j}}}{H}) U_{p_{i+1,j}}$$

$$+ (\frac{V_{p_{i,j}}}{2S} - \frac{1}{S^2 \beta} - \frac{\rho^*_{p_{i,j+1}} - \rho^*_{p_{i,j-1}}}{4S^2 \beta \rho^*_{p_{i,j}}}) U_{p_{i+1,j+1}} - \frac{U_{i+1,j}}{N_m} = (\frac{U^2_{p_{i,j}}}{H}) \tag{C-13}$$

$$(\frac{1}{N_m} + \frac{U_{p_{i,j}}}{H})V_{p_{i+1,j}} - \frac{V_{i+1,j}}{N_m} - \frac{E^*_{i+1,j}}{\beta N_m} = (\frac{U_{p_{i,j}} \cdot V_{p_{i,j}}}{H}) \qquad (C\text{-}14)$$

$$-(\frac{V_{i,j}}{2S} + \frac{1}{S^2\beta} + \frac{E^*_{i,j}}{2S\beta})\rho^*_{p_{i+1,j-1}} + (\frac{U_{i,j}}{H} + \frac{2}{S^2\beta} + \frac{4\alpha\rho^*_{p_{i,j}}}{\beta})\rho^*_{p_{i+1,j}}$$

$$+ (\frac{V_{i,j}}{2S} - \frac{1}{S^2\beta} + \frac{E^*_{i,j}}{2S\beta})\rho^*_{p_{i+1,j+1}} = (\frac{U_{i,j} \cdot \rho^*_{p_{i,j}}}{H}) \qquad (C\text{-}15)$$

$$E^*_{i+1,j+1} - E^*_{i+1,j} - 4\alpha S\rho^*_{p_{i+1,j}} = 0 \qquad (C\text{-}16)$$

Also equation (3-21a) can be written in a simplified finite difference form after applying the boundary conditions at the wall as follows:

$$\gamma_{i+1,n+2} = (1.54\beta N_m \rho_R / R^* N_R^{1/2})[(\frac{K_{np}/S}{1 + K_{np}/S})U_{p_{i+1,n+1}} + R^* U_{i+1,n+1}/S]U^{1/2}_{i+1,n+1} \qquad (C\text{-}17)$$

Combining equation (C-17) with equation (3-21) gives

$$\dot{m}^*_{i+1} = DPR_{i+1} = \rho^*_{p_{i+1,n+2}}(\sigma V_{p_{i+1,n+2}} + \sigma_w \lambda/\beta) - \sigma'_w \rho^*_{pb}(1.54\beta N_m \rho_R / R^* N_R^{1/2})[(\frac{K_{np}/S}{1 + K_{np}/S})U_{p_{i+1,n+1}} + R^* U_{i+1,n+1}/S]U^{1/2}_{i+1,n+1}/\beta \qquad (C\text{-}18)$$

Let

$$\alpha 1_{i,j} = -(\frac{V_{i,j}}{2S} + \frac{1}{S^2 N_R})$$

$$\alpha 2_{i,j} = (\frac{U_{i,j}}{H} + \frac{2}{S^2 N_R})$$

$$\alpha 3_{i,j} = \left(\frac{V_{i,j}}{2S} - \frac{1}{S^2 N_R}\right)$$

$$\beta 1_{i,j} = \left(-\frac{V_{p_{i,j}}}{2S} - \frac{1}{S^2\beta} + \frac{\rho^{*}_{p_{i,j+1}} - \rho^{*}_{p_{i,j-1}}}{4S^2\beta\rho^{*}_{p_{i,j}}}\right)$$

$$\beta 2_{i,j} = \left(\frac{1}{N_m} + \frac{2}{S^2\beta} + \frac{U_{p_{i,j}}}{H}\right)$$

$$\beta 3_{i,j} = \left(\frac{V_{p_{i,j}}}{2S} - \frac{1}{S^2\beta} - \frac{\rho^{*}_{p_{i,j+1}} - \rho^{*}_{p_{i,j-1}}}{4S^2\beta\rho^{*}_{p_{i,j}}}\right)$$

$$\gamma 1_{i,j} = \left(\frac{1}{N_m} + \frac{U_{p_{i,j}}}{H}\right)$$

$$\eta 1_{i,j} = -\left(\frac{V_{i,j}}{2S} + \frac{1}{S^2\beta} + \frac{E^{*}_{i,j}}{2S\beta}\right)$$

$$\eta 2_{i,j} = \left(\frac{U_{i,j}}{H} + \frac{2}{S^2\beta} + \frac{4\alpha\rho^{*}_{p_{i,j}}}{\beta}\right)$$

$$\eta 3_{i,j} = \left(\frac{V_{i,j}}{2S} - \frac{1}{S^2\beta} + \frac{E^{*}_{i,j}}{2S\beta}\right)$$

$$C1_{i,j} = \left(\frac{U^2_{i,j} + P_i}{H}\right)$$

$$C2_{i,j} = (\xi U_{i,j})$$

$$C3_{i,j} = \left(\frac{U^2_{p_{i,j}}}{H}\right)$$

$$C4_{i,j} = \left(\frac{U_{p_{i,j}} \cdot V_{p_{i,j}}}{H}\right)$$

$$C5_{i,j} = \left(\frac{U_{i,j} \cdot \rho^{*}_{p_{i,j}}}{H}\right)$$

$$C = -4\alpha S$$

$$CC = (1.54\beta N_m \rho_R / R^{*} N_R)$$

$$CK = (K_{np}/S)/(1 + K_{np}/S)$$

Then equations (C-11) to (C-16) and equation (C-18) can be written in shortened form as follows:

$$\alpha 1_{i,j} U_{i+1,j-1} + \alpha 2_{i,j} U_{i+1,j} + \alpha 3_{i,j} U_{i+1,j+1} + P_{i+1}/H = C1_{i,j} \quad \text{(C-19)}$$

$$V_{i+1,j+1} - V_{i+1,j} + \xi U_{i+1,j} = C2_{i,j} \quad \text{(C-20)}$$

$$\beta 1_{i,j} U_{p_{i+1,j-1}} + \beta 2_{i,j} U_{p_{i+1,j}} + \beta 3_{i,j} U_{p_{i+1,j+1}} - U_{i+1,j}/N_m = C3_{i,j} \quad \text{(C-21)}$$

$$\gamma 1_{i,j} V_{p_{i+1,j}} - V_{i+1,j}/N_m - E^*_{i+1,j}/\beta N_m = C4_{i,j} \quad \text{(C-22)}$$

$$\eta 1_{i,j} \rho^*_{p_{i+1,j-1}} + \eta 2_{i,j} \rho^*_{p_{i+1,j}} + \eta 3_{i,j} \rho^*_{p_{i+1,j+1}} = C5_{i,j} \quad \text{(C-23)}$$

$$E^*_{i+1,j+1} - E^*_{i+1,j} + C\rho^*_{p_{i+1,j}} = 0 \quad \text{(C-24)}$$

$$DPR_{i+1} = \rho^*_{p_{i+1,n+2}} (\sigma V_{p_{i+1,n+2}} + \sigma_w \lambda/\beta)$$

$$-\sigma'_w \rho^*_{pb} \cdot CC[CK \cdot U_{p_{i+1,n+1}} + R^* U_{i+1,n+1}/S] U^{1/2}_{i+1,n+1}/\beta \quad \text{(C-25)}$$

where $i = 1(1)m$ for all equations (C-19) to (C-25),

and $j = 2(1)n+1$ for all equations except (C-22) where $j = 3(1)n+2$

Equations (C-19) to (C-25) can be expanded to give (6n+1) equations for fixed value of i and different values of j. Using the boundary

conditions with these equations, then the unknowns that one is looking for will be as follows:

Phase	Unknowns	No. of Unknowns
fluid phase	$U_{i+1,2}, U_{i+1,3}, \ldots\ldots, U_{i+1,n+1}$	n
	$V_{i+1,3}, V_{i+1,4} \ldots, V_{i+1,n+1}$	n-1
	P_{i+1}	1
particle phase	$U_{p_{i+1,2}}, U_{p_{i+1,3}}, \ldots\ldots, U_{p_{i+1,n+1}}$	n
	$V_{p_{i+1,3}}, V_{p_{i+1,4}}, \ldots, V_{p_{i+1,n+1}}$	
	$V_{p_{i+1,n+2}}$	n
	$\rho^{*}_{p_{i+1,2}}, \rho^{*}_{p_{i+1,3}}, \ldots\ldots\ldots, \rho^{*}_{p_{i+1,n+1}}$	n
	$E^{*}_{i+1,3}, E^{*}_{i+1,4}, \ldots, E^{*}_{i+1,n+1}$	
	$E^{*}_{i+1,n+2}$	n
	$\dot{m}^{*}_{i+1}$	1
	Total	(6n+1)

So the number of equations is equal to the number of unknowns, so the system of equations can be solved, and the method of solution is discussed in sections 3.3 and 4.3 for the channel and diffuser flows respectively.

Appendix D

TABLES OF COMPUTER PROGRAM VARIABLES

SYMBOL**	EXPLANATION
M,N	number of grid steps in the X- and Y- directions respectively.
H,S	Step sizes in the X- and Y- directions respectively.
W	h, half the channel width.
R	R^*, dimensionless radius of a particle.
AKNP	K_{np}, particle Knudsen number.
ANG	tan θ, where θ is half the diffuser angle.
ANM	N_m, momentum-transfer number.
ANR	N_R, Reynolds number.
ALPHA	α, electrostatic charge parameter.
BETA	β, diffusive Peclet number.
SIGMA	σ, sticking probability accounts for electro-viscous forces.
SIGMAW	σ_w, sticking probability accounts for adhesive forces at the wall.
SIGMWP	σ_w', lifting probability accounts for lift forces at the wall.
LAMBDA	λ, surface adhesion parameter.
DENTR	ρ_R, density ratio as defined.
PDENT	ρ_{pb}^*, dimensionless packed bed density.
C1(I,J)	$C1_{i,j}$, given in Appendix C.
C2(I,J)	$C2_{i,j}$ given in Appendix C.
C3(I,J)	$C3_{i,j}$, given in Appendix C.

**Also see list of symbols on pages xxi, xxii, xxiii and xxiv

SYMBOL**	EXPLANATION
C4(I,JB)	$C4_{i,j+1}$, given in Appendix C
C5(I,J)	$C5_{i,j}$, given in Appendix C.
ALPHA1(I,J)	$\alpha 1_{i,j}$, given in Appendix C.
ALPHA2(I,J)	$\alpha 2_{i,j}$, given in Appendix C.
ALPHA3(I,J)	$\alpha 3_{i,j}$, given in Appendix C.
ALPH13(I,2)	$\alpha 13_{i,2} = \alpha 1_{i,2} + \alpha 3_{i,2}$.
BETA1(I,J)	$\beta 1_{i,j}$, given in Appendix C.
BETA2(I,J)	$\beta 2_{i,j}$, given in Appendix C.
BETA3(I,J)	$\beta 3_{i,j}$, given in Appendix C.
BETA13(I,2)	$\beta 13_{i,2} = \beta 1_{i,2} + \beta 3_{i,2}$
BETA23(I,NC)	$\beta 23_{i,n+1} = \beta 2_{i,n+1} + CK \cdot \beta 3_{i,n+1}$
GAMA1(I,JB)	$\gamma 1_{i,j+1}$, given in Appendix C.
GAMA(I,ND)	$\gamma_{i,n+2}$, as defined in Eq. (C-17) after replacing i+1 with i.
ETA1(I,J)	$\eta 1_{i,j}$, given in Appendix C.
ETA2(I,J)	$\eta 2_{i,j}$, given in Appendix C.
ETA3(I,J)	$\eta 3_{i,j}$, given in Appendix C.
ETA4(I,NC)	$\eta 4_{i,n+1} = (1+S\sigma'_w \gamma_{i,n+2} \rho^*_{pb} / \rho^*_{p_{i,n+1}}) / [1-S(1-\sigma)E^*_{i,n+2} + S\sigma_w \lambda]$.
ETA13(I,2)	$\eta 13_{i,2} = \eta 1_{i,2} + \eta 3_{i,2}$.
ETA23(I,NC)	$\eta 23_{i,n+1} = \eta 2_{i,n+1} + \eta 3_{i,n+1} \cdot \eta 4_{i,n+1}$.
A(II,JJ)	A, matrix of coefficients of matrix equation AX=B
B(JJ)	B, column vector
U(IB,J)	$U_{i+1,j}$, axial velocity of fluid phase.
P(IB)	P_{i+1}, fluid static pressure.
V(IB,J)	$V_{i+1,j}$, normal velocity of fluid phase.

SYMBOL**	EXPLANATION
UP(IB,J)	$U_{p_{i+1,j}}$, axial velocity of particle phase.
VP(IB,J)	$V_{p_{i+1,j}}$, normal velocity of particle phase.
ROHP(IB,J)	$\rho^*_{p_{i+1,j}}$, particle concentration.
ROHU(IB,J)	$\rho^*_{p_{i+1,j}} U_{p_{i+1,j}}$, mass flow of particles in the X-direction.
ROHV(IB,J)	$\rho^*_{p_{i+1,j}} V_{p_{i+1,j}}$, mass flow of particles in the Y-direction.
E(IB,J)	$E^*_{i+1,j}$, Electric field intensity.
DPR(IB)	$\dot{m}^*_{i+1}$, rate of deposition of particles.

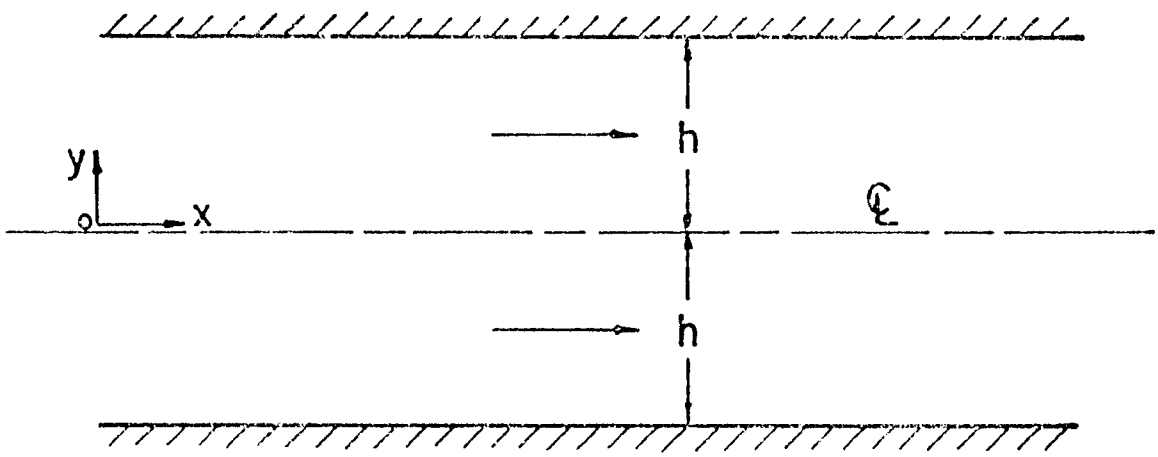

FIG. 3.1 CHANNEL FLOW CONFIGURATION

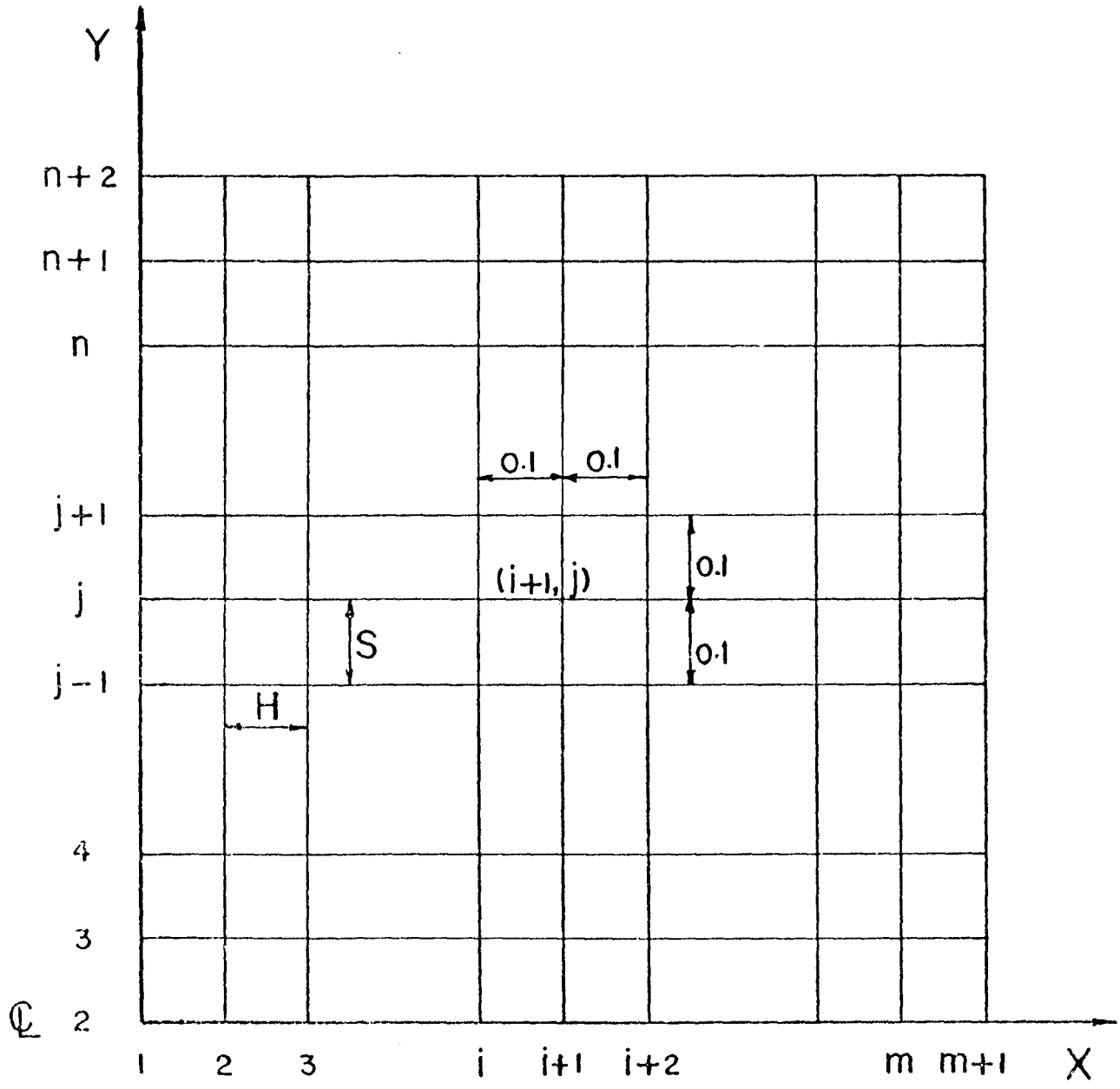

FIG. 3.2 FINITE DIFFERENCE GRID OF CHANNEL FLOW

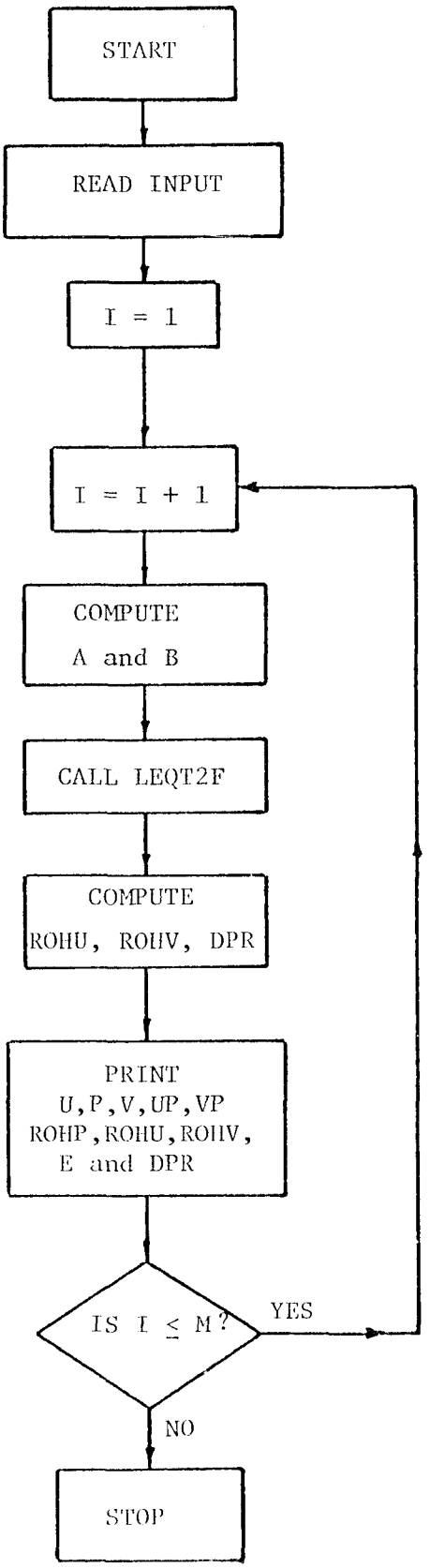

FIG. 3.3 COMPUTER FLOW CHART FOR CHANNEL FLOW

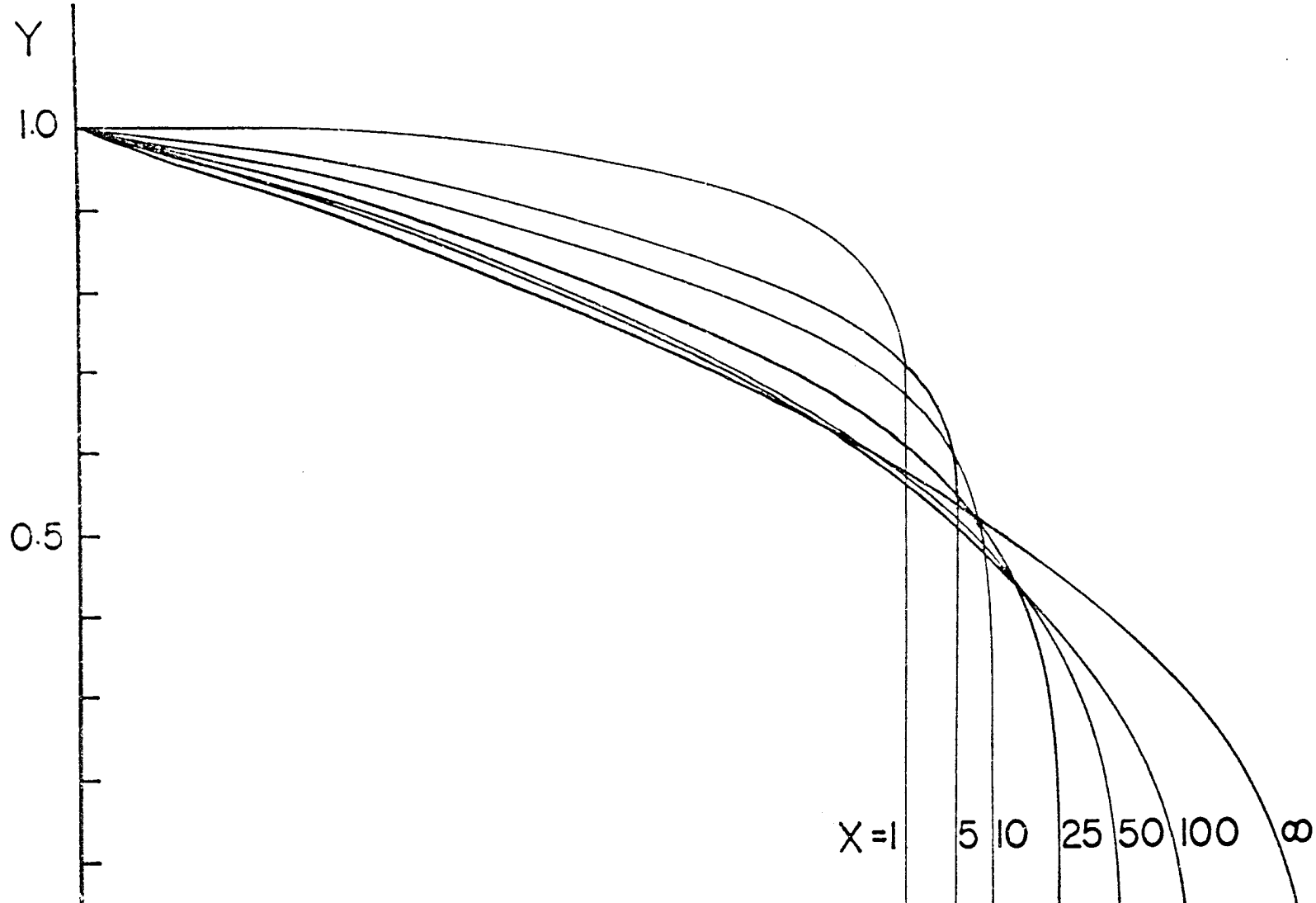

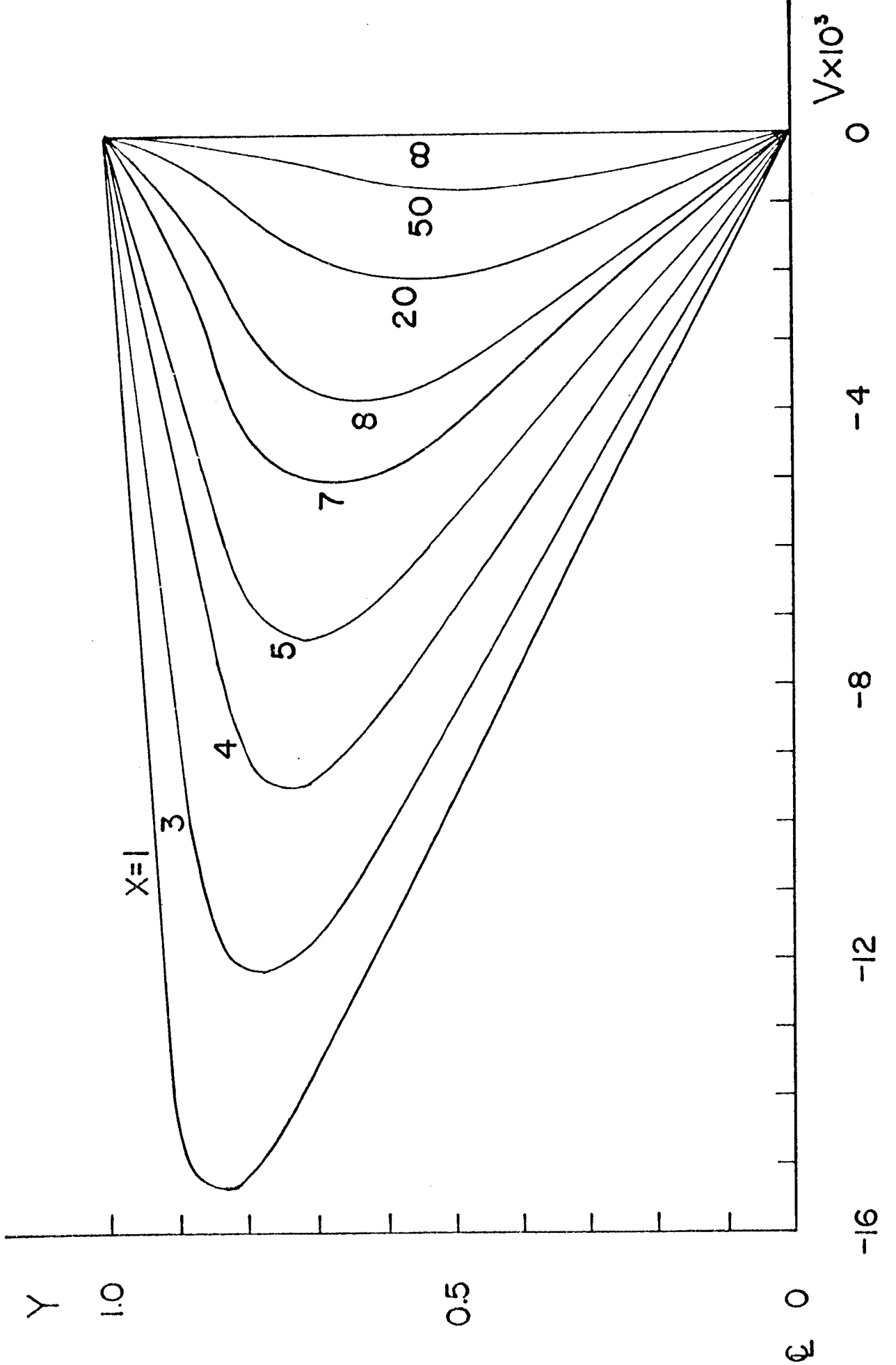

FIG. 3.5 VERTICAL VELOCITY DISTRIBUTION OF FLUID PHASE IN A CHANNEL FLOW

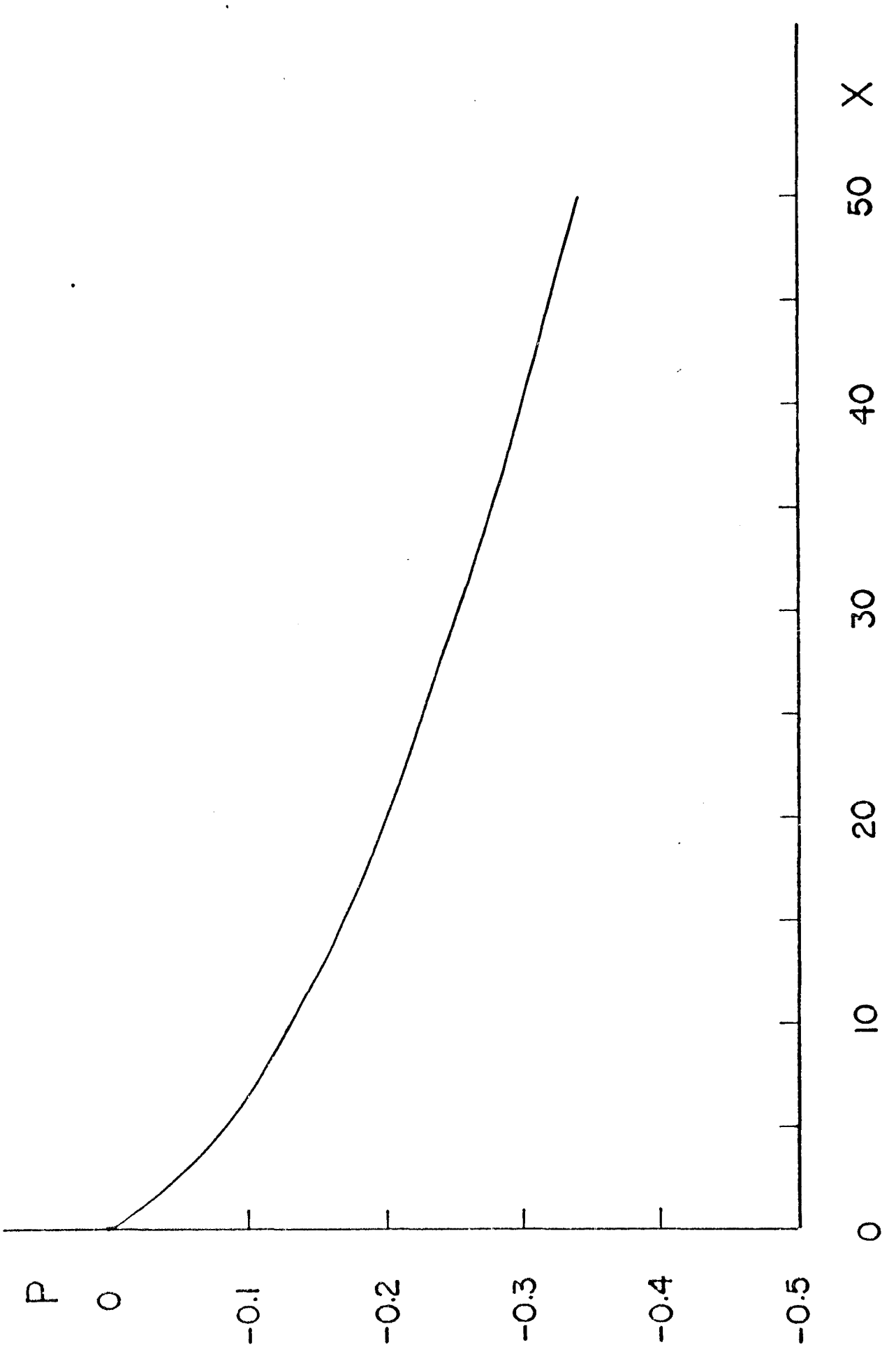

FIG. 3.6 AXIAL DISTRIBUTION OF FLUID STATIC PRESSURE IN A CHANNEL FLOW

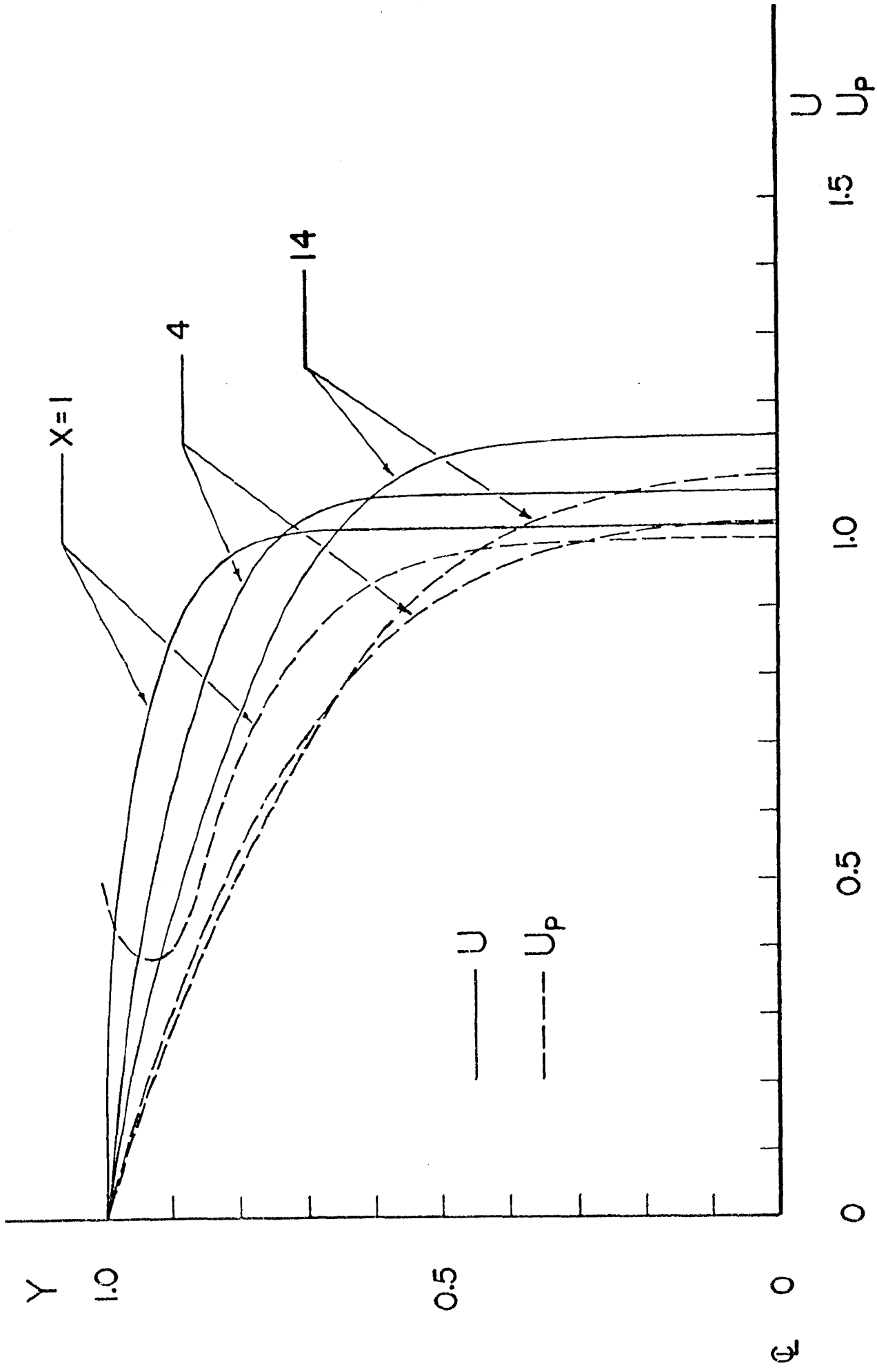

FIG. 3.7 COMPARISON OF AXIAL VELOCITIES OF FLUID AND PARTICLE PHASES WITH NO DEPOSITION IN A CHANNEL FLOW
(K_{np} = 0.0001, N_m = 2, N_R = 1000, α = 0, β = 40, σ = 0.5, $\sigma_w\lambda$ = 0, σ_w' = 0)

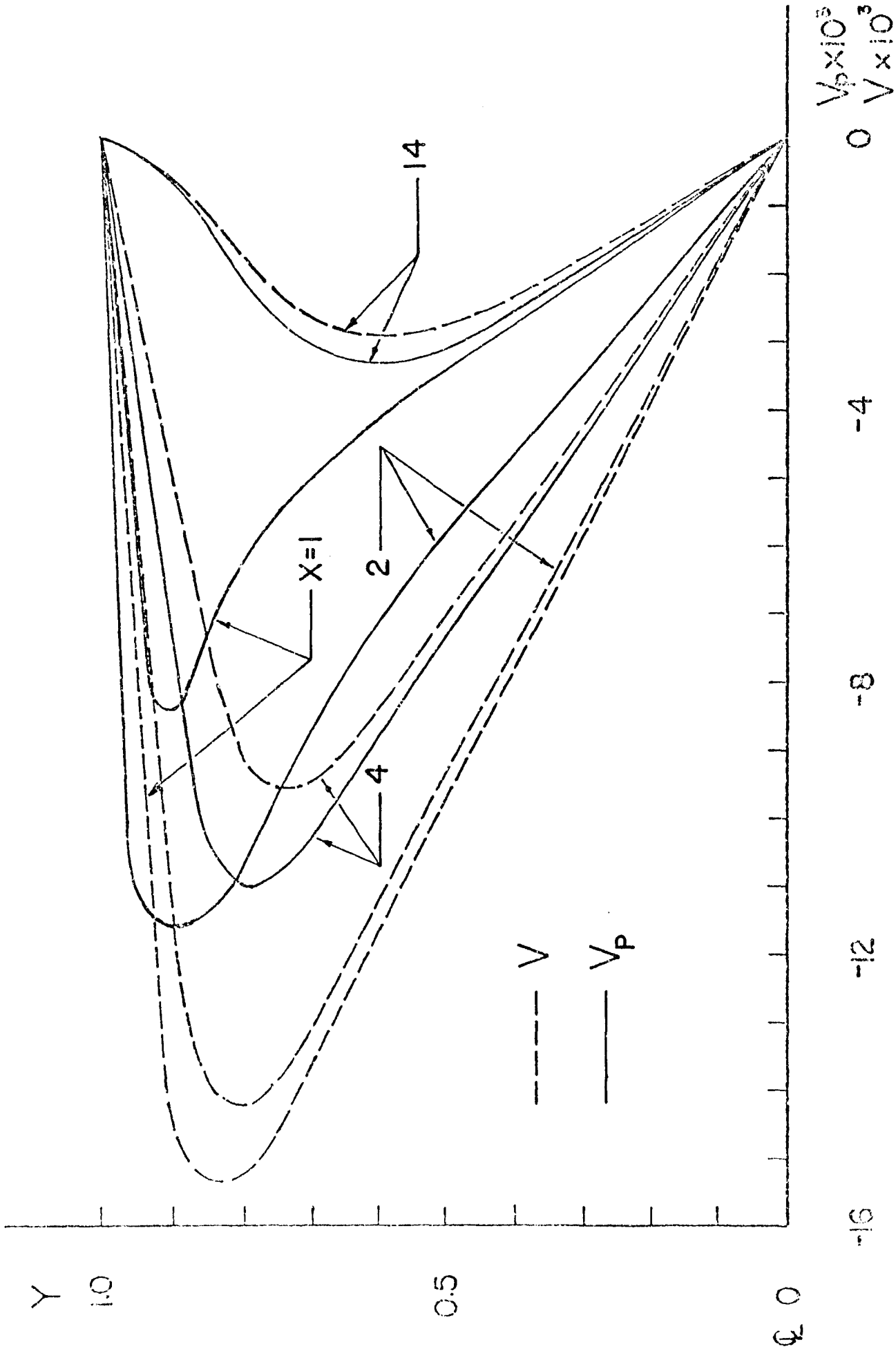

FIG. 3.3 COMPARISON OF VERTICAL VELOCITIES OF FLUID AND PARTICLE PHASES WITH NO DEPOSITION IN A CHANNEL FLOW

($K_{np} = 0.0001$, $N_m = 2$, $N_R = 1000$, $\alpha = 0$, $\beta = 40$, $\sigma = 0.5$, $\sigma_w \lambda = 0$, $\sigma_w' = 0$)

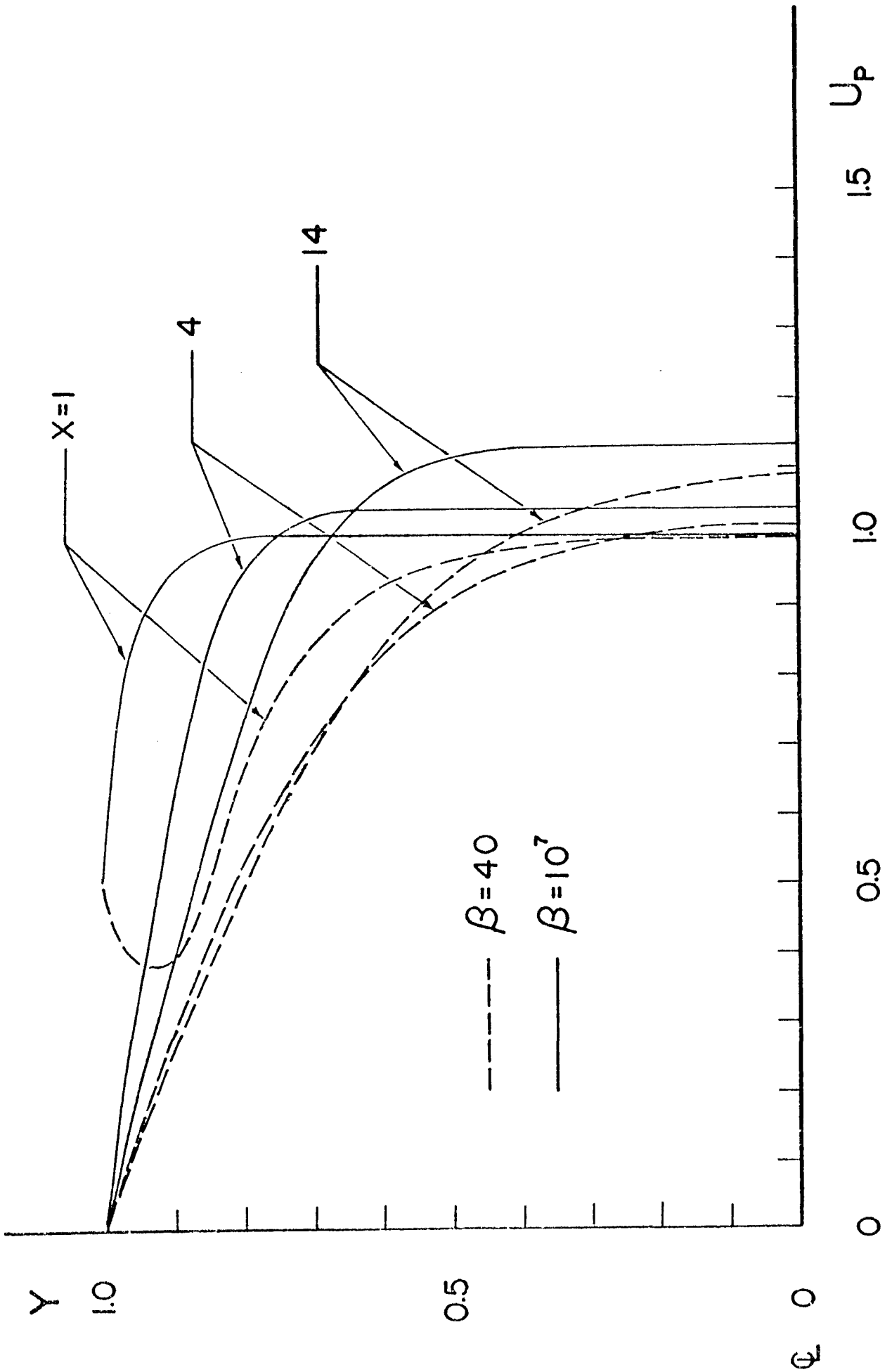

FIG. 3.9 EFFECT OF DIFFUSIVE PECLET NUMBER (β) ON AXIAL VELOCITY DISTRIBUTION OF PARTICLES WITH NO DEPOSITION IN A CHANNEL FLOW

(K_{np}= 0.0001, N_m= 2, N_R= 1000, α = 0, σ = 0.5, $\sigma_w\lambda$ = 0, σ_w' = 0)

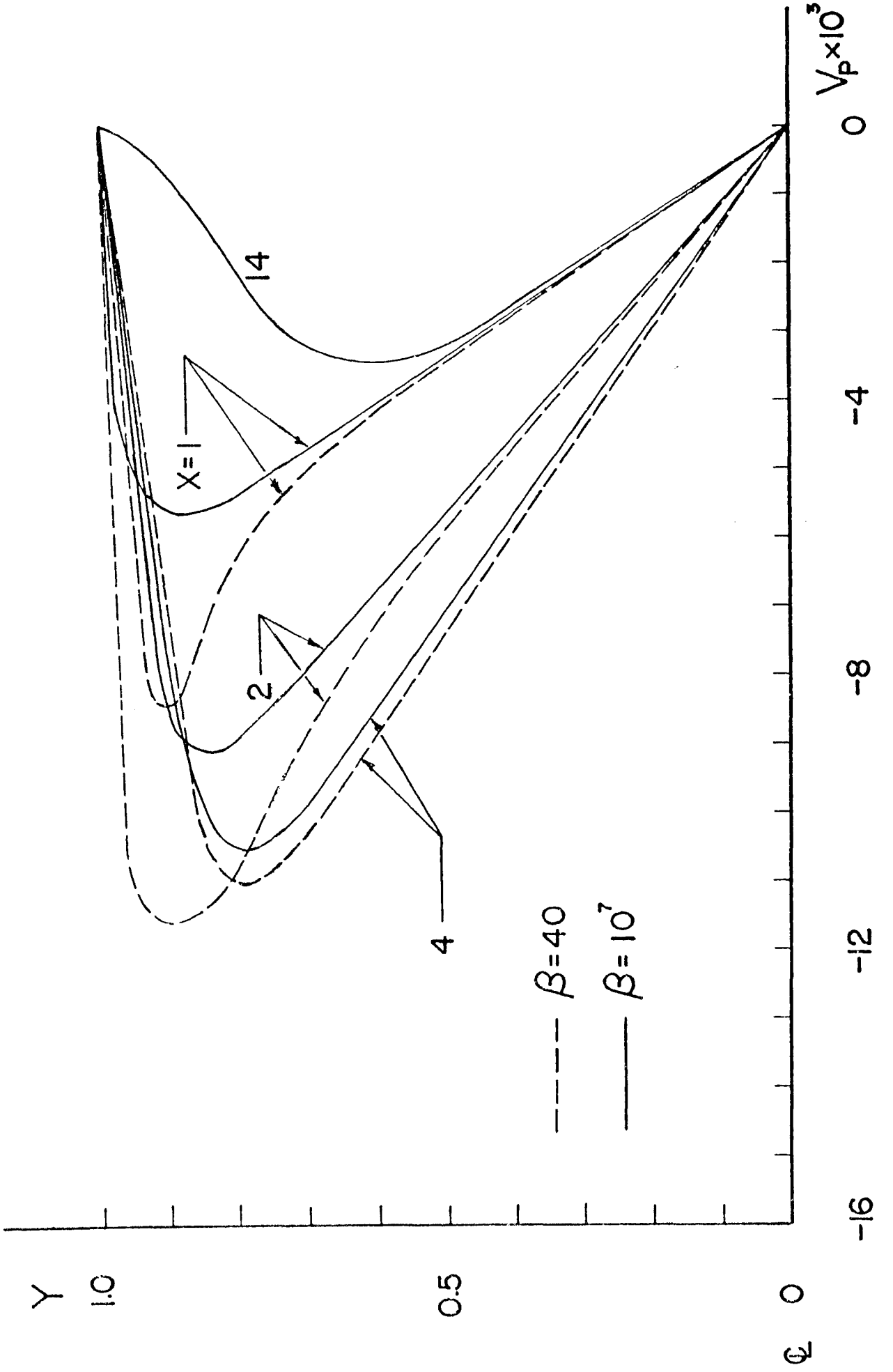

FIG. 3.10 EFFECT OF DIFFUSIVE PECLET NUMBER ON VERTICAL VELOCITY DISTRIBUTION OF PARTICLES WITH NO DEPOSITION IN A CHANNEL FLOW

($K_{np} = 0.0001$, $N_m = 2$, $N_R = 1000$, $\alpha = 0$, $\sigma = 0.5$, $\sigma_w' = 0$, $\sigma_w = 0$).

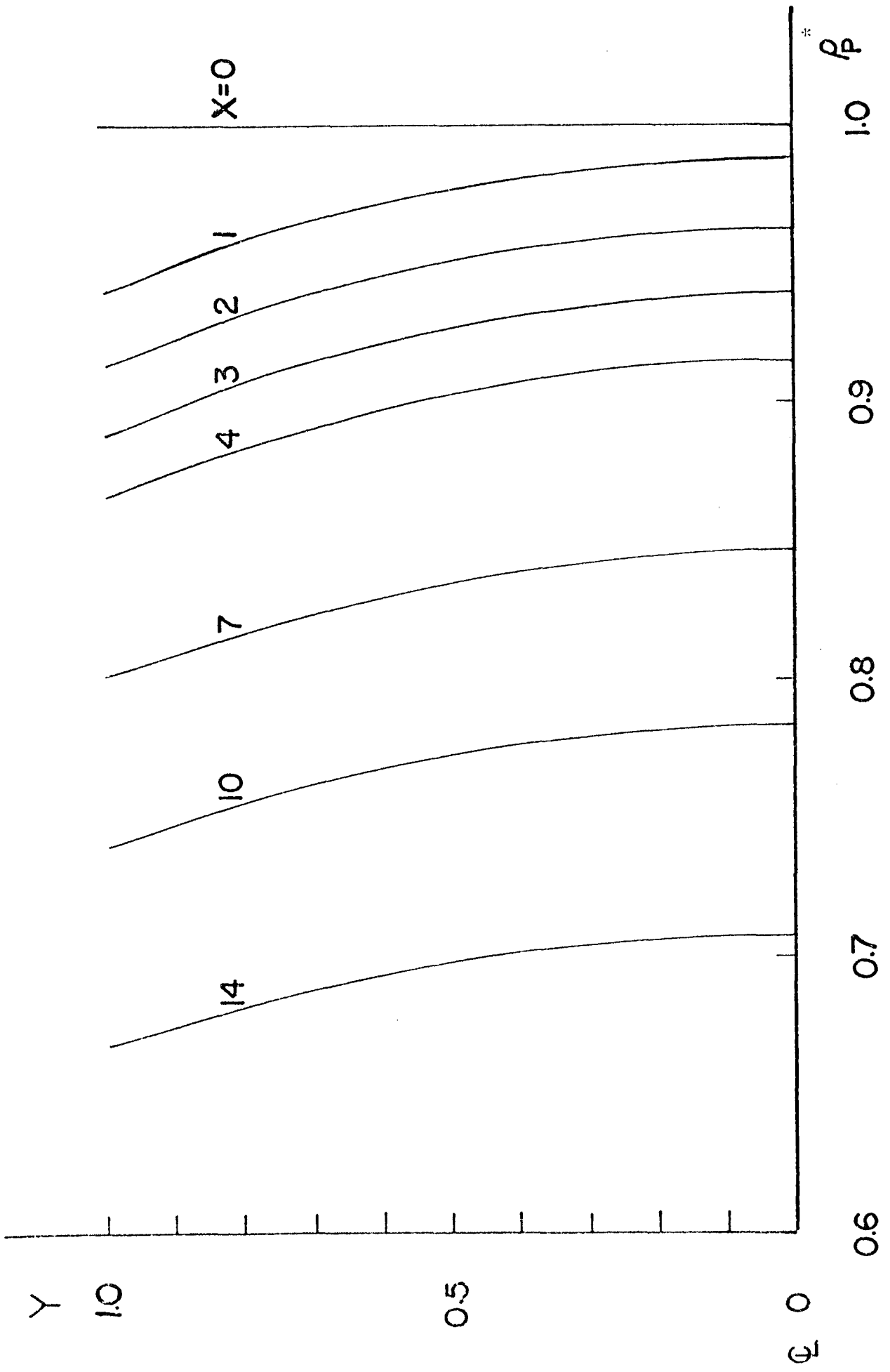

FIG. 3.11 DISTRIBUTION OF PARTICLE CONCENTRATION DUE TO ADHESION ONLY WITH VERY LOW DIFFUSIVE PECLET NUMBER IN A CHANNEL FLOW

(K_{np}= 0.0001, N_m= 2, N_R= 1000, α = 0, β = 4, σ = 0.5, $\sigma_w\lambda$= 0.1, σ_w'= 0)

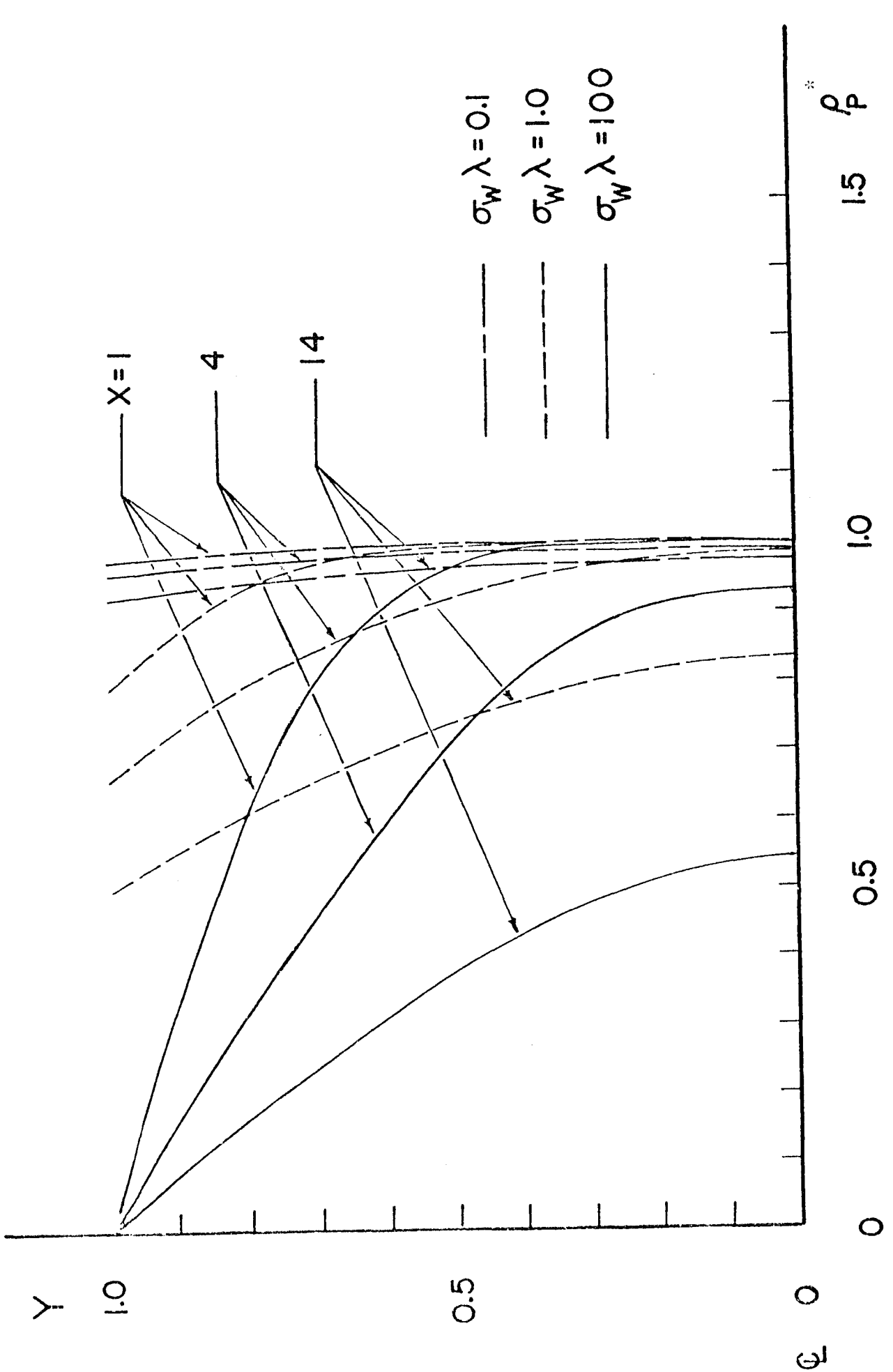

FIG. 3.12 EFFECT OF SURFACE ADHESION ON PARTICLE CONCENTRATION WITH LOW DIFFUSIVE PECLET NUMBER IN A CHANNEL FLOW

(K_{np}= 0.0001, N_m= 2, N_R= 1000, α = 0, β = 40, σ = 0.5, σ_w' = 0)

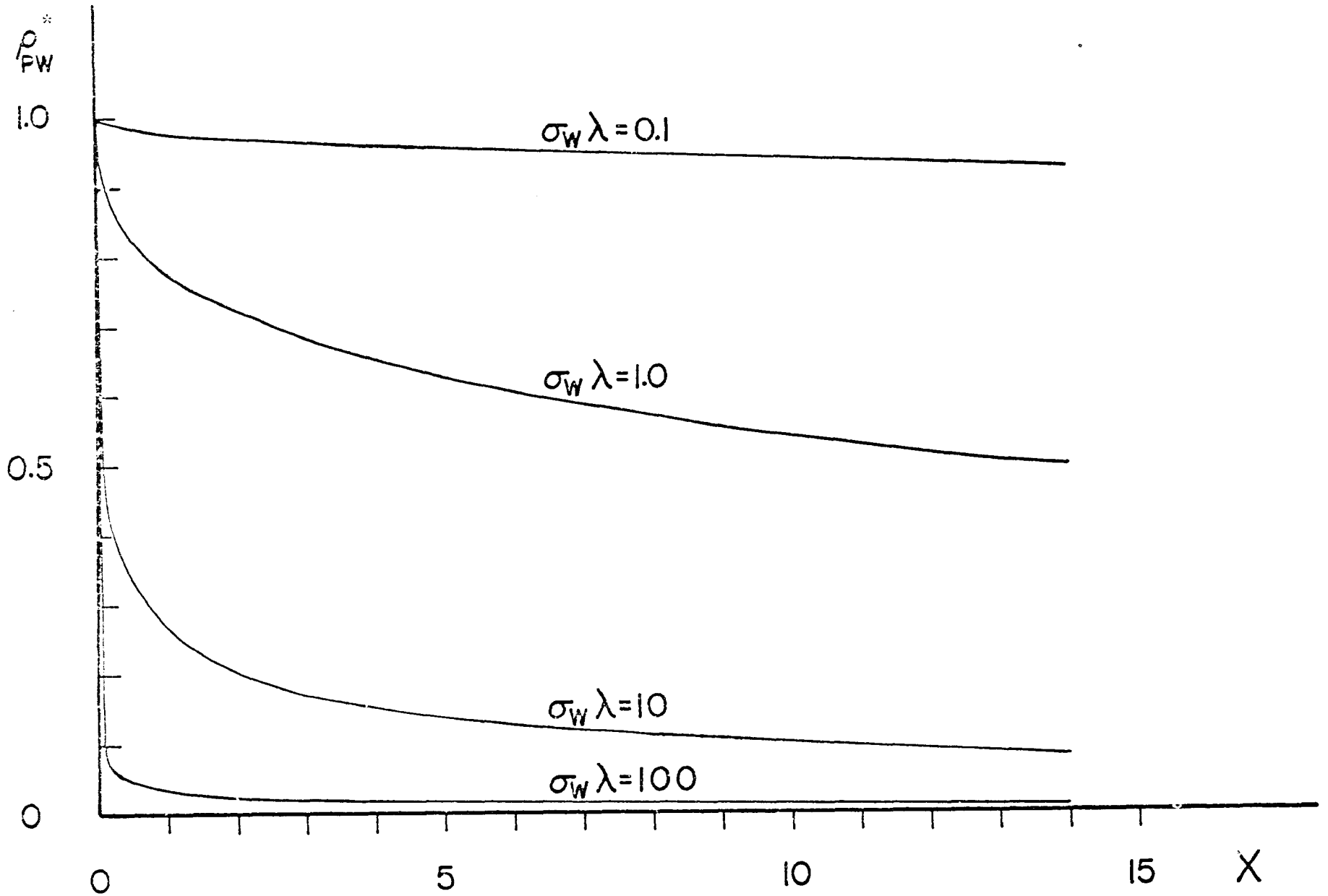

FIG. 3.13 EFFECT OF SURFACE-ADHESION ON AXIAL DISTRIBUTION OF PARTICLE CONCENTRATION AT WALL IN CASE OF ADHESION ONLY AND LOW DIFFUSIVE PECLET NUMBER IN A CHANNEL FLOW

(K_{np} = 0.0001, N_m = 2, N_R = 1000, α = 0, β = 40, σ = 0.5, σ_w' = 0)

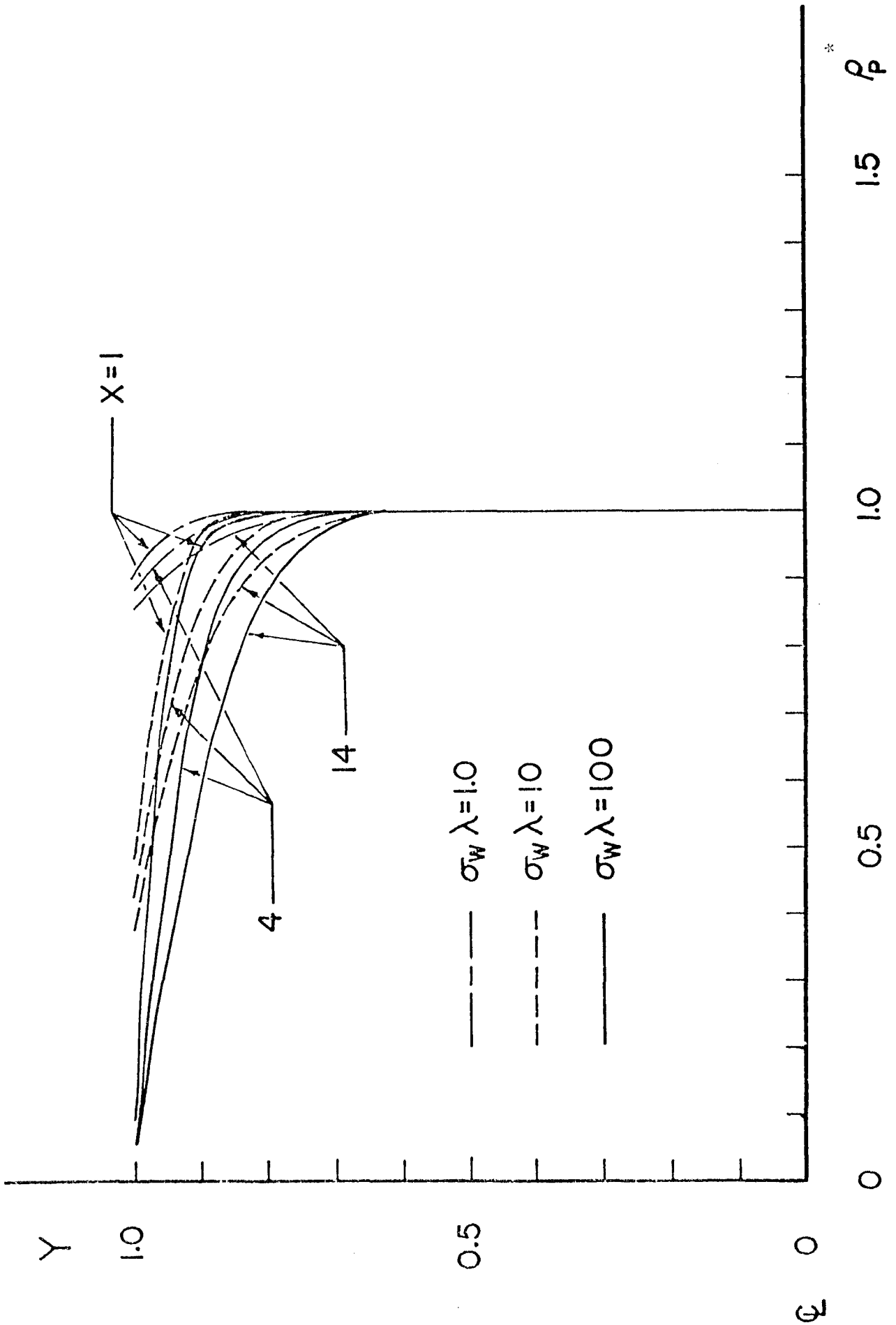

FIG. 3.14 EFFECT OF SURFACE ADHESION ON PARTICLE CONCENTRATION WITH HIGH DIFFUSIVE PECLET NUMBER IN A CHANNEL FLOW

($K_{np} = 0.0001$, $N_m = 2$, $N_R = 1000$, $\alpha = 0$, $\beta = 10^7$, $\sigma = 0.5$, $\sigma_w' = 0$)

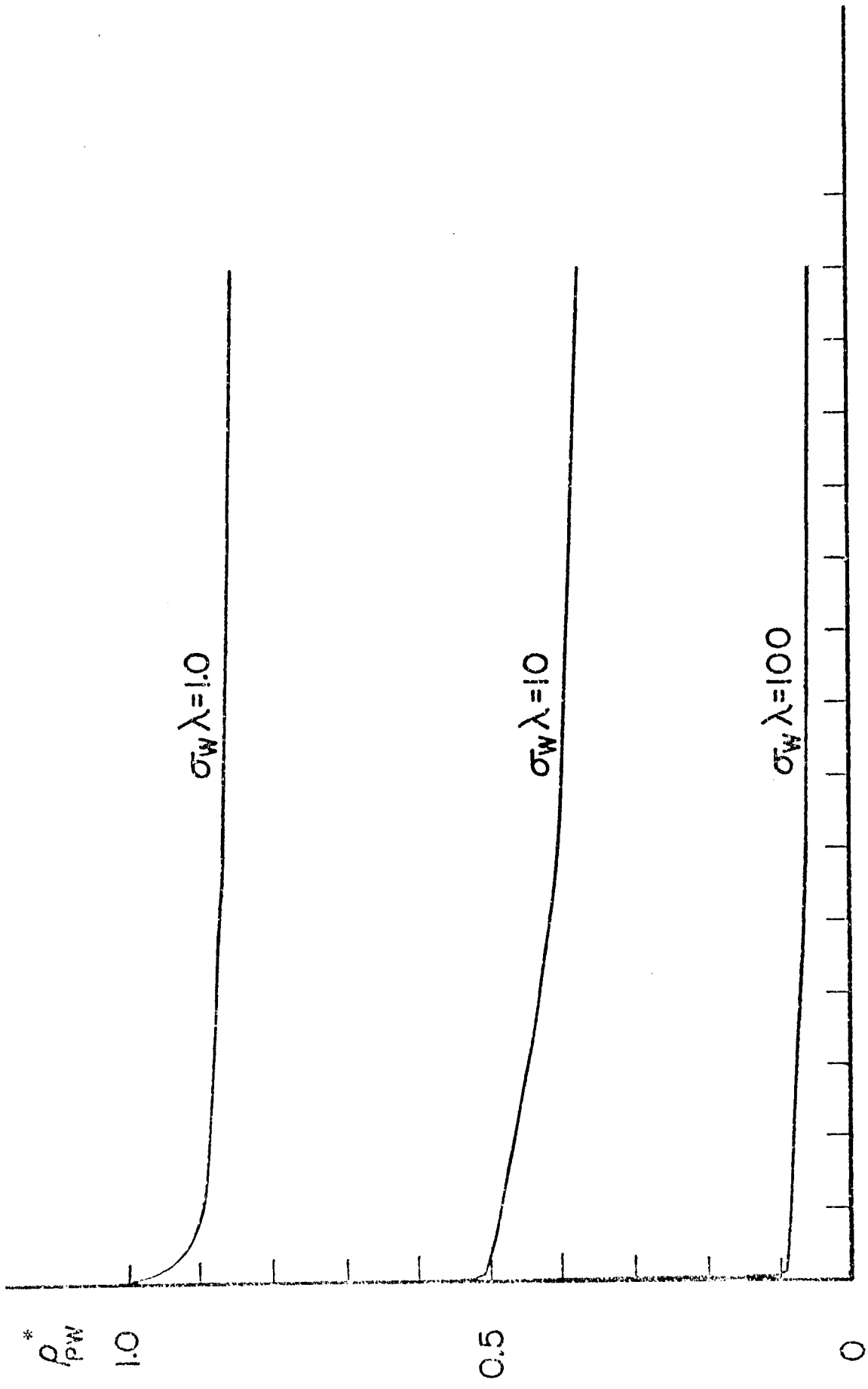

FIG. 3.15 EFFECT OF SURFACE ADHESION ON AXIAL DISTRIBUTION OF PARTICLE CONCENTRATION AT WALL IN CASE OF ADHESION ONLY AND HIGH DIFFUSIVE PECLET NUMBER IN A CHANNEL FLOW
(K_{np} = 0.0001, N_m = 2, N_R = 1000, α = 0, β = 10^7, σ = 0.5, σ_w = 0)

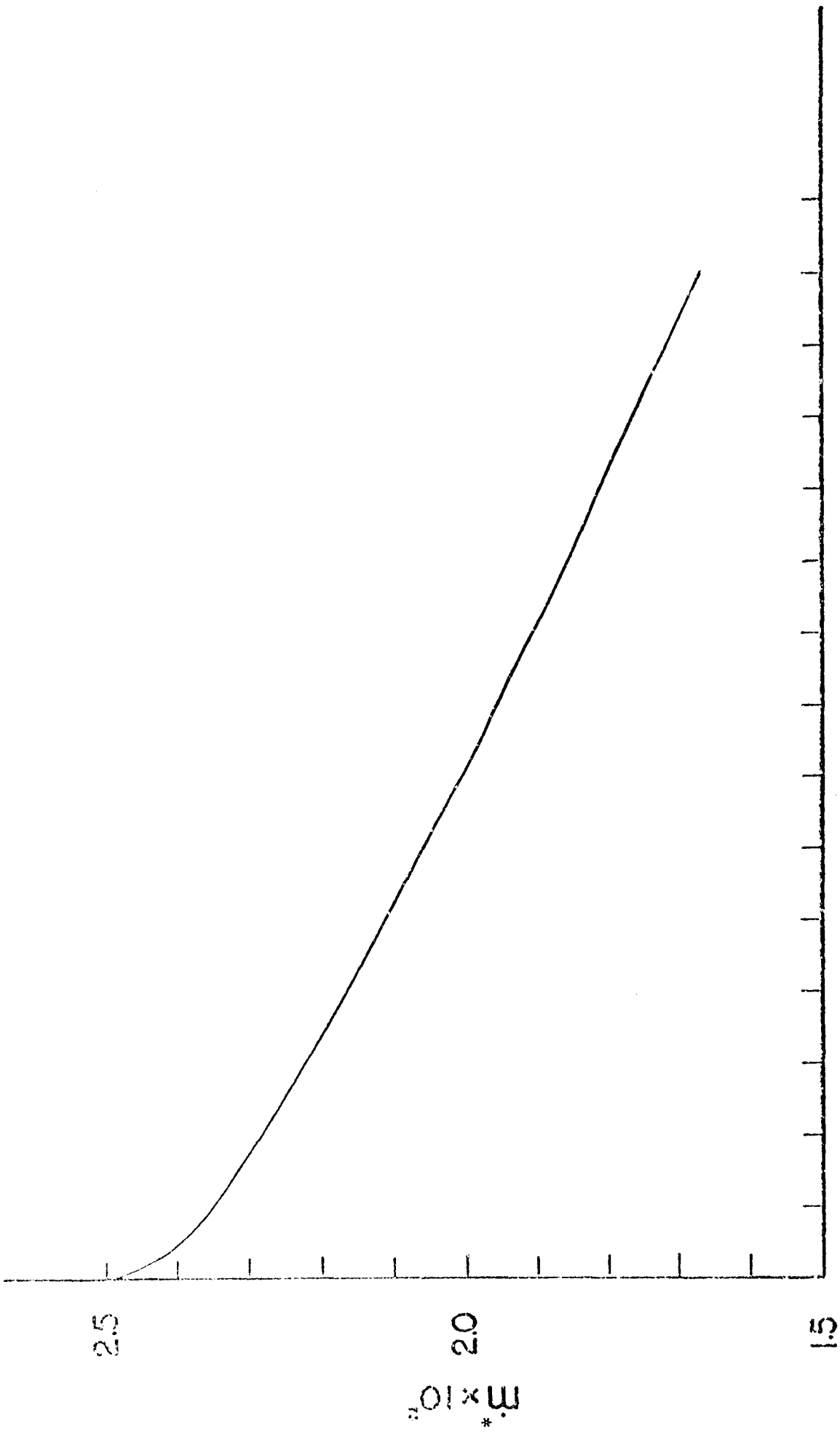

FIG. 3.16 AXIAL DISTRIBUTION OF RATE OF DEPOSITION OF PARTICLES DUE TO ADHESION ONLY ($\sigma_w^2 = 0.1$) WITH VERY LOW DIFFUSIVE PECLET NUMBER IN A CHANNEL FLOW

($K_{np} = 0.0001$, $N_m = 2$, $N_R = 1000$, $\alpha = 0$, $\beta = 4$, $\sigma = 0.5$, $\sigma_w' = 0$)

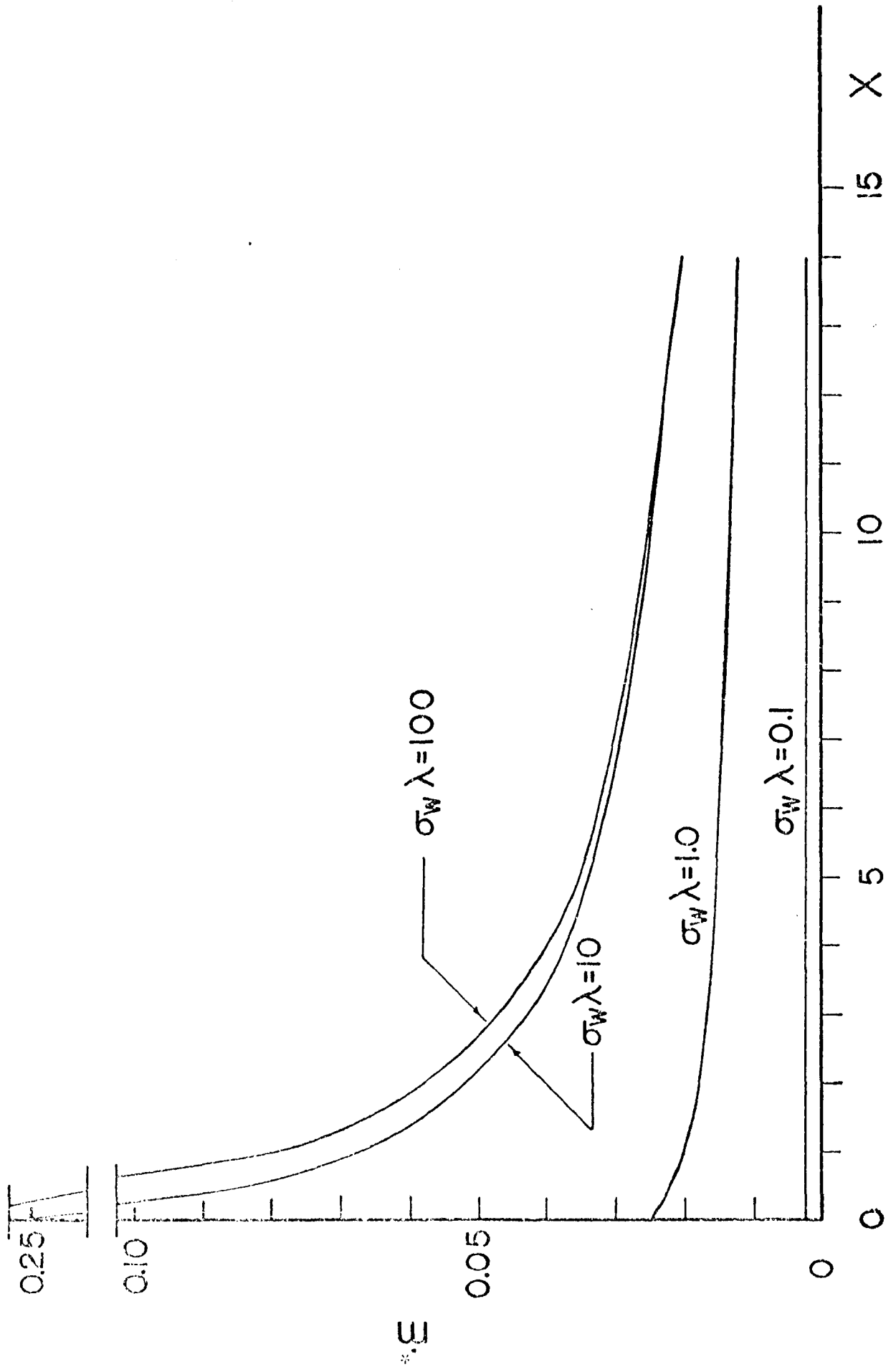

FIG. 3.17 EFFECT OF SURFACE ADHESION ON RATE OF DISPOSITION DUE TO ADHESION ONLY WITH LOW DIFFUSIVE PECLET NUMBER IN A CHANNEL FLOW

(K_{np} = 0.0001, N_m = 2, N_R = 1000, α = 0, β = 40, σ = 0.5, σ_w' = 0)

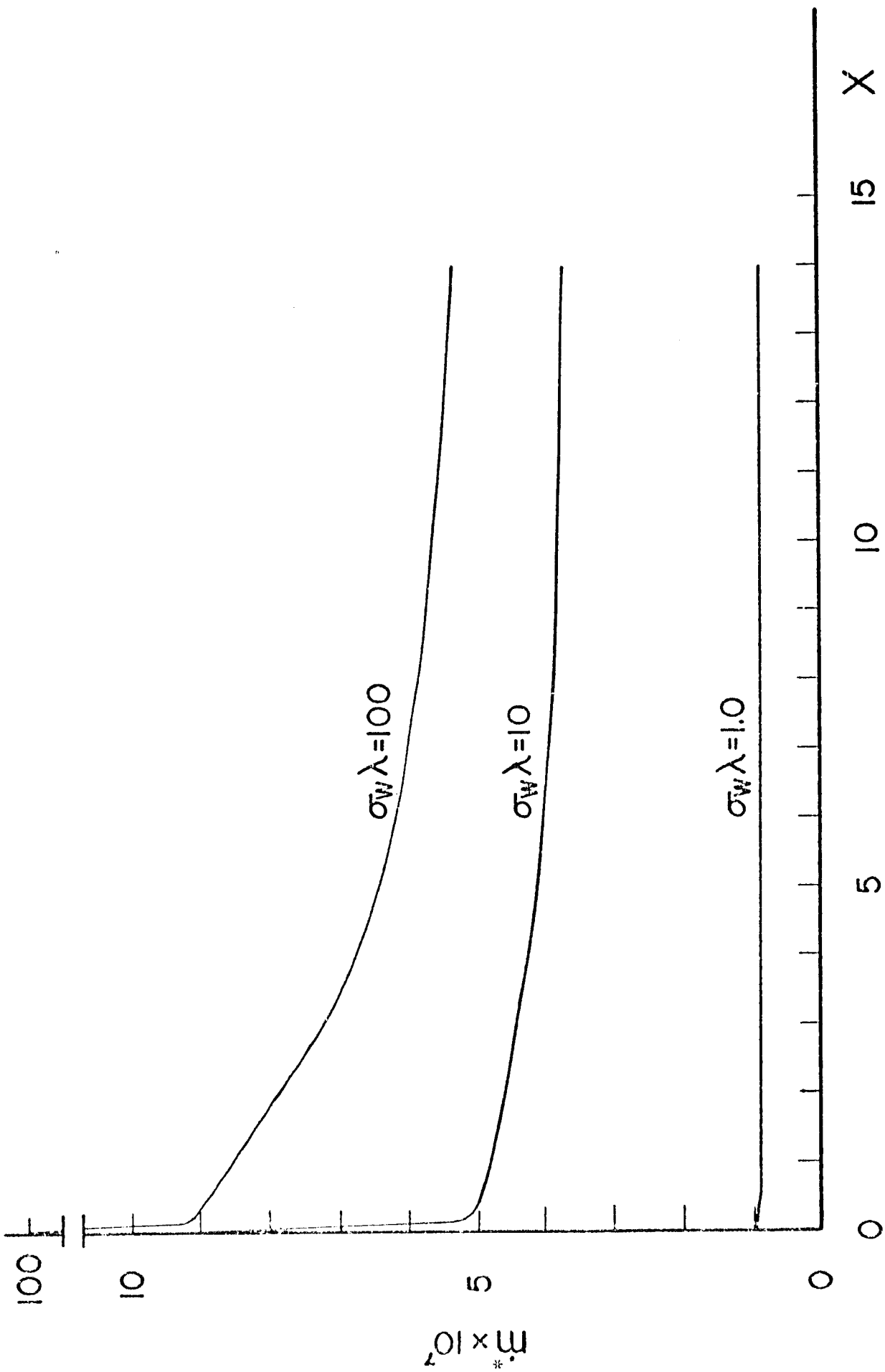

FIG. 3.18 EFFECT OF SURFACE ADHESION ON RATE OF DEPOSITION DUE TO ADHESION ONLY WITH HIGH DIFFUSIVE PECLET NUMBER IN A CHANNEL FLOW

(K_{np} = 0.0001, N_m = 2, N_R = 1000 α = 0 $\beta = 10^7$. σ = 0.5 σ_w' = 0)

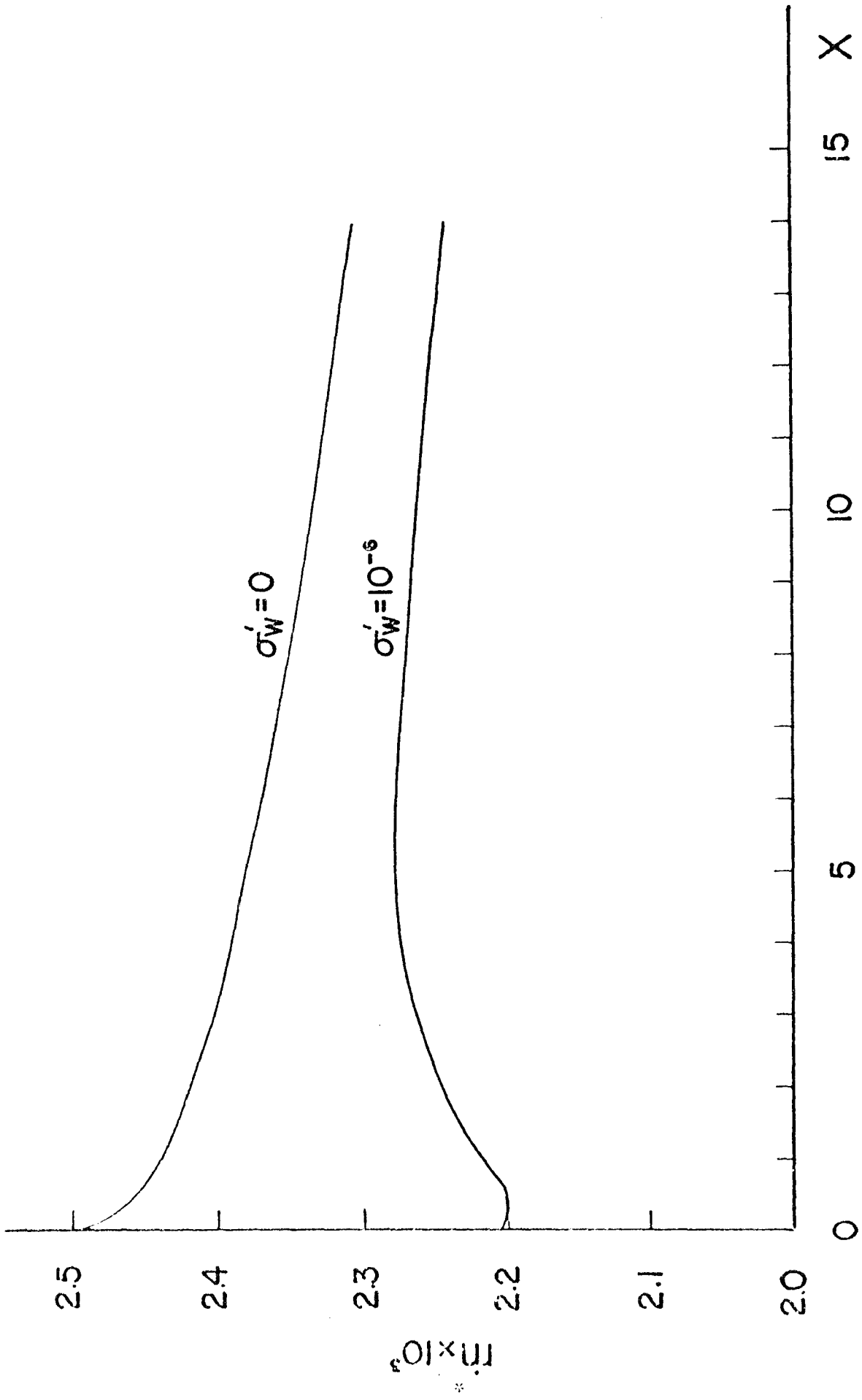

FIG. 3.19 EFFECT OF LIFT FORCES AT WALL ON RATE OF DEPOSITION OF PARTICLES IN CASE OF NO ELECTRIC CHARGE IN A CHANNEL FLOW

($K_{mp} = 0.0001$, $K_m = 2$, $K_R = 1000$, $R^* = 0.002$, $\alpha = 0$, $\beta = 40$, $\sigma = 0.5$, $\sigma_w^\lambda = 0.1$, $\rho_R = 300$, $\rho_{pb}^* = 0.3$)

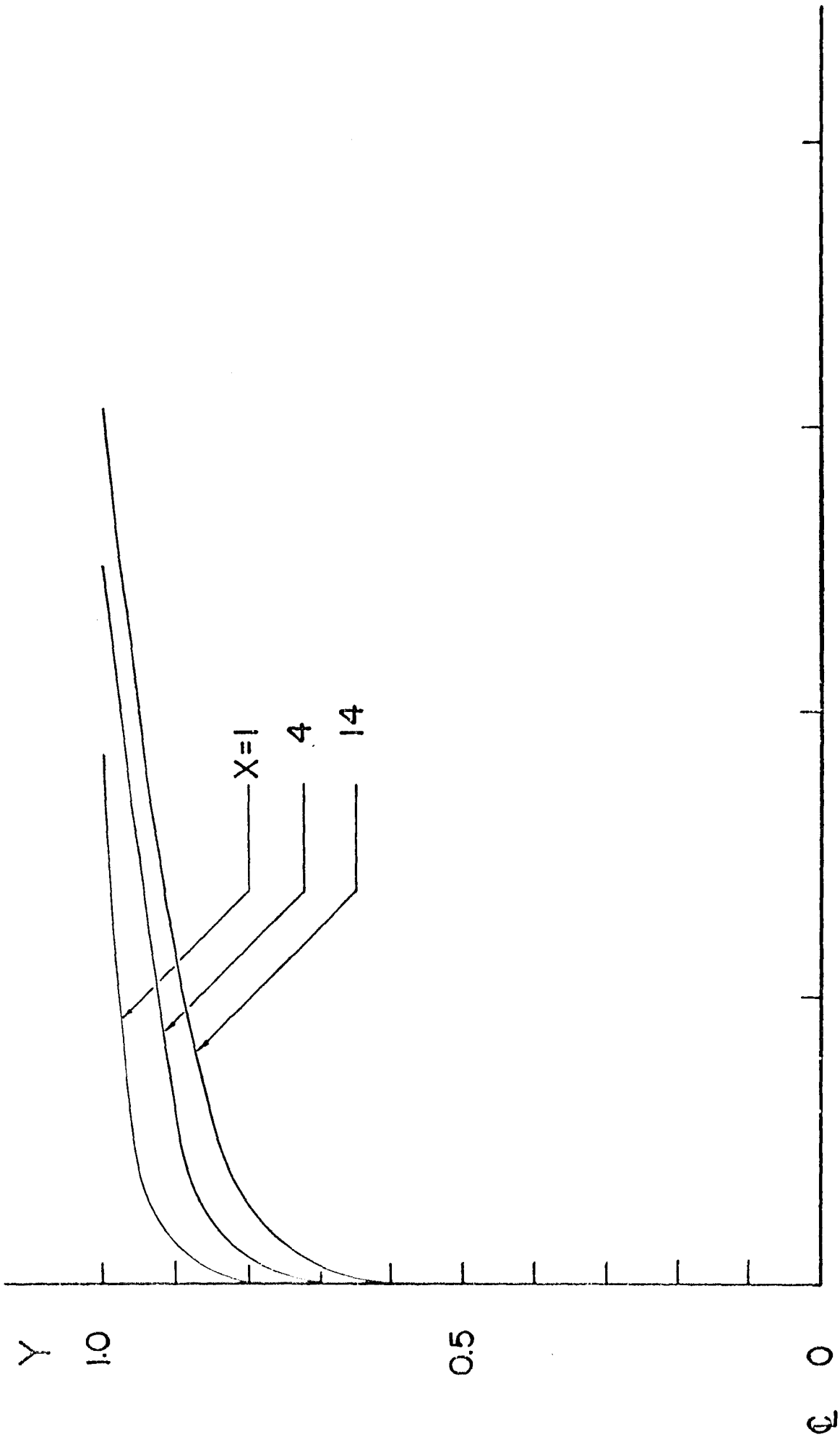

FIG. 5.20 DISTRIBUTION OF PARTICLE CONCENTRATION DUE TO ELECTRIC CHARGE ONLY IN A CHANNEL FLOW

($K_{np} = 0.0001$, $K_m = 2$, $N_R = 1000$, $\delta = 1.0$, $\delta = 10^7$, $\sigma = 0.5$, $\sigma_w^\lambda = 0$, $\sigma_w = 0$)

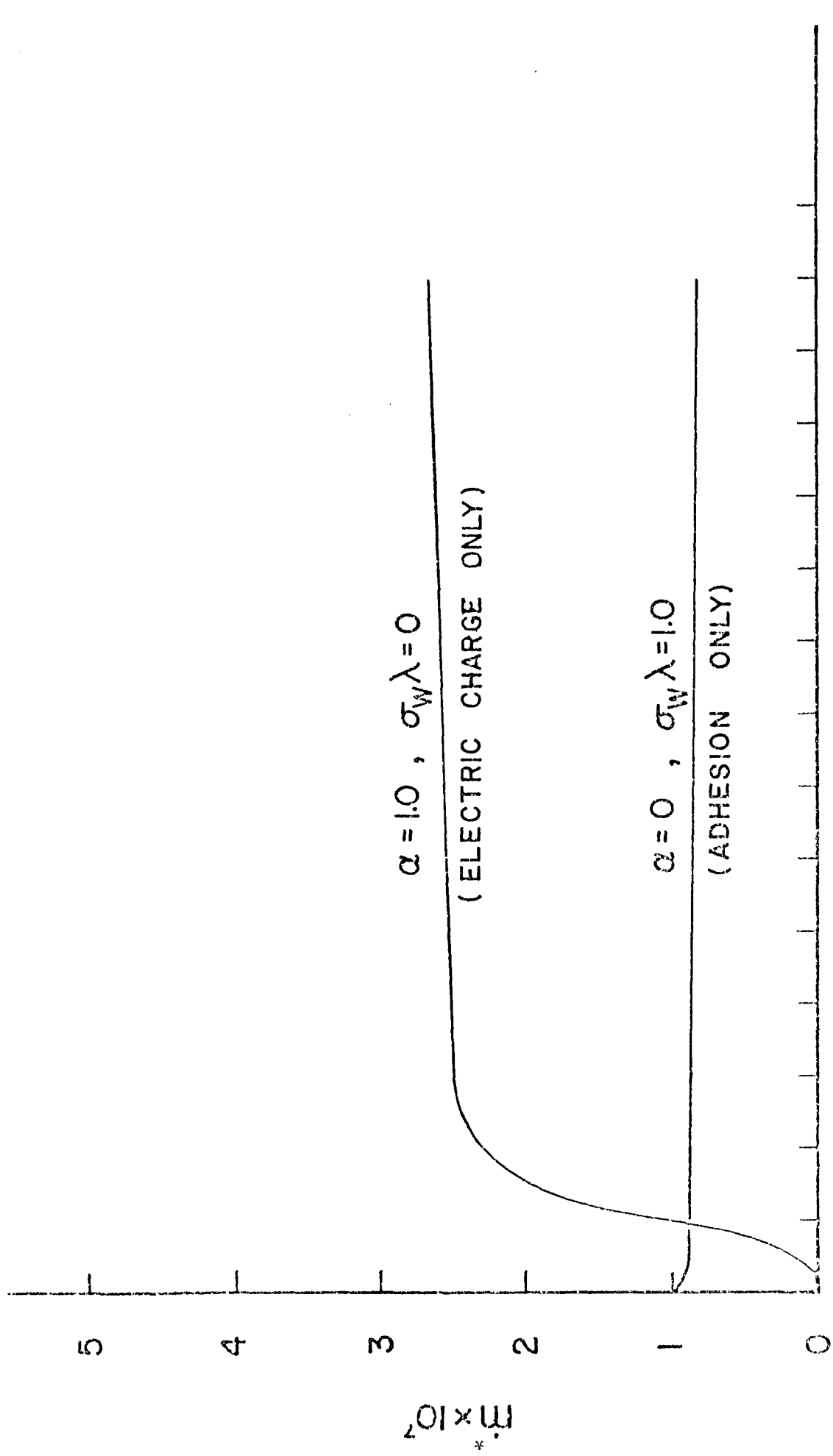

FIG. 3.21 EFFECT OF ELECTROSTATIC CHARGE AND SURFACE ADHESION ON AXIAL DISTRIBUTION OF RATE OF DEPOSITION OF PARTICLES IN A CHANNEL FLOW

($K_{np} = 0.0001$, $N_m = 2$, $N_R = 1000$, $\beta = 10^7$, $\sigma = 0.5$, $\sigma_w' = 0$)

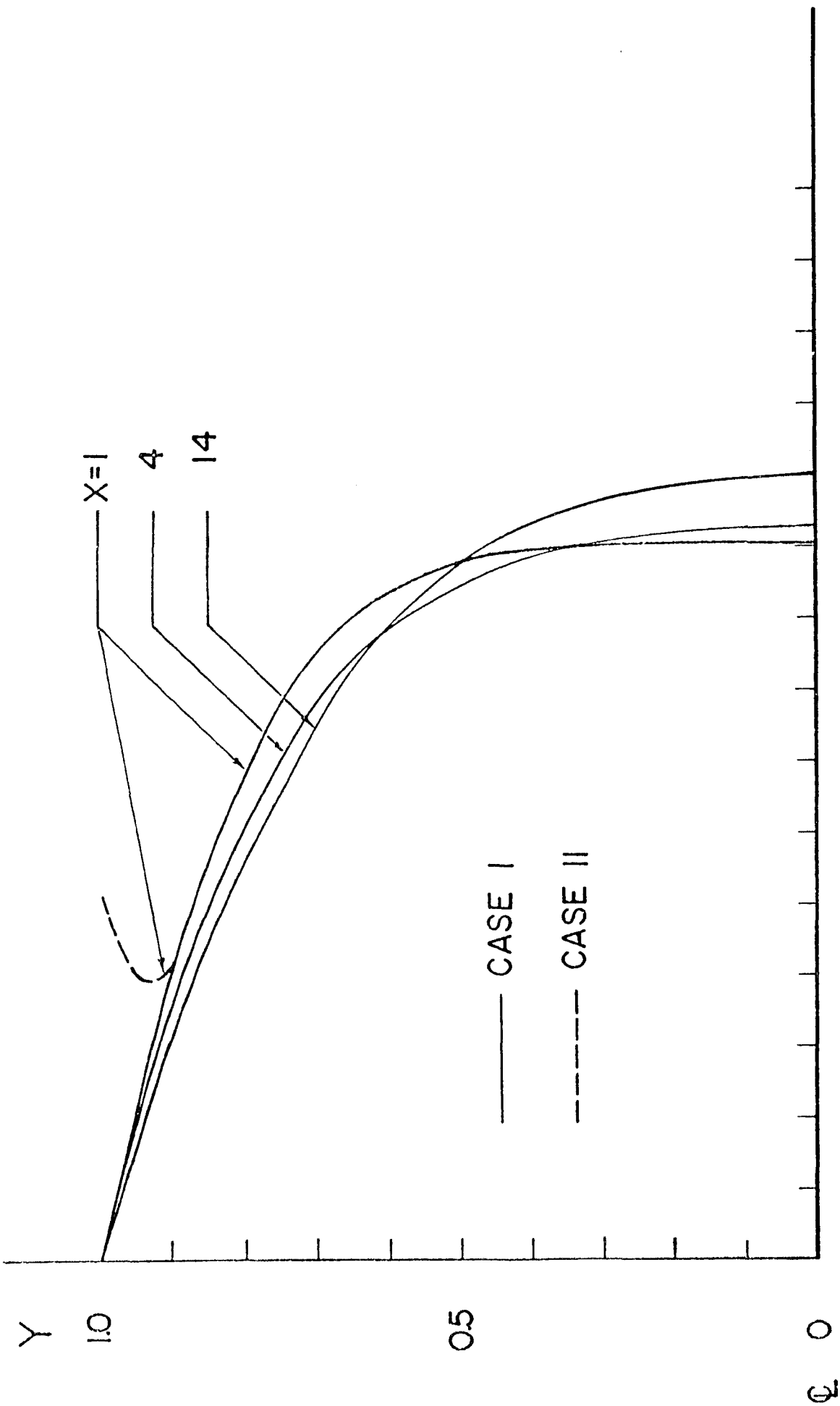

FIG. 3.22 COMPARISON OF AXIAL VELOCITY DISTRIBUTION OF PARTICLES IN CASES I & II IN A CHANNEL FLOW

($K_{pp} = 0.0001$, $N_m = 2$, $N_R = 1000$, $R^* = 0.002$, $\alpha = 1.0$, $\beta = 40$, $\sigma = 0.5$, $\sigma_w = 0.1$, $\sigma_w' = 10^{-6}$, $\sigma_R = 300$, $\sigma_{pb}^* = 0.3$)

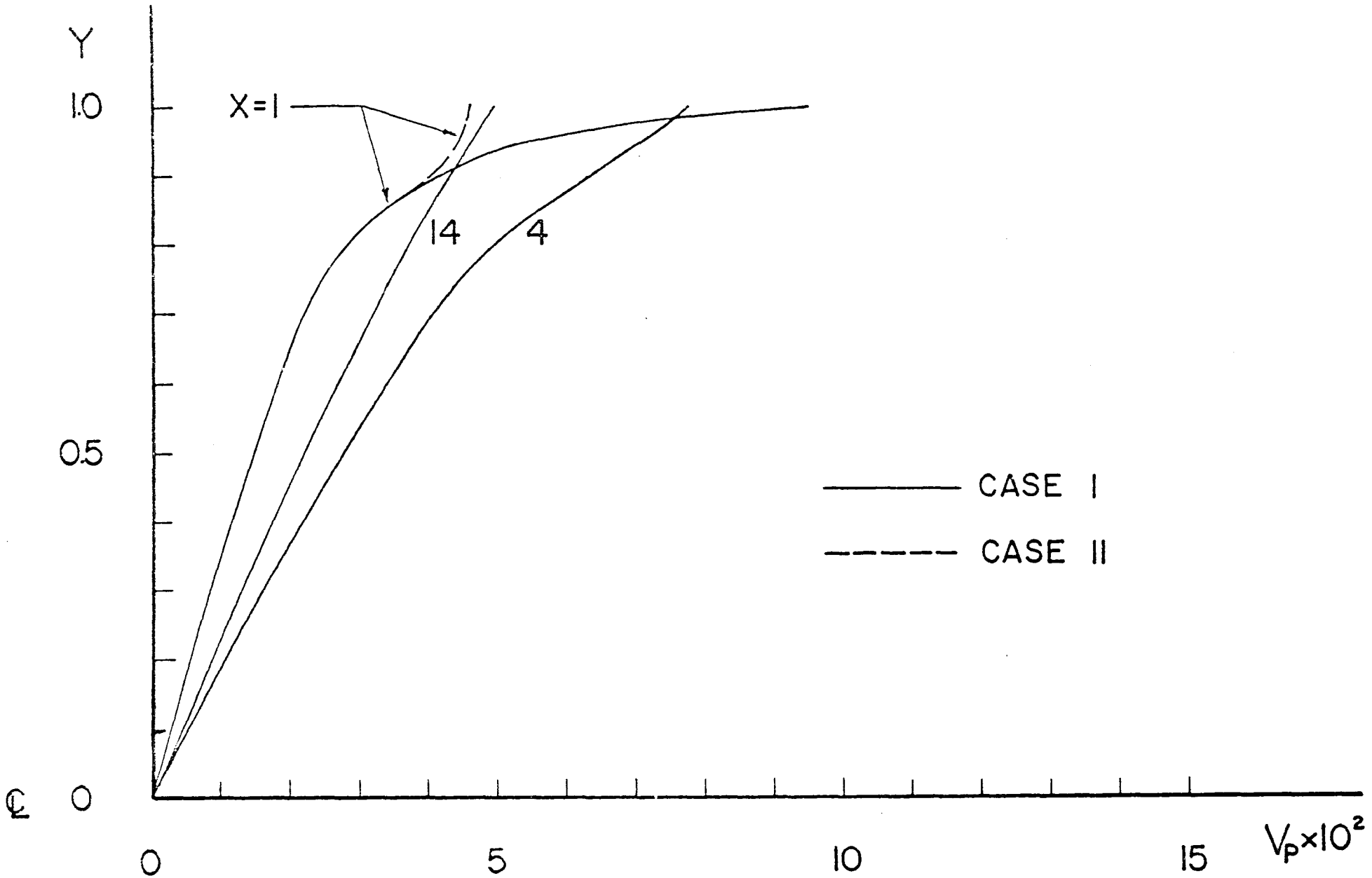

FIG. 3.23 COMPARISON OF VERTICAL VELOCITY DISTRIBUTION OF PARTICLES IN CASES I & II IN A CHANNEL FLOW

(K_{np} = 0.0001, N_m = 2, N_R = 1000, R^* = 0.002, α = 1.0, β = 40, σ = 0.5, σ_w/λ = 0.1, σ_w' = 10^{-6}, ρ_R = 300, ρ_{pb}^* = 0.3)

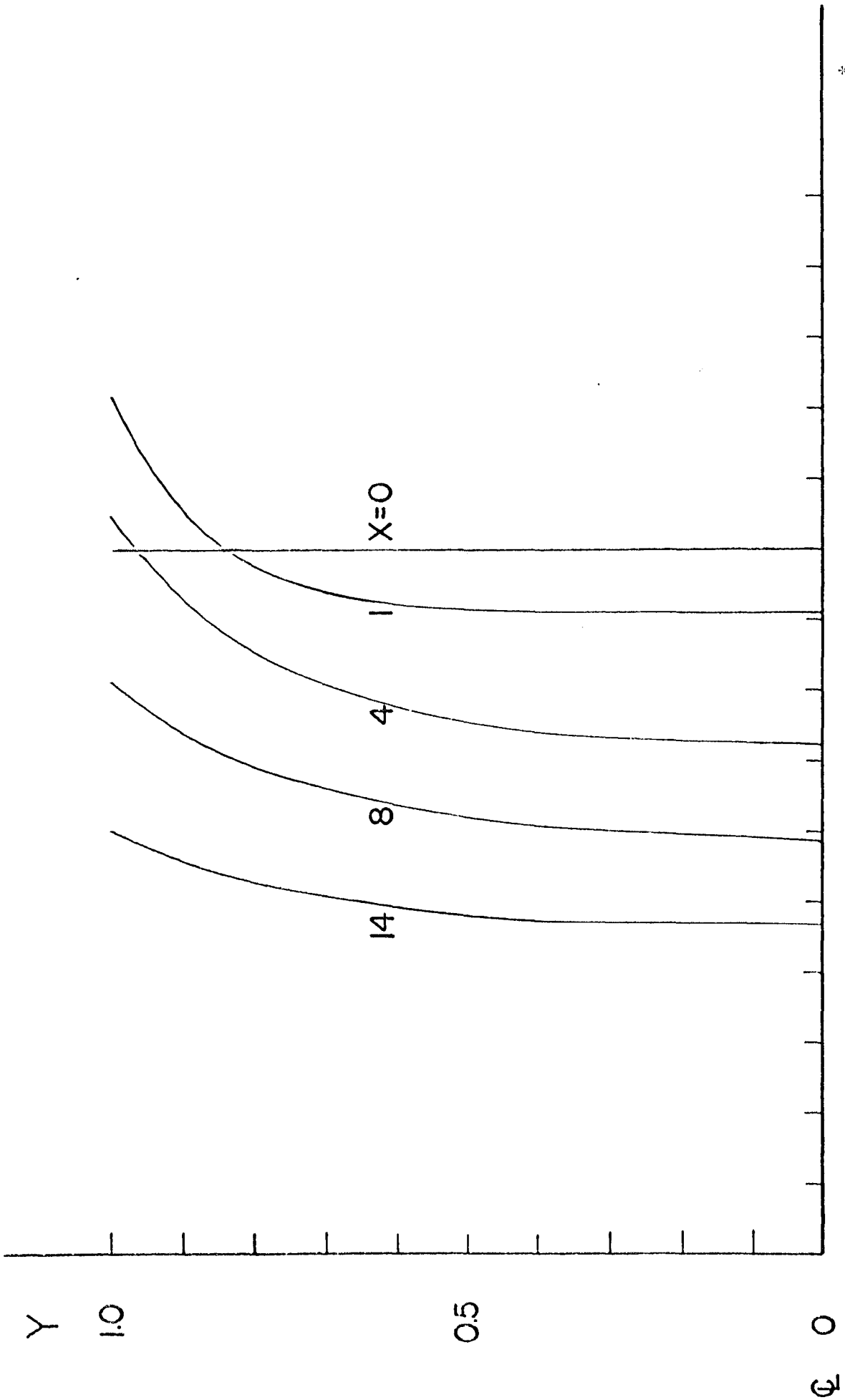

FIG. 3.24 PARTICLE CLOUD DENSITY DISTRIBUTION (CONCENTRATION) IN CASES I & II IN A CHANNEL FLOW

(κ_{np} = 0.0001, κ_m = 2, N_R = 1000, R^* = 0.002, α = 1.0, β = 40, σ = 0.5, σ_w' = 0.1, σ_w = 10^{-6}, σ_R = 300, σ_{pb}^* = 0.3)

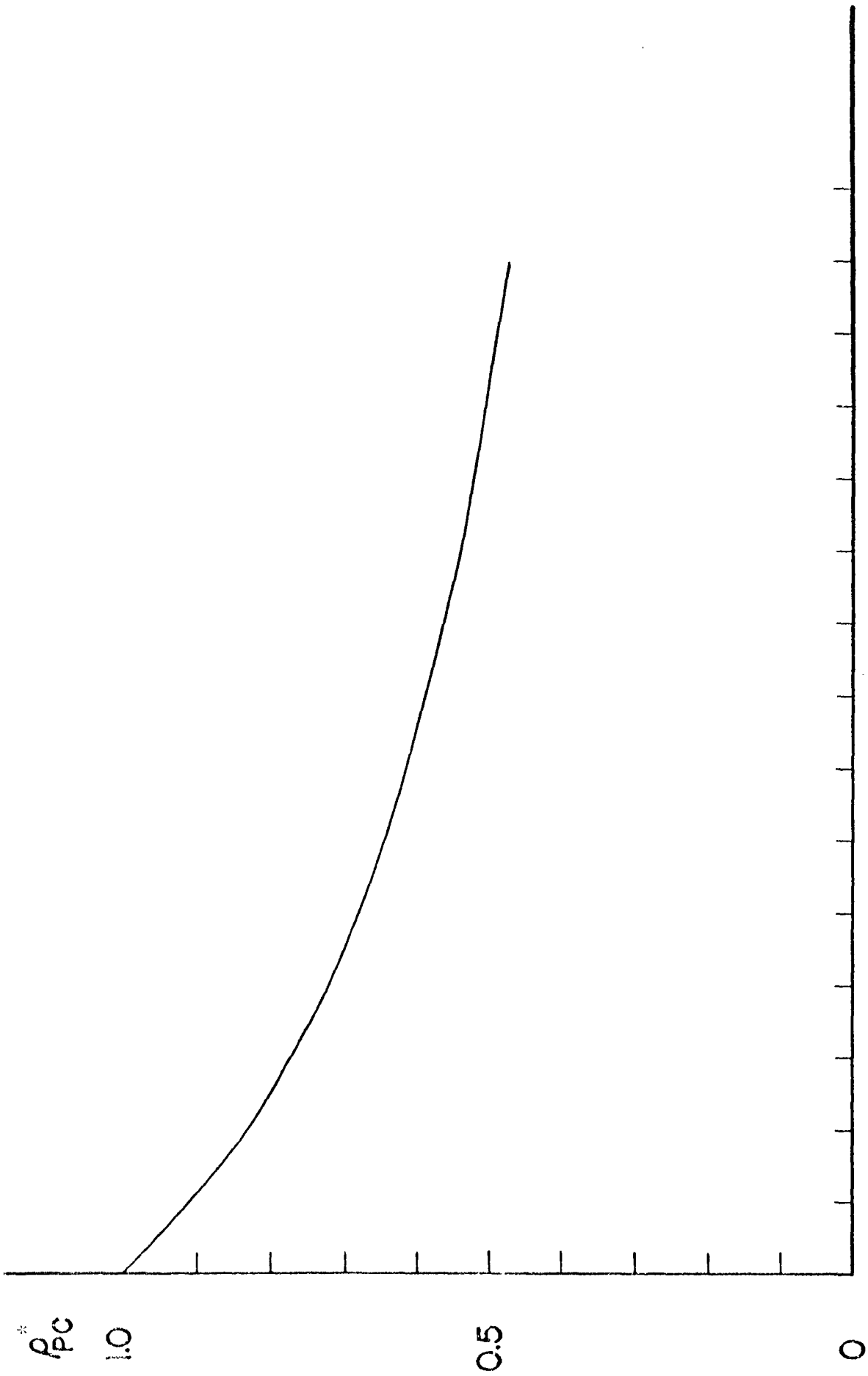

FIG. 3.25 AXIAL DISTRIBUTION OF PARTICLE CONCENTRATION AT CHANNEL CENTERLINE IN CASES I & II IN A CHANNEL FLOW

(K_{np} = 0.0001, N_m = 2, N_R = 1000, R^* = 0.002, α = 1.0, β = 40, σ = 0.5, σ_w = 0.1, σ_w' = 10^{-6}, ρ_R = 300, ρ_{pb}^* = 0.3)

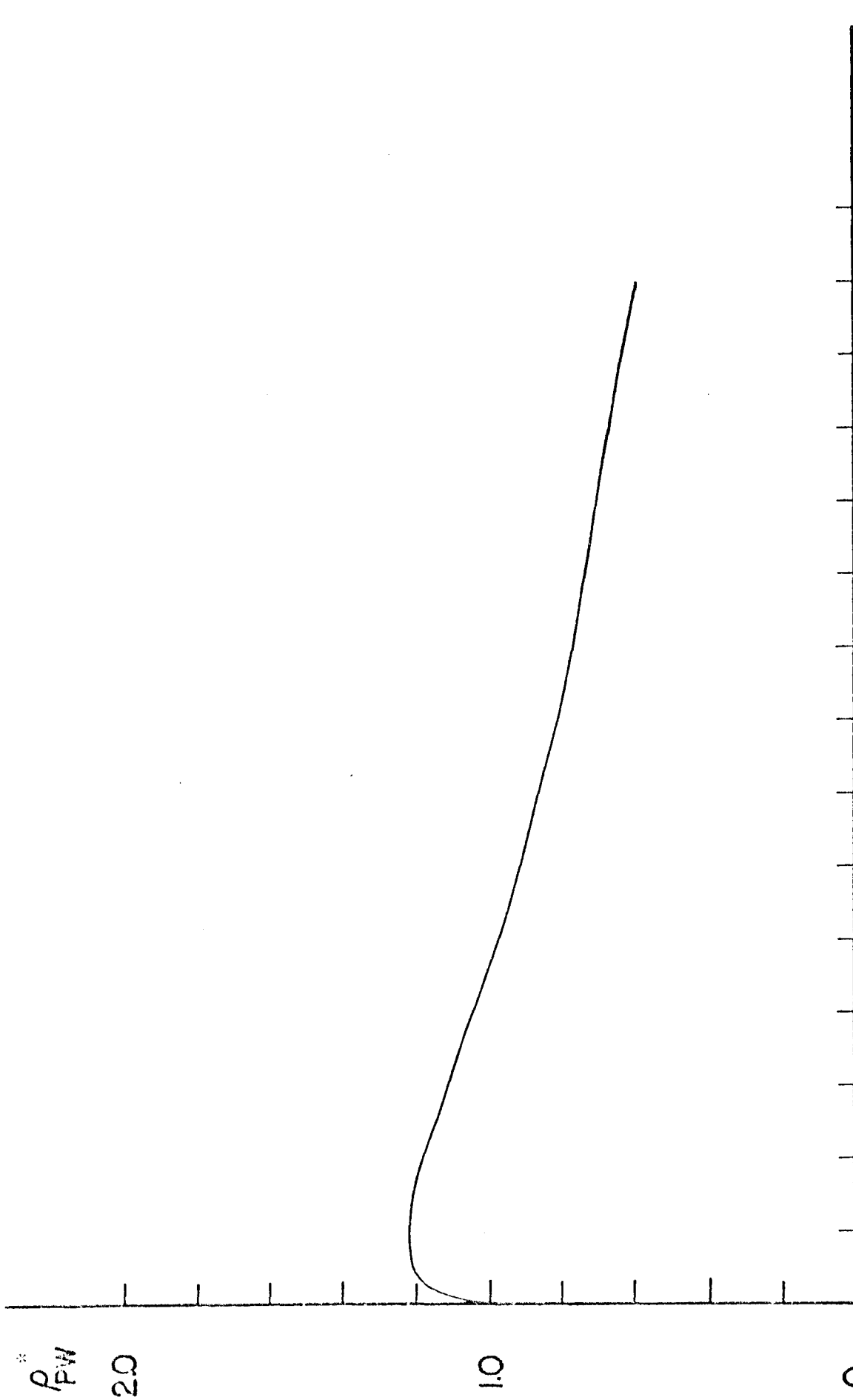

FIG. 3.26 AXIAL DISTRIBUTION OF PARTICLE CONCENTRATION AT WALL IN CASES I & II IN A CHANNEL FLOW

(K_{np} = 0.0001, K_m = 2, K_R = 1000, R^* = 0.002, α = 1.0, β = 40, σ = 0.5, $\sigma_W\lambda$ = 0.1, $\sigma'_W = 10^{-6}$, ρ_R = 300, ρ^*_{pb} = 0.3)

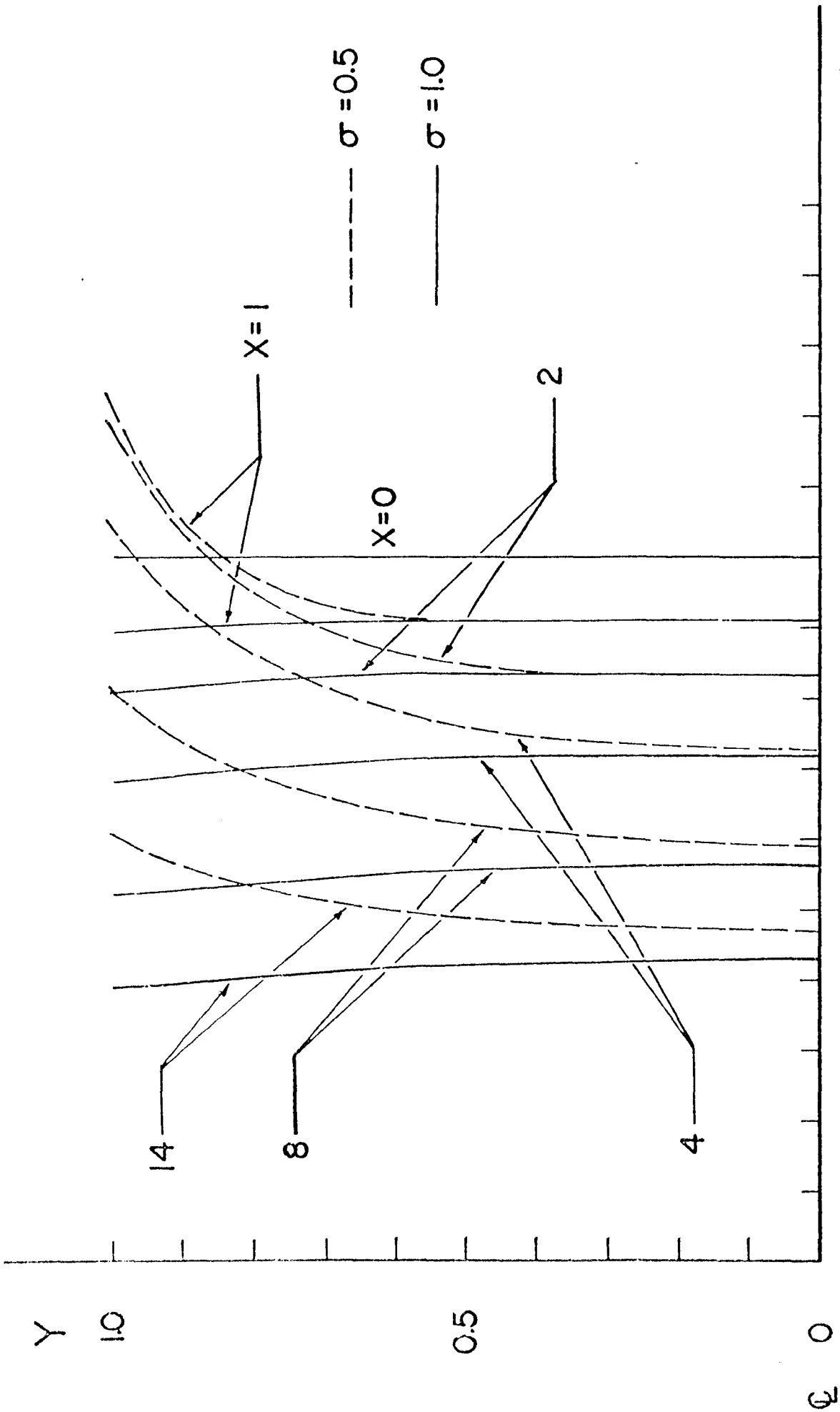

FIG. 3.27 EFFECT OF ELECTROVISCOUS-STICKING FACTOR (σ) ON PARTICLE CONCENTRATION IN CASES I & II IN A CHANNEL FLOW

(K_{hp} = 0.0001, N_m = 2, N_R = 1000, R^* = 0.002, α = 1.0, β = 40, $\sigma_w\lambda$ = 0.1, σ'_w = 10^{-6}, ρ_R = 300, ρ^*_{pb} = 0.3)

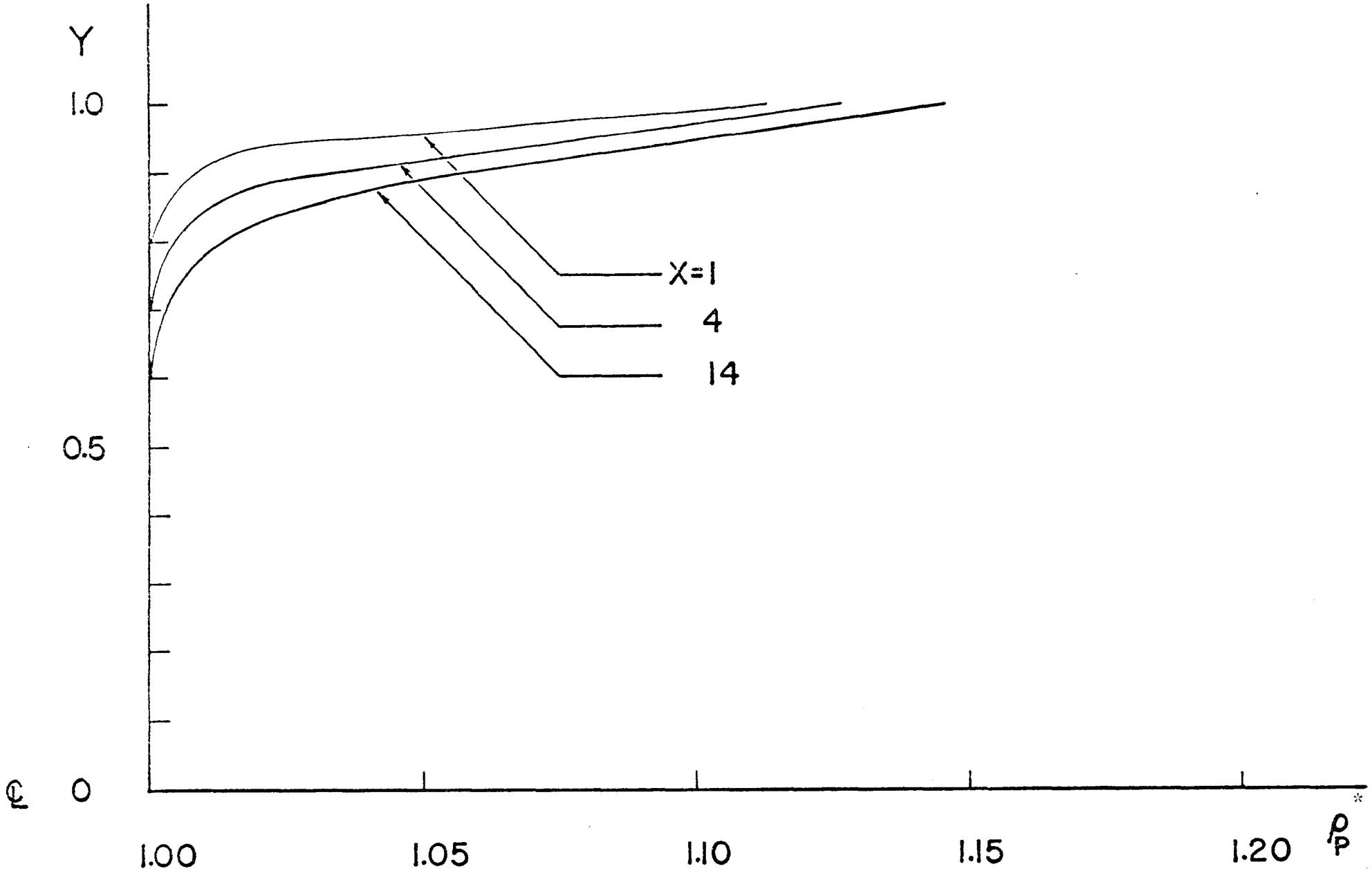

FIG. 3.28 DISTRIBUTION OF PARTICLE CONCENTRATION AT HIGH DIFFUSIVE PECLET NUMBER IN A CHANNEL FLOW

($K_{np} = 0.0001$, $N_m = 2$, $N_R = 1000$, $R^* = 0.002$, $\alpha = 1.0$, $\beta = 10^7$, $\sigma = 0.5$, $\sigma_w\lambda = 1.0$, $\sigma_w' = 10^{-10}$, $\rho_R = 300$, $\rho_{pb}^* = 0.3$)

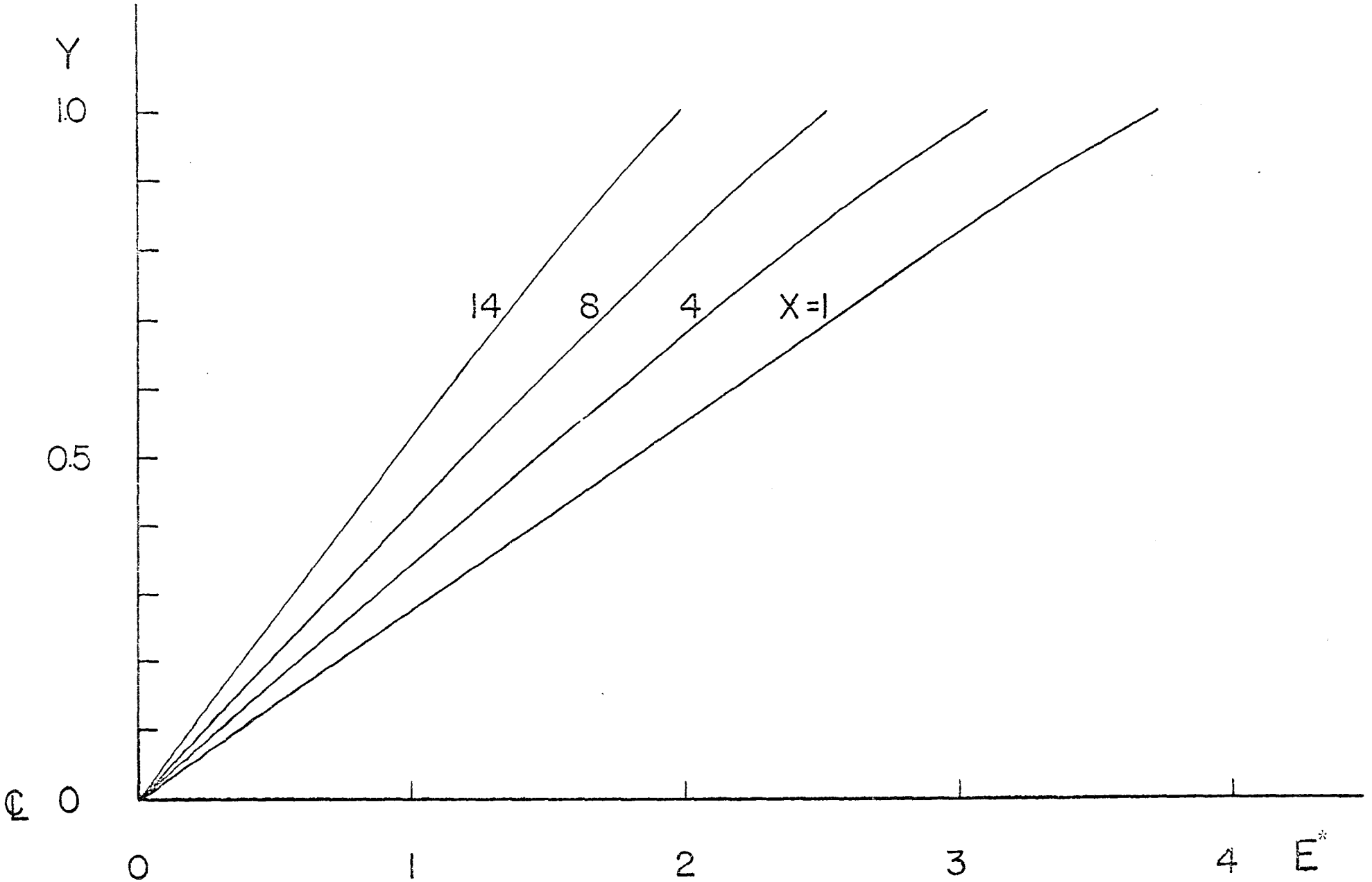

FIG. 3.29 DISTRIBUTION OF ELECTRIC FIELD INTENSITY IN CASES I & II WITH LOW DIFFUSIVE PECLET NUMBER

($K_{np} = 0.0001$, $N_m = 2$, $N_R = 1000$, $R^* = 0.002$, $\alpha = 1.0$, $\beta = 40$, $\sigma = 0.5$, $\sigma_w\lambda = 0.1$, $\sigma_w' = 10^{-6}$, $\rho_R = 300$, $\rho_{pb}^* = 0.3$)

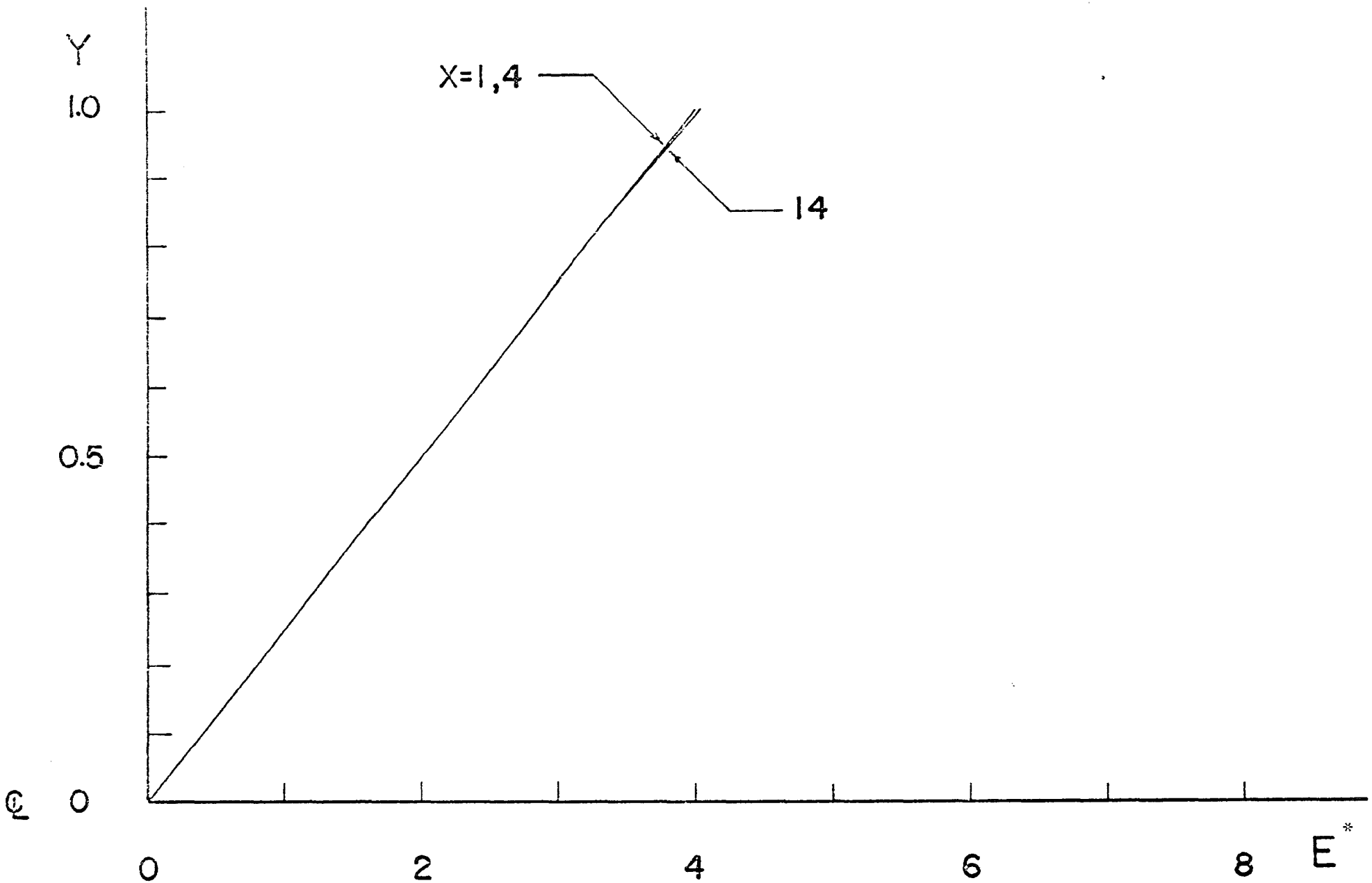

FIG. 3.30 DISTRIBUTION OF ELECTRIC FIELD INTENSITY IN CASES I & II WITH HIGH DIFFUSIVE PECLET NUMBER IN A CHANNEL FLOW

(K_{np}= 0.0001, N_m= 2, N_R= 1000, R^*= 0.002, α = 1.0, β = 10^7, σ = 0.5, $\sigma_w\lambda$ = 1.0, σ_w' = 10^{-10}, ρ_R= 300, ρ^*_{pb}= 0.3)

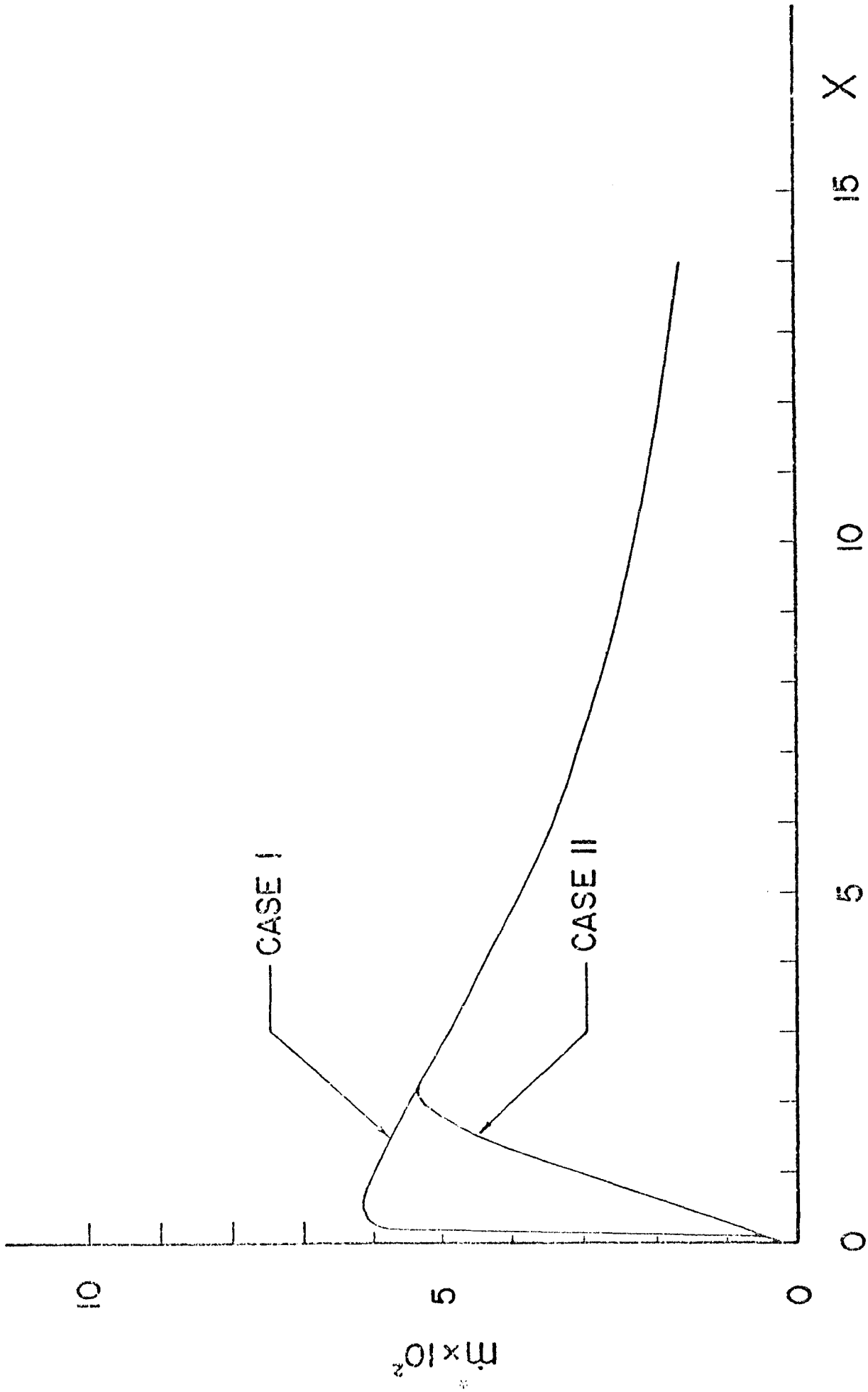

FIG. 3.31 EFFECT OF PARTICLE SLIP CONDITION AT WALL ON RATE OF DEPOSITION OF PARTICLES IN A CHANNEL FLOW (K_{np} = 0.0001, N_m = 2, N_R = 1000, R^* = 0.002, α = 1.0, β = 40, σ = 0.5, $\sigma_w\lambda$ = 0.1, σ_w' = 10^{-6}, ρ_R = 300, ρ^*_{pb} = 0.3)

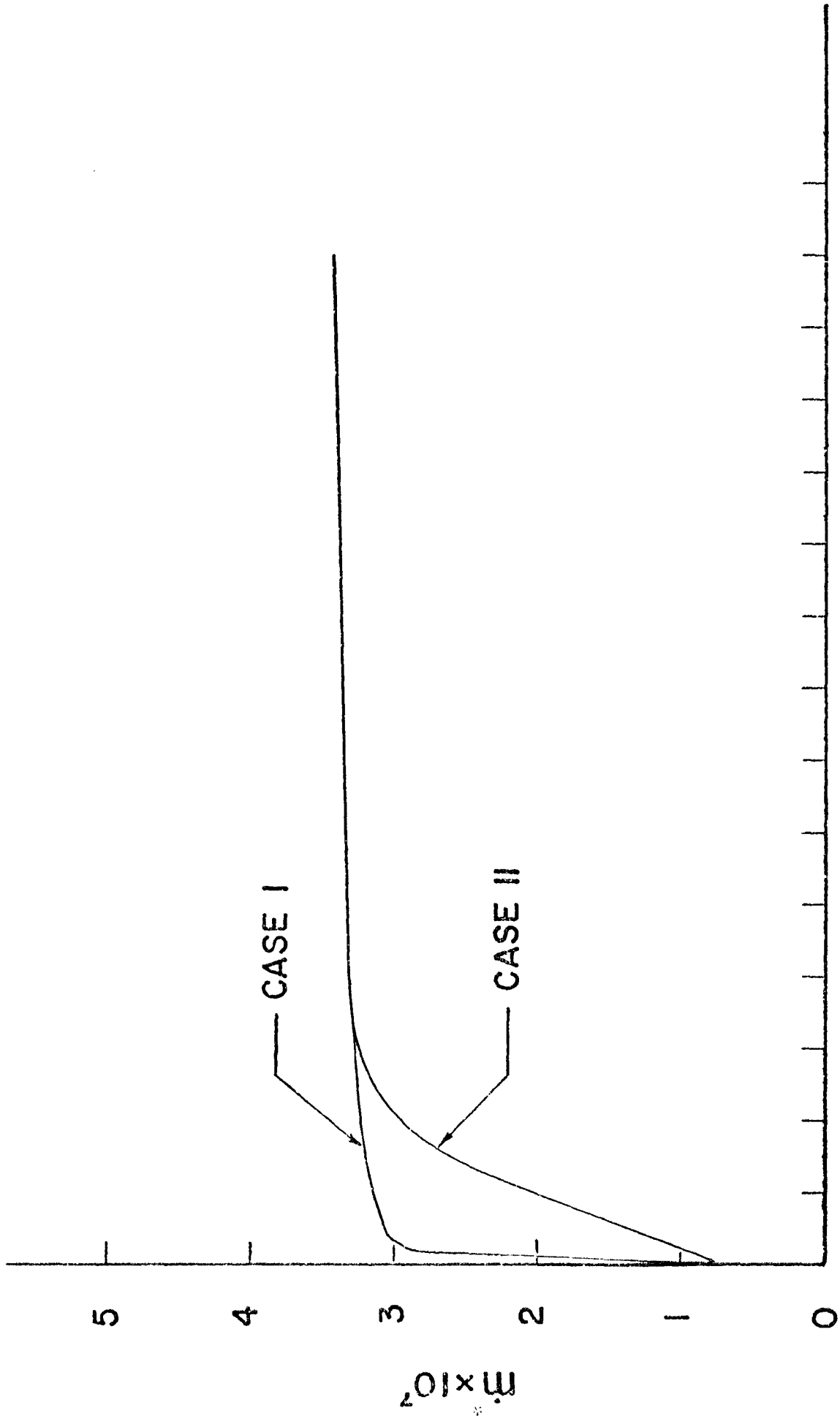

FIG. 3.32 EFFECT OF PARTICLE SLIP CONDITION AT WALL ON RATE OF DEPOSITION AT HIGH DIFFUSIVE PECLET NUMBER IN A CHANNEL FLOW

($K_{np} = 0.0001$, $N_m = 2$, $N_R = 1000$, $R^* = 0.002$, $\alpha = 1.0$, $\beta = 10^7$, $\sigma = 0.5$, $\sigma_w\lambda = 1.0$, $\sigma_w' = 10^{-10}$, $\rho_R = 300$, $\rho_{pb}^* = 0.3$)

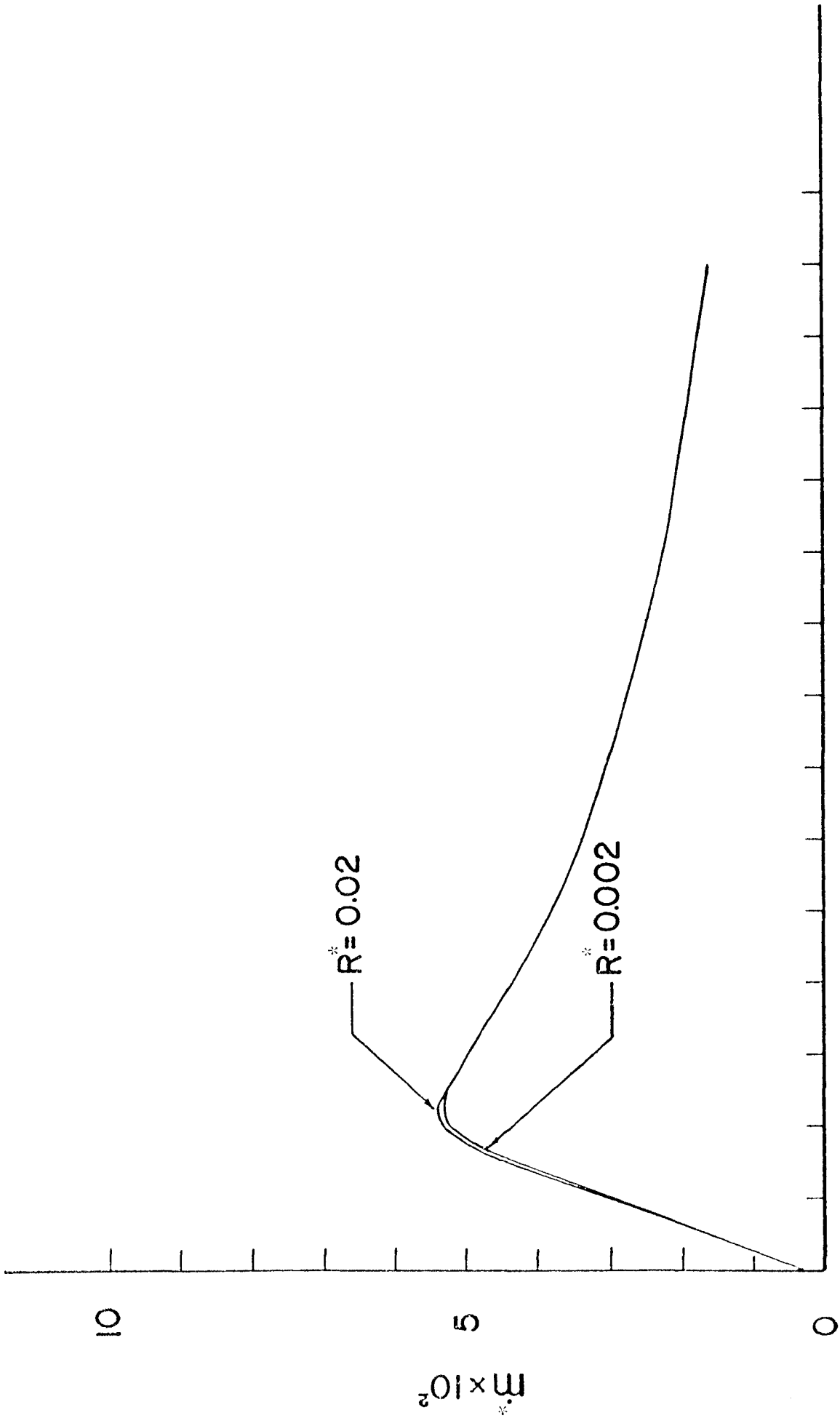

FIG. 3.33 EFFECT OF PARTICLE SIZE ON RATE OF DEPOSITION IN A CHANNEL FLOW

($K_{np} = 0.0001$, $N_m = 2$, $N_R = 1000$, $\alpha = 1.0$, $\varepsilon = 40$, $\sigma = 0.5$, $\sigma_{w^2} = 0.1$, $\sigma'_w = 10^{-6}$, $\rho_R = 300$, $\rho^*_{pb} = 0.3$)

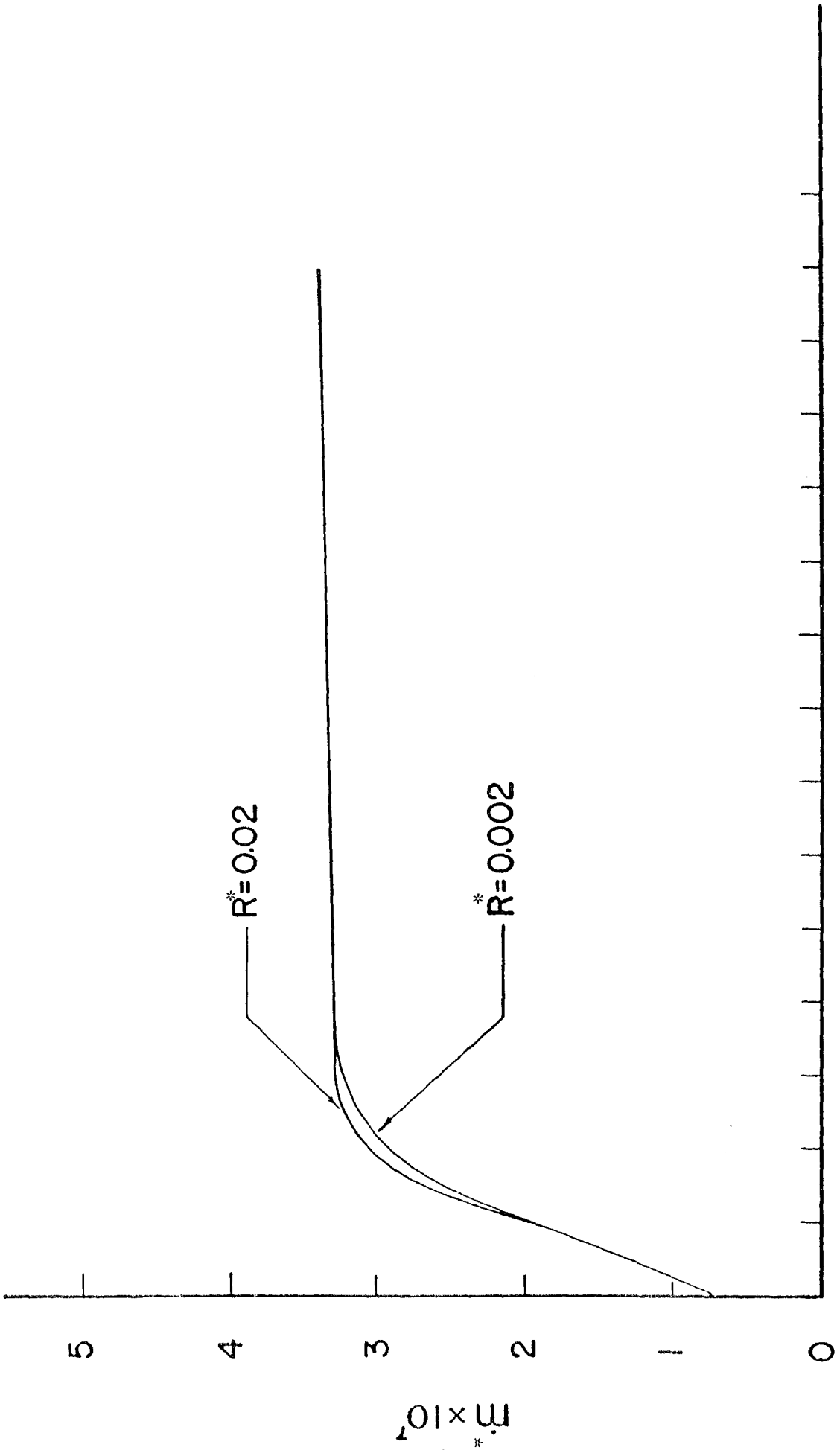

FIG. 3.34 EFFECT OF PARTICLE SIZE ON RATE OF DEPOSITION AT HIGH DIFFUSIVE PECLET NUMBER IN A CHANNEL FLOW
(K_{np} = 0.0001, N_{Pe} = 2, N_R = 1000, ε = 1.0, β = 10^7, σ = 0.5, σ_{w^+} = 1.0, σ_w = 10^{-10}, ρ_R = 300, ρ^*_{pb} = 0.3)

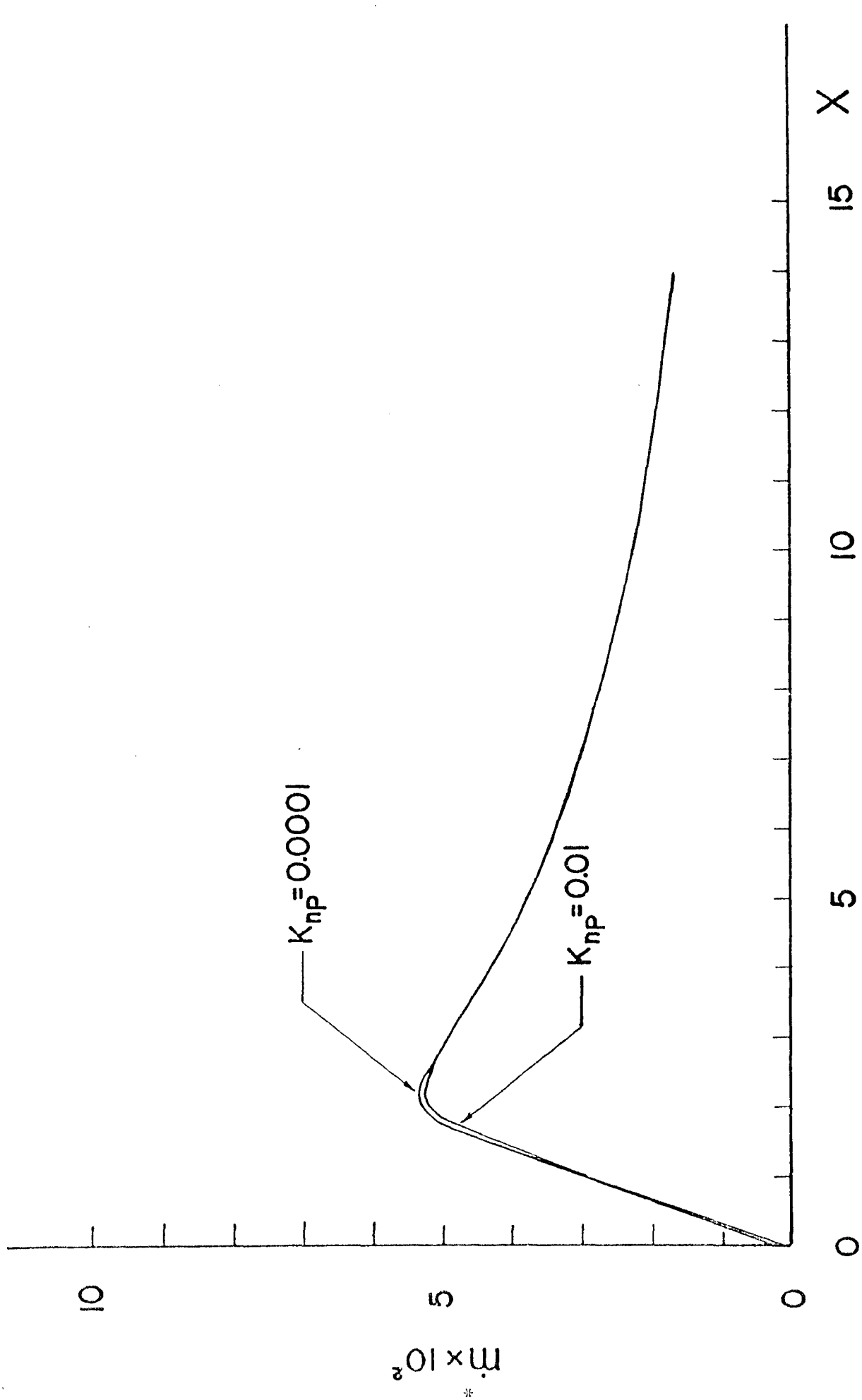

FIG. 3.35 EFFECT OF PARTICLE KNUDSEN NUMBER ON RATE OF DEPOSITION IN A CHANNEL FLOW

(G_m = 2, N_R = 1000, R^* = 0.002, α = 1.0, δ = 40, σ = 0.5, σ_w = 0.1, σ_w' = 10^{-6}, ρ_R = 300, ρ^*_{pb} = 0.3)

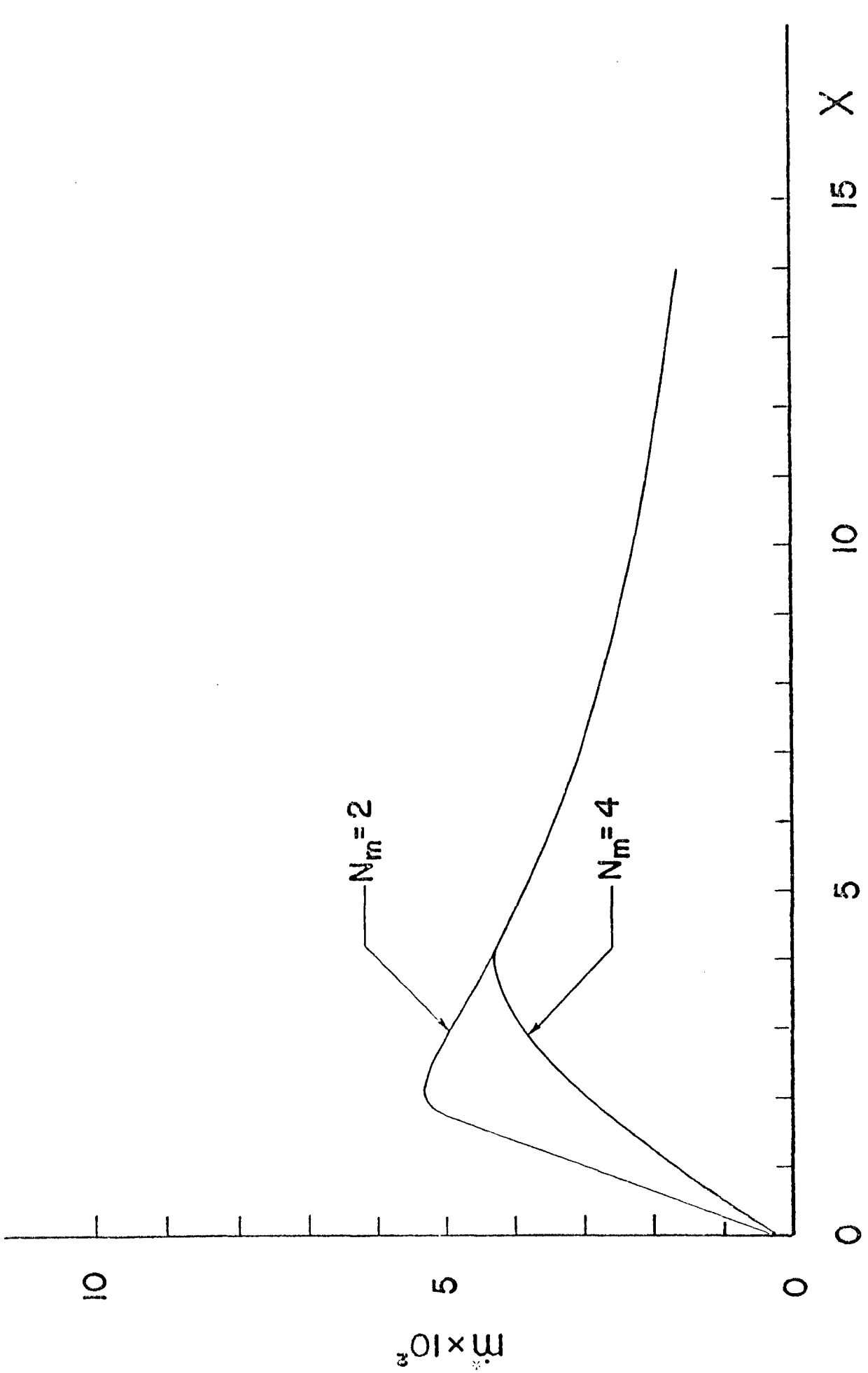

FIG. 3.36 EFFECT OF MOMENTUM-TRANSFER NUMBER ON RATE OF DEPOSITION IN A CHANNEL FLOW

($K_{np} = 0.0001$, $N_R = 1000$, $R^* = 0.002$, $\alpha = 1.0$, $\beta = 40$, $\sigma = 0.5$, $\sigma_w\lambda = 0.1$, $\sigma'_w = 10^{-6}$, $\rho_R = .300$, $\rho^*_{pb} = 0.3$)

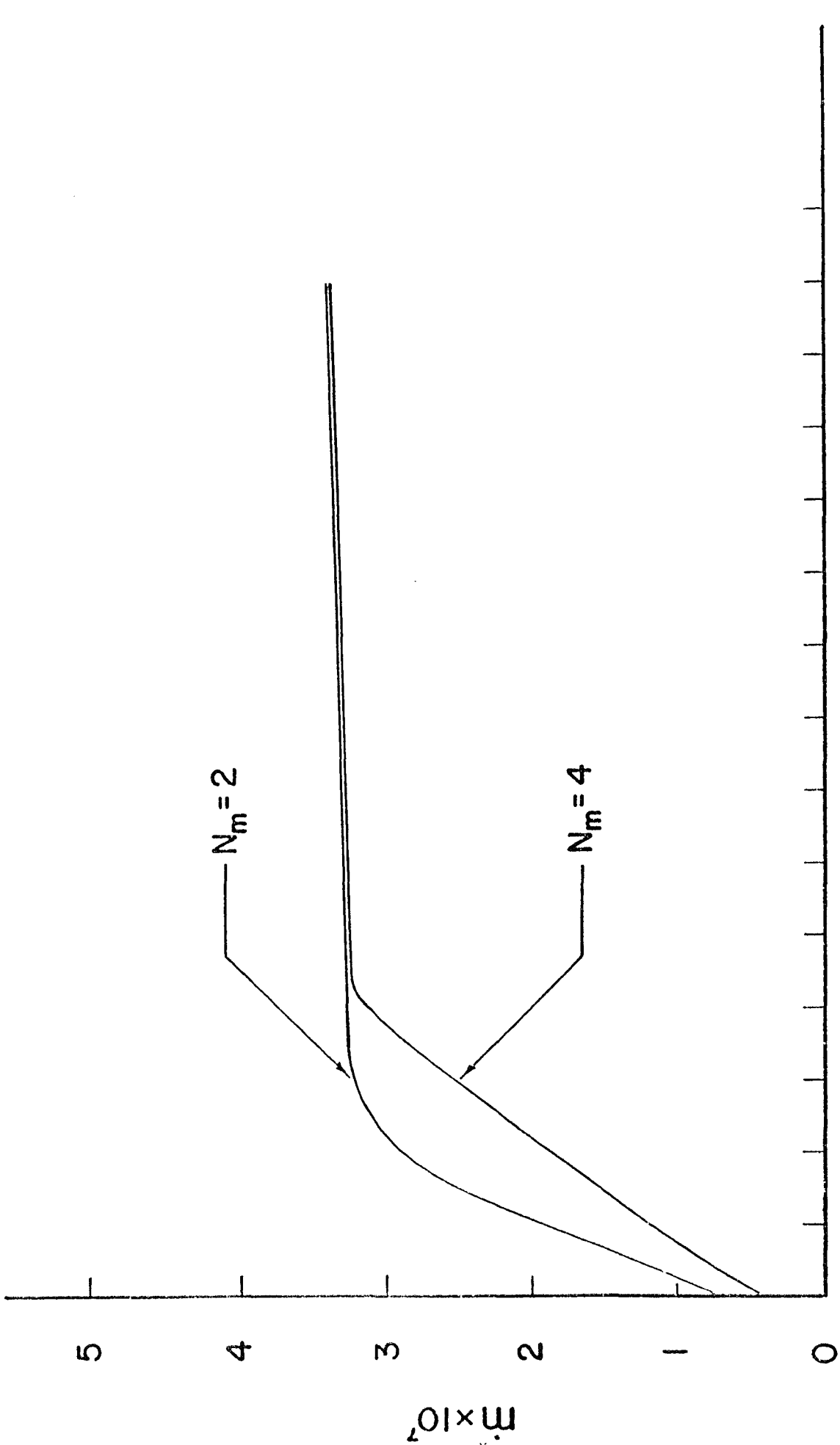

FIG. 3.37 EFFECT OF MOMENTUM-TRANSFER NUMBER ON RATE OF DEPOSITION AT HIGH DIFFUSIVE PECLET NUMBER IN A CHANNEL FLOW

($K_{np} = 0.0001$, $N_R = 1000$, $R^* = 0.002$, $\alpha = 1.0$, $\beta = 10^7$, $\sigma = 0.5$, $\sigma_w \lambda = 1.0$, $\sigma_w' = 10^{-10}$, $\rho_R = 300$, $\rho_{pr}^* = 0.3$)

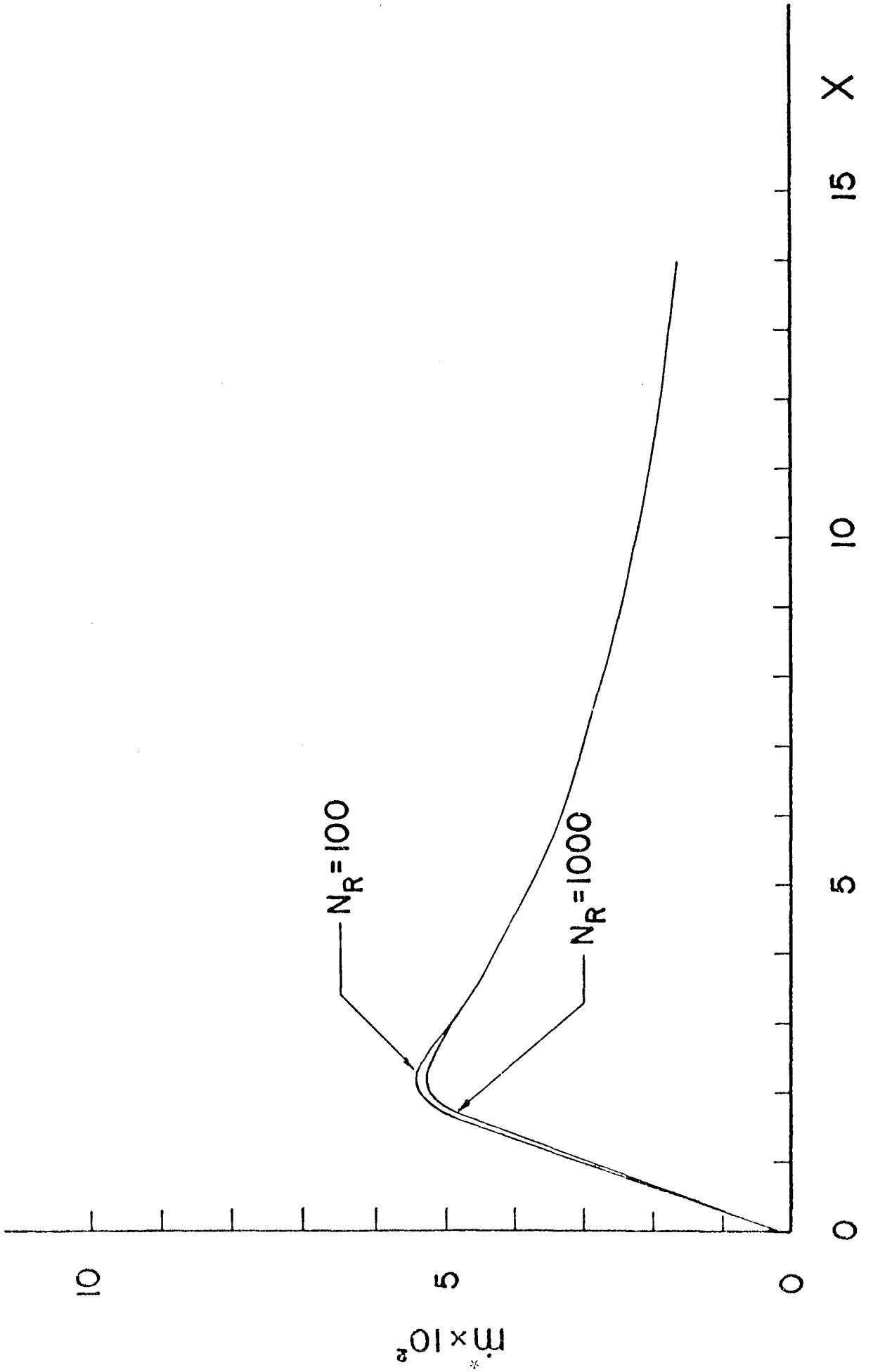

FIG. 3.36 EFFECT OF REYNOLDS NUMBER ON RATE OF DEPOSITION IN A CHANNEL FLOW

($K_{np} = 0.0001$, $N_n = 2$, $R^* = 0.002$, $\alpha = 1.0$, $\delta = 40$, $\sigma = 0.5$, $\sigma_w \lambda = 0.1$, $\sigma_w' = 10^{-6}$, $\sigma_R = 300$, $\rho_{pb}^* = 0.3$)

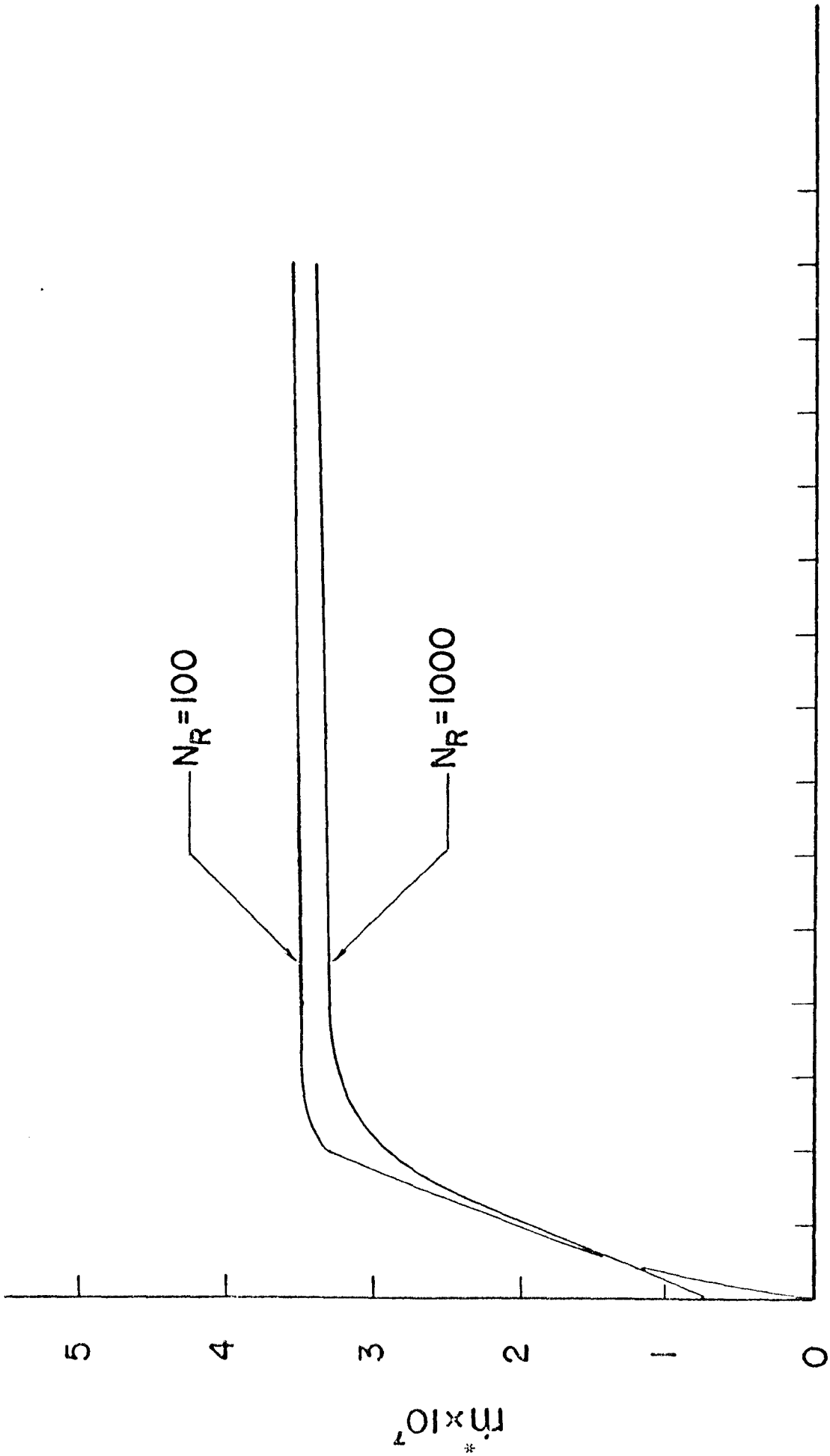

FIG. 3.39 EFFECT OF REYNOLDS NUMBER ON RATE OF DEPOSITION AT HIGH DIFFUSIVE PECLET NUMBER IN A CHANNEL FLOW

($K_{np} = 0.0001$, $N_m = 2$, $R^* = 0.002$, $\alpha = 1.0$, $\beta = 10^7$, $\sigma = 0.5$, $\sigma_w^{\lambda} = 1.0$, $\sigma_w' = 10^{-10}$, $c_R = 300$, $c^*_{pb} = 0.3$)

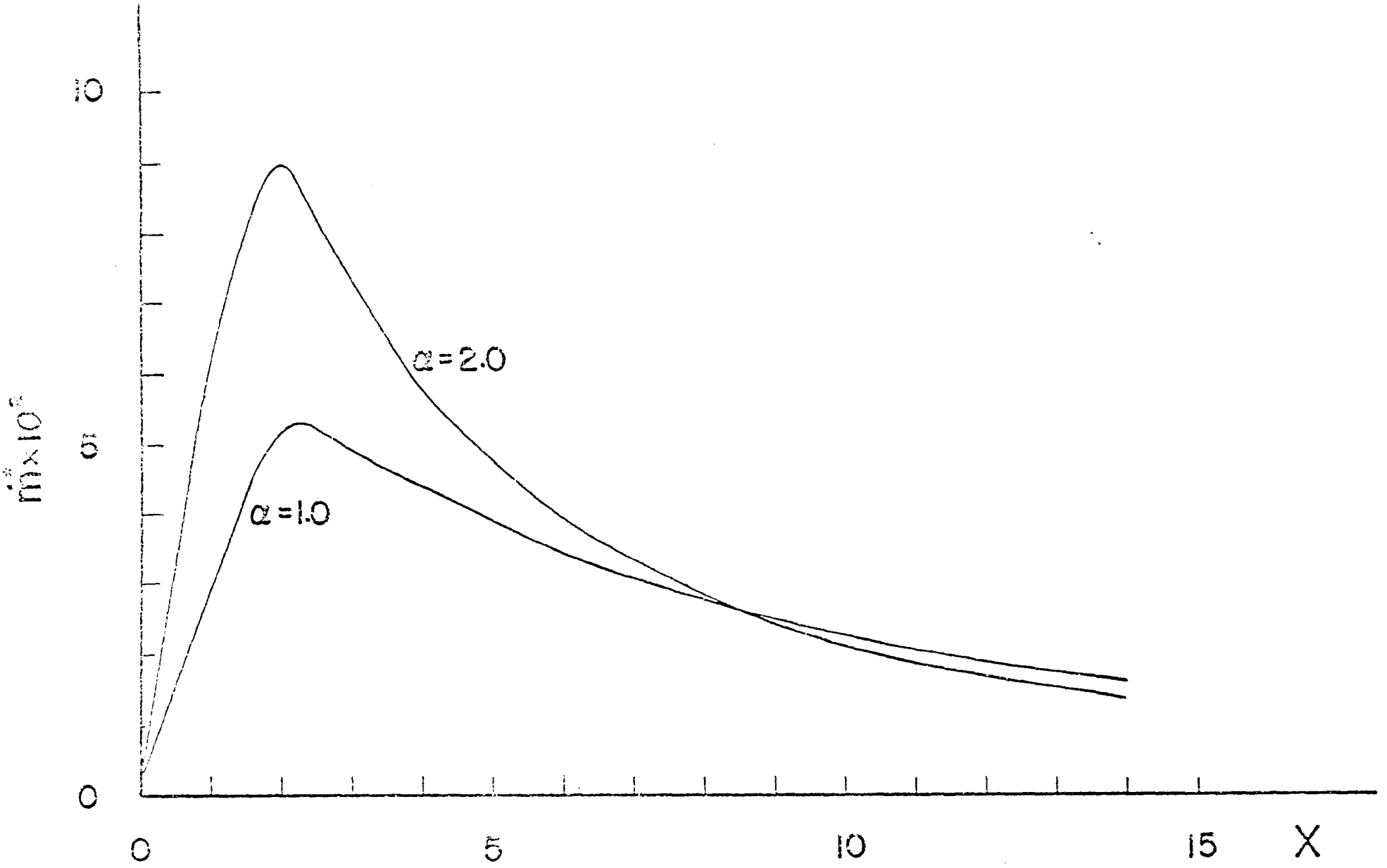

FIG. 3.40 EFFECT OF ELECTROSTATIC CHARGE ON RATE OF DEPOSITION IN A CHANNEL FLOW

($K_{np} = 0.0001$, $N_m = 2$, $N_R = 1000$, $R^* = 0.002$, $\beta = 40$, $\sigma = 0.5$, $\sigma_w\lambda = 0.1$, $\sigma_w = 10^{-6}$, $\rho_R = 300$, $\rho^*_{pb} = 0.3$)

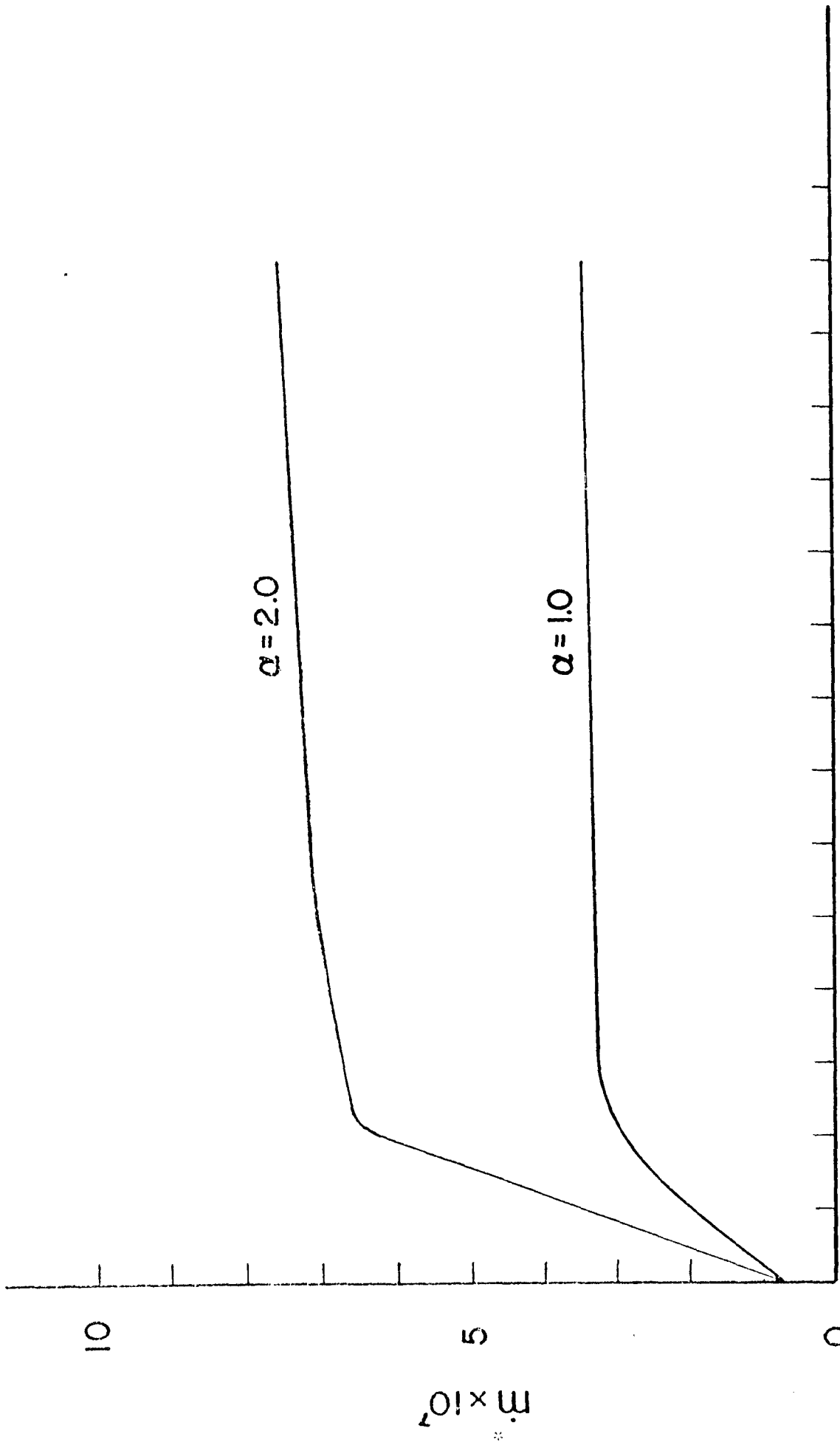

FIG. 3.1 EFFECT OF ELECTROSTATIC CHARGE ON RATE OF DEPOSITION AT HIGH DIFFUSIVE PECLET NUMBER IN A CHANNEL FLOW

($K_{np} = 0.0001$, $K_m = 2$, $K_R = 1000$, $R^* = 0.002$, $\beta = 10^7$, $\sigma = 0.5$, $\sigma_w^\lambda = 1.0$, $\sigma_w = 10^{-10}$, $\rho_R = 300$, $\rho_{pb}^* = 0.3$)

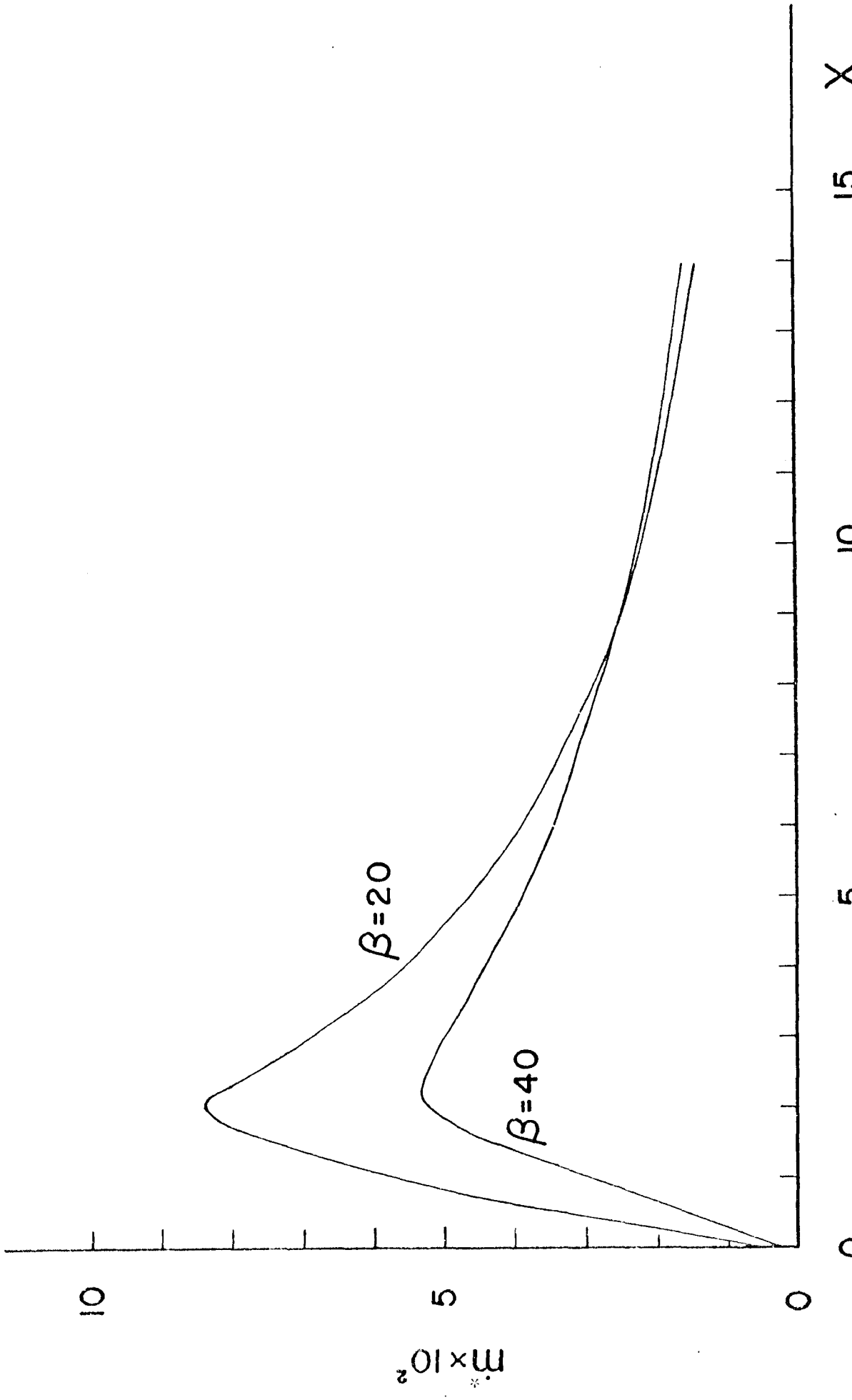

FIG. 3.42 EFFECT OF DIFFUSIVE PECLET NUMBER ON RATE OF DEPOSITION IN A CHANNEL FLOW

(K_{np} = 0.0001, N_m = 2, N_R = 1000, R^* = 0.002, α = 1.0, σ = 0.5, σ_w^* = 0.1, σ_w' = 10^{-6}, ρ_R = 300, ρ_{pb}^* = 0.3)

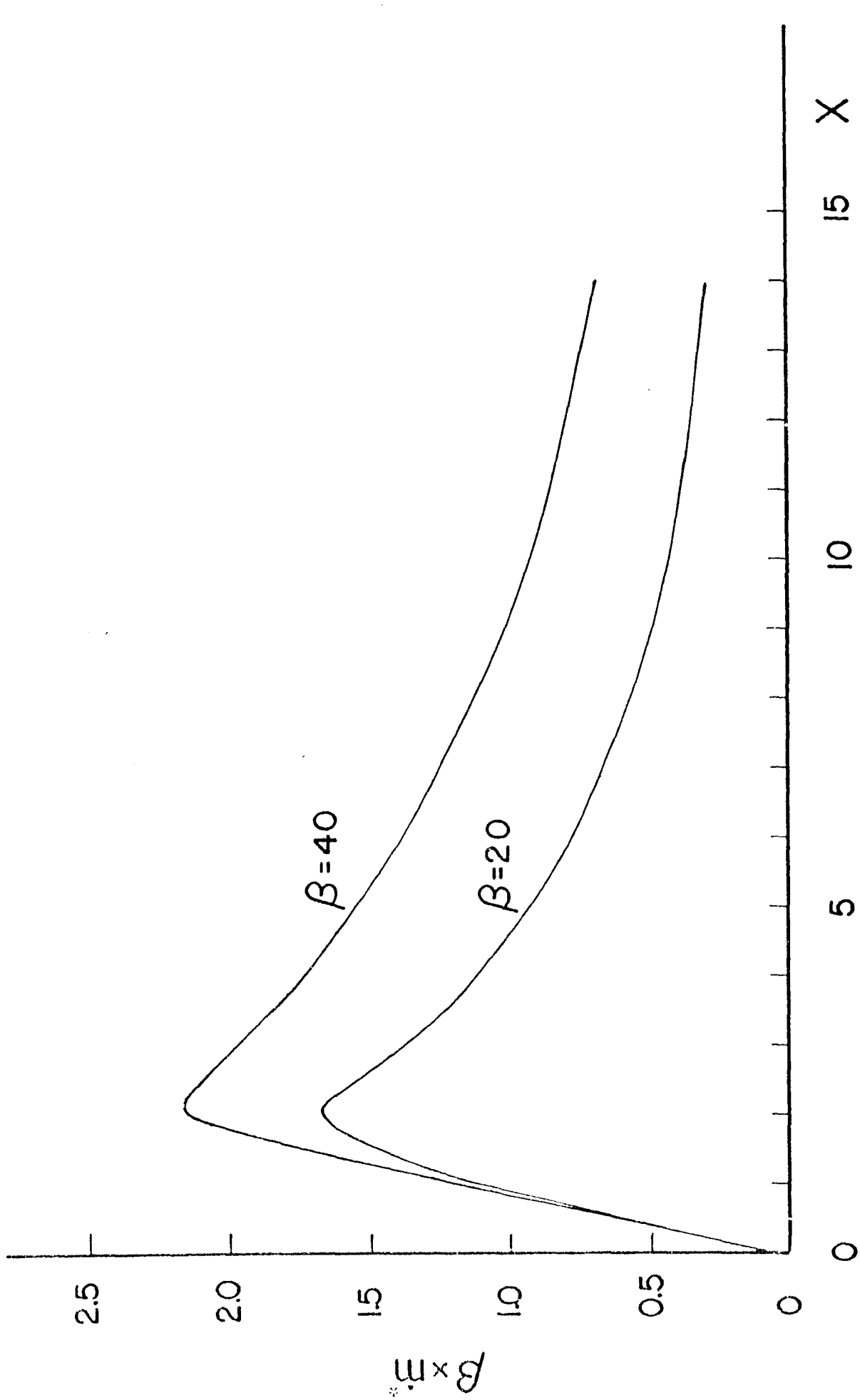

FIG. 3.43 EFFECT OF DIFFUSIVE PECLET NUMBER ON MODIFIED RATE OF DEPOSITION, $\dot{m}^*$ IN A CHANNEL FLOW

(K_{np} = 0.0001, N_m = 2, N_R = 1000, R^* = 0.002, α = 1.0, σ = 0.5, σ_w = 0.1, σ_w' = 10^{-6}, ρ_R = 300, c^*_{pb} = 0.3)

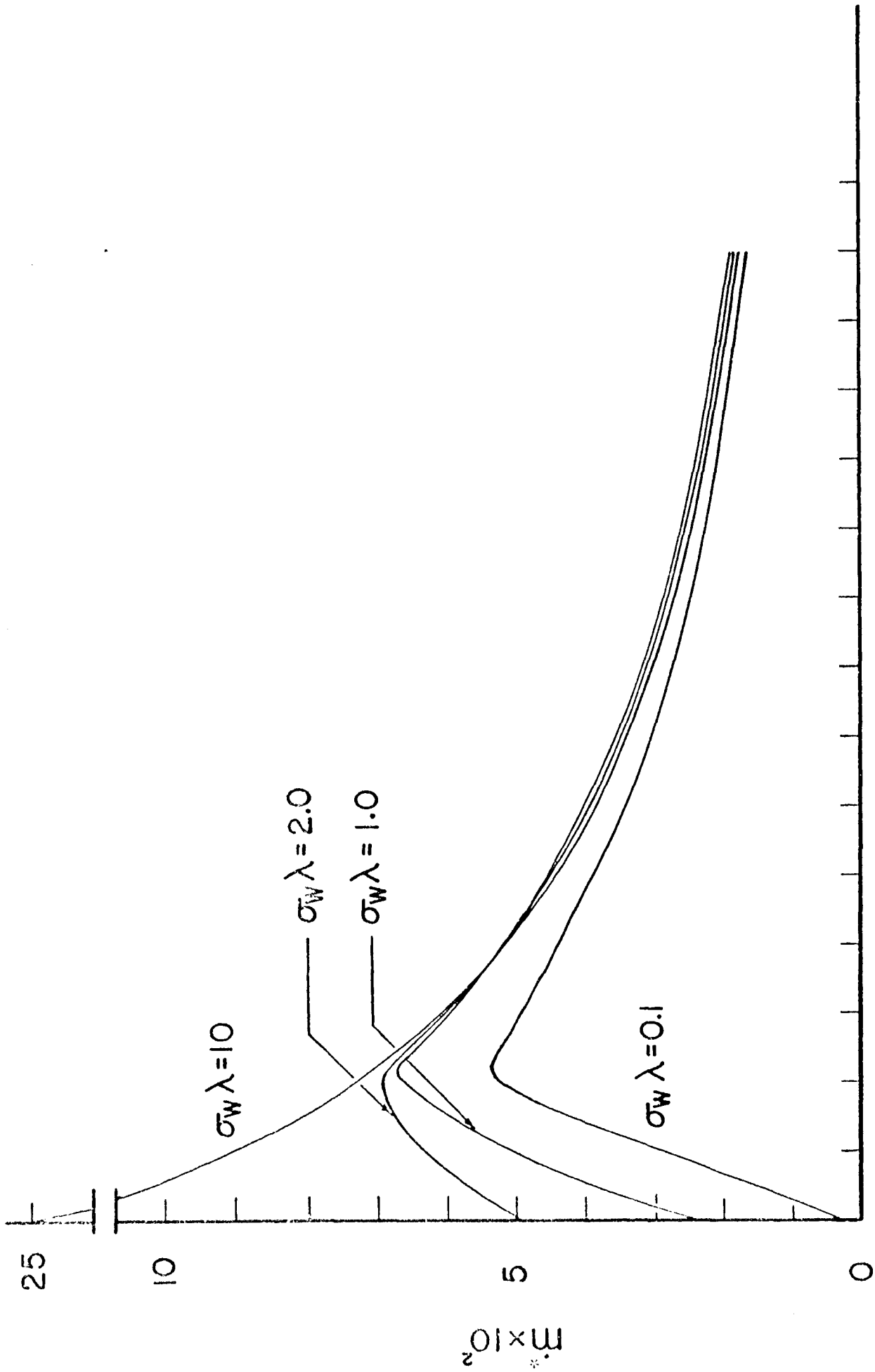

FIG. 3.44 EFFECT OF SURFACE ADHESION ON RATE OF DEPOSITION IN A CHANNEL FLOW

(K_{np} = 0.0001, N_m = 2, N_R = 1000, R^* = 0.002, α = 1.0, δ = 40, σ = 0.5, σ_w' = 10^{-6}, P_R = 300, c^*_{pb} = 0.3)

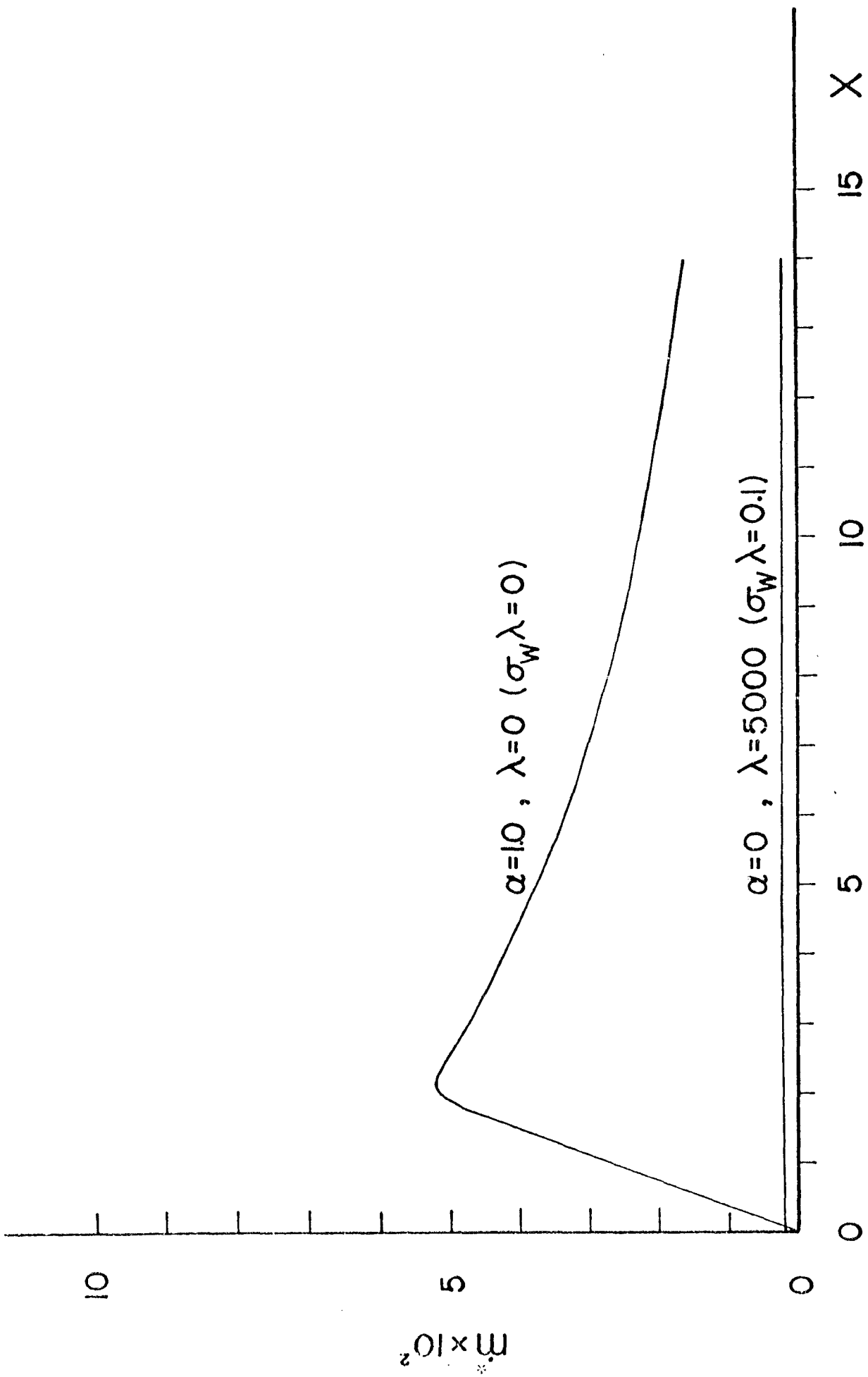

FIG. 5.45 EFFECT OF ELECTROSTATIC CHARGE AND SURFACE ADHESION ON RATE OF DEPOSITION IN A CHANNEL FLOW

(K_{np} = 0.0001, N_m = 2, N_R = 1000, R^* = 0.002, δ = 40, σ = 0.5, σ_w' = 10^{-6}, ρ_R = 300, ρ^*_{pb} = 0.3)

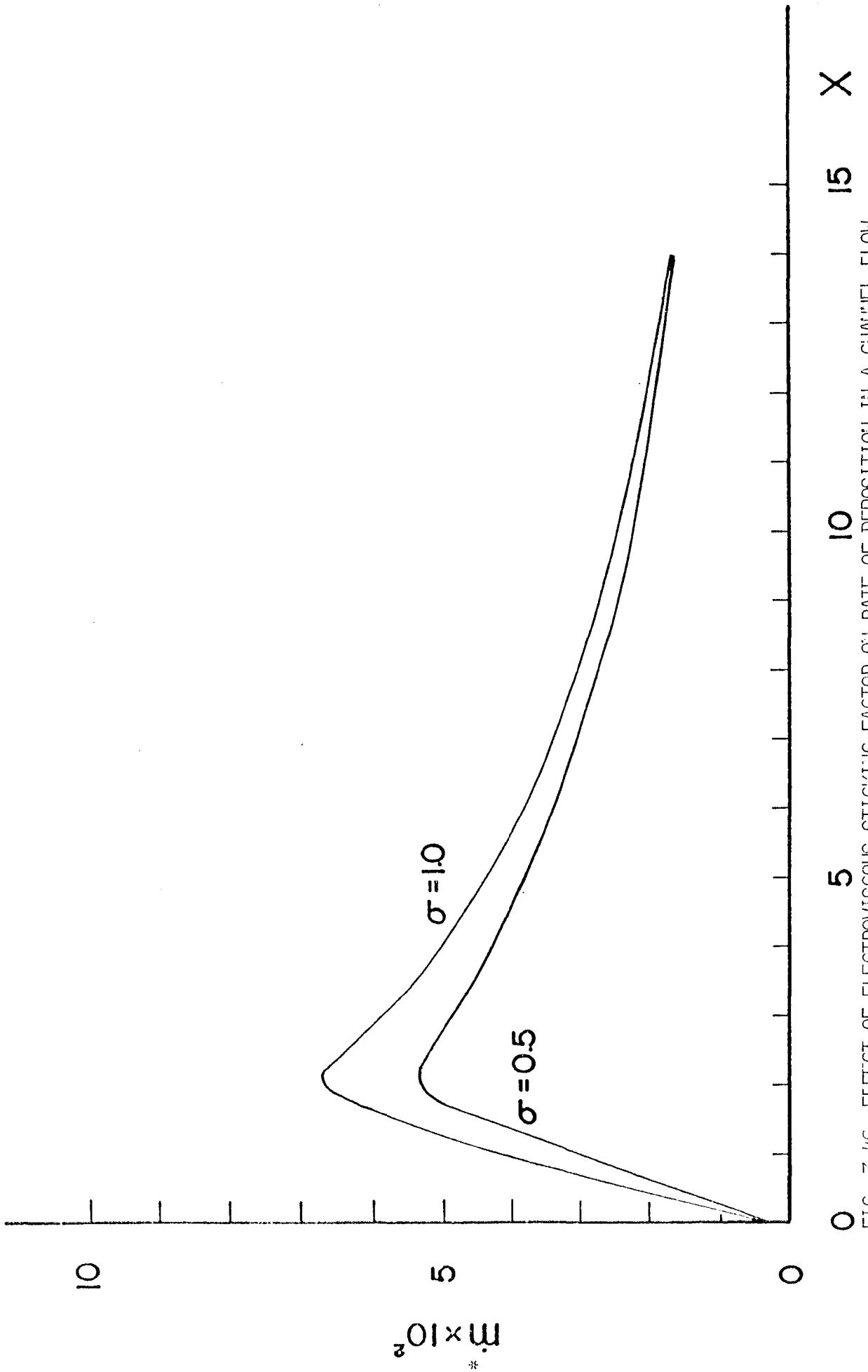

FIG. 3.46 EFFECT OF ELECTROVISCOUS-STICKING FACTOR ON RATE OF DEPOSITION IN A CHANNEL FLOW

($K_{np} = 0.0001$, $N_m = 2$, $N_R = 1000$, $R^* = 0.002$, $\alpha = 1$, $\beta = 40$, $\sigma_w\lambda = 0.1$, $\sigma_w' = 10^{-6}$, $\rho_R = 300$, $\rho_{pb}^* = 0.3$)

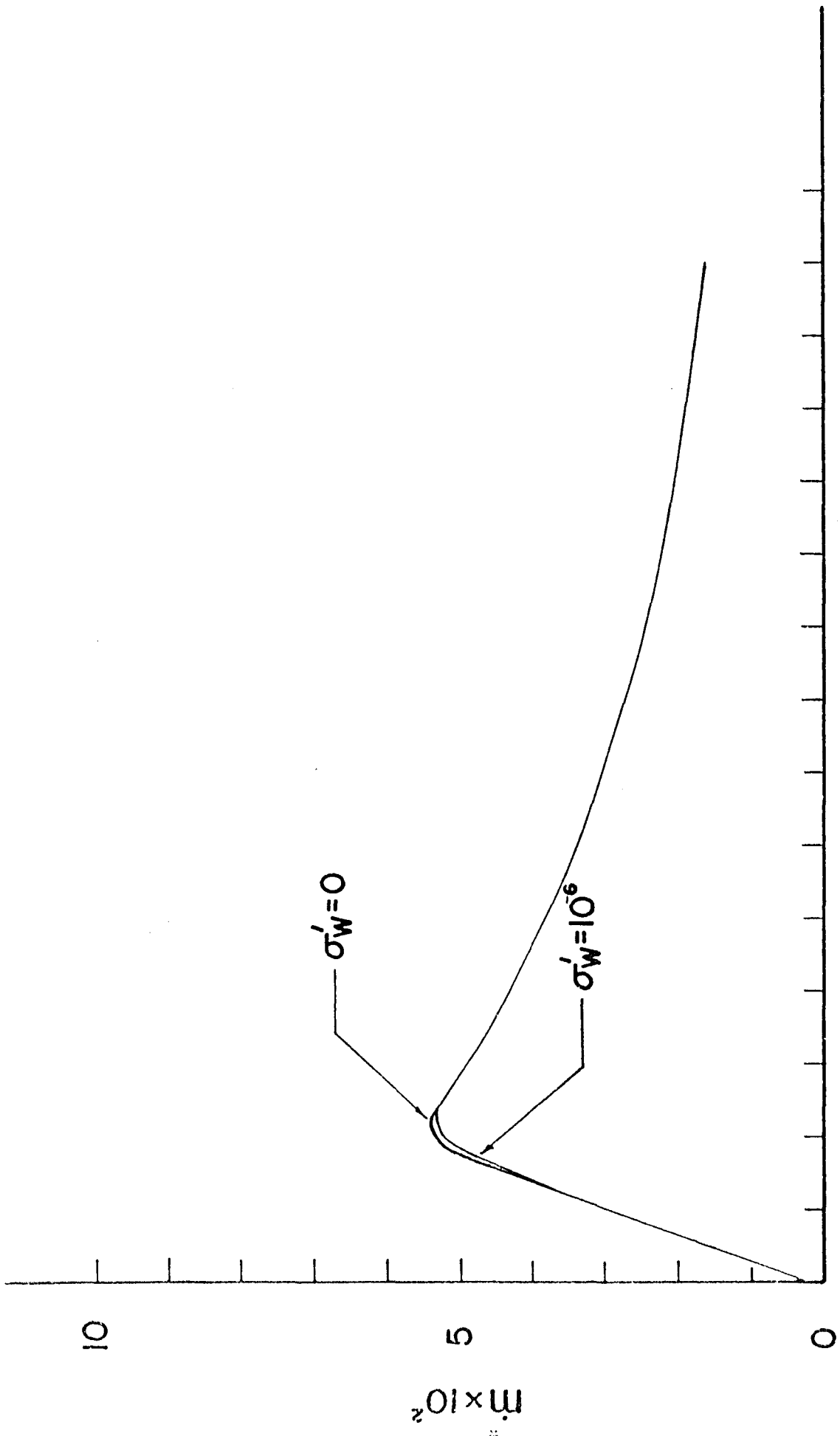

FIG. 3.47 EFFECT OF LIFT FORCES AT WALL ON RATE OF DEPOSITION IN A CHANNEL FLOW

(K_{np} = 0.0001, N_m = 2, N_R = 1000, R^* = 0.002, α = 1.0, β = 40, σ = 0.5, σ_w^{λ} = 0.1, ρ_R = 300, ρ^*_{pb} = 0.3)

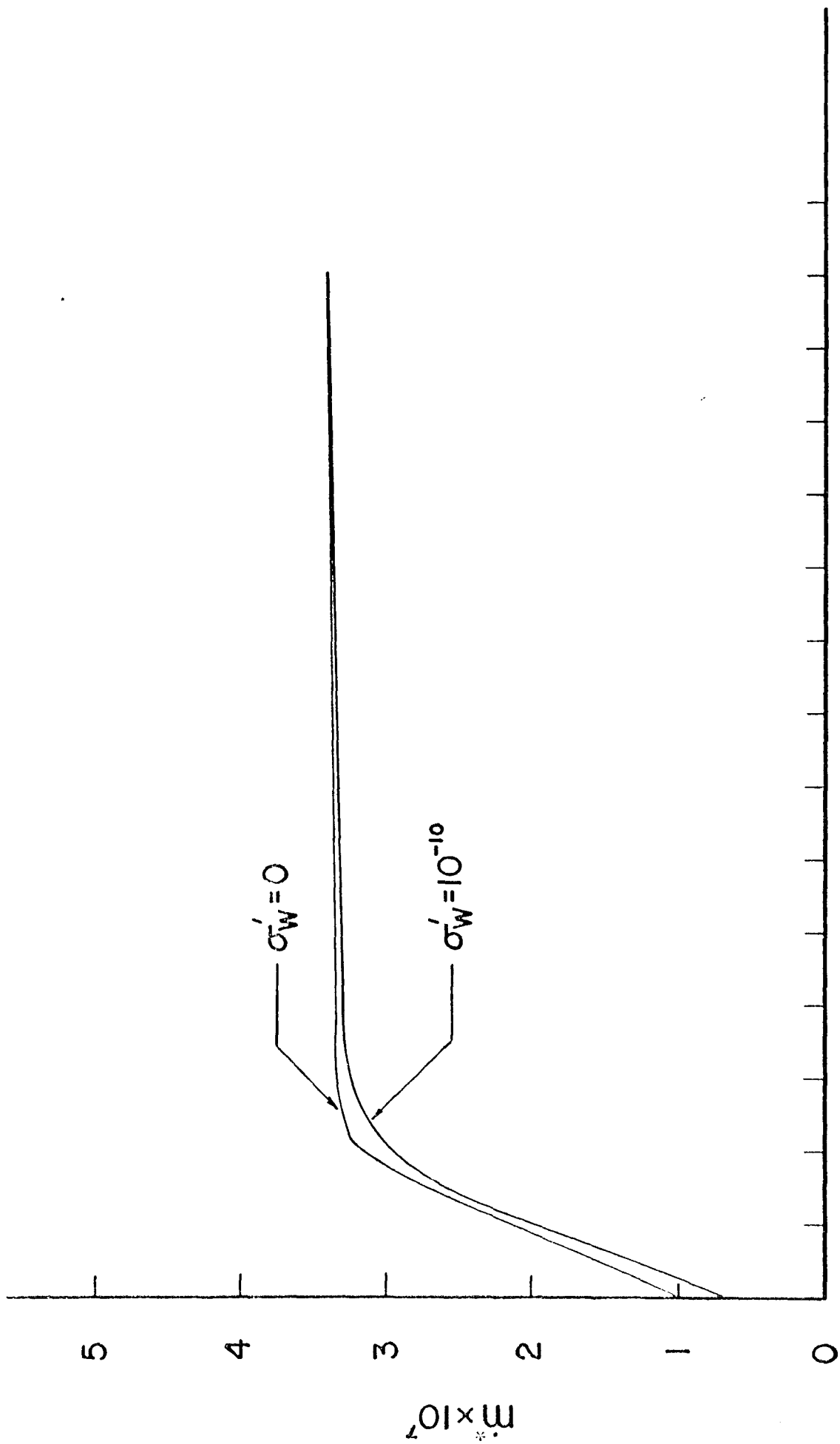

FIG. 3.43 EFFECT OF LIFT FORCES AT WALL ON RATE OF DEPOSITION AT HIGH DIFFUSIVE PECLET NUMBER IN A CHANNEL FLOW

($K_{np} = 0.0001$, $N_m = 2$, $N_R = 1000$, $R^* = 0.002$, $\alpha = 1.0$, $\beta = 10^7$, $\sigma = 0.5$, $\sigma_w\lambda = 1.0$, $\rho_R = 300$, $\rho^*_{pb} = 0.3$)

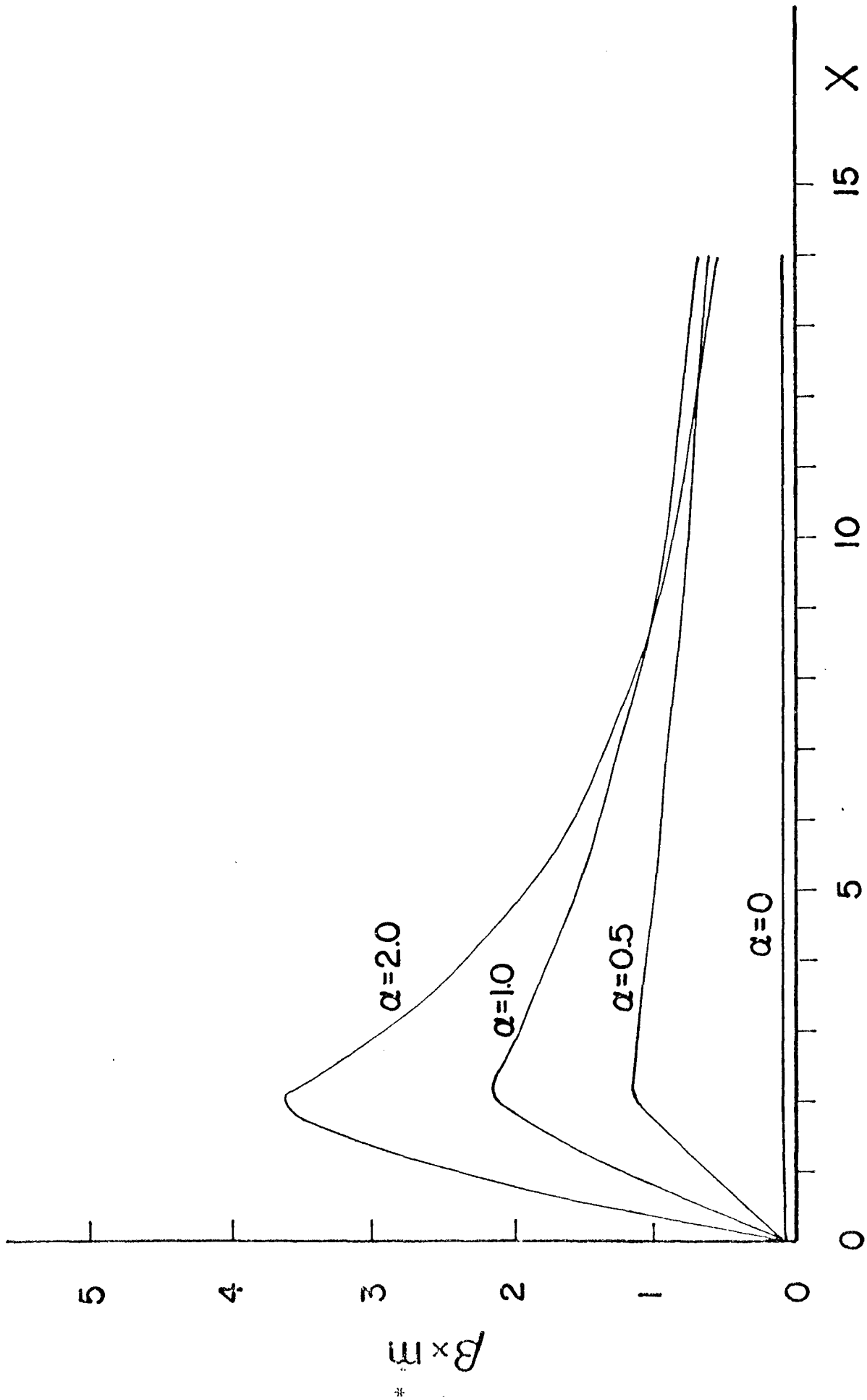

FIG. 3.49 EFFECT OF ELECTROSTATIC CHARGE ON MODIFIED RATE OF DEPOSITION IN A CHANNEL FLOW

(K_{np} = 0.0001, N_m = 2, N_R = 1000, R^* = 0.002, β = 40, σ = 0.5, σ_w^λ = 0.1, σ_w = 10^{-6}. ρ_R = 300, ρ^*_{pb} = 0 3)

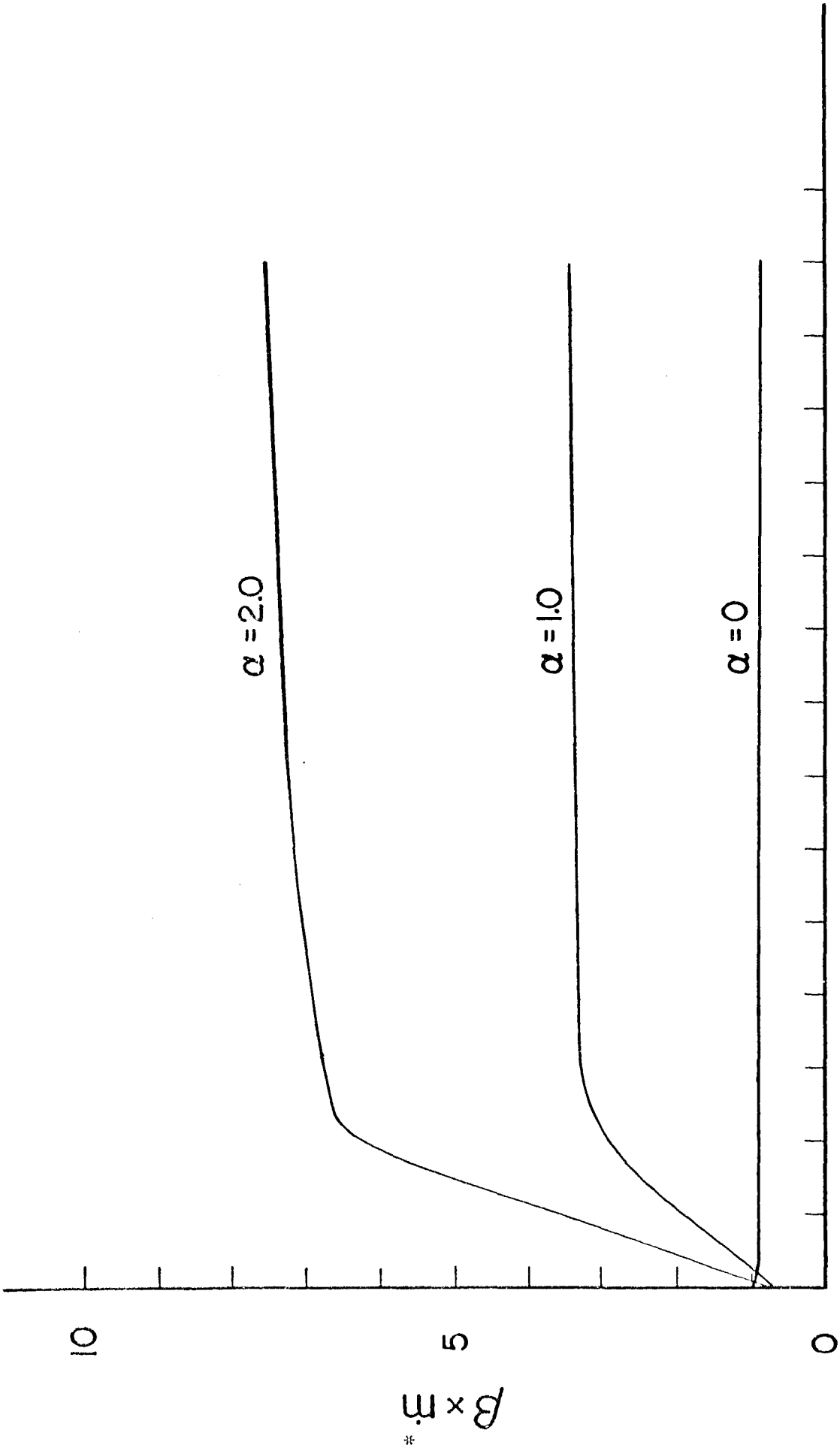

FIG. 3.50 EFFECT OF ELECTROSTATIC CHARGE ON MODIFIED RATE OF DEPOSITION AT HIGH DIFFUSIVE PECLET NUMBER IN A CHANNEL FLOW

(K_{np} = 0.0001, N_m = 2, N_R = 1000, R^* = 0.002, Pe = 10^7, σ = 0.5, σ_w' = 1.0, σ_w' = 10^{-10}, ρ_R = 300, ρ_{pb}^* = 0.3)

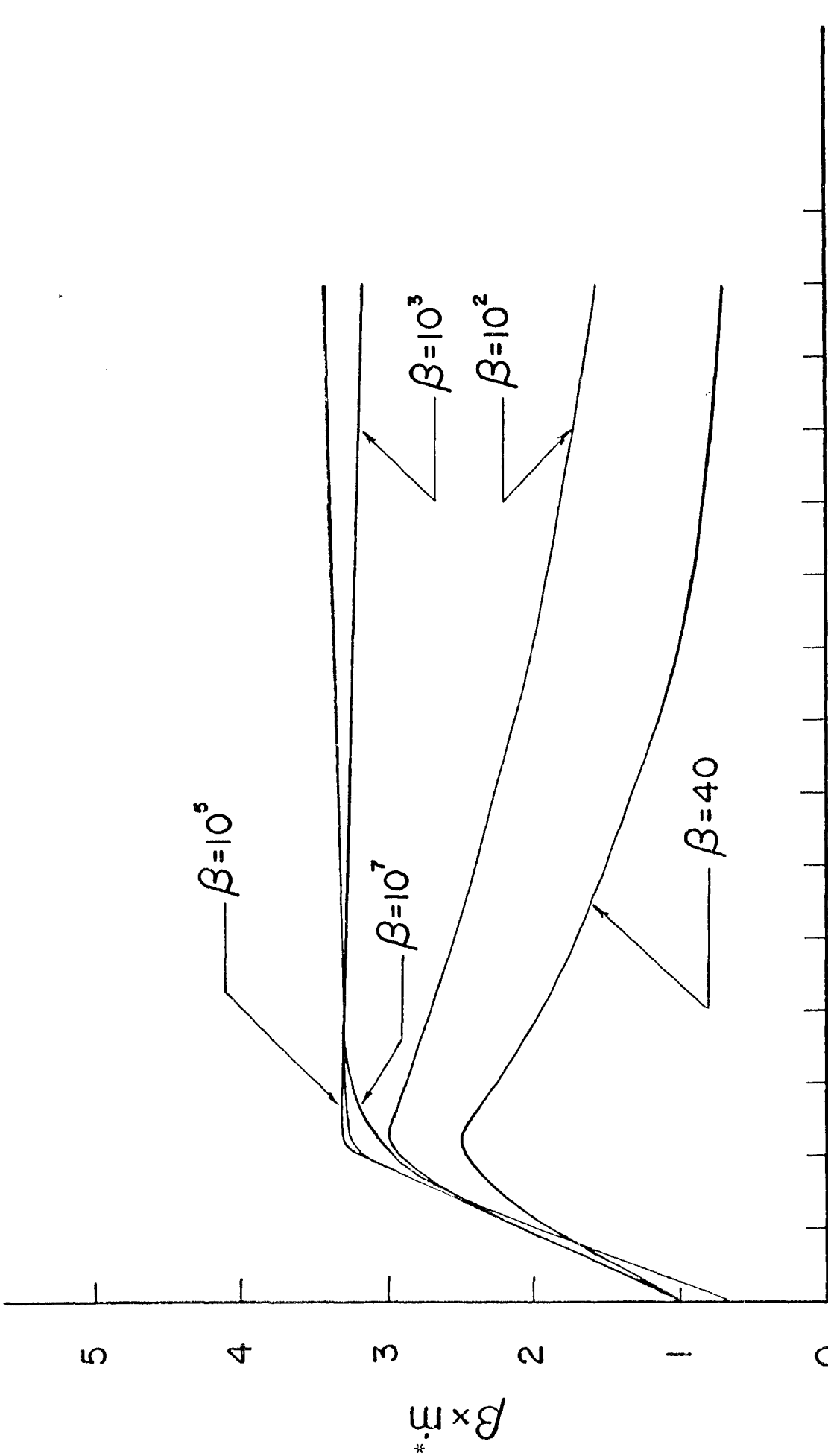

FIG. 3.51 EFFECT OF DIFFUSIVE PECLET NUMBER ON MODIFIED RATE OF DEPOSITION IN A CHANNEL FLOW

(K_{np} = 0.0001, N_m = 2, N_R = 1000, R^* = 0.002, α = 1.0, σ = 0.5, σ_w = 1.0, σ_w' = 10^{-10}, ρ_R = 300, ρ^*_{pb} = 0.3)

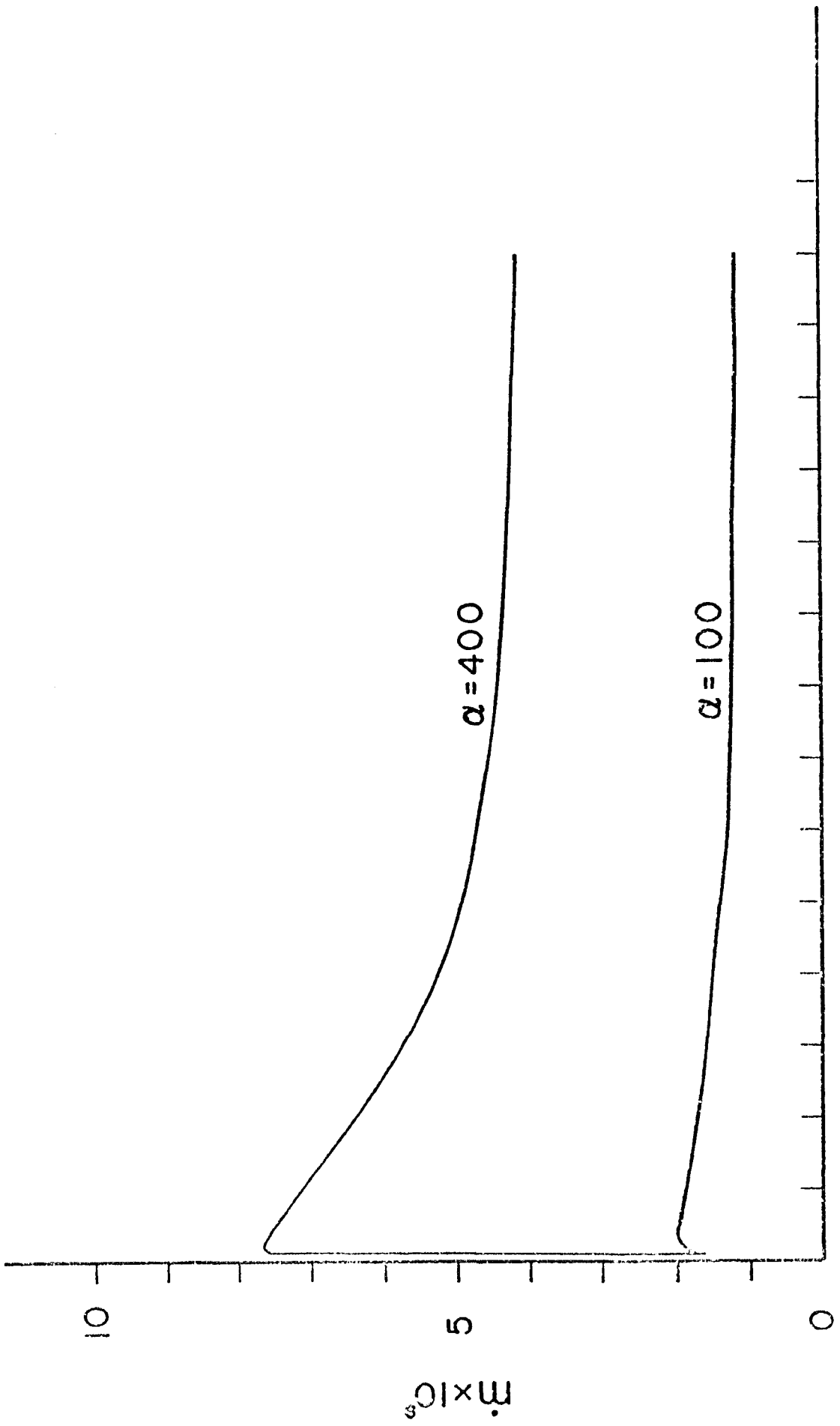

FIG. 3.52 EFFECT OF ELECTROSTATIC CHARGE ON RATE OF DEPOSITION AT HIGH SURFACE ADHESION IN A CHANNEL FLOW
($K_{np} = 0.0001$, $N_m = 67.8$, $N_R = 1000$, $R^* = 0.01$, $\varepsilon = 6.23 \times 10^9$, $\sigma = 0.5$, $\sigma_w^{\lambda} = 1000$, $\sigma_w' = 0$, $\rho_R = 300$, $\rho^*_{pb} = 0.3$)

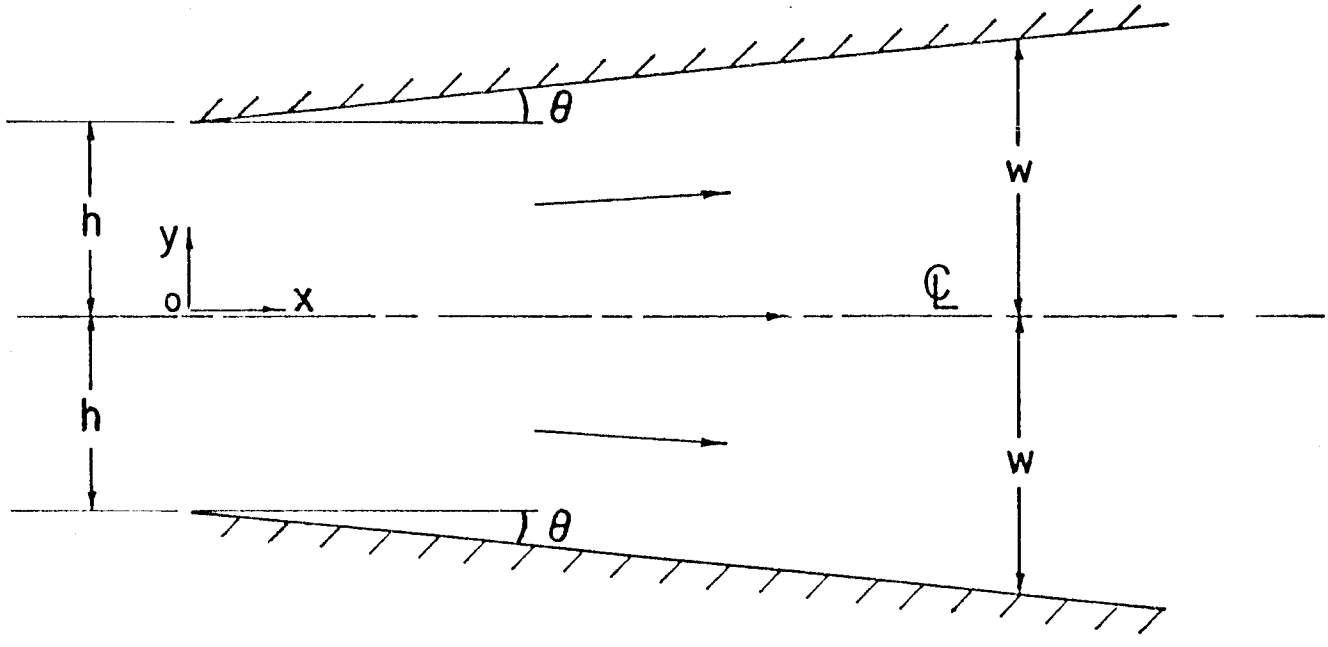

FIG. 4.1 DIFFUSER FLOW CONFIGURATION

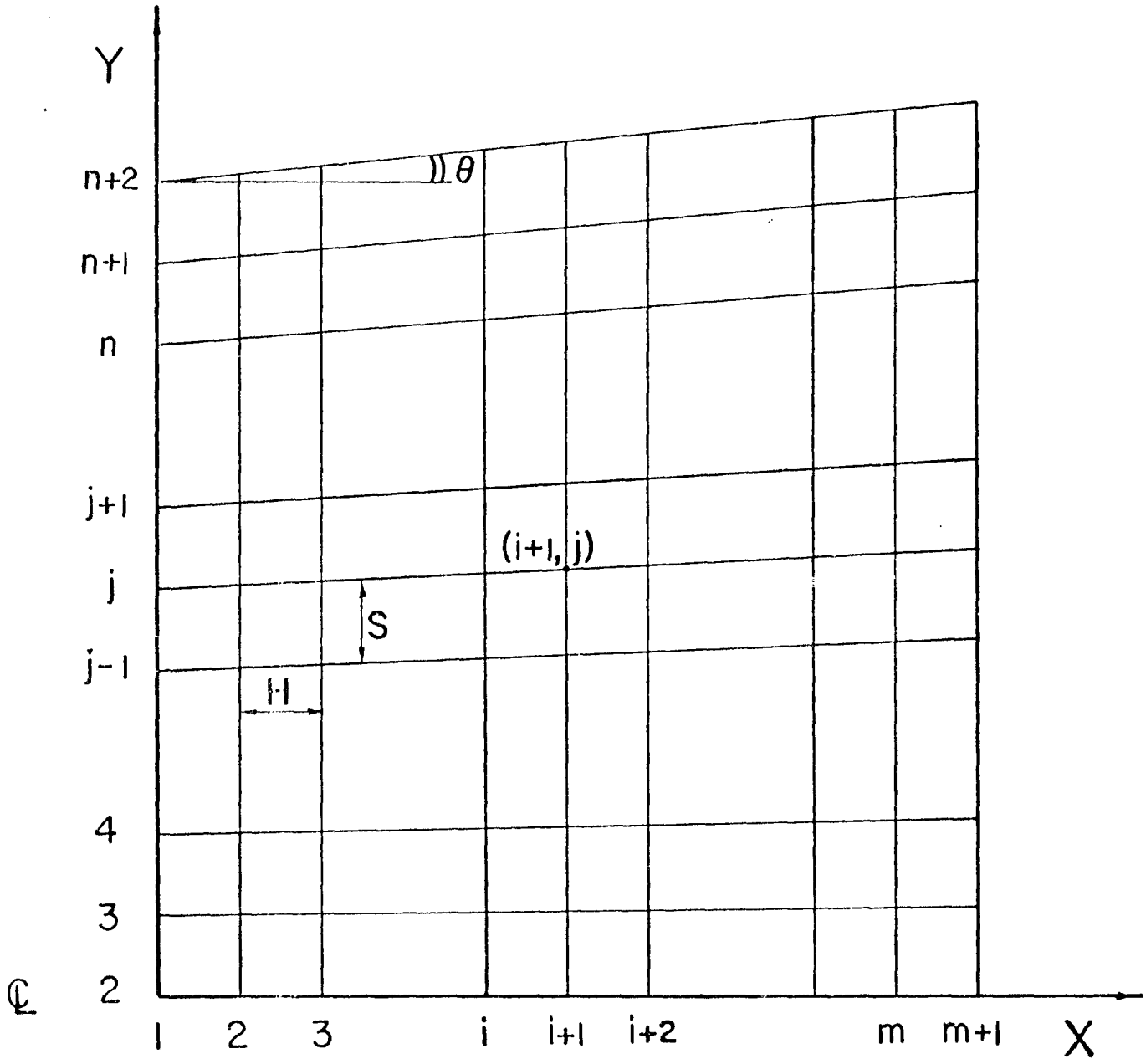

FIG. 4.2 FINITE DIFFERENCE GRID OF DIFFUSER FLOW

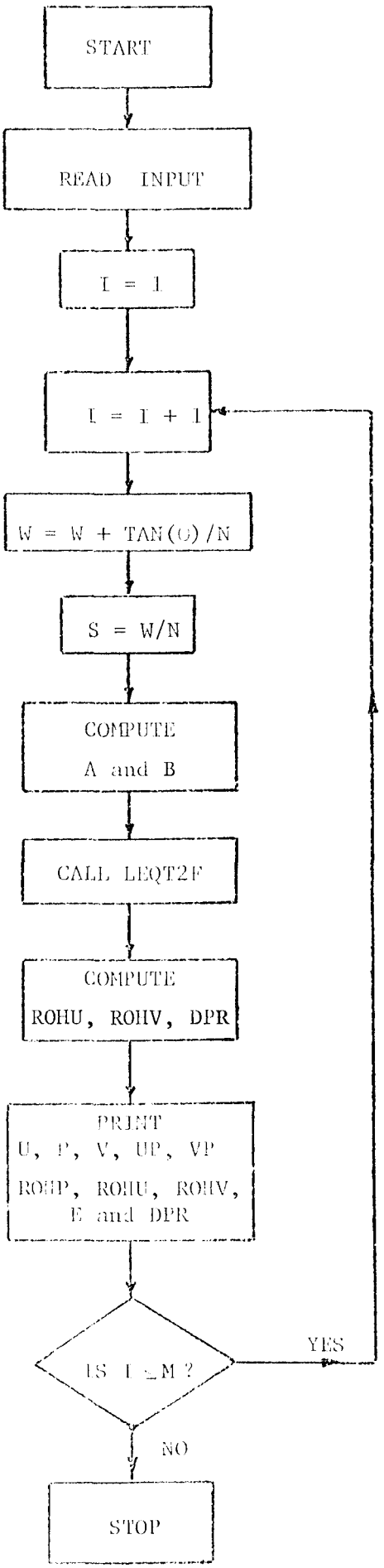

FIG. 4.3 COMPUTER FLOW CHART FOR DIFFUSER FLOW

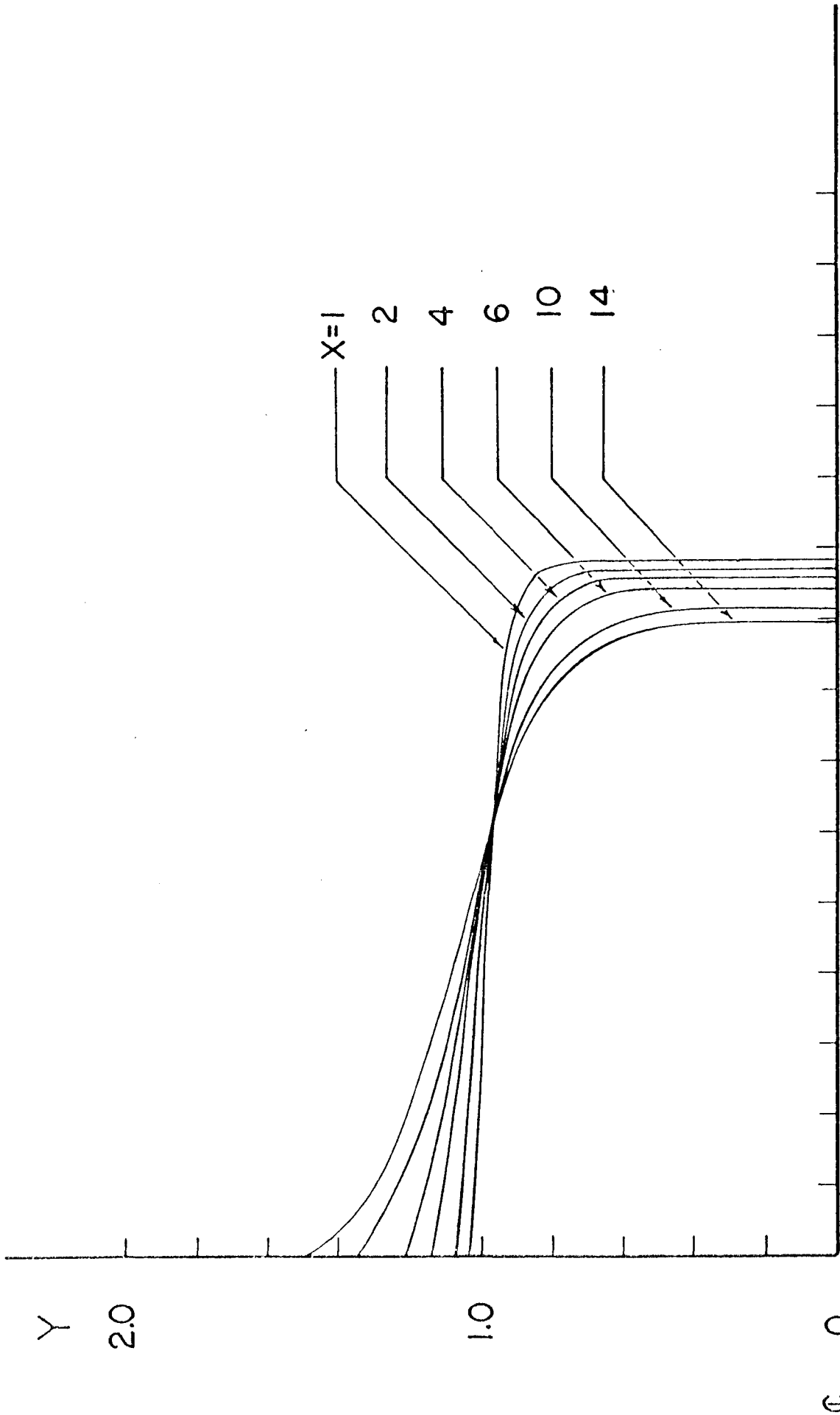

FIG. 4.4 AXIAL VELOCITY DISTRIBUTION OF FLUID PHASE FOR $\theta = 2^\circ$ IN A DIFFUSER FLOW

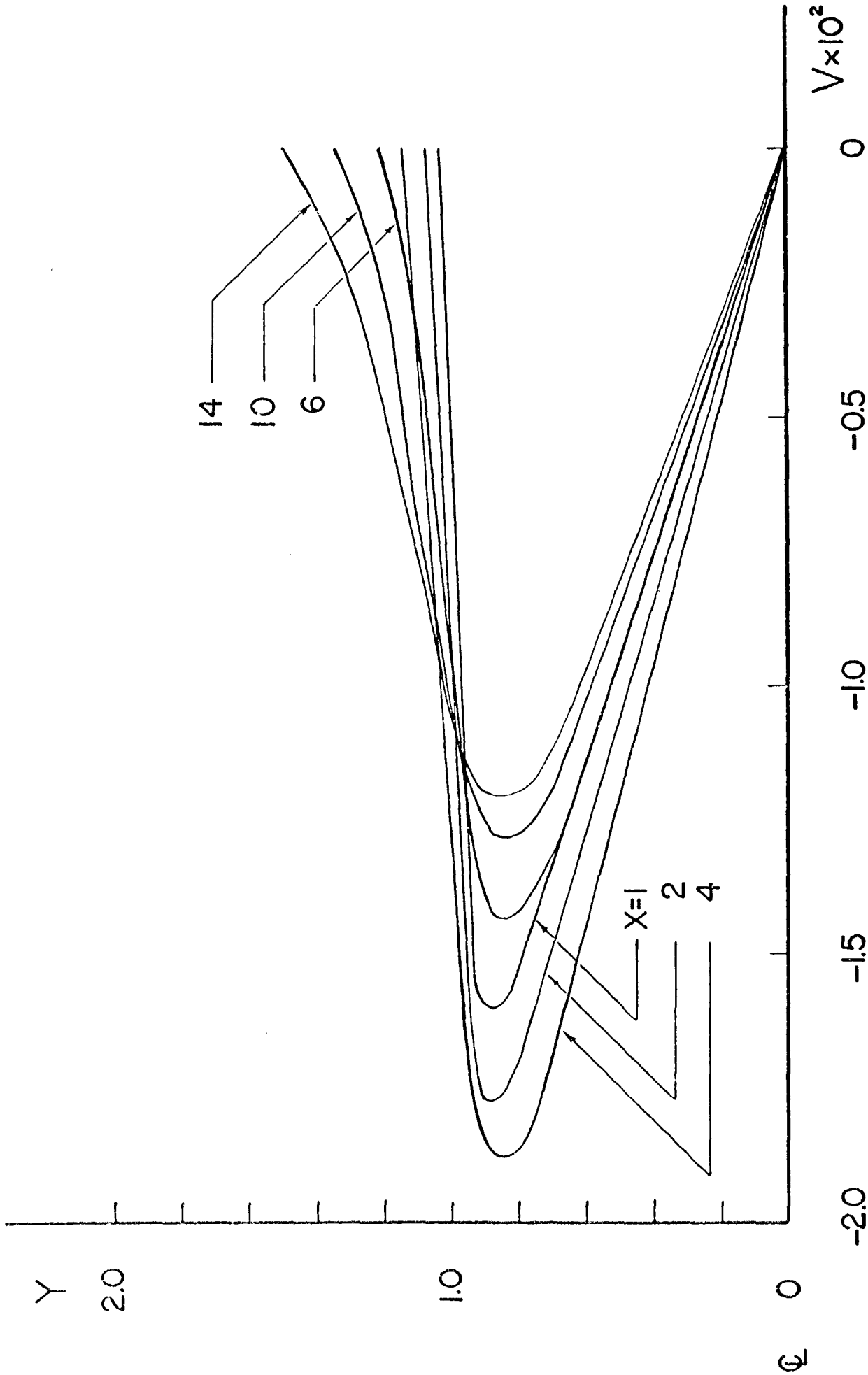

FIG. 4.5 VERTICAL VELOCITY DISTRIBUTION OF FLUID PHASE FOR $\theta = 2^\circ$ IN A DIFFUSER FLOW

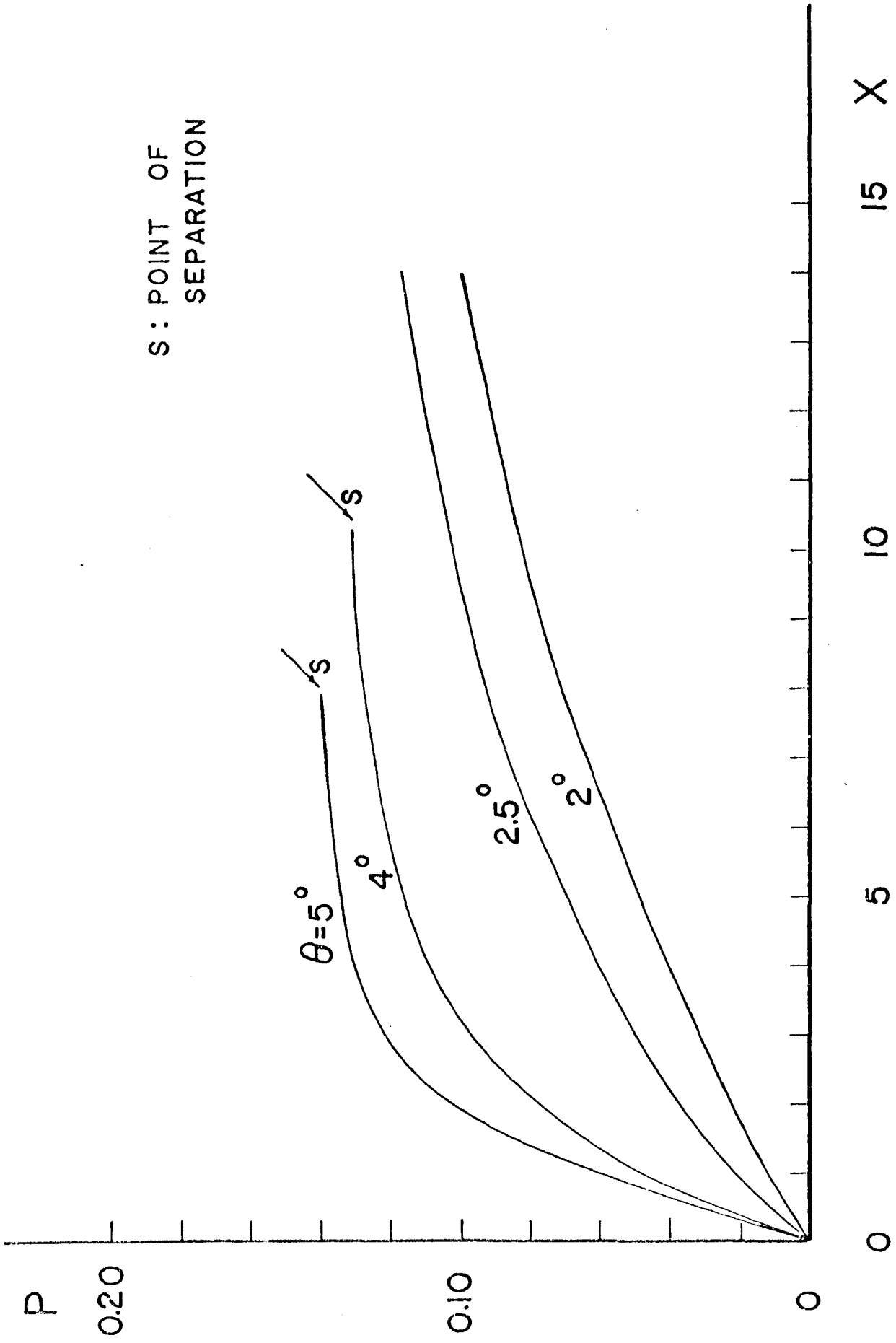

FIG. 4.6 EFFECT OF DIFFUSER ANGLE ON FLUID STATIC PRESSURE DISTRIBUTION

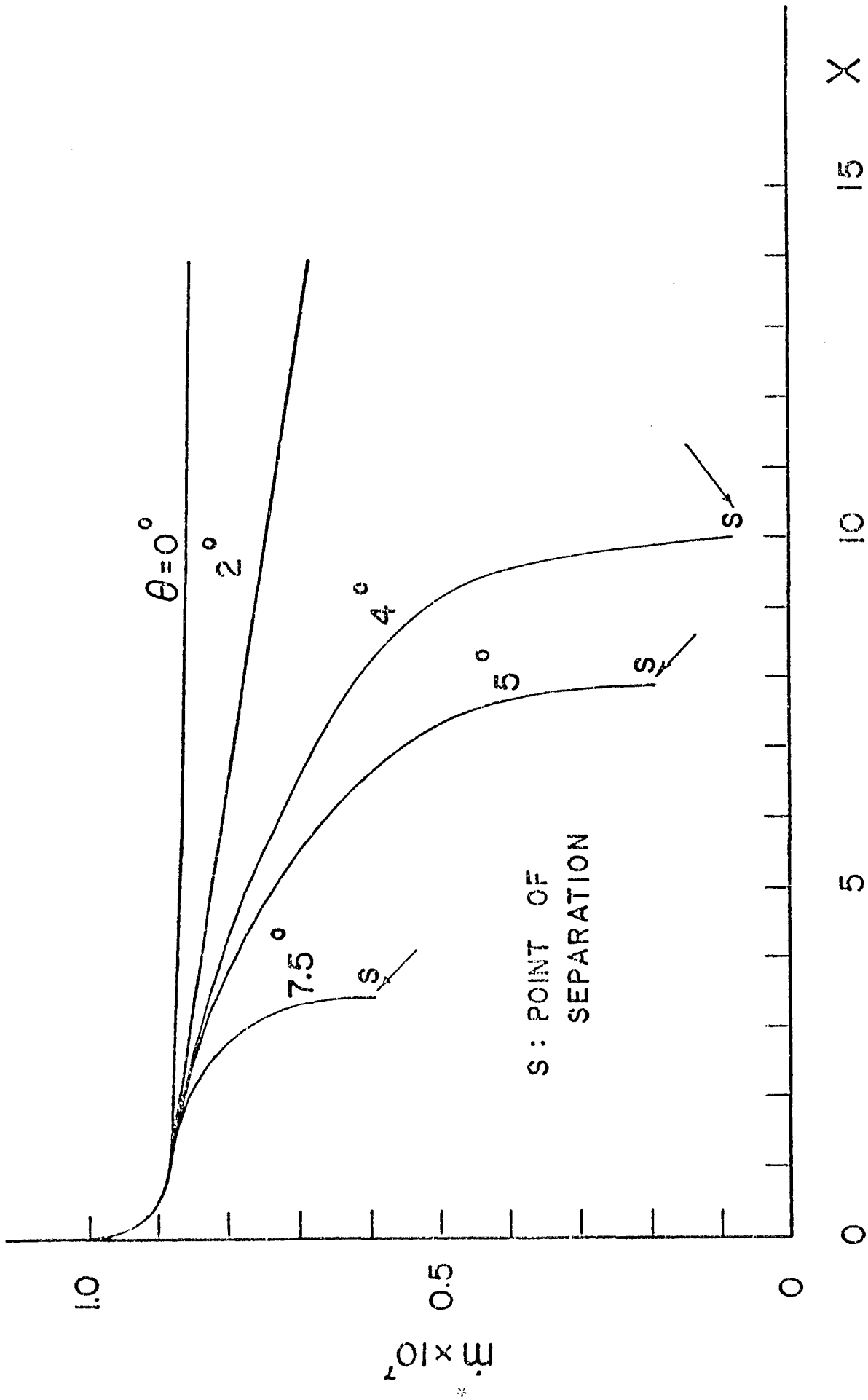

FIG. 4.7 EFFECT OF DIFFUSER ANGLE ON RATE OF DEPOSITION DUE TO ADHESION ONLY

(K_{np} = 0.0001, N_m = 2, N_R = 1000, R^* = 0.002, α = 0, $\beta = 10^7$, σ = 0.5, $\sigma_w\lambda$ = 1.0, σ_w' = 0, ρ_R = 300, ρ^*_{pb} = 0.3)

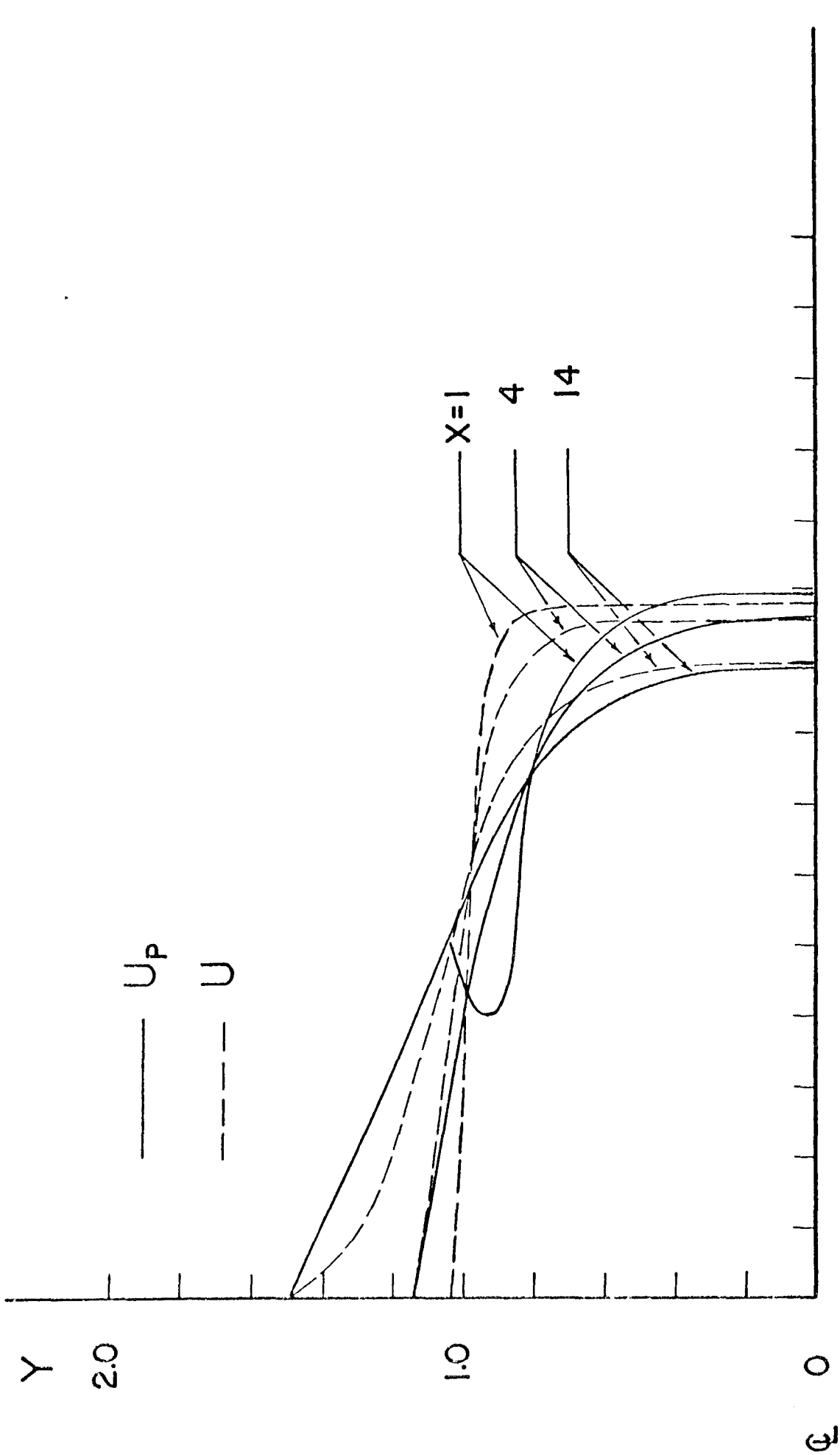

FIG. 4.8 COMPARISON OF AXIAL VELOCITIES OF FLUID AND PARTICLE PHASES IN A DIFFUSER FLOW

(K_{np} = 0.0001, N_m = 2, N_R = 1000, R^* = 0.002, α = 1.0, β = 40, θ = 2°, τ = 0.5, σ_w = 0.1, σ_w' = 10^{-6}, σ_R = 300, σ^*_{pb} = 0.3)

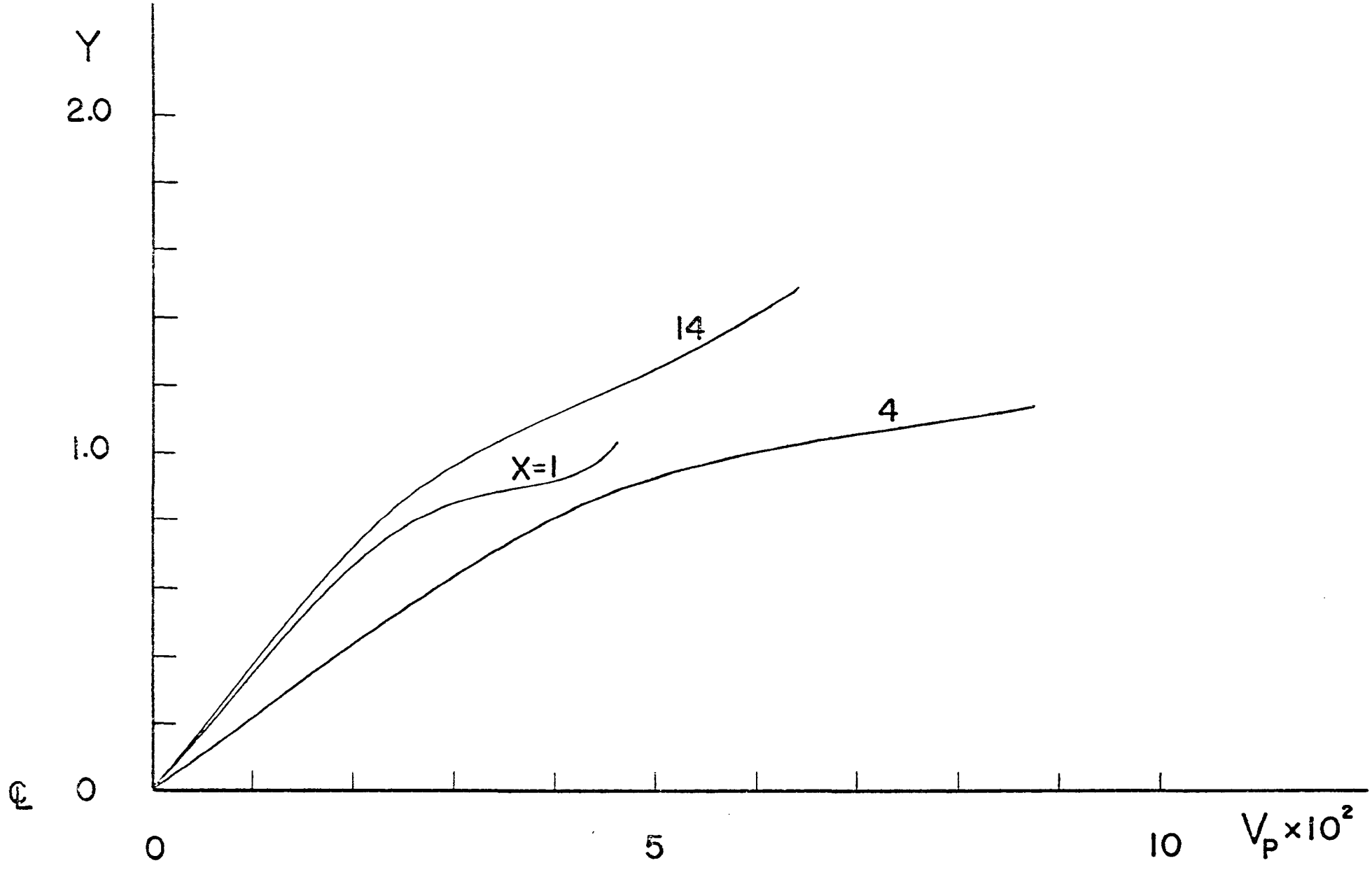

FIG. 4.9 VERTICAL VELOCITY DISTRIBUTION OF PARTICLES IN A DIFFUSER FLOW

(K_{np} = 0.0001, N_m = 2, N_R = 1000, R^* = 0.002, α = 1.0, β = 40, θ = 2°, σ = 0.5, $\sigma_w\lambda$ = 0.1, $\sigma'_w = 10^{-6}$, ρ_R = 300, ρ^*_{pb} = 0.3)

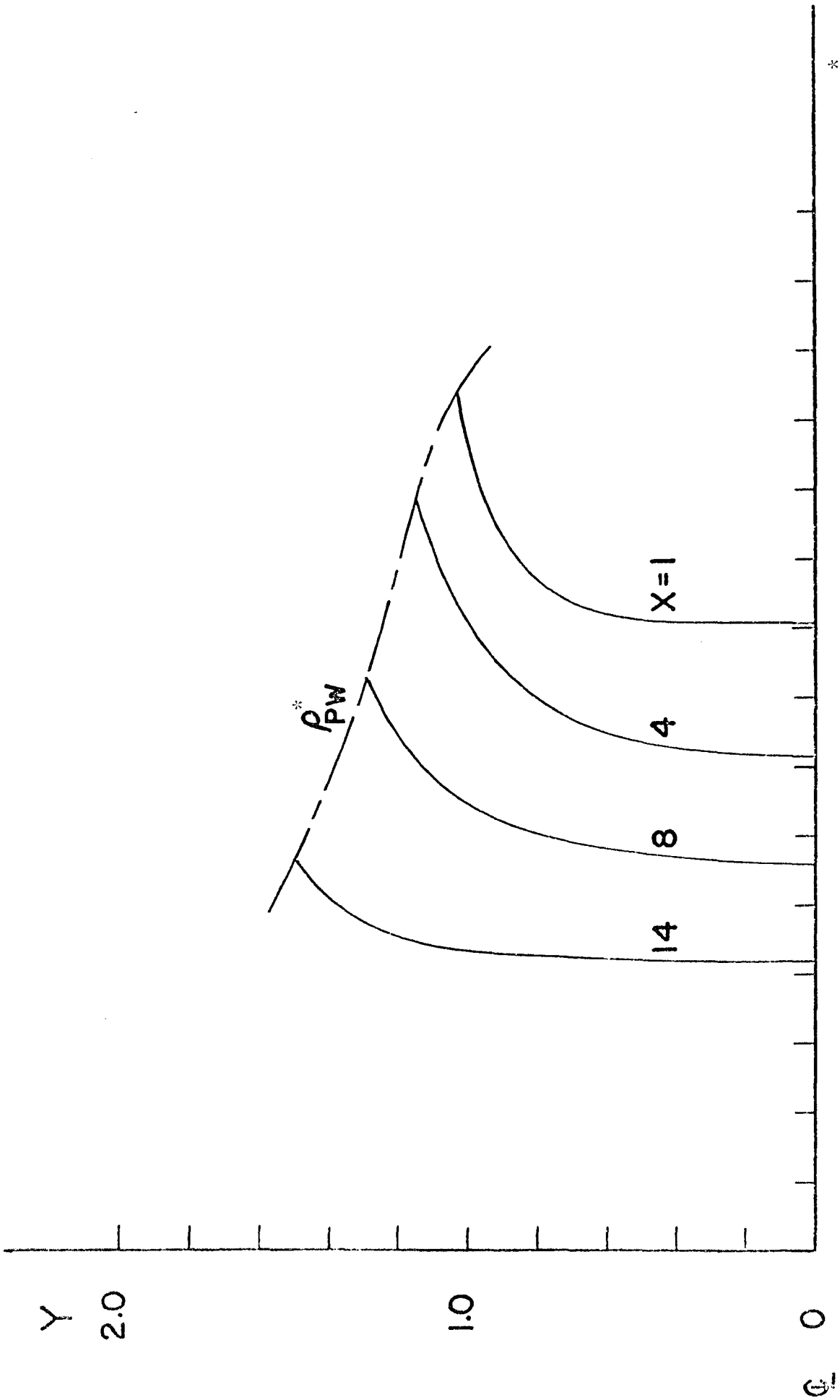

FIG. 4.10 DISTRIBUTION OF PARTICLE CONCENTRATION IN A DIFFUSER FLOW

(K_{np} = 0.0001, N_m = 2, N_R = 1000, R^* = 0.002, α = 1.0, β = 40, Θ = 2°, σ = 0.5, σ_w = 0.1, σ_w' = 10^{-6}, ρ_R = 300, ρ_{pb}^* = 0.3)

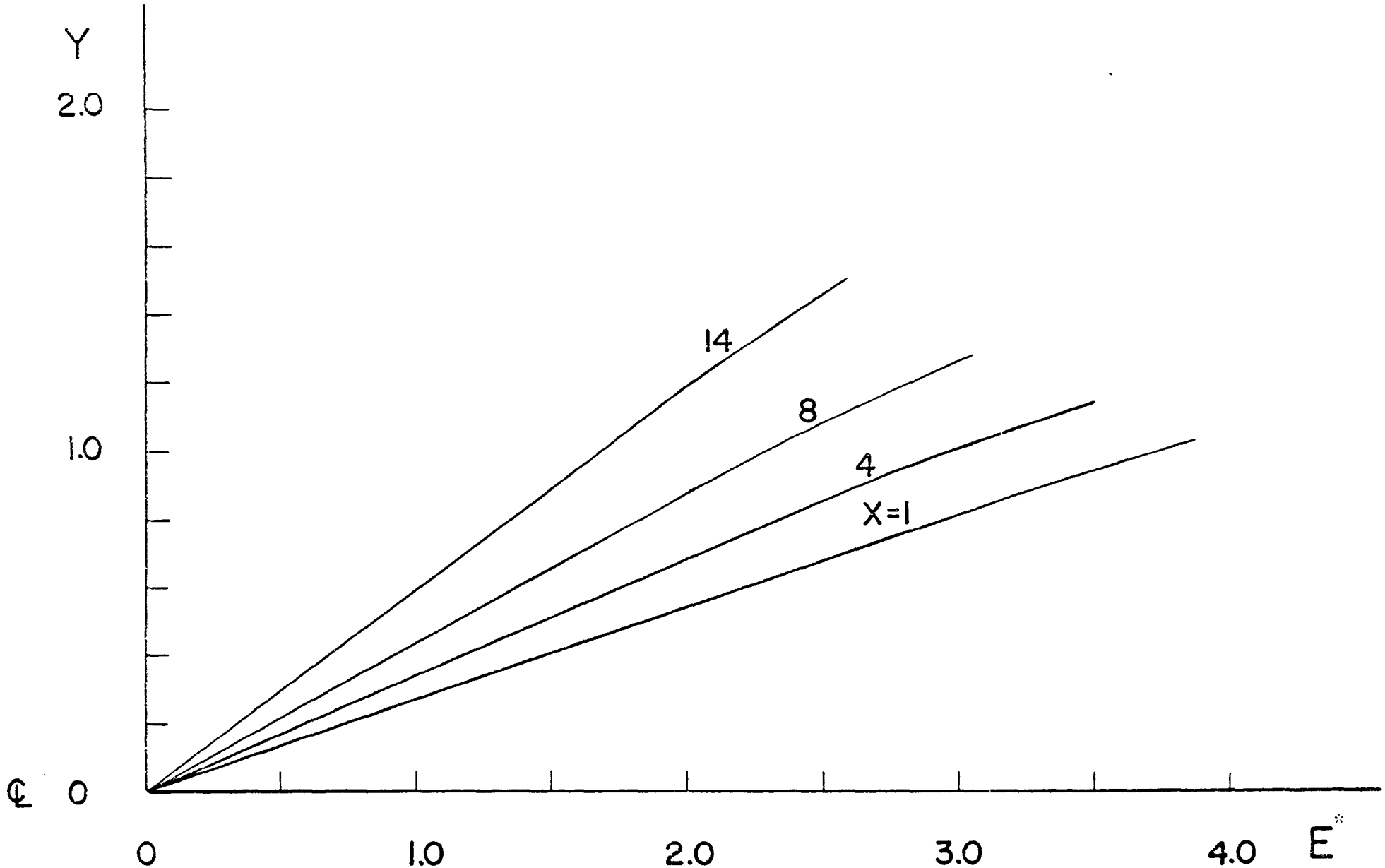

FIG. 4.11 DISTRIBUTION OF ELECTRIC FIELD INTENSITY IN A DIFFUSER FLOW

(K_{np} = 0.0001, N_m = 2, N_R = 1000, R^* = 0.002, α = 1.0, β = 40, θ = 2°, σ = 0.5, $\sigma_w\lambda$ = 0.1, σ'_w = 10^{-6}, ρ_R = 300, ρ^*_{pb} = 0.3)

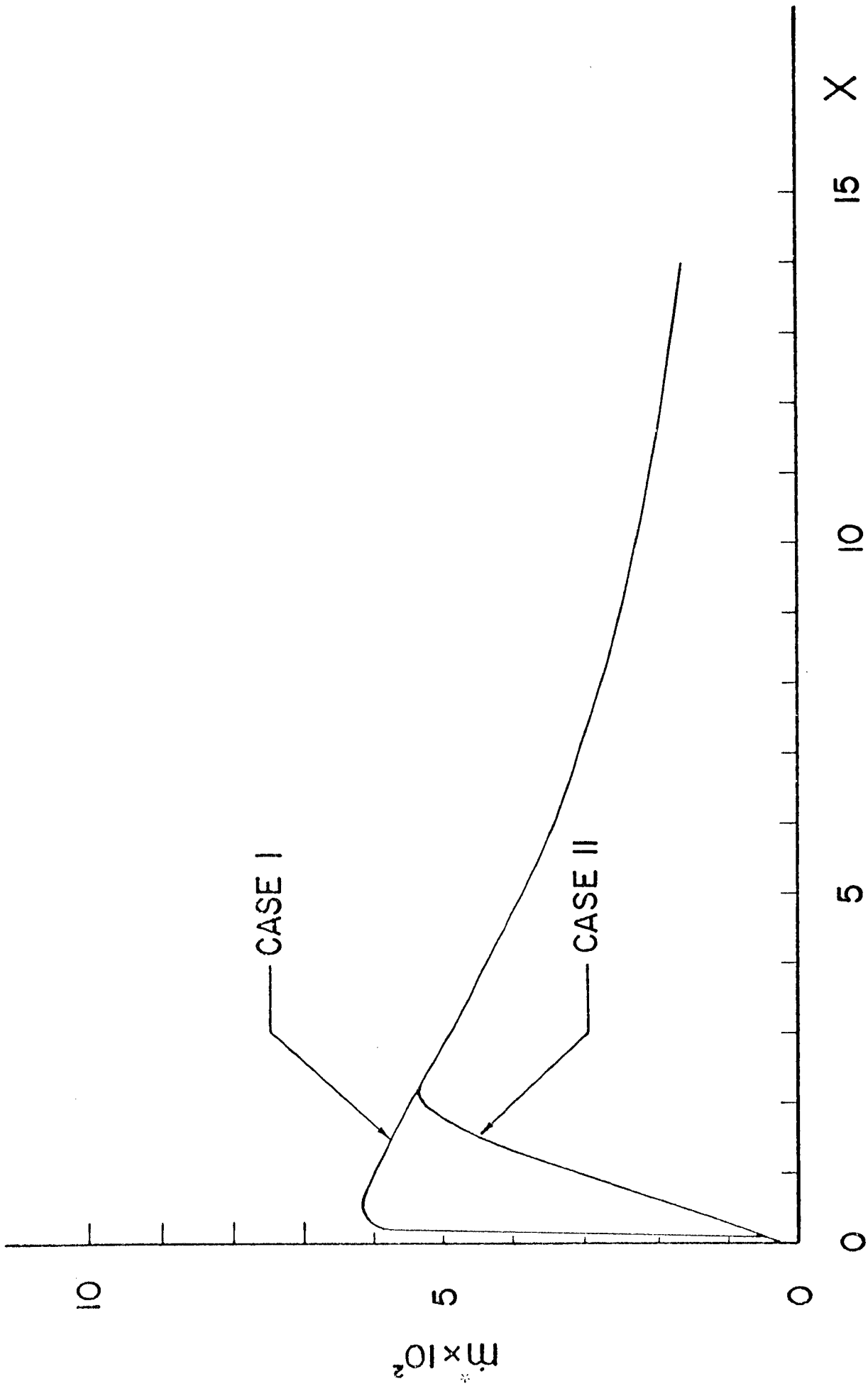

FIG. 4.12 EFFECT OF PARTICLE SLIP CONDITION AT WALL ON RATE OF DEPOSITION IN A DIFFUSER FLOW
($K_{np} = 0.0001$, $N_m = 2$, $N_R = 1000$, $K^* = 0.002$, $\alpha = 1.0$, $\beta = 40$, $\theta = 2°$, $\sigma = 0.5$, $\sigma_w' = 0.1$, $\sigma_w' = 10^{-6}$, $\rho_R = 300$, $\rho_{Pb}^* = 0.3$)

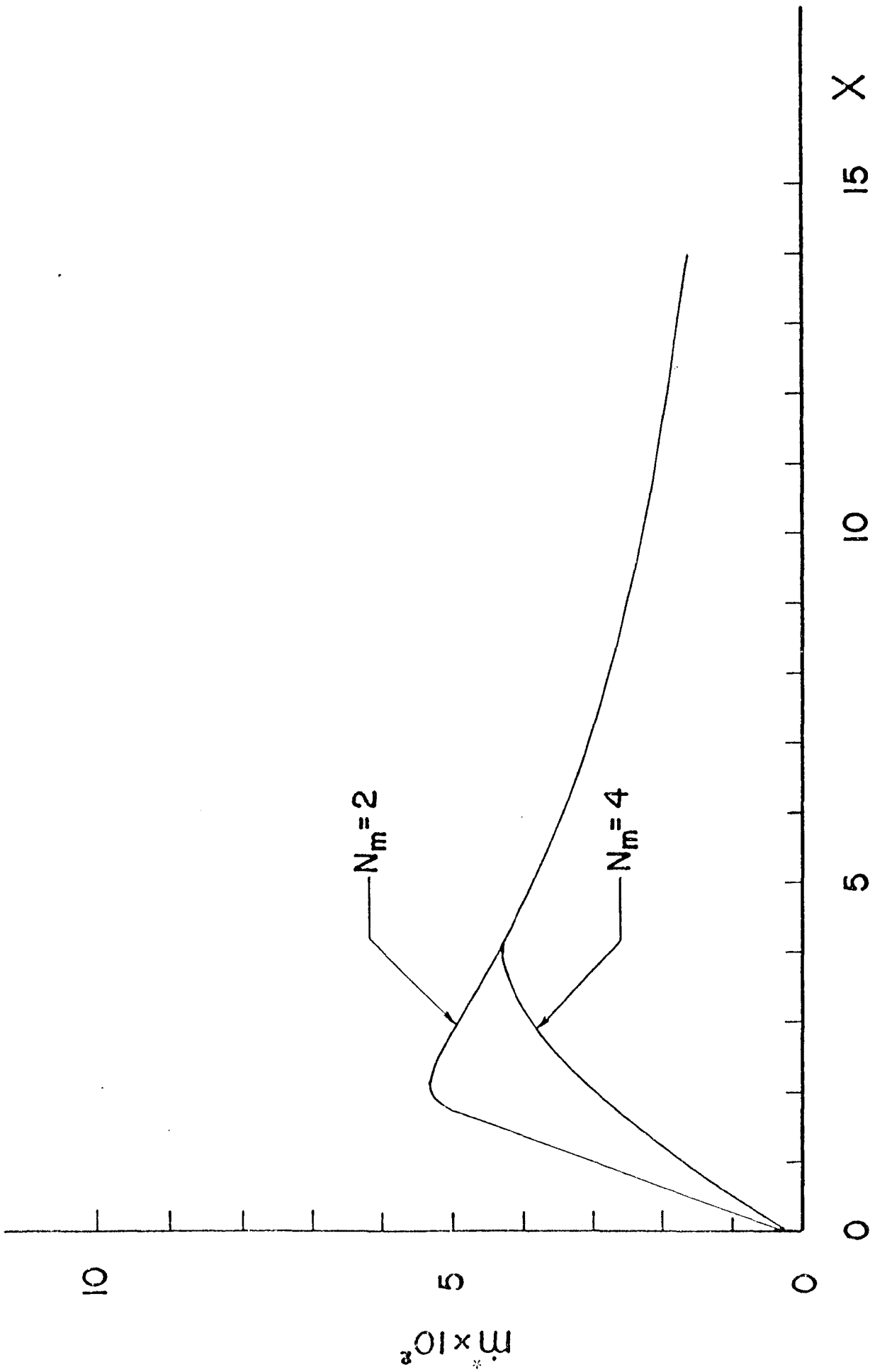

FIG. 4.13 EFFECT OF MOMENTUM-TRANSFER NUMBER ON RATE OF DEPOSITION IN A DIFFUSER FLOW
($K_{np} = 0.0001$, $N_R = 1000$, $R^* = 0.002$, $\alpha = 1.0$, $\beta = 40$, $\theta = 2°$, $\sigma = 0.5$, $\sigma_{w\lambda} = 0.1$, $\sigma_w' = 10^{-6}$, $\rho_R = 300$, $p^*_{pb} = 0.3$)

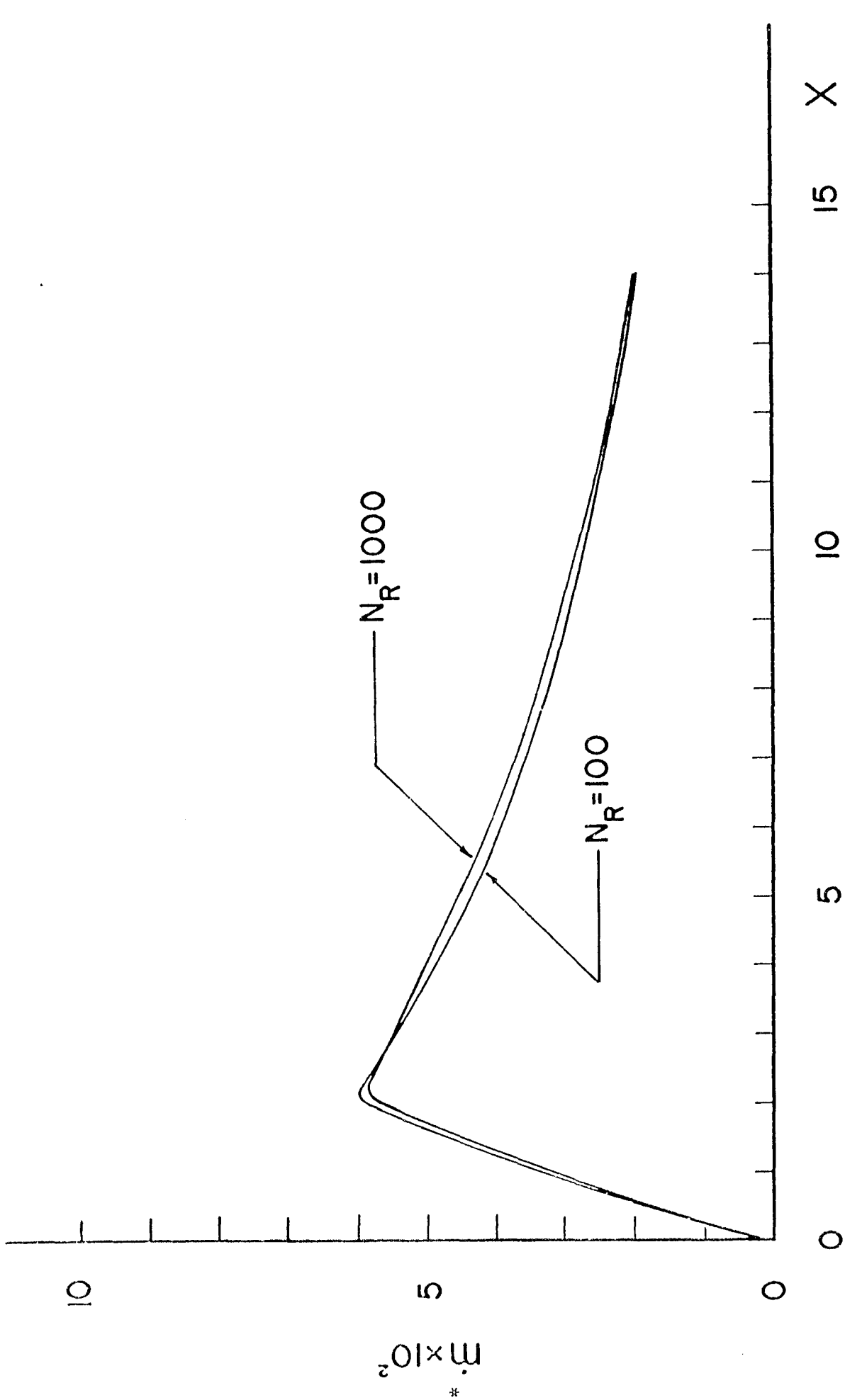

FIG. 4.14 EFFECT OF REYNOLDS NUMBER ON RATE OF DEPOSITION IN A DIFFUSER FLOW
(K_{np} = 0.0001, N_m = 2, R^* = 0.002, α = 1.0, β = 40, Θ = 2°, σ = 0.5, $\sigma_{w\lambda}$ = 0.1, σ_w' = 10^{-6}, ρ_R = 300, c^*_{Pb} = 0.3)

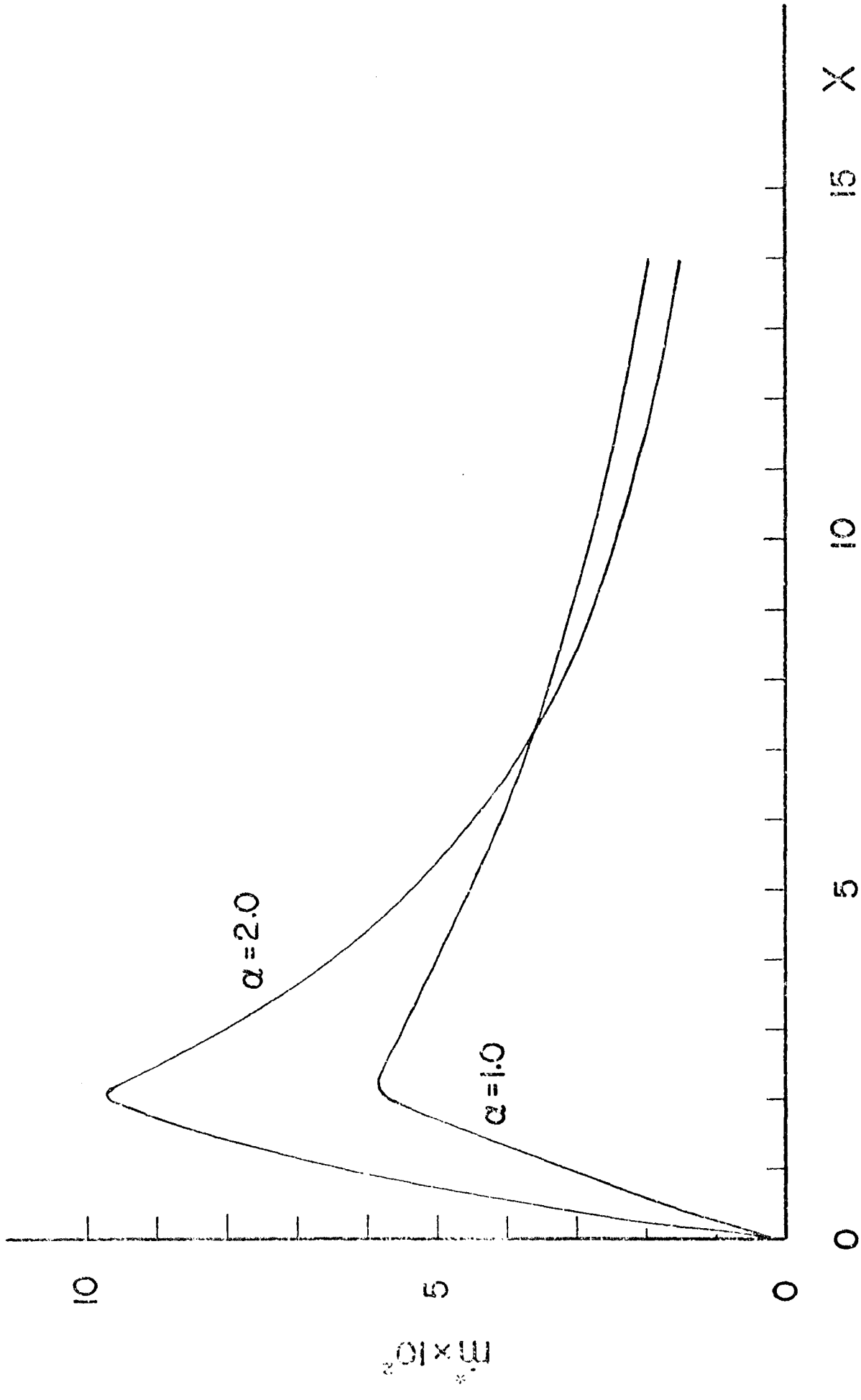

FIG. 4.15 EFFECT OF ELECTROSTATIC CHARGE ON RATE OF DEPOSITION IN A DIFFUSER FLOW

($K_{np} = 0.0001$, $N_m = 2$, $N_R = 1000$, $R^* = 0.002$, $\beta = 40$, $\theta = 2^\circ$, $\sigma = 0.5$, $\sigma_w{}^\lambda = 0.1$, $\sigma_w' = 10^{-6}$, $\rho_R = 300$, $\rho_{pb}^* = 0.3$)

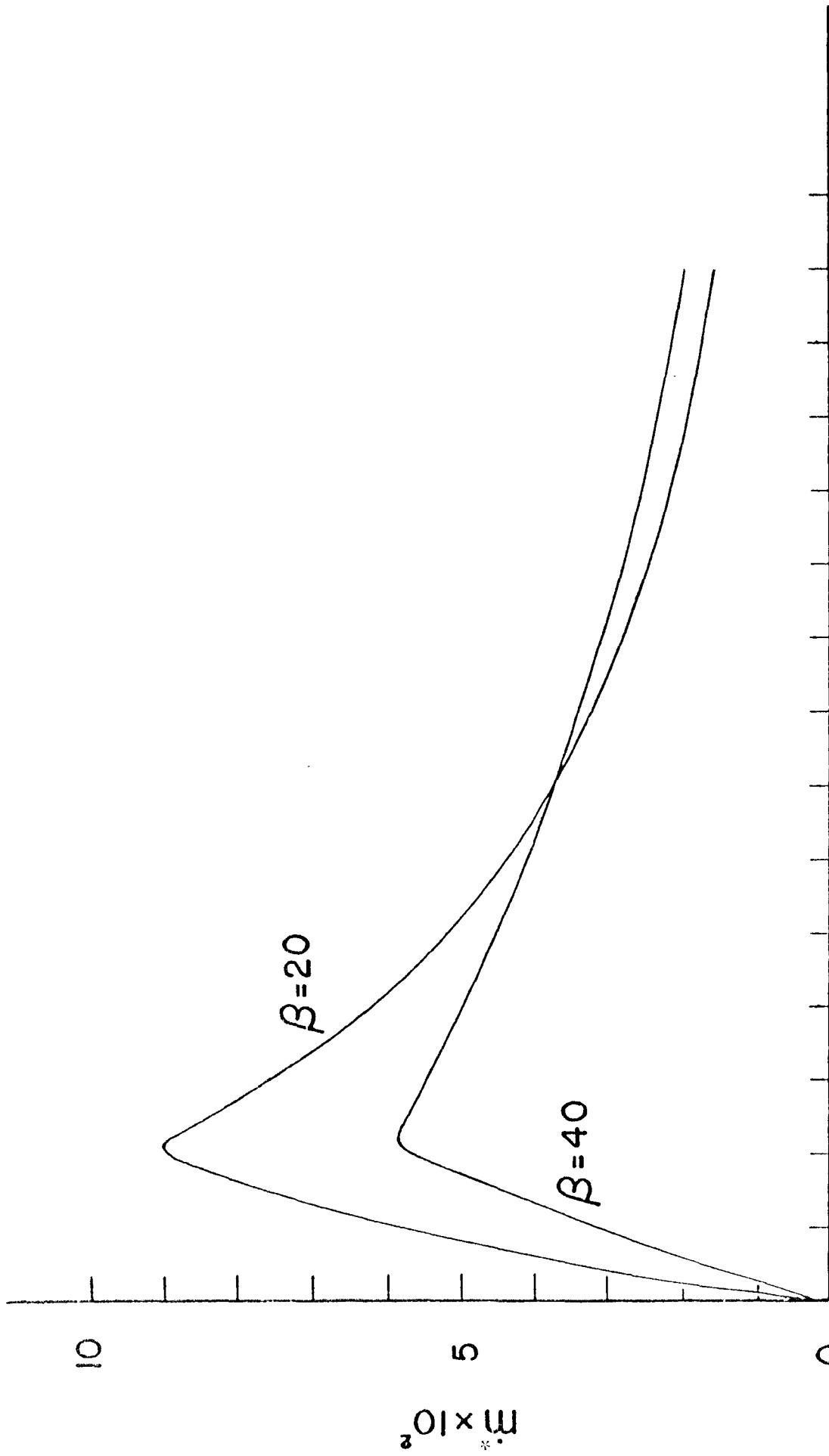

FIG. 4.16 EFFECT OF DIFFUSIVE PECLET NUMBER ON RATE OF DEPOSITION IN A DIFFUSER FLOW

(K_{np} = 0.0001, N_m = 2, N_R = 1000, R^* = 0.002, a = 1.0, θ = 2°, σ = 0.5, σ_w^{λ} = 0.1, σ_w' = 10^{-6}, ε_R = 300, ε_{pb}^* = 0.3)

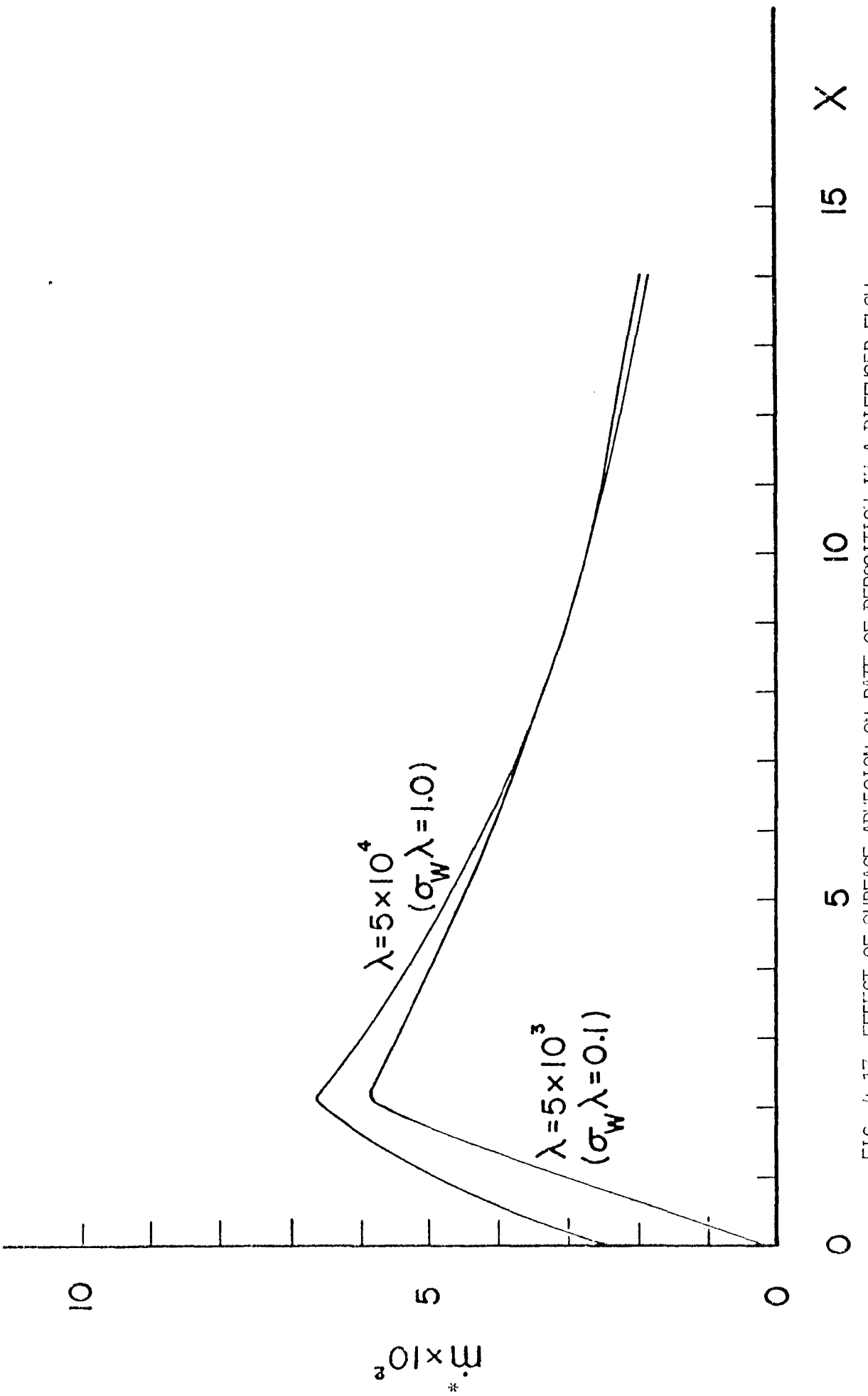

FIG. 4.17 EFFECT OF SURFACE ADHESION ON RATE OF DEPOSITION IN A DIFFUSER FLOW

(K_{np} = 0.0001, N_m = 2, N_R = 1000, R^* = 0.002, α = 1.0, β = 40, θ = 2°, σ = 0.5, σ_w' = 10^{-6}, c_R = 300, c_{pb}^* = 0.3)

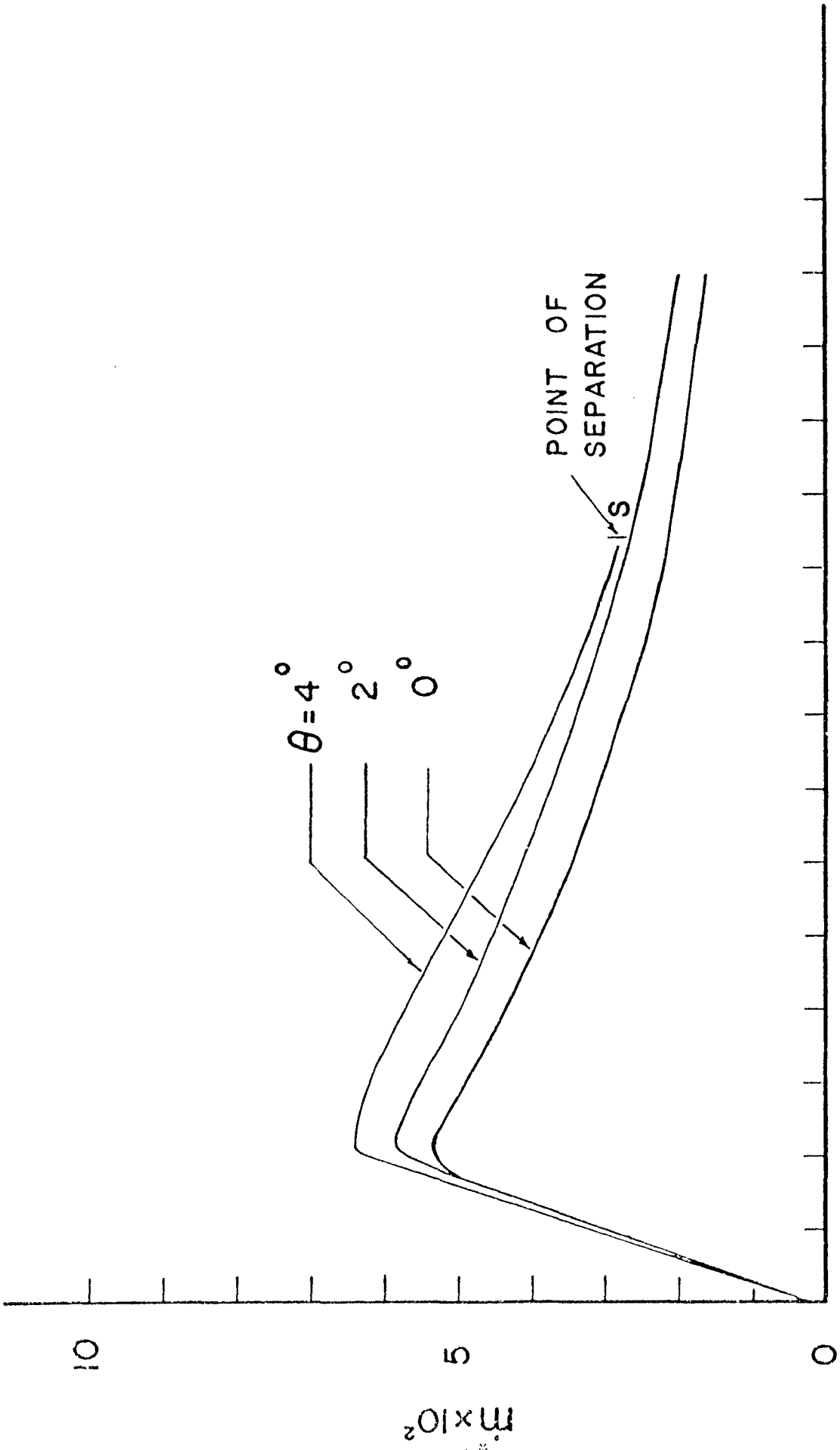

FIG. 4.18 EFFECT OF DIFFUSER ANGLE ON RATE OF DEPOSITION AT LOW DIFFUSIVE PECLET NUMBER

($K_{n_P} = 0.0001$, $N_m = 2$, $N_R = 1000$, $R^* = 0.002$, $\alpha = 1.0$, $\beta = 40$, $\sigma = 0.5$, $\sigma_w^\lambda = 0.1$, $\sigma_w' = 10^{-6}$, $\sigma_R = 300$, $\sigma_{pb}^* = 0.3$)

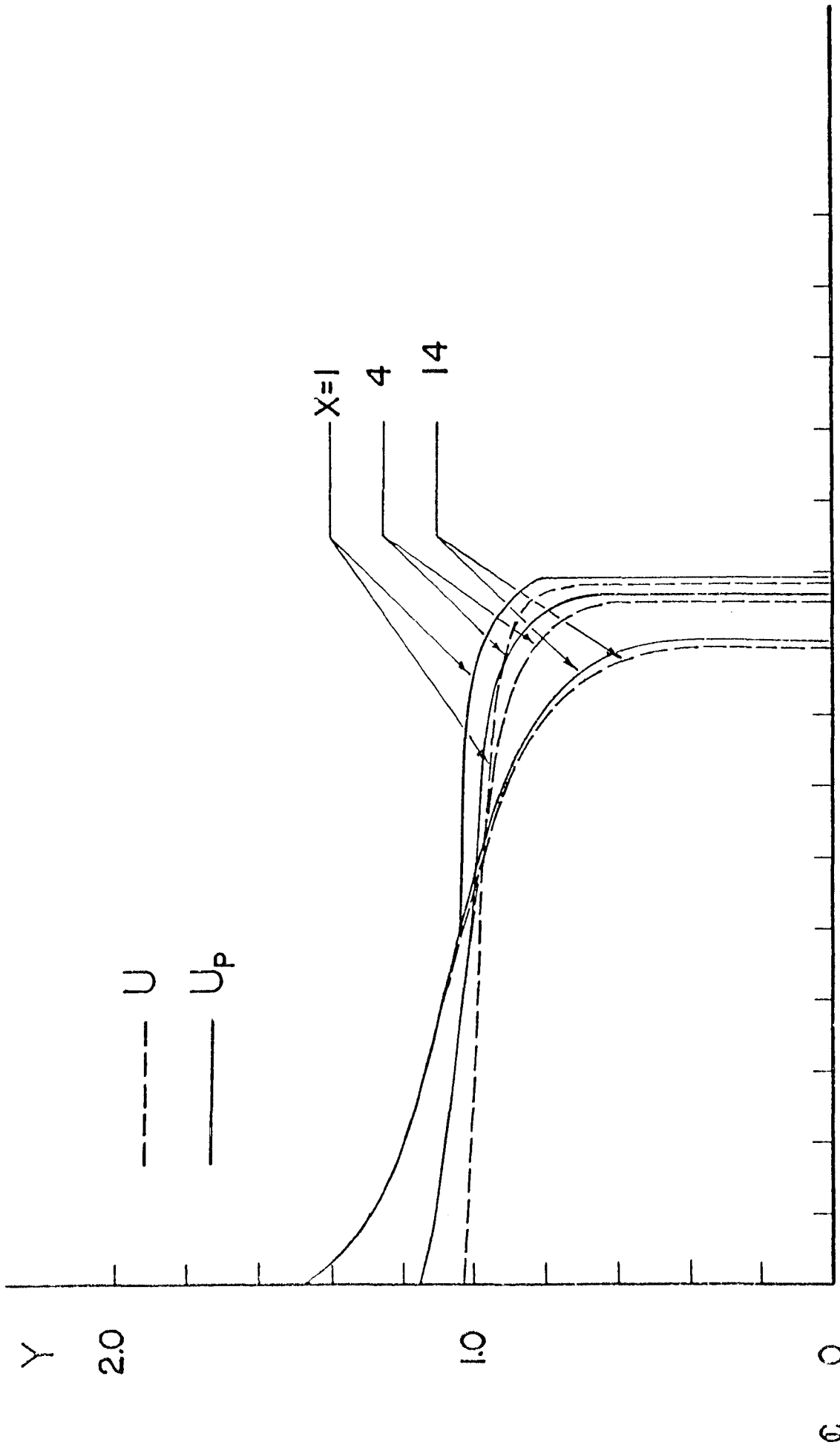

FIG. 4.19 COMPARISON OF AXIAL VELOCITY PROFILES OF FLUID AND PARTICLE PHASES AT HIGH DIFFUSIVE PECLET NUMBER IN A DIFFUSER FLOW (K_{mp} = 0.0001, N_m = 2, N_R = 1000, R^* = 0.002, α = 1.0, $\beta = 10^7$, $\theta = 2°$, σ = 0.5. σ_{w^2} = 1.0, $\sigma_w = 10^{-10}$, ρ_R = 300, ρ^*_{pb} = 0.3)

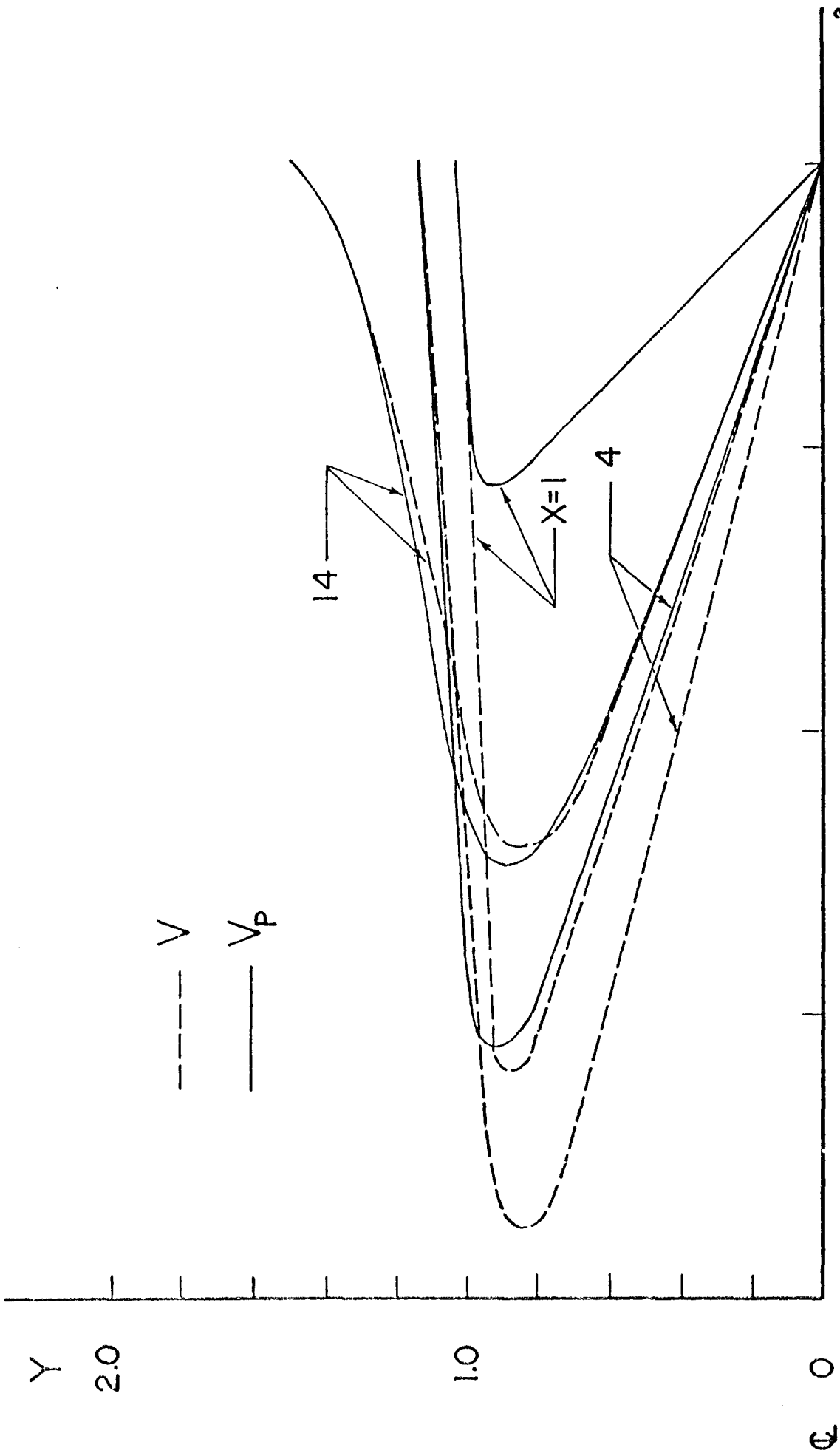

FIG. 4.20 COMPARISON OF VERTICAL VELOCITY PROFILES OF FLUID AND PARTICLE PHASES AT HIGH DIFFUSIVE PECLET NUMBER IN A DIFFUSER FLOW

(K_{np} = 0.0001, N_m = 2, N_R = 1000, R^* = 0.002, α = 1.0, ε = 10^7, θ = 2°, σ = 0.5, $\sigma_w \lambda$ = 1.0, σ_w' = 10^{-10}, σ_R = 300, σ_{pb}^* = 0.3)

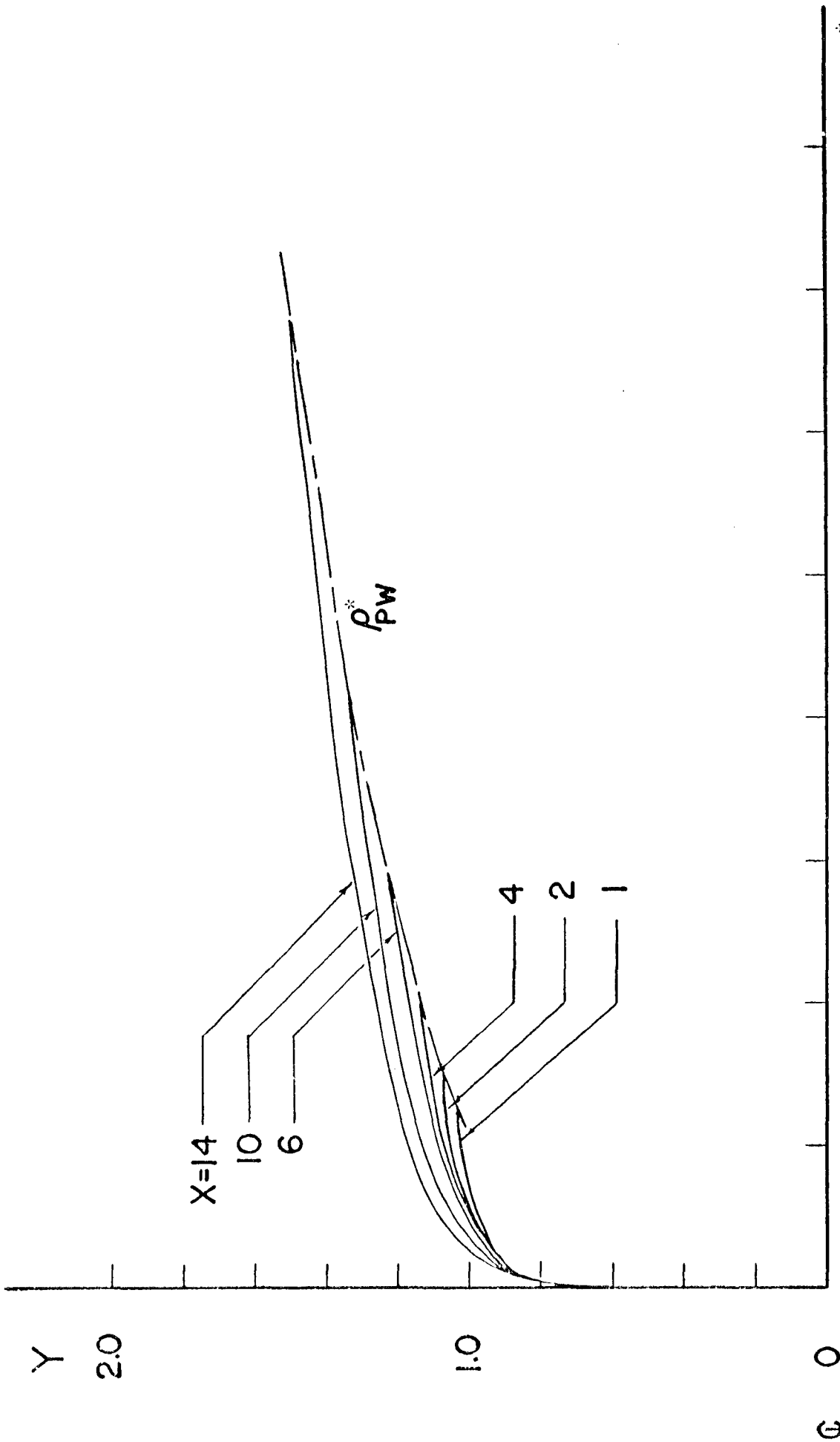

FIG. 4.21 DISTRIBUTION OF PARTICLE CONCENTRATION AT HIGH DIFFUSIVE PECLET NUMBER IN A DIFFUSER FLOW
(K_{np} = 0.0001, N_n = 2, N_R = 1000, R^* = 0.002, α = 1.0, β = 10^7, Θ = 2^o, σ = 0.5, σ_w' = 1.0, σ_w' = 10^{-10}, ϵ_R = 300, c_{pb}^* = 0.3)

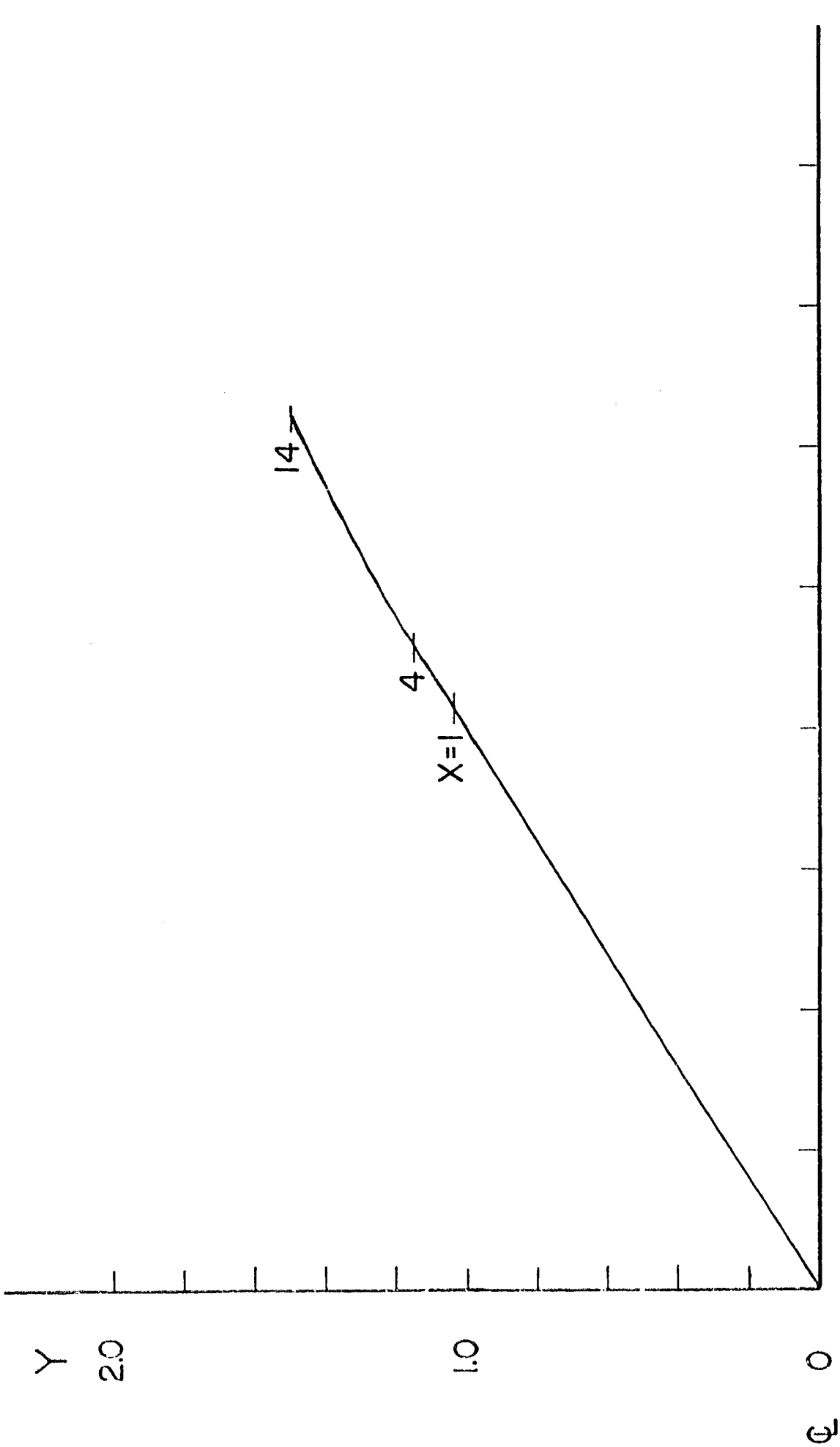

FIG. 4.22 DISTRIBUTION OF ELECTRIC FIELD INTENSITY AT HIGH DIFFUSIVE PECLET NUMBER IN A DIFFUSER FLOW
(K_{np} = 0.0001, N_m = 2, N_R = 1000, R^* = 0.002, α = 1.0, β = 10^7, θ = 2°, σ = 0.5, σ_w = 1.0, σ'_w = 10^{-10}, ρ_R = 300, ρ^*_{pb} = 0.3)

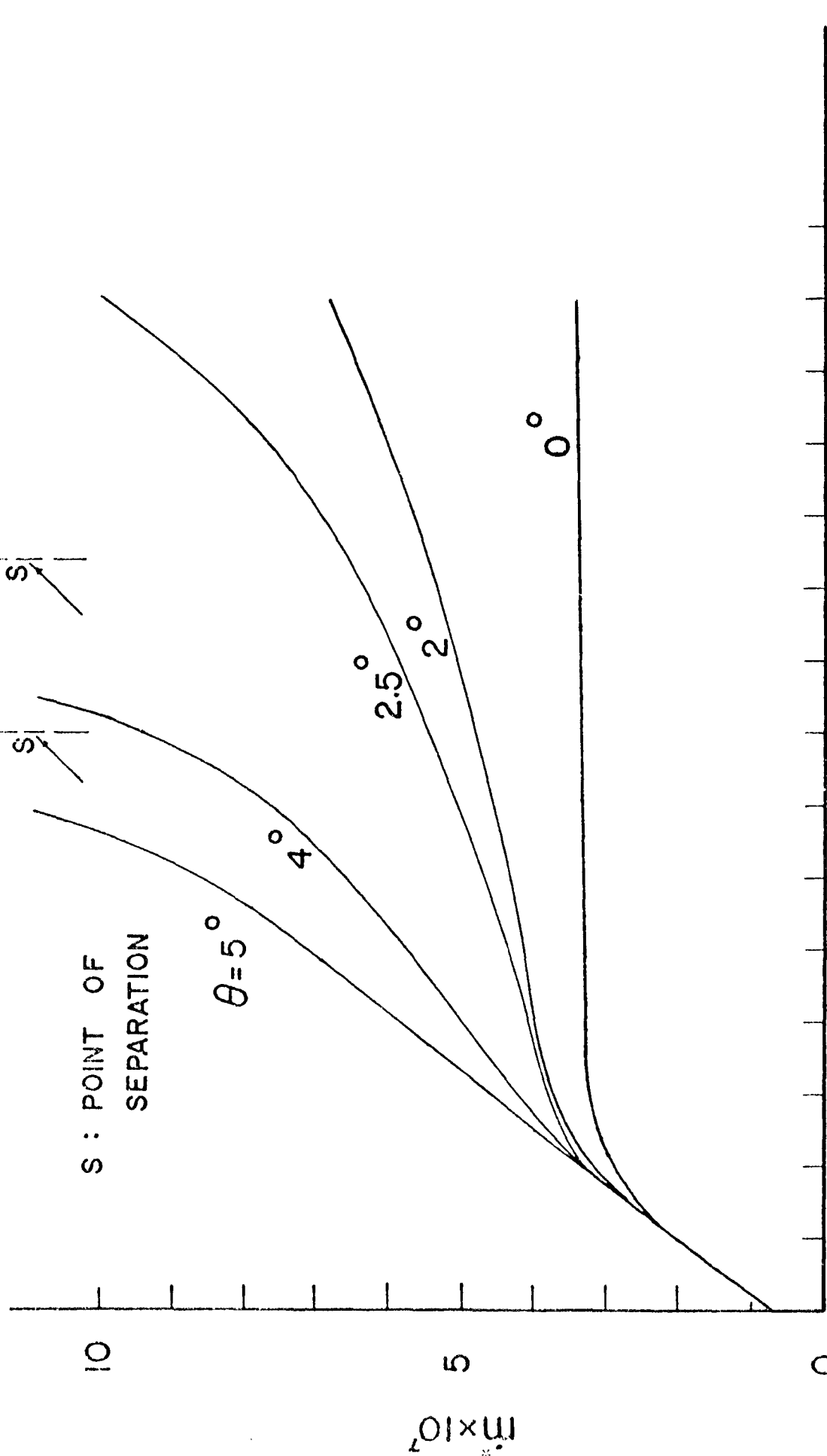

FIG. 4.23 EFFECT OF DIFFUSER ANGLE ON RATE OF DEPOSITION AT HIGH DIFFUSIVE PECLET NUMBER

($N_{np} = 0.0001$, $N_m = 2$, $N_R = 1000$, $R^* = 0.002$, $\alpha = 1.0$, $\beta = 10^7$, $\sigma = 0.5$, $\sigma_w' = 1.0$, $\sigma_w = 10^{-10}$, $\sigma_R = 300$, $\sigma_{pb}^* = 0.3$)

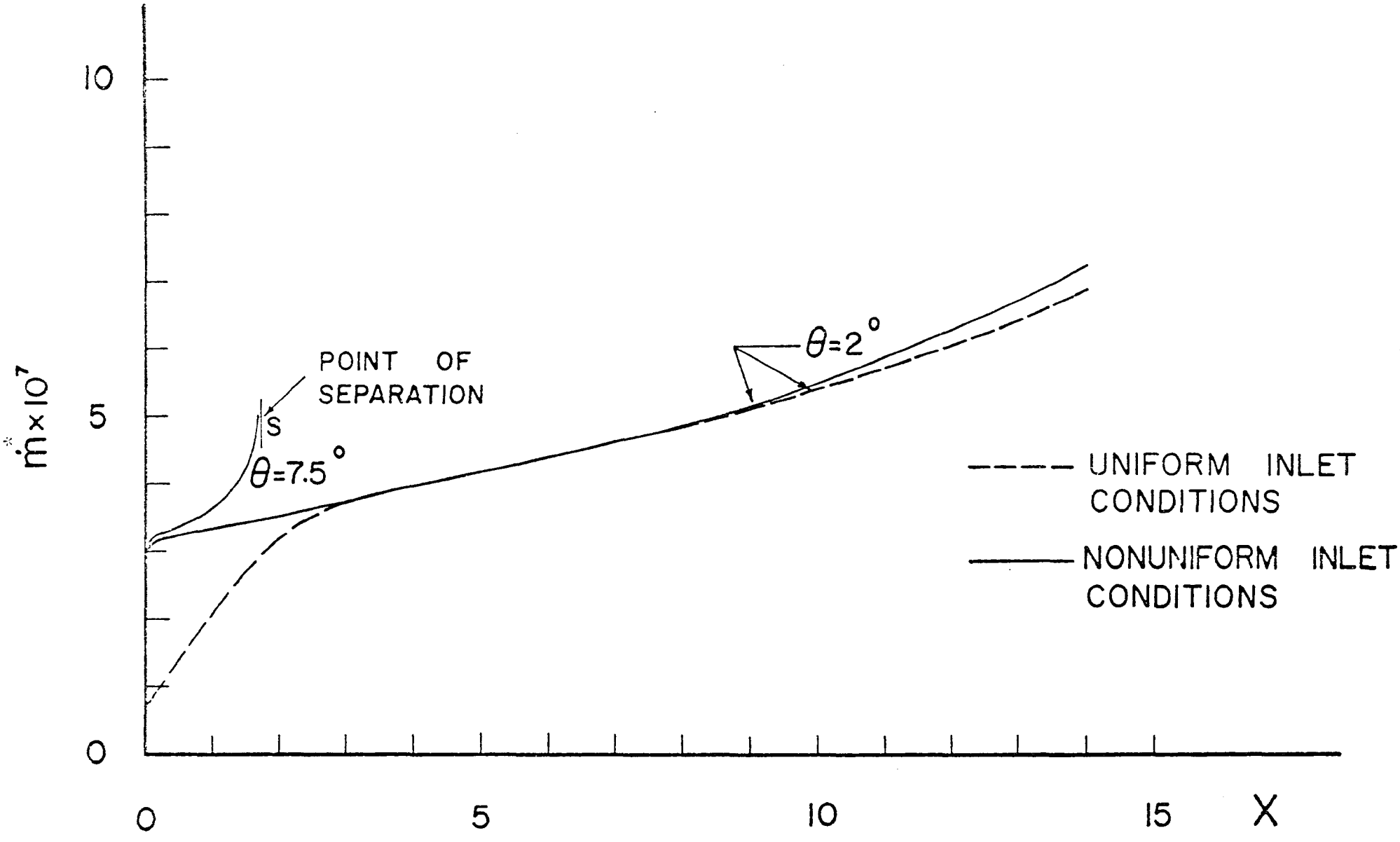

FIG. 4.24 EFFECT OF DIFFUSER ANGLE AND INLET CONDITIONS ON RATE OF DEPOSITION

(K_{np} = 0.0001, N_m = 2, N_R = 1000, R^* = 0.002, α = 1.0, $\varepsilon = 10^7$, σ = 0.5, $\sigma_w\lambda$ = 1.0, $\sigma_w' = 10^{-10}$, ρ_R = 300, ρ^*_{pb} = 0.3)

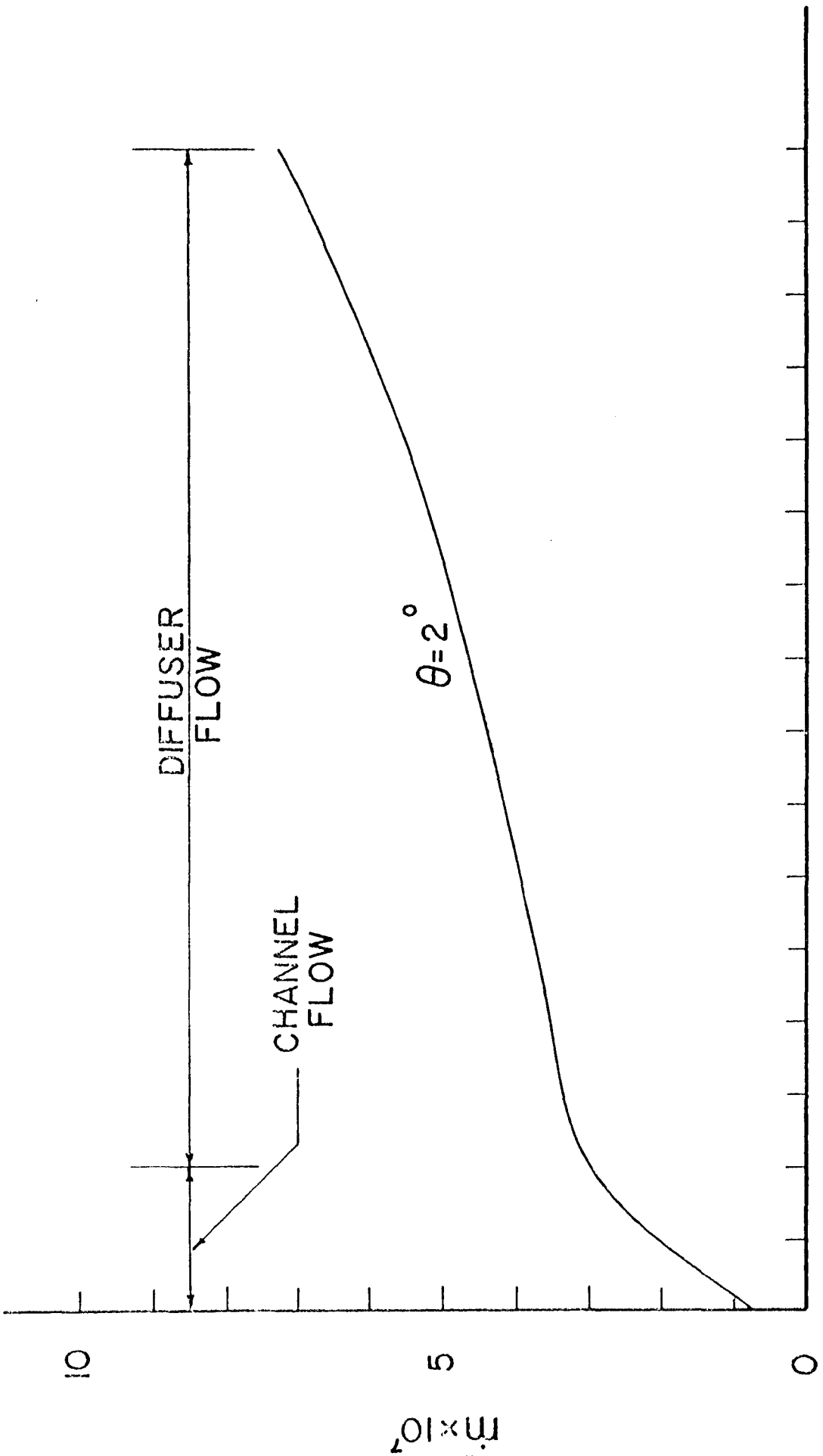

FIG. 4.25 AXIAL DISTRIBUTION OF RATE OF DEPOSITION IN CASE OF A CHANNEL CONNECTED TO A DIFFUSER OF 4° ANGLE

($K_{np} = 0.0001$, $N_m = 2$, $N_R = 1000$, $P^* = 0.002$, $\alpha = 1.0$, $\beta = 10^7$, $\sigma = 0.5$, $\sigma_w^{\lambda} = 1.0$, $\sigma_w' = 10^{-10}$, $\sigma_R = 300$, $\sigma_{pb}^* = 0.3$)

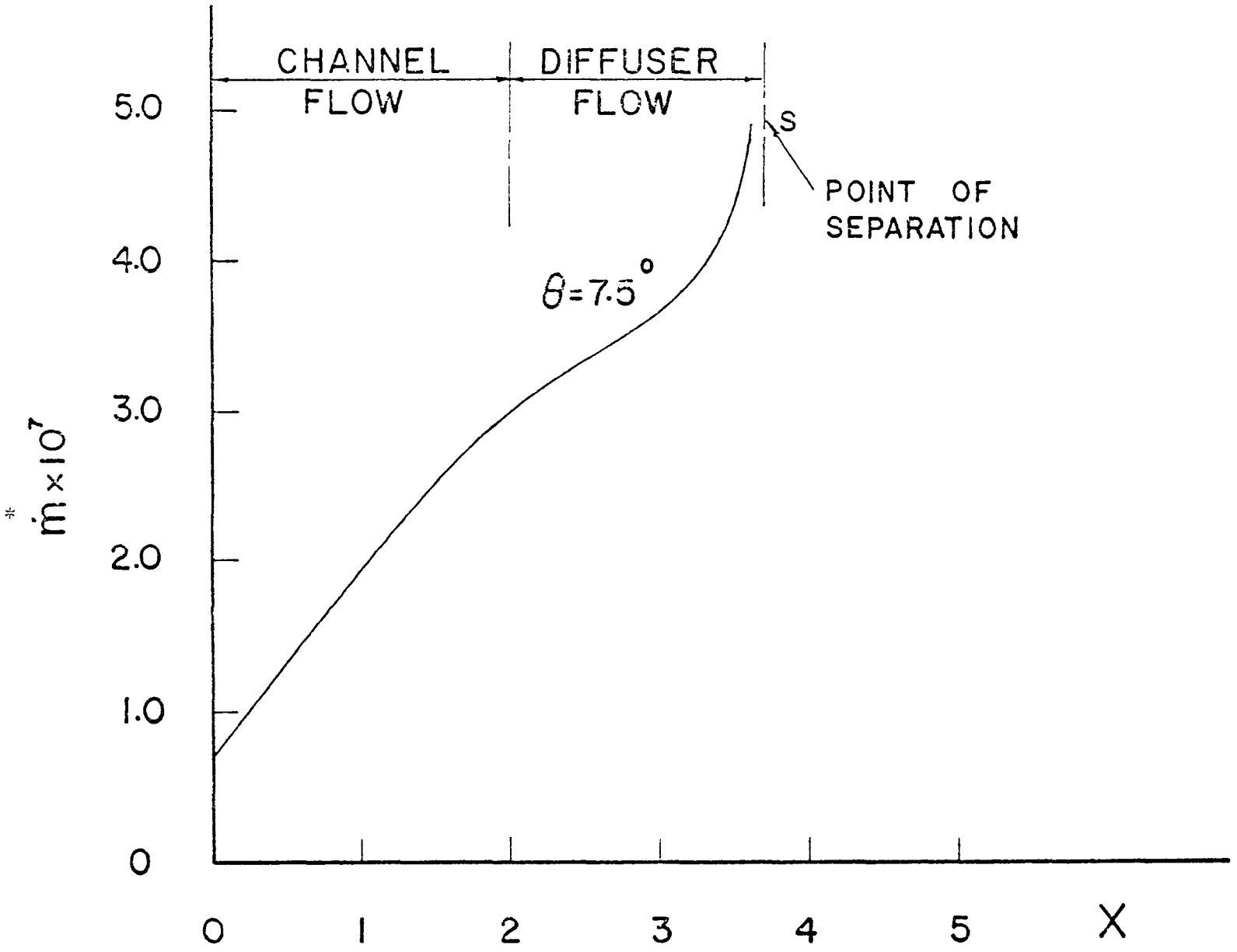

FIG. 4.26 AXIAL DISTRIBUTION OF RATE OF DEPOSITION IN CASE OF A CHANNEL CONNECTED TO A DIFFUSER OF 15° ANGLE

(K_{np} = 0.0001, N_m = 2, N_R = 1000, R^* = 0.002, α = 1.0, $\beta = 10^7$, σ = 0.5, $\sigma_w\lambda$ = 1.0, $\sigma_w' = 10^{-10}$, ρ_R = 300, ρ_{pb}^* = 0.3)

VITA

SHAWKI MAHMOUD ELDIGHIDY was born in . He enrolled in COLLEGE OF ENGINEERING, CAIRO UNIVERSITY, EGYPT, as a freshman in 1963. He received his B.S. Degree with high honors in 1968.

He worked as an instructor in the Mechanical Engineering Department, EIN SHAMS UNIVERSITY, CAIRO, EGYPT, from 1968 to 1971.

He received his M.S. Degree with highest honors (G.P.A. = 4.0) in 1973, from NEWARK COLLEGE OF ENGINEERING (NCE)*, NEWARK, NEW JERSEY, U.S.A.

He was awarded a college teaching fellowship in 1973 and a research assistantship in 1974, he served as a teaching and research assistant in 1973, 1974 and 1975 during his doctoral program in NEW JERSEY INSTITUTE OF TECHNOLOGY (NJIT), NEWARK, NEW JERSEY, U.S.A.

---

*Known as New Jersey Institute of Technology as of January 1, 1975.